Monte Carlo Modelling of Tumour Growth, Hypoxia and Radiotherapy in Head and Neck Squamous Cell Carcinoma

Wendy M. Harriss

A report submitted for acceptance
as a thesis for the degree of
Doctor of Philosophy
from the School of Chemistry and Physics
University of Adelaide, South Australia, Australia

September 2011

Table of Contents

I. LIST OF FIGURES

II. LIST OF TABLES

ii) Oxic tumour Conventional Schedule simulation total cell kill results in terms of the number of 2 Gy fractions required to achieve total "basal" (stem, transit and level 1 differentiating cell) and stem cell only elimination, for accelerated repopulation (AR) onset times, and alpha beta ratios

APPENDIX C:

i) Moderately Hypoxic tumour simulation cell kill results for the total elimination of all stem transit and level 1 differentiating cells, for various onset times of accelerated repopulation (AR) and reoxygenation (ROx). Schedule numbers can be referred to in Tables 6.1 and 7.1 of this report.

ii) Oxic tumour simulation cell kill results for the total elimination of all stem transit and level 1 differentiating cells, for various onset times of accelerated repopulation (AR). Schedule numbers can be referred to in Tables 6.1 and 7.1 of this report.

III. ABREVIATIONS

AR	–	accelerated repopulation
BED	–	biological effective dose
CT	–	computed tomography
DNA	–	deoxyribonucleic acid
FHV	–	Fractional hypoxic volume
Gy	–	Gray = 1 Joule / Coulomb
HNSCC	–	head and neck squamous cell carcinoma
HP	–	hypoxic percentage (of cells in a tumour)
HYP-RT	–	'Hypoxic Radiotherapy' simulation model
IMRT	–	intensity modulated radiotherapy
KeV	–	kilo electron volt
KVp	–	kilo voltage potential
LET	–	linear energy transfer
LQ	–	linear quadratic (theory of cell survival)
M	–	molar
MV	–	mega voltage (x-ray beam)
MeV	–	mega electron volt
NTCP	–	normal tissue complication probability
OER	–	oxygen enhancement ratio
pO_2	–	partial pressure of oxygen
PTV	–	planning target volume
RBE	–	relative biological effectiveness
ROx	–	reoxygenation (during radiotherapy)
RT	–	radiotherapy
SCC	–	squamous cell carcinoma
SF_2	–	surviving fraction of cells after 2 Gy irradiation
TCP	–	tumour control probability
T_D	–	tumour double time
T_{pot}	–	potential tumour doubling time (equal to T_D when all cells are cycling clonogenic cells)

IV. ABSTRACT

Tumour hypoxia is the inadequate supply of oxygen in living tissue. Hypoxia is a major problem in the treatment cancer with ionising radiation because of the associated increase in radioresistance of hypoxic tumour cells. This effect can cause up to a three fold increase in the radiation dose required to kill the hypoxic cells compared to well oxygenated cells. Many locally advanced head and neck tumours exhibit hypoxia to some degree, and there is direct evidence that hypoxic tumour sub-volumes and their associated mean oxygenation levels have a direct influence on local tumour control after radiotherapy (Nordsmark 2005).

Currently, head and neck cancer radiotherapy local control rates lie at approximately 80% for early stage disease, but reduce significantly (often below 50%) for locally advanced tumours. Efforts to improve these statistics through dose and fractionation modifications in randomised clinical trials have been made in recent decades using alternate fractionation schedules, but the average prognosis has not improved significantly.

The effects of tumour reoxygenation during fractionated radiotherapy can assist in re-sensitising previously hypoxic tissue; however the complex dynamics and patient dependent characteristics of this phenomenon make the benefits difficult to quantify. Head and neck cancers, specifically head and neck squamous cell carcinoma (HNSCC), have also been shown to experience the phenomenon of accelerated repopulation during fractionated radiotherapy. Accelerated repopulation enhances cellular proliferation as a response to the trauma caused by treatment, and contributes to the low HNSCC local control rates after radiotherapy.

The modelling work developed for this report was undertaken to better understand the mechanisms and quantitative effects of HNSCC cellular kinetics and tumour oxygenation during growth and radiotherapy. The goal of individualising treatment planning for this disease was the motivation for developing the model. A key aim was to produce an end product to be used as an efficient and user-friendly radiobiological tool for the input on tumour specific properties such as tumour oxygenation and reoxygenation onset time, to investigate their effects on cell kill during radiotherapy.

To this end, a Monte Carlo model, named *HYP-RT (for **HYP**oxic-**R**adio**T**herapy simulation)*, was developed. *HYP-RT* simulates the tumour cell division process according to epithelial proliferative hierarchy, starting from a single stem cell. Monte Carlo methods were used to simulate the probabilistic nature of the biological and radiobiological mechanisms and parameters incorporated into the model, e.g. the distribution of cell cycle times (normal or exponential) and oxygenation levels (normal or log-normal), and the randomised methods of cell kill and oxygenation increase during treatment. Probabilistic methods were also used to make decisions during cell division, as to the type of daughter cell products that would emerge after the division of a mother cell.

After the growth of a 10^8 cell tumour, an algorithm was developed to model the effects of fractionated radiotherapy. This algorithm was designed to simulate the oxygen dependent radiosensitivity of individual tumour cells, as well as the effects of gradual reoxygenation and accelerated repopulation (through loss of stem cell division asymmetry). Both reoxygenation and accelerated repopulation could be onset at varying times after the start of treatment. Experimental animal work using HNSCC (FaDu cell line) xenografts was undertaken during this research, and showed that reoxygenation occurred very late in an accelerated radiation schedule (40 Gy in 2 weeks), indicating the need to investigate a range of reoxygenation onset times in the model (0 to 3 weeks).

Dynamic cell data was stored in a pre-allocated vector (the *Cellarray*) containing just over 10^8 object elements, with each element representing one tumour cell. This enabled efficient random access to the data. Linked list methods were used to chronologically order cells in the *Cellarray* based on their times of division. Model efficiency was paramount during model development, to ensure convenient use of the model for the current work and potential future research. Using linked list methods, the goal of a one hour maximum computation time to grow and treat a tumour was successfully achieved.

The model source code was written with the FORTRAN 95 programming language (complier v7.1.0, *Lahey Computer Systems* Inc.*)*, within the Visual Studio (2003, *Microsoft Corporation*) framework. Two additional graphical user interface programs were developed using the JAVA programming language (Java SE Development Kit 6.17), to 1) read in and interpret tumour data files, and 2) allow for the input of key tumour parameters before a simulation (or batches of simulations) and iteration over multiple parameter sets.

Cellular data and key algorithm parameters were written out to file at regular intervals (1000 hours by default), during tumour growth and before and after every dose fraction during treatment, for retrospective analysis. This data included the tumour pO_2 distribution, the instantaneous tumour growth rate and the number of cells of various types comprising the tumour.

Simulation results showed that tumour growth rate was strongly dependent on the percentage of stem cells in the tumour (modelled to be approximately 1% during growth). Incorporating a "moderately" hypoxic oxygen distribution increased tumour doubling times significantly, from 37 days for oxic tumours up to 65 days for moderately hypoxic tumours. This was attributed to the effects of oxygen dependent cell cycle slowing, cellular quiescence and necrosis.

Simulated conventional radiotherapy (5x2 Gy/wk) required on average an extra 16 Gy in total to achieve tumour control for moderately hypoxic compared to well oxygenated tumours. The effects of both accelerated repopulation and reoxygenation significantly altered the total doses required for tumour control, with accelerated repopulation effects dominating model outcomes. Accelerated repopulation and reoxygenation were found to be dependent on one another, making simulations of every combination of onset time for each effect necessary during model analysis.

During accelerated repopulation, a dose per fraction of 2.5 to 3.0 Gy was required to control the extra cell growth in an otherwise 2 Gy per fraction schedule. This equated to an extra 5 Gy being requiring to maintain tumour control for every week that the onset accelerated repopulation was brought toward the start of treatment. The benefits of reoxygenation reduced as the time of onset was delayed, with +1 Gy required to maintain tumour control for every week that reoxygenation was delayed.

Conventional fractionation simulation results had good agreement with standard Linear Quadratic theory, for the dose required to control well oxygenated tumours. However, comparison results were mixed for more complex cases involving hypoxic tumours with and without accelerated repopulation. When modelling altered fractionation schedules, simulation outcomes in terms of the total doses required for tumour control, agreed well with the prescriptions from published clinical trials. The most beneficial schedule, based on predicted total dose as well as biological effective doses (BED's) calculations for normal tissues, was the 10x1.1 Gy/week schedule (Pinto *et al.* 1991). However, there were up to 30 Gy differences in total dose and BED results when simulating

specific sets of tumour parameters for the same radiation schedule, highlighting the need for individualisation of treatment planning to improve the therapeutic ratio.

Four newly designed altered schedules were also simulated with the *HYP-RT* model. Results showed that using a concomitant boost at the beginning, rather than at the end of treatment, or using a "less aggressive" continuous hyper-accelerated radiotherapy (CHART) schedule (compared to the UK CHART schedule) may have potential therapeutic benefits compared to existing clinical schedules. Altering the oxygen enhancement ratio (OER) curve based on dose per fraction for the altered fractionation schedules, changed model results significantly for hyperfractionated schedules (up to 20 Gy). This highlighted the critical nature of the OER curve in predictive radiobiological tumour models.

In summary, the current research has involved the development, analysis and use of an efficient Monte Carlo tumour growth and radiotherapy model (*HYP-RT*). The model simulates a biologically plausible epithelial cell hierarchy, a large number of individual cells, tumour hypoxia, and the dynamics of reoxygenation and accelerated repopulation during radiotherapy. The user can input the desired oxygen distribution to describe the degree of tumour hypoxia as well as and the times of onset of treatment related effects, among many other cellular parameters. The model provides quantitative results regarding the total dose required to control a tumour, for a given fractionation schedule and tumour parameter set. It is hoped that computer models such as *HYP-RT* will be used in the near future as a tool to aid in the individualisation of radiotherapy planning, based on specific tumour experimental/imaging information, to improve prognosis for patients with HNSCC.

V. STATEMENT OF AUTHENTICITY

This work contains no material which has been accepted for the award of any other degree or diploma in any university or other tertiary institution, and to the best of my knowledge and belief, contains no material previously published or written by another person, except where due reference has been made in the text.

I give consent to this copy of my thesis when deposited in the University Library, being made available for loan and photocopying, subject to the provisions of the Copyright Act 1968. The author acknowledges that copyright of published works contained within this thesis resides with the copyright holder(s) of those works.

I also give permission for the digital version of my thesis to be made available on the web, via the University's digital research repository, the Library catalogue, the Australasian Digital Theses Program (ADTP) and also through web search engines, unless permission has been granted by the University to restrict access for a period of time.

Signed:……

Dated:……..

VI. ACKNOWLEDGEMENTS

I wish to give thanks to the School of Chemistry and Physics at the University of Adelaide, in accepting me into their postgraduate research program, and awarding me a scholarship which enabled me to study full time during the initial years of my PhD candidature. I also thank the University of Adelaide for further financial support which assisted in my attendance at several conferences and for the purchase of computer and experimental work equipment. Thank you to Dr Judith Pollard for your many years of dedicated work as the post-gradate Medical Physic program coordinator.

I am extremely grateful to have been accepted and welcomed into the Department of Medical Physics at the Royal Adelaide Hospital, and would like to whole-heartedly thank my supervisors Associate Professor Eva Bezak, Chief Medical Physicist, and Professor Eric Yeoh, Director of Radiation Oncology, for the their years of assistance, patience and support.

Eva, you have treated me with respect and kindness and have always given me your time when I have needed it, despite you very hectic schedule! I appreciate your efforts and consider working and studying with you an honour. I have very much enjoyed my time studying under your guidance, right from our first meeting at the beginning of my honours year in 2003.

Professor Yeoh, your support towards the Department of Medical Physics, and to post-gradate students is so very much appreciated. Thank you for your clinical guidance during my PhD research and for all of the wonderful editing work! I also appreciate your help in terms of financial support which assisted in funding my attendance at multiple conferences and workshops, as well as for these equipment needed for the animal experiments component of my research.

I would like to give kind thanks to Associate Professor Loredana Marcu, Senior Medical Physicist at the Royal Adelaide Hospital, for helping me to choose the direction of my research, for her kind support, and for her radiobiological knowledge which has assisted me greatly. Thanks also go to Professor Tim van Doorn and Dr Judith Pollard, for their supervision and guidance in the early years of this work.

Appreciation goes to all of the people that I have collaborated with, especially during the multi-disciplinary phase of animal experimental work, which was a new and exciting challenge for me. Thank you to Dr Tina Lavranos and Mrs Donna Fenu for their animal handling and cell line expertise, Dr Carlene Cullinane for the FaDu cell line donation, Professor Albert van der Kogel for the immunohistochemical imaging assistance, Mr Jim Manavis for tumour excise and cross-section advice and preparation, IMVS staff for animal handling and anaesthetic advice, Professor Cathy Malcontenti-Wison and Dr Peter Wong for *OxyLab* system assistance and equipment loan, and Mr Maarten Hermans, who joined the department as part of his masters work from the Technical University, Eidenhoven in the Netherlands, for his willing assistance and friendship during many hours of animal preparation and irradiation.

The Department of Medical Physics at the Royal Adelaide Hospital has been a welcoming and positive environment to study, with all team members showing me support and kindness during my candidature. Kind thanks go to the whole team and especially to Christine Robinson for her administrative assistance and caring friendship which has (and continues to) mean a great deal to me.

The love and support of my family, Lesley, John and Laura, my Grandparents, and my dear husband Dr Damien Phillips, have helped me immensely during my years of study. Thank you my family, your love has helped me to remain calm, focussed and remember what really matters in life. Damien, you have helped me more than I can put into words. You have assisted me emotionally and technically in achieving my goals for the model and getting to the finishing line of this long but extremely rewarding project. Thank you from the bottom of my heart for all that you do for me, for sharing your programming skills, for your patience, and most of all for your unconditional love.

VII. PUBLICATIONS & PRESENTATIONS

Publications in refereed journals

- Harriss-Phillips W. M., Bezak E., Yeoh K. (2011), *Monte Carlo radiotherapy simulations of accelerated repopulation and reoxygenation for hypoxic head and neck cancer.* Br J Radiol. **84** 903–918.
- Harriss W.M., Bezak E., Yeoh K., Hermans M. (2010), *Measurement of reoxygenation during fractionated radiotherapy in head and neck squamous cell carcinoma xenografts*. Australas Phys Eng Sci Med. **33** 251-63.
- Tuckwell W.M., Bezak E., Yeoh K., Marcu L.(2008), *Efficient Monte Carlo modelling of individual tumour cell propagation for hypoxic head and neck cancer*. Phys Med Biol. **53** 4489-507. (Note: published in my former name of W. M. Tuckwell).
  - ***Awarded the status of one of the top 20 articles in Phys Med Biol in 2008***

Published book chapters

- Harriss W. M. (2011), *Radiobiological modelling of tumour hypoxia and radiotherapy*. Recent Advances and Research Updates: Medical Physics. [ISSN 0972-4699] Chapter 16, 257-278.

Papers in preparation

- Harriss-Phillips W. M., Bezak E., Yeoh K. *Development of a radiobiological Monte Carlo model of hypoxic head and neck cancer and radiotherapy, HYP-RT.* To be submitted to Computational and Mathematical Methods in Medicine.

- Marcu L.M., Harriss-Phillips W.M., ***In silico*** *modelling of tumour response to treatment: current status.* To be submitted as a review paper to Computational and Mathematical Methods in Medicine.

Conference oral and poster presentations

International

- Harriss W.M., Bezak E., Yeoh K. (2009), *Computer and tumour xenograft modelling: dynamic hypoxia in head & neck radiotherapy*. Poster presentation. World Congress on Medical Physics and Biomedical Engineering. Munich, Germany.

- Tuckwell W.M., Bezak E., Yeoh K. (2008), *Monte Carlo Modelling of Hypoxic Head and Neck Squamous Cell Carcinoma and Radiotherapy*. Oral presentation. European Society for Therapeutic Radiology and Oncology Conference. Barcelona, Spain.

National

- Harriss-Phillips W.M., Bezak E., Yeoh K. (2011), *Observation of Hypoxia in HNSCC Xenografts during Fractionated Radiotherapy*. Oral presentation. Engineering and Physics Sciences in Medicine Conference. Darwin, Australia.
  - ***Awarded best Radiobiology proffered paper by Keynote speaker, Professor Wolfgang Dorr***

- Harriss-Phillips W.M., Bezak E., Yeoh K. (2011), *Simulations of Hypoxic HNSCC with Clinical Trial and New Radiotherapy Schedules using the HYP-RT model*. Oral presentation. Engineering and Physics Sciences in Medicine Conference. Darwin, Australia.

- Harriss W.M., Bezak E., Yeoh K. (2010), *Predicting individualised responses of hypoxic head and neck cancer to radiotherapy using Monte Carlo modelling.* Oral presentation. 3rd Modelling of Tumours "MOT" Meeting. Adelaide, Australia.

- Harriss W.M., Bezak E., Yeoh K. (2010), *Algorithm development and simulation outcomes for hypoxic head and neck cancer radiotherapy using a MC model: HYP-RT.* Oral presentation. Engineering and Physics Sciences in Medicine Conference. Melbourne, Australia.

- Harriss W.M., Bezak E., Yeoh K. (2009), *Computer and tumour xenograft modelling: dynamic hypoxia in head & neck radiotherapy*. Poster presentation. RANZCR, AIR, FRO, ACPSEM Combined Scientific Meeting. Brisbane, Australia.

- Harriss W.M., Bezak E., Yeoh K., Hermans M. (2009), *Computer and tumour xenograft modelling: dynamic hypoxia in head & neck radiotherapy*. Poster presentation. Engineering and Physics Sciences in Medicine Conference. Canberra, Australia.

- Harriss W.M., Bezak E., Yeoh K. (2008), *Monte Carlo modelling of head and neck cancer oxygenation.* Oral presentation. 2nd Modelling of Tumours "MOT" Meeting. Adelaide, Australia.

- Tuckwell W.M., Marcu L., Bezak E. (2006), *Individualising radiotherapy planning through Monte Carlo modelling of radiobiological principles for head and neck carcinoma*. Oral presentation. Engineering and Physics Sciences in Medicine Conference. Noosa, Australia.

- Tuckwell W.M., van Doorn T., Marcu L. (2005), *Temporal tumour modelling for individualised radiotherapy planning of head and neck cancer*. Oral presentation. Engineering and Physics Sciences in Medicine Conference. Noosa, Australia.

Other presentations

- Harriss W.M., Bezak E., Yeoh K. (2010), *Investigating the impact of reoxygenation in radiotherapy of hypoxic head and neck cancer using MC simulation and xenograft models*. Oral presentation. Royal Adelaide Hospital, *Medical Research Staff Prize Competition*. Adelaide, Australia.

- Harriss W.M., Bezak E., Yeoh K. (2010), *Predicting the responses of hypoxic head and neck cancer to radiotherapy using MC modelling.* Oral presentation (presented by E. Bezak). ACPSEM Queensland Branch Symposium. Brisbane, Australia.

- Harriss W.M., Marcu L., Bezak E. (2006), *Monte Carlo modelling of hypoxia and radiotherapy for head and neck cancer.* Oral presentation. University of Adelaide, Medical Physics and Biomedical Engineering *Postgraduate Student Paper Competition*. Adelaide, Australia.
  - Awarded first prize in the Medical Physics category

- Harriss W.M., van Doorn T., Marcu L. (2005), *Temporal tumour modelling for individualised radiotherapy planning of head and neck cancer*. Oral presentation. University of Adelaide, Medical Physics and Biomedical Engineering *Postgraduate Student Paper Competition*. Adelaide, Australia.
  - Awarded equal first prize in the Medical Physics category

- Harriss W.M., van Doorn T. (2004), *Increasing the efficiency of a temporal tumour growth model*. Oral presentation. University of Adelaide, Medical Physics and Biomedical Engineering Postgraduate Student Paper Competition. Adelaide, Australia.

For my family

Chapter 1

Introduction

1.1. Head and Neck Squamous Cell Carcinoma Overview

1.1.1. Disease Outline

Squamous Cell Carcinoma of the Head and Neck (HNSCC) describes malignant disease arising in the epithelial lining of the upper air and digestive organs and structures such as the oral cavity, larynx, tongue, pharynx, oesophagus and sinuses. HNSCC is often a rapidly growing and aggressive disease, presenting at an advanced stage and with metastatic (usually nodal) spread.

Cancers of the head and neck account for approximately 3% of all human malignancies with approximately 500,000 cases diagnosed world wide each year (Bourhis 2006). Approximately 90% of head and neck cancers are squamous cell carcinomas (Wong 1996), while the remainder are carcinomas which arise from glandular structures in the head and neck (adenocarcinomas, adenocystic tumours) and others cancers such as lymphomas and melanomas which arise from non-epithelial cells. HNSCC was the sixth most common form of cancer diagnosed in North America in both male and females in the nineteen nineties (Vokes 1993).

Despite aggressive treatment strategies such as radiotherapy targeting the primary tumour site, local recurrence is a common pattern of treatment failure of HNSCC. The high local recurrence rates after treatment have been attributed to the effects of accelerated tumour proliferation and the low cellular oxygenation levels (tumour hypoxia) which increases the resistance of the tumour cells to ionising radiation.

1.1.2. Tumour Hypoxia

Hypoxia arises in tissue due to inadequate delivery of oxygen through the vascular system to the cells in the tissue. The proportion of tumours exhibiting hypoxia is estimated to be 50%, although the percentage of hypoxic cells within a tumour has been reported to vary from 1% to 100% (Nordsmark 2005). Head and neck cancers in particular commonly exhibit tumour hypoxia, with approximately 70% of locally advanced tumours presenting with hypoxic tumour sub-regions based on the use of a set oxygenation threshold to define hypoxia, e.g. a partial pressure of oxygen (pO_2) threshold of 2.5 or 5.0 mm Hg (Becker 1998, Rischin 2006).

It has been long established that tumour hypoxia is a factor contributing towards the resistance of many types of tumours including HNSCC to radiotherapy, having a significant adverse effect on patient outcome (Nordsmark 2005, Nordsmark 1996). Analysis of randomised clinical trial data with patients separated into low and high oxygenation groups has shown that the difference in the time to recurrence and patient death rate can be up to 30% and 10% respectively in the two groups after 5 years (Adam 1999, Nordsmark 2005).

The term commonly used to quantitatively describe the impact of oxygenation on radiation induced cell death is the Oxygen Enhancement Ratio (OER). OER is usually described as a function of pO_2 and describes the increase in radiosensitivity of cells with increasing oxygenation, with anoxic cells (no oxygen) having the lowest OER value of 1.0 and fully oxygenated cells having a high OER value of 2.5 to 3.0 (Alper 1979).

The number of active tumour cells usually decreases during fractionated radiotherapy as the tumour regresses, reducing the demand for oxygen. Therefore, an initially hypoxic tumour may become more oxygenated during the course of treatment. The process of gradual increase of oxygenation levels during treatment has been named reoxygenation, which has the potential to increase overall tumour control probability (TCP) as tumour cells become re-sensitised to ionising radiation. However, it is usually

challenging to predict and measure oxygenation levels in human tumours before and during treatment because of the measurement process logistics and the dynamic nature of tumour hypoxia, which makes the impact of hypoxia on treatment outcome difficult to quantify.

1.1.3. Treatment of Head and Neck Squamous Cell Carcinoma

1.1.3.1. Treatment Modalities and Strategies

Surgery, radiotherapy and chemotherapy may be used alone or in combination to control HNSCC, however radiotherapy is the most common form of treatment. Approximately 50% of head and neck tumour patients receive radiotherapy alone, and the other 50% receive combinations of radiotherapy, chemotherapy and surgery in an attempt to cure their disease (radical treatment intent), failing which palliation may be sought. The goal of curative radiotherapy is to deliver a high dose to the tumour mass to kill all tumour cells that have the potential to grow back the tumour, while sparing the surrounding normal tissues to minimise treatment side effects.

The conventional radiotherapy treatment schedules used to treat HNSCC involves one 2 Gy fraction delivered 5 days per week, with a total prescription dose in the range of 60 to 80 Gy (Fu 2000, Horiot 1997). A consequence of increasing the total dose and/or dose per fraction to improve TCP is to increase normal tissue reactions above tolerance levels. Common normal tissue reactions during HNSCC radiation treatments include mucositis and inflammation of the epithelial lining which may lead to difficulty in swallowing, hoarseness, dryness of the mouth, and weight loss. Consequences of treatment breaks to allow a patient to recover from acute (early) reactions can be detrimental for rapidly growing tumours such as HNSCC because of the phenomenon of accelerated repopulation, discussed below.

Carcinomas can exhibit more rapid cell growth as a response to the cell damage incurred during treatment. The mechanisms responsible for this rapid growth, named Accelerated Repopulation (AR), include shortening of the cell cycle, recruitment of

non-cycling (quiescent G0 phase) cells back into the cell cycle and the loss of asymmetric stem cell division. Stem cells usually divide into one stem cell and one more differentiated cell, but as division asymmetry is lost there is a higher chance of a stem cell diving into two stem cells. This mechanism has been reported to be primarily responsible for the near exponential tumour growth rates observed in HNSCC induced after the beginning of treatment (Fowler 1991, Marcu 2004, Withers 1988).

When applying the linear quadratic (LQ) theory of cell survival, HNSCCs have a high average alpha beta ratio (α/β) because of their initial fast response to treatment and the effects of accelerated repopulation. As such, the total time of treatment rather than fraction size is the critical factor in achieving a high TCP for these tumours. The importance of overall treatment time on outcome has been reported in multiple retrospective clinical trial studies (Peters 1997, Withers 1995, Withers 1988, Fowler 1991).

Acceleration of radiation schedules to shorten the overall treatment time can help to minimise the effects of AR. However, acceleration of treatment is limited by normal tissue tolerances for the organs and structures surrounding the planning target volume (PTV) in radiotherapy treatment plan. Consequently, treatment schedules should be designed to minimise overall time (and maximise total dose) without increasing normal tissue reactions above acceptable levels. This may be achieved using a schedule with two or three dose fractions per day instead of the standard single fraction; however the dose per fraction must be reduced.

Optimising the fractionation schedule for each patient in terms of the dose per fraction, days per week of treatment and the total dose to minimise normal tissue effects and achieve a high TCP remains one of the fundamental challenges in head and neck radiotherapy. The potential to improve outcome by tailoring the radiation schedule to the properties of each tumour has already been discussed in a number of clinical trial reports (Horiot 1994, Nordsmark 2005, Rischin 2006), and will be the focus of the modelling results presented in this report.

1.1.3.2. Current Radiotherapy Prognosis

The average 5 year survival rate for patients diagnosed with head and neck cancer is approximately 50%, which has not changed significantly over the past two decades (Reid 2000, Wong 1996). Currently, when treated with radiation as the sole treatment modality, tumour local control rates are approximately 80% for early stage disease, but fall to well below 50% for locally advanced tumours (Dinshaw 2006, Fu 2000, Nordsmark 2004, Rosenthal 2004).

Efforts to improve HNSCC treatment outcomes through dose and fractionation modifications have been made in recent decades, however the average prognosis has not improved significantly (Dinshaw 2006, Koukourakis 2006, Stadler 1998). Possible causes for the lack of improvement in average tumour local control (LC) rates include the failure of current treatment strategies to take into account the variations in individual tumour properties such as oxygenation, the timing of reoxygenation and the rate of accelerated repopulation during radiotherapy.

It has been shown in clinical trials that some types of cancer, including head and neck cancer, have improved TCP when treated with hyper-fractionated and/or accelerated radiotherapy schedules for certain patient groups (Fu 2000, Nordsmark 2005). However, in view of the logistics of delivering more than one treatment fraction per day with at least six hours between fractions to allow for normal tissue repair, it is still common practice to use the conventional 2 Gy per day, 5 day per week radiotherapy.

1.2. Radiotherapy Response Prediction using Computer Modelling

1.2.1. The Need for Computer Models

Modern treatment delivery methods for external beam radiotherapy employ techniques such as intensity modulated radiation therapy (IMRT) and image guided radiation therapy (IGRT) to deliver high radiation doses to the tumour planning target volume (PTV) or multiple PTV's with ever increasing accuracy and precision. However, to greatly improve outcomes for individual patients will be necessary to explore in more detail the radiobiological processes that occur in human tumours and to predict optimal treatment plans for the individual patient.

Radiation Oncologists may be able to benefit from computer models which enable optimal radiation dose prescriptions to be predicted based on the procedures. A computer model could potentially be used to predict the time at which it is necessary to re-assess tumour size and oxygenation during a course of fractionated radiotherapy, so that re-planning and scheduling can be performed to optimise outcome.

There is considerable published evidence supporting the value of computer modelling concentrating on oxygen distributions within a tumour (Dasu 2005, Dionysiou 2004, Duchting 1985, Harting 2007). Previous work modelling accelerated repopulation in tumours has shown the large impact of the timing and degree of this phenomenon on treatment outcome (Marcu 2004, Trott 1991). The wide variations in tumour properties in the patient population for HNSCC such as repopulation rate, oxygenation level and reoxygenation onset time (between patient and within regions of each individual tumour) provide rationale for the development of computer models that can simulate the response of a tumour at the cellular level throughout the course of radiotherapy.

The process of tailoring the radiation plan to the radiobiological response of a specific tumour is referred to as the "individualisation" of treatment planning. Challenges that lie ahead involve not only obtaining the required individual patient data (before and

during treatment) but also in devising the best methods and models in which the information can be used to optimise treatment.

1.2.2. The Use of Computer Models for Predicting Radiotherapy Outcome

Computer models (*in silico* models) are an efficient way to complement the results from radiotherapy clinical trials, by predicting the effects of individual tumour properties on treatment outcome during conventional and altered fractionated radiation schedules. Models not only allow patient specific biological data consideration, but can also incorporate temporal changes in parameter values and ranges to more accurately reflect the dynamic biological processes within the tumour during treatment, compared to more static mathematical (equation based) models.

Many of the computer models developed in the previous and current decade have been developed with patient individualisation in mind (an overview of models reported upon will be presented in chapter 3). This has been in-line with the advancements in imaging modalities such as 4D computer tomography (CT) and cone beam CT, as well as biological imaging such as positron emission tomography (PET) with markers such as F^{18}-Misonodazole for imaging hypoxia. These imaging modalities have the potential to reveal individual tumour (intra-tumour temporal and spatial characterisation) information to be used in computer models.

1.2.2.1. The Monte Carlo Modelling Technique

Individualisation of treatment and the use of cell based stochastic computer models are becoming more sought after with the increase in capability of off-the-shelf computer systems, making the development and implementation of sophisticated models more accessible.

Monte Carlo methodology involves the use of random number generation and probability distributions for decision making within the algorithm (stochastic

modelling). Monte Carlo methods of modelling tumour growth and the effect of radiation on a cell population are particularly advantageous for modelling the statistical nature of the biological and radiobiological mechanisms involved, such as the distribution of cell kinetic values, the range in oxygen levels among the tumours cells and the fate of a tumour cell if targeted with radiation.

When considering tumour hypoxia, computer models are particularly advantageous because of the wide distribution of oxygenation levels among the cells within a single tumour. Monte Carlo modelling allows the entire range of oxygen levels (oxygenation histogram) to be used in assigning cellular oxygen levels to the cell population in terms. The cellular oxygen levels may be allocated to cells using oxygen probability distributions (pO_2 histograms) or by the modelling of blood vessel networks. Computer models can further incorporate temporal changes to parameters, making it possible to model changes in cellular oxygenation throughout treatment. Currently, radiobiological Monte Carlo models are still under investigation and are not available commercially for clinical implementation.

1.3. Aims of the Current Study

As the beneficial effect of inter-fraction reoxygenation and the detrimental effect of accelerated repopulation greatly influence cell kill efficiency, there is great potential to exploit these two phenomena if individual tumour information collection can be performed and treatment planning performed based on radiobiological computer models of tumour response.

The aim this work is to develop a tumour growth and radiotherapy computer model to simulate and predict tumour control outcomes after fractionated treatment, taking into account the effects of reoxygenation and accelerated repopulation in oxic and hypoxic head and neck tumours. The aims for the development of the tumour growth algorithm are to propagate a virtual oxic or hypoxic tumour on a cell by cell basis, starting from a

single epithelial stem cell, up to a tumour comprised of 10^8 cells with a realistic proliferative hierarchy.

The radiotherapy effect algorithm aims to simulate fractionated radiotherapy based on conventional strategies as well as altered clinical trial and new fractionation schedules and quantify the impact of reoxygenation and accelerated repopulation on the total dose required to achieve total cell kill and hence tumour control. The model will enable a virtual tumour to be grown much faster than any *in vivo* tumour system and provide quantitative results on the cellular level in terms of the rate of cell kill at any time point during radiotherapy and the relative effects of the mechanisms and parameters values modelled.

Ultimately, the model would be researched and verified to the extent that it would be ready for making predictions to assist radiation oncology clinicians and medical physicists to design individualised radiotherapy treatment schedules, however clinical implementation will not form part of the current work presented in this report.

A summary of the research aims are presented below:

- To develop a temporal tumour growth model algorithm using cellular properties including cell cycle time, cell type and oxygenation level, to propagate a virtual hypoxic tumour comprised of individual head and neck squamous cell carcinoma cells.

- To develop a radiation effect model algorithm to simulate the fractionated radiotherapy treatment of a virtual tumour, incorporating the effects of accelerated repopulation and reoxygenation of hypoxic tumours.

- To develop the model to be intuitive and simple to use, with the flexibility to allow for algorithm extension as new radiobiological developments and experimental data are reported in the future.

- To incorporate Monte Carlo methods in the model to allow the random nature of cellular biology and radiobiology to be simulated when allocating cellular properties and division characteristics and when modelling radiation induced effects such as cell death probability and tumour reoxygenation.

- To allow for the analysis of the number of individual tumours cells throughout tumour evolution and to further analyse the changes in the percentages of different cells types present in the tumour and their changing oxygenation levels.

- To perform experimental work in an animal model to quantify the level of oxygen increase and the timing of reoxygenation onset during fractionated radiotherapy.

- To analyse the parameter values necessary in modelling the mechanisms of accelerated repopulation and reoxygenation and to quantify the differences in the total dose required to achieve tumour control for well oxygenation versus hypoxic tumours, and the effects of accelerated repopulation and reoxygenation on tumour cell kill.

- To model a selection of randomised clinical trial radiation schedules for comparison of model outcomes with published data, and to apply the model to the simulation of new treatment schedules tumours with various oxygenation levels and accelerated repopulation and reoxygenation onset times to predict any potential benefits of the new versus the existing schedules.

1.4. Thesis Outline

Chapter 2 begins with an overview of head and neck cancer biology and radiobiology including human head and neck anatomy, epithelial cell biology and HNSCC progression, and continues with an introduction to radiobiological theories such as the

oxygen effect, the phenomenon of accelerated repopulation and fractionation effects in radiotherapy.

Chapter 3 forms a review of the past and current tumour model literature, with an emphasis on models incorporating tumour hypoxia. Deterministic as well as stochastic Monte Carlo models and their progression throughout the past 60 years are outlined, with a focus on the more recent Monte Carlo models.

Chapters 4 and 5 present the results and discussion from the development of the current Monte Carlo model (*HYP-RT*). The tumour growth algorithm involving individual cell division and data storage will be outlined, with results presented on the computational efficiency and the model parameter values used. This is followed by an outline of the radiotherapy effect algorithm, discussing the key features of tumour reoxygenation and accelerated repopulation.

Experimental results are presented from animal work using a human FaDu cell line to propagate HNSCC tumour xenografts in a mouse model. The aims of this work were to explore the timing and degree of reoxygenation of tumours *in vivo*, during an accelerated course of radiotherapy. The computer modelling results in these two chapters focus on the effects of repopulation and reoxygenation on the number of conventional fractions (2 Gy) required to kill all tumour cells that have the potential to grow back the tumour, which are compared with LQ therapy and clinical data.

Following the use of the model to simulate conventional radiotherapy, Chapter 6 reports upon the simulation of altered fractionation schedules that were reported to provided a benefit in clinical trials by increasing the therapeutic ratio. Modelling results show the predicted potential benefits of different clinical trial schedules when different combinations of tumour oxygenation, accelerated repopulation onset time and reoxygenation onset time are simulated.

The total doses required to achieve tumour control in the model are compared to clinical trial dose prescriptions and local control rates reported at 2 to 5 years after radiotherapy. A biological effective dose analysis is also reported on where the doses to acute and late reacting normal tissues has been estimated to provide a basis whereby

schedules may be ranked, considering that at all schedules were simulated until 100% TCP had been achieved.

Chapter 7 extends the simulation work and reports on new fractionation schedule simulation outcomes, where the new schedules were designed in an attempt to improve the therapeutic ratio compared to existing clinical schedules. A biological effective dose analysis was also conducted for the new schedules.

Chapter 8 concludes the report with a summary of the modelling techniques used, the key findings obtained during development and use of the tumour growth and radiotherapy effect algorithms and plans for extending the model in the future.

Chapter 2

An Overview of Head and Neck Cancer Radiobiology

2.1. Biology of Head and Neck Squamous Cell Carcinoma

2.1.1. Head and Neck Anatomy

The head and neck form one of the most complex anatomical regions of the human body. It is responsible for many functions that are critical for survival and quality of life, including breathing, digestion, speech, smell and taste. A cross sectional diagram (Figure 2.1) illustrates some of the sites constituting the human head and neck region. Sites that are commonly involved with HNSCC include the larynx, oral cavity, oropharynx, nasopharynx, hypopharynx and upper oesophagus, with disease of the oral cavity and oropharynx having the worst prognosis (Dinshaw 2006).

Figure 2.1. A cross sectional illustration of the human head and neck region displaying many of the constituent sites affected by squamous cell carcinoma (www.macmillan.org.uk).

The various sites constituting the head and neck region are lined by epithelial cell layers. The squamous cells which line the epithelial layers are more flat and elongated in shape

compared to the more cube like shape of basal cells, and are located in the superficial strata (Figure 2.2). The shape of the squamous cells assists in making the tissue resistant to fluid leakage beyond the epithelial layers, while other epithelial cells perform roles such as the secretion of mucous and saliva.

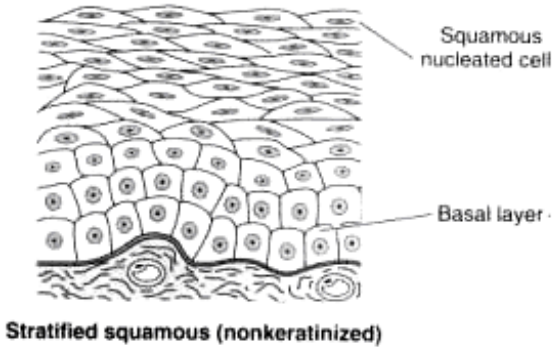

Figure 2.2. Epithelial non-keratinised stratified squamous cell structure (Henrikson 1997).

The squamous cells of the epithelial lining are regularly replaced by a small population of dividing stem (clonogenic) and transit (limited generation) cells in the basal layers (Aarnaes 1993, Wright 1984). As the superficial layers of the lining are reached, cells become more differentiated and specific in terms of their function and protein generation (e.g. keratin).

Epithelial cell layers can be highly differentiated with a very small proportion of stem cells or less differentiated, depending on the role of the tissue. Epithelial tissue of the internal head and neck structures are often described as ortho-keratinising or non-keratinising; unlike skin epithelium which are described as keratinising because cells differentiate rapidly and form thick keratin layers (Figure 2.3).

2.1.2. Head and Neck Squamous Cell Carcinoma Biology

Patients with head neck cancer often present with hoarseness, throat pain, tongue ulcers, or a painless neck lump (Mehanna 2010). Current evidence does not support the benefits (earlier diagnosis) of screening of the general population through visual examination or other routine methods (Mehanna 2010). However, as imaging modality accuracy and

precision increase with advancements in technology, earlier diagnosis and improvements in patient prognosis may be possible.

2.1.2.1. Carcinogenesis of HNSCC

Squamous cell carcinoma (SCC) is a malignant disease resulting from the deregulation and rapid proliferation of cells in the epithelial lining layers. The theory of epithelial homeostasis implies that cell production in the deeper layers of the epithelium is normally well balanced by loss of cells from superficial layers. However, in the case of SCC cell propagation significantly outweighs cell loss, through processes such as apoptosis and sloughing of the superficial layers at the surface. SCC can be classified by degree of differentiation (well or poorly differentiating) corresponding to the histological appearance of samples obtained from biopsies.

Factors such as smoking and alcohol affect the incidence and prognosis of HNSCC (Becker 2000, Mehanna 2010). Environmental factors including exposure to wood and cement dusts and increasingly in the developed world the human papilloma virus, have been identified as increasing the risk of developing HNSCC. Although the exact reasons for the initiation of cell to a malignant phenotype in many cancers including HNSCC are unknown.

The progression of the disease from a non-malignant phenotype (with regulated cell propagation) to a malignant phenotype is thought to be the result of a single successful malignant (stem) cell phenotype (existing in a field of pre-malignant stem cells), and the consequent propagation of a colony of cells. As the colony of cells grow to form a clinically dateable tumour, they may gain further deoxyribonucleic acid (DNA) mutations, and produce abnormal quantities of proteins promoting further growth and decreased differentiation. A schematic illustration of the pathogenesis and progression of HNSCC is shown in Figure 2.3.

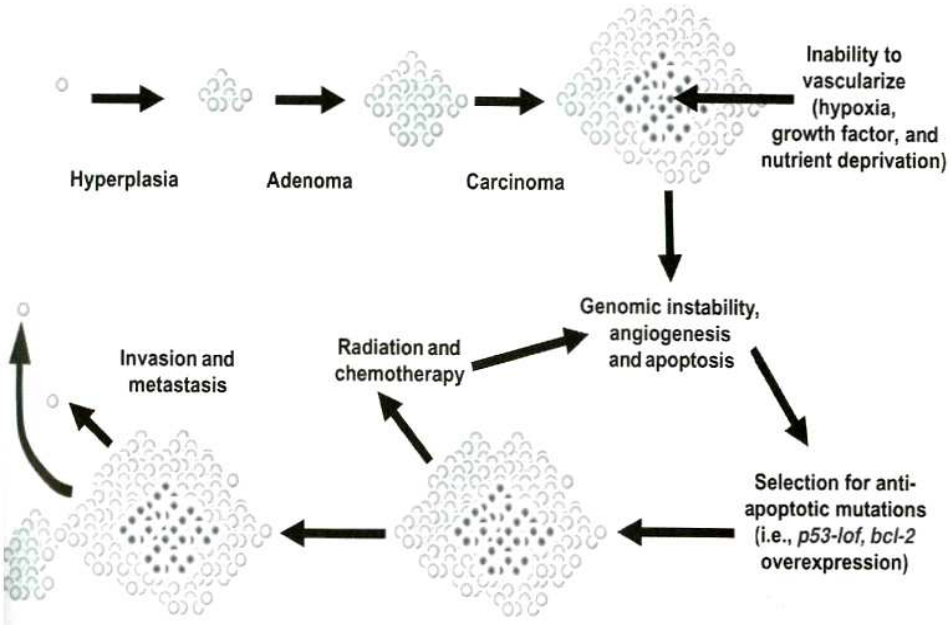

Figure 2.3. Carcinogenesis of carcinomas from a single mutated cell to a malignant and invasive tumour (Le 2004, Hall 2006).

Gene expression studies have shown that bio-markers related to carcinogenesis are also important in predicting treatment prognosis. These bio-markers include epidermal growth factor receptor (EGFR) expression, cyclin-D1 or cyclin-E expression, serum soluble IL-2 receptor concentrations and loss of chromosome arm 18q. HNSCC has been linked to gene mutations and/or altered changed protein levels in hundreds of different genes including TP53, VEGF, CDNKA(p16), KRT4, KRT5, and DAP-kinase (Lallemant 2010, Villaret 2000, Wang 2000).

2.1.2.2. Tumour Hypoxia in HNSCC

Normal tissue oxygenation levels in non-diseased tissue are commonly in the range of 20 to 100 mm Hg, with an average of 40 mm Hg in the head and neck region (Adam 1999). Tumours often have significantly reduced pO_2 levels in the range of 0 to 10 mm Hg for head and neck cancers and involved lymph nodes (Lartigau 1998, Adam 1999).

A tumour mass generally grows in an exponential fashion up to 1 to 2 mm in diameter, limited by oxygenation and nutrient diffusion distances from surrounding tissue (Conti 2002). Restricted tumour growth may continue, although the process of angiogenesis (neovascularisation) is soon required to overcome oxygen deficiency and allow the

tumour mass to be sustained and grow beyond approximately 1 cm in diameter (McElwain 1979).

The reduced pO_2 levels of the tumour tissue occurs because of the high metabolism and therefore oxygen consumption rate of tumour cells relative to normal tissue as well as the irregular nature of the tumour vascularature (Ljungkvist 2002). Vessels often grow in a chaotic manor, forming networks which do not supply oxygen evenly to all regions of the tumour. The vessels may be spaced too far apart, dilated or improperly formed and exhibit faults such as vessel shunts, blind ends and leaks (Vaupel 2004).

The link between hypoxia and induced angiogenesis has been verified experimentally in a study involving the hypoxia inducible factor (HIF-1) protein and the vascular endothelial growth factor (VEGF) gene, which was proven to be a HIF-1 regulated in the mid 1990's (Forsythe 1996). The process of angiogenesis is thought to be initiated once the oxygen diffusion limit for the tissue (100 to 200 µm) has been reached, but may also depend on the oxygen consumption rate and the types of cells involved (Gray 1953, Tannock 1972).

Regions of tissue experiencing short terms reductions in oxygen supply are defined as acutely or temporarily hypoxic. The more permanent form of hypoxia is called chronic hypoxia, affecting cells that are beyond the diffusion limit of a functioning blood vessel (Figure 2.4). Both forms of hypoxia can occur anywhere within the tumour mass; however large regions of chronic hypoxia (and necrosis) are more likely to form near the centre of large tumours.

Both forms of hypoxia are not only important when considering the treatment of HNSCC, but also because they have been linked to malignant cell progression and the increased metastatic potential of hypoxic tumours (Hill 1990).

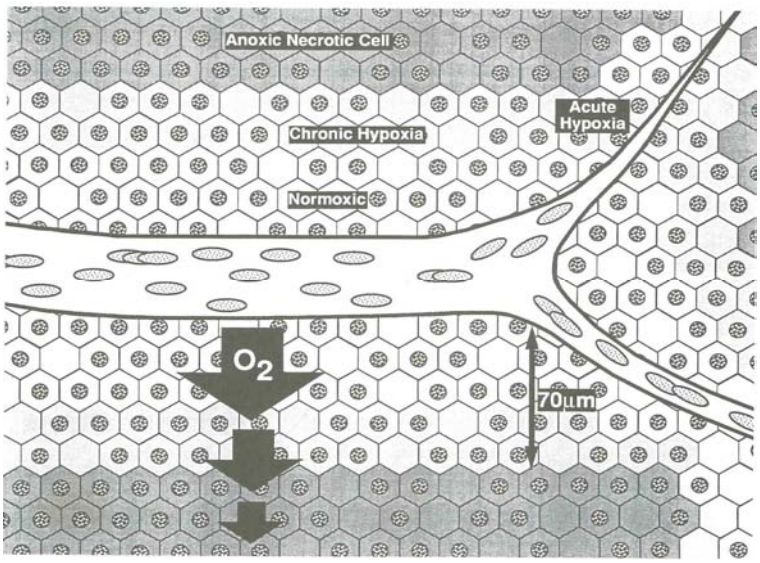

Figure 2.4. Development of hypoxia in tissue, comparing chronic hypoxia which arises due to limited oxygen diffusion, with acute hypoxia arising from temporarily non-functioning blood vessels (Brown 1990, Hall 2006).

Tumour cells with pO_2 levels lower than the normal level for their tissue type can experience delayed cell cycle progression due to extension of the G2 and mitotic phases of the cell cycle (Webster 1998). When experiencing extremely low oxygen conditions less than approximately 1 mm Hg cells may be arrested in the G0 quiescent phase (Amellem 1991, Douglas 2005, Royds 1998) and survive in this state for a number of days (Durand 1998, Ljungkvist 2005).

The low oxygenation threshold for inducing cell quiescence emphasises the high proportion of tumour cells have low to mid-ranged oxygenation (pO_2 between 1 and 10 mm Hg) and consequently the ability to proliferate while having increased radioresistance.

Traditional techniques for assessing the oxygenation levels of tumours include the polarographic micro-electrode technique, where redox reactions at the electrode tip produce a current proportional to the local oxygen concentration. The Eppendorf electrode device employs a similar method to produce a histogram of oxygen values within tissue. Other techniques include the use of a fibre optic probe (OxyLab, *Oxford Scientific* Ltd.), positron emission tomography (PET) (using biological markers such as misonidazole (MISO), nitroimidazole-pentafluoropropyl acetamide (EF5), azomycin

arabinoside (FAZA) and radioactive isotopes such as F^{18}, Cu^{60} and Cu^{62}), electron paramagnetic resonance (EPR) imaging and immunohistochemical fluorescence imaging using biological markers such as *Pimonidazole*.

Depending on the technique used, cellular or tissue oxygenation may be reported in different ways, such as the percentage of hypoxic cells (with pO_2 less than a set threshold e.g. 5.0 mm Hg), the relative area of hypoxic cell immunohistochemical staining in a tumour cross section (usually pO_2 < 10 mm Hg), the pO_2 distribution (histograms from Eppendorf probe studies), or the relative uptake of radioactive tracers (PET imaging). Tumour hypoxia and reoxygenation measurements using the fibre-optic probe technique on HNSCC xenografts will be discussed in more detail in Chapter 4.

The percentages of tumour cells with pO_2 levels below 2.5, 5.0 and 10.0 mm Hg from a selection of HNSCC Eppendorf studies are displayed in Figure 2.5. These studies have either reported the median or mean values for the pO_2 percentages; however the data ranges reported in each study were relatively large. For example, the study by Nordsmark and group involving patients from seven different radiotherapy centres reported the tumour cell hypoxic percentages ($HP_{mm\ Hg}$) to range from 0% to 97% and 0% to 100% for $HP_{2.5}$ and $HP_{5.0}$ respectively.

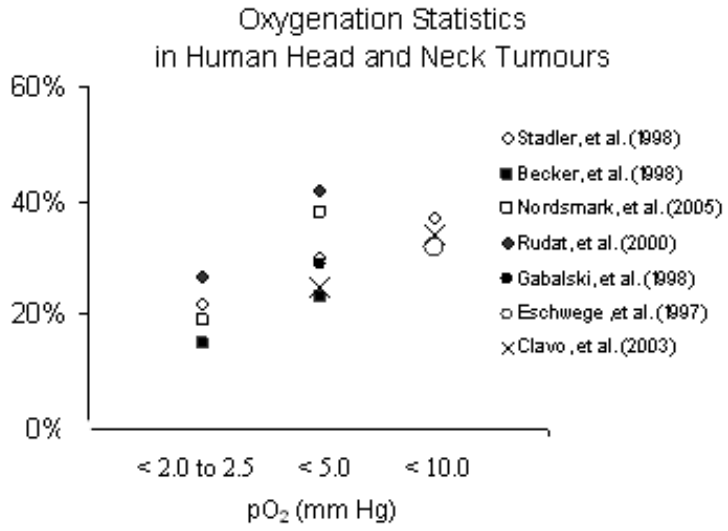

Figure 2.5. Human in vivo Eppendorf tumour oxygenation (pO_2) measurement data from HNSCC patients prior to radiotherapy (adapted from pO_2 data reported from the references provided in the legend).

2.2. Tumour Radiobiology Overview

2.2.1. Introduction

2.2.1.1. Radiation Induced Cell Death

The x-ray beams utilised for conventional radiotherapy treatments are generated by linear accelerators (linacs). Linacs initially accelerate electron beams up to a nominated energy commonly in the range of 4 to 25 MeV. When x-ray generation is required the accelerated electrons undergo Bremsstrahlung interactions inside the high density target within the head of the linac which produces the x-ray beam used for treatment. The x-ray beam contains photons within a spectrum of energies, with the maximum energy approximately equal to the initial electron beam energy and the mean energy equal to one third of the initial electron beam energy. Common nominal beam energies describing clinical x-ray beams from linacs are 4, 6, 10 and 18 MV.

The dominant process for the interaction of high energy photons in water, and other tissue equivalent materials, is the Compton Effect. Compton interactions involve the transfer of energy from a photon to an outer shell atomic electron. The increase in energy allows the electrons to leave the atom with sufficient kinetic energy to overcome the Coulomb forces previously binding it to the atom. After the photon has transferred part of its energy to the electron it is scattered at an angle dependent on its initial angle and the energy transferred.

The released Compton electron may interact directly within a cell and produce damage such as DNA strand breaks or be involved in chemical reactions that produce free radical species in the cell. Oxidising free radicals are particularly potent because they have an unpaired valence electron making them highly likely to interact and damage nearby molecules, including DNA. The method of free radical induced DNA damage is often called an indirect or two-step radiation induced damage process.

DNA strand breaks are currently understood to be the key mechanism of radiation induced cell death, with the accumulation of double strand breaks, i.e. damage to both sides of the DNA double helix, considered to be the trigger for inducing cellular apoptosis (Steel 2002). Approximately 40 double strand breaks, 1000 single strand breaks and 1000 base pair damage events are caused per 1 Gy of ionising radiation (Ward 1994, Steel 2002). After receiving a 2 Gy dose of ionising radiation most cell types in the human body will approximately halve in quantity, with the surviving fraction of cells known as the SF_2. Thus, the SF_2 for most types of cells is approximately 0.5, however this value can vary greatly for cells from different individuals, for healthy versus tumour cells and for *in vitro* cell lines because of the altered environmental conditions (Steel 2002, Bjork-Eriksson 2000).

Poisson theory provided the first mathematical model aiming to explain the random nature of radiation induced cell kill, with tumour control probability (P_n) expressed as a function of the expected number surviving number of clonogenic (colony forming) tumour cells, a, and the actual number of surviving cells, n (Equation 2.1). P_n is equivalent to *TCP* for the case of n equal to zero (Equation 2.2).

$$P_n = \frac{a^n e^{-a}}{n!} \tag{2.1}$$

$$TCP = P_0 = e^{-a} \tag{2.2}$$

This work led to the development of theories such as multi-target single hit theory and the linear quadratic (LQ) model of cell survival (Equation 2.3). This enabled the calculation of TCP for a course of fractionated radiotherapy to be calculated in terms of an exponential dose response (Equations 2.4 and 2.5), where *SF* is the surviving fraction of cells, N_0 is the original number of cells, N is the final number of cells, D is the total dose, d is the dose per fraction and α and β are tissue specific terms of the LQ model.

$$\frac{N_0}{N} = SF = e^{-\alpha D - \beta d D} \tag{2.3}$$

$$TCP = e^{-N_0 SF} \tag{2.4}$$

$$TCP = e^{-N_0 e^{-\alpha D - \beta d D}} \tag{2.5}$$

The LQ model was developed assuming that DNA strand breaks are the source of lethal radiation induced cell damage, where single strand breaks are linearly dependent on dose and double strand breaks occur due to simultaneous single strand breaks on opposing DNA base pairs which are dependent on the square of the dose. The α and β terms in the model represent the probability of these two cell damage mechanisms.

2.2.1.2. Relative Biological Effectiveness

The Relative Biological Effectiveness (RBE) of a radiation beam describes the relative efficiency of cell kill for different radiation beams compared to mono-energetic 250 KVp x-rays. The different beam modalities deposit energy at different rates in tissue, known as the Linear Energy Transfer (LET) which quantifies the energy transferred to the medium per unit path length (2 KeV/µm for 250 KVp x-ray beams). Standard radiotherapy treatment beams produced by linear accelerators (electron and x-ray beams) have low LET values and RBE values of 1, while neutron, alpha, and other heavy ion beams are classed as high LET radiation and have RBE values of 5 to 20 (ICRP 2007). Consequently, high LET radiation beams require less total dose to achieve a high TCP compared to low LET radiation beams.

High LET radiation beams have optimal damage efficiency when the rate of energy deposition corresponds spatially to the distance between the two strands of the DNA double helix (approximately 20 Angstroms or 2 nm) (Hall 2006). This energy deposition distance occurs at approximately 100 KeV per µm in most tissue types (Hall 2006, Barendsen 1968). The increase in cell kill efficiency per unit radiation dose occurs because of the high likelihood of causing direct double stand breaks. This direct damage is less dependent on tissue oxygenation or the creation of free radicals, which will be discussed in the next section. Despite the benefits of high LET radiation beams,

treatment is difficult to implement clinically because of the expense of installation and running the necessary equipment.

In the current work low LET x-ray irradiation has been modelled. Consequently, consideration of tumour oxygenation is relevant because of the significant impact on cellular radiosensitivity and the treatment of hypoxic tumours.

2.2.1.3. The 5 R's of Radiobiology

The discipline of radiobiology has been of interest to physicists, biologists and clinicians since the discovery of x-rays and their potential for biological imaging and control of disease in the late nineteenth and early twentieth century. In the last few decades the topics of interest to radiation oncology radiobiologists have been broken down into the *5 R's of Radiobiology*. This decade some radiobiologists have extended the list of key topics to include effects such as the *Recovery* of the tissue and *Remote* cell kill (bystander effects). The sections below are an overview of these topics; with detailed information regarding *Reoxygenation* and *Repopulation* because they are most relevant to the model described in this report.

2.2.1.3.1. Repair

DNA repair is carried out in the hours proceeding radiation exposure, with an average half life of 1 hour and with the majority of all DNA damage repaired within 4 to 6 hours (Núñez 1995). Repair rates depend on variables such as the cell type involved, the proliferative status of the cell, the immune system of the patient and the degree of damage that the cell received. Fractionation of treatment is not desirable for optimising TCP; however fractionation is often necessity to allow for the repair of normal tissues and to keep normal tissue complication probability (NTCP) within the acceptable limits.

The term *repair* is very general. When considering tumour cells, the DNA and the genetic make up of the cells are not normal and therefore repair is difficult to define. Cells may attempt to repair DNA damage using the opposing side of the DNA double helix as a

template; however this process may be performed incorrectly. When both sides of the double helix at the same point in the DNA are damaged repair is more difficult.

Incorrect DNA repair may be sufficient and allow the cell to continue to function and divide, however the cell is left genetically altered/mutated. Mechanisms of incorrect repair include chromosome cross linking, chromosome breakage (increasing the total number of chromosomes) and incorrect base pair repair. For tumour cells which are the target in radiotherapy, incorrect repair is not important, however for normal tissues exposed to the primary beam or to secondary scattered radiation, incorrect repair can lead to the development of secondary cancers.

2.2.1.3.2. Radiosensitivity

The sensitivity of cells to ionising radiation is a term used to define the level of dose required to kill the cells involved and stop clonogenic proliferation of the population. The SF_2 value of a cell line is a common term used to define cellular radiosensitivity. However, *in vivo* and *in vitro* SF_2 values may differ because of variable cellular environmental conditions, and so data should be considered carefully. Radiosensitivity of cells in a tumour depend on many factors during and within hours of irradiation, including the phase of the cell cycle, the local oxygenation of the tissue, the inherent repair mechanism efficiency of the DNA, and the cell proliferation rate.

2.2.1.3.3. Redistribution /Reassortment

The cell cycle can be separated into four main phases: the mitotic (M) phase, the G1 and G2 gaps phases and the synthesis (S) phase (Figure 2.6). The redistribution effect occurs due to the preferential killing of cells in the more radiosensitive phases of the cell cycle. Experiments designed to determine the radiosensitivity of the different cell cycle phases were first made on Chinese hamster cells (Sinclair 1965) with results showing that the M phase is more radiosensitive than the G1 and G2 gap phases and that the S phase is the most radioresistant phase.

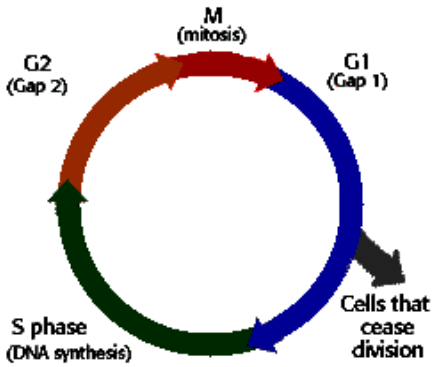

Figure 2.6. The four main phases of the cell cycle starting with the first gap phase (G1), followed by the DNA synthesis phase (S), the second gap phase (G2), and with completion in the Mitosis phase (M).

For a population of cells cycling at random through the cell cycle, a dose of radiation will leave a greater proportion of cells in the S phase. This creates an accumulation of cells in the S and then the G2 and M phases in the hours following the irradiation, i.e. temporary cell synchronisation.

If cells are left to cycle for number of generations (a few days) the accumulation of cells in a single phase will reduce as *redistribution* through the cell cycle occurs for the cell population. However, if subsequent dose of radiation is given a short time after the first dose (approximately half the average cell cycle time), many cells will be in the M phase and more efficient cell kill will occur. Due to the natural random distribution of cells about the cell cycle and the rate of redistribution after a dose of radiation, this effect is very difficult to take advantage of during radiotherapy.

2.2.1.3.4. Repopulation

Repopulation of normal (healthy) cells is important for minimising normal tissue complication probability (NCTP), while the repopulation of tumour cells can compromise TCP. Cells that have proliferative capacity and are able to propagate a tumour cell colony of more than 50 cells are classed as clonogenic. If any tumorous or healthy clonogenic cells survive a dose of radiation there is a probability that repopulation may occur.

In theory, a single tumour cell has the potential to re-grow the tumour if it survives irradiation. Survival may be because of the absence of direct DNA damage or due to effective DNA repair. The rate of cell proliferation after irradiation may increase to compensate for the damage to the cell population, a phenomenon commonly named *accelerated repopulation.*

2.2.1.3.5. Reoxygenation

The presence of oxygen in a cell assists in fixing-in radiation induced DNA damage, making the damage more permanent. Low oxygenation levels (tumour hypoxia) therefore results in reduced cell repair along with reduced free radical production, and consequently an increased resistance to standard linac radiotherapy treatment.

The detrimental effects of low oxygenation can be partially reversed as the tumour shrinks during treatment and has increased access to oxygen. This process of gradual oxygen increase is called tumour *reoxygenatation*. The rate of tumour reoxygenation is likely to be different for every tumour and depends on factors such as the local tumour environment, the survival of blood vessels during therapy and the oxygen consumption rate of surviving tumour cells.

2.2.2. Tumour Hypoxia and Reoxygenation in HNSCC Radiotherapy

2.2.2.1. The Oxygen Enhancement Ratio

The presence of molecular oxygen results in the DNA damage becoming more permanent or fixed, known as the *oxygen effect* or the *oxygen fixation hypothesis*. Damage may have been caused by direct interaction with an electron or by interaction with highly potent free radical species. Oxygen found in the water (H_20) molecule also assists in the chemical chain reaction required to produce the free radicals (Figure 2.7).

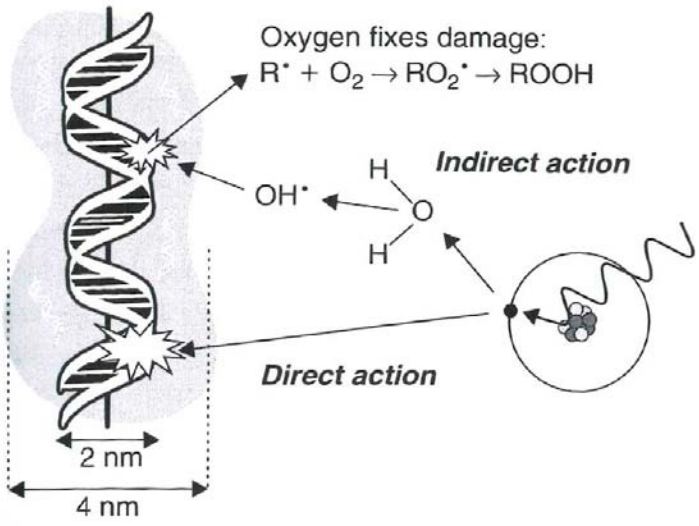

Figure 2.7. An illustration of two ionising radiation cell damage processes with DNA as the target (Hall 2006). The indirect process involves liberation of an atomic electron which then reacts, producing highly reactive free radicals that can cause DNA damage. With oxygen present, this damage is "fixed". Other damage mechanisms are also shown which involve liberation of an electron followed by direct DNA damage.

Multiple studies have shown that decreased cellular oxygen levels affect tumour cells as well as healthy cells, *in vitro* and *in vivo*, by altering their sensitivity to ionising radiation (Gray 1953, Hill 1971, Wright 1957). The factor used to express the decreased radiosensitivity of cells experiencing reduced oxygenation is named the Oxygen Enhancement Ratio (OER). OER is defined as the amount of dose reduction required for cells of a given oxygenation level compared to anoxic cells (no oxygen) to obtain the same effect, i.e. a low OER value if hypoxic and a high OER value if oxic. The OER has been reported to be high as 3 oxic cells compared to anoxic cells (Elkind 1965).

Alper and Howard-Flanders formulated OER as a function of pO_2 (Equation 2.6), and found that values of 3 for both *m* and *k* provided a good fit with experimental data (Alper 1956, Alper 1979). The *m* parameter represents the maximum ratio of the doses required to kill a cell with low oxygenation (hypoxic or anoxic) compared to one with high oxygenation (oxic or normoxic), and *k* is a constant of the equation.

$$OER = \frac{mpO_2 + k}{pO_2 + k} \qquad (2.6)$$

Kirkpatrick and group have also formulated OER using empirical data (Kirkpatrick 2004) based on the work of Elkind (Equation 2.7).

$$OER = 1 + 0.81(pO_2{}^{0.616})/(1 + 0.324pO_2{}^{0.616}) \qquad (2.7)$$

Equation 2.7, along with the curves representing the influence of dose per fraction on the OER, is presented in Figure 2.8 (Dasu 1998, 1999, Kirkpatrick 2004). The reduction in OER for cells exposed to small dose fractions (< 2 Gy) has important implications for hyperaccelerated radiation schedules.

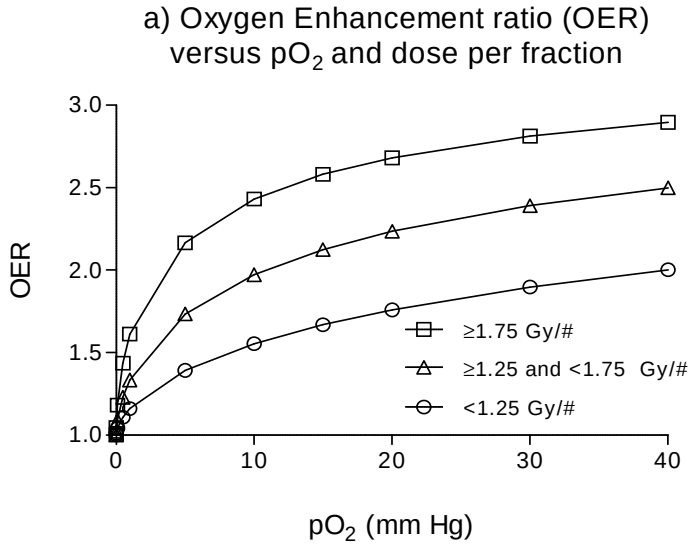

Figure 2.8. The oxygen enhancement ratio of irradiated cells of increasing oxygenation (pO_2) for the conventional (2 Gy) dose per fraction and for decreasing dose per fraction (Dasu 1998, 1999, Kirkpatrick 2004).

There have been reported differences between the radiosensitivity of acutely versus chronically hypoxic cells because of the decreased repair capacity of the chronically hypoxic cells (Denekamp 1999, Denekamp 1998). This effect has not been included in this work but may be considered in the future.

2.2.2.2. Hypoxia and Tumour Control in HNSCC Radiotherapy

There is evidence that the hypoxic sub-volume of a tumour and the mean oxygenation level have a direct influence on the local control (LC) for head and neck tumours (Nordsmark 2005, Gatenby 1988, Dunst 2003, Stadler 1999, Stadler 1998, Brizel 1999).

Past strategies to overcome the radio-resistance associated with low tumour oxygenation have included the use of hyperbaric oxygen and breathing of oxygen rich air (carbogen) before or during treatment (Brown 1999, Lee 1996, Marcu 2006). In the last decade, efforts have been directed towards locating hypoxic regions (with PET and CT imaging modalities), by targeting hypoxic tumour sub-regions with higher doses of radiotherapy (dose painting) and the use of cytotoxic or reoxygenating drugs that preferentially bind to hypoxic cells (*Tirapazamine* and *Misonidazole*).

These methods although beneficial in some studies have not been shown to have significant advantages compared to standard treatment, taking into consideration the side effects of the drugs, logistics of drug delivery, patient tolerance, and overall improvements in local tumour control (Marcu 2006, Corry 2004, Kaanders 2004, Lee 1996).

2.2.3. Accelerated Repopulation in HNSCC Radiotherapy

A natural response of epithelial cells to physical trauma, including damage from a dose of radiation, is an increase in cellular proliferation of the surviving cells. In the case of acutely responding normal tissues, this effect assists in the fast and recovery of the tissue and restored functionality. In the case of tumour tissues, this rapid or *accelerated* repopulation has a detrimental effect on tumour control probability because of the extra clonogenic tumour cells that are generated, especially if the total treatment time is relatively long (Withers 1988).

There are a number possible cellular mechanisms attributed to accelerated repopulation, with the key mechanism thought to be the increase in the stem cell symmetrical division

probability (Marcu 2004, Withers 1988). Other mechanisms include a decrease in cell cycle time, recruitment of the cells from the G0 quiescent phase of the cell cycle, and de-differentiation of cells to a more stem cell like state.

It is likely that a number of these mechanisms are induced simultaneously, however their times of onset after trauma such as a fractionated radiotherapy require further study (Begg 1991, Fowler 1991, Marcu 2004, Withers 1988). In this work, symmetrical stem cell division has been modelled as the sole mechanism of accelerated repopulation.

The total time of treatment is a key parameter in controlling tumours which undergo accelerated repopulation. This has been evaluated in large clinical studies which have correlated tumour control to the number of weeks of treatment with fractionation schedules of various total time durations (Maciejewski 1989, Peters 1997, Withers 1988, Trott 1991, Trott 1999).

Other reports focus on a single clinical trial comparing conventional schedules to schedules with a planned break (Terhaard 2005). The published reports conclude that on average, HNSCC accelerated repopulation onset time or "kick off" is in the order of 2 to 4 weeks, and may be as high as 5 weeks (Brenner 1993, Maciejewski 1989, Peters 1997, Trott 1991, Withers 1988). However as accelerated repopulation onset times vary for individual tumours, the modelling of this effect has been analysed in detail in Chapter 5.

Some radiotherapy schedules that have concomitant chemotherapy treatment may have more delayed tumour accelerated repopulation onset; however this mechanism has not been considered in this report.

2.2.4. Fractionating Radiotherapy Treatment

2.2.4.1. Aims and Techniques

Fractionation decreases the overall average slope the resultant cell survival curve, compared to the delivery of a single large dose. In the example shown (Figure 2.9) the

difference in overall cell survival between after the delivery of four 2 Gy fractions, compared to one 8 Gy fraction is significant, with approximately 37% versus 1% cell survival. This difference is primarily because of the repair of sub-lethally damaged cells between dose fractions. The level of cell repair depends on the cell type irradiated and the length of time between the dose fractions.

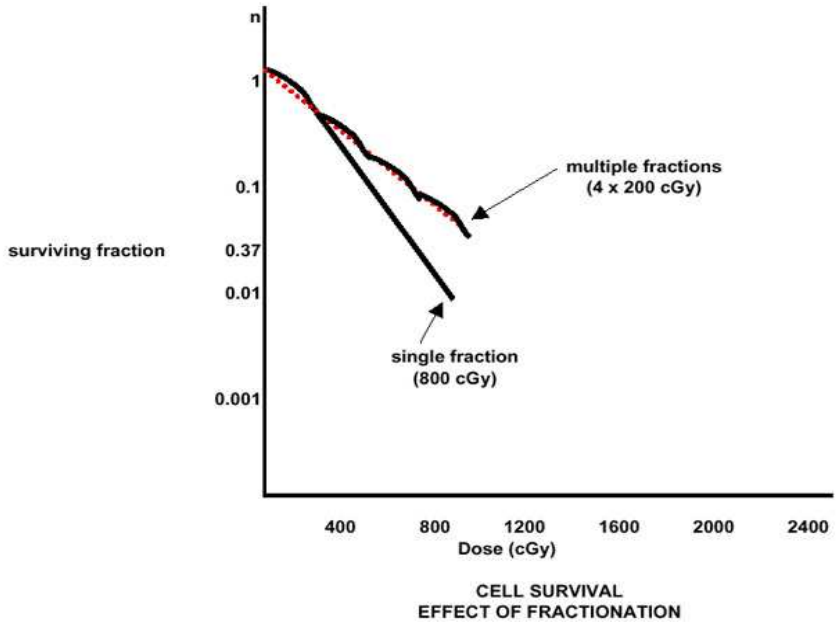

Figure 2.9. The fractionation effect on cell survival in Radiotherapy, where four dose fractions are compared to a single dose fraction (Dasu 1998, 1999, Kirkpatrick 2004).

For head and neck cancers, a seven week course of 2 Gy per day, 5 days a week (total dose of 70 Gy) is the convention for most radiation oncology centres around the world and is also commonly used as the control arm in the majority of head and neck radiotherapy clinical trials. The strategy of altering a fractionation schedule by decreasing total treatment time (accelerated treatment) is beneficial for minimising accelerated repopulation in tumours as well as patient convenience. However, accelerating treatment may require a total dose reduction to avoid late normal tissue effects.

To decrease the duration of treatment significantly the average dose per day must correspondingly be increased. Therefore, unless weekend days are used, multiple fractions (2 or 3) per day are required (hyperfractionation). During a hyperfractionated schedule it is important to allow sufficient time for the sub-lethally damaged normal cell

to repair. As discussed in the previous section, reducing the dose per fraction can also have implications on the radiosensitivity of hypoxic cells.

Apart from purely accelerated and hyperfractionated schedules, other strategies to improve treatment outcome include dose escalation (increased total dose and time) and a combination of acceleration and hyperfractionation, such as continuous hyperfractionated accelerated radiotherapy (CHART) and concomitant boost approaches. Overall, a balance is required to maximise total radiation dose, minimise duration of treatment (to overcome accelerated repopulation) and minimise normal tissue effects.

2.2.4.2. HNSCC Clinical Trial Review

Randomised clinical trials of altered fractionation schedules for HNSCC have been carried out since the 1980's. Most of the trials with statistically significant results collected data from a large number of patients and reported patient follow up results after 2 to 5 years. A tabulated summary of 14 phase II and III randomised clinical trials is located in Appendix A, in which conventional therapy control arm data are compared to data from one or more altered fractionation schedules, using radiation as the sole modality of treatment. Details regarding the altered fractionation schedules modelled in this work will be presented in chapter 5.

In general, the data from HNSCC clinical trials indicate that LC can be improved by approximately 10% to 20% for advanced disease (stage 3 and 4) through the use of hyperfractionation and combined hyperfractionation and acceleration of treatment. Strategies to increase the total radiation dose by including a treatment break have not been found to improve the therapeutic ratio (of TCP to NTCP) compared to conventional treatments.

In a small number of HNSCC clinical trials, extra information has been collected from patients, such as tumour potential doubling time (T_{pot}) and the labelling index (LI) of cells from biopsies. Results have shown that certain sub-groups of patients had better outcomes than others for tumours of the same stage. For example, LC was improved in tumours with a low T_{pot} values by up to 40% compared with the average of 10% to 20%

for the group of patients in the control arm of the trial (Horiot 1997). However in this trial, the difference in outcome was not observed in the altered fractionation arm.

Tumour oxygenation data is not generally available from large multi-centre clinical trial reports. The available data primarily contains information on tumour stage, patient age, and outcomes of treatment for radiation alone or radiation with chemotherapy. When oxygenation has been measured in trial patients, tumour oxygenation parameters have been correlated with LC and survival outcomes (Nordsmark 2005). Because of the limited oxygen specific trial data it is currently difficult to predict the benefit of specific altered schedules for tumours with different oxygenation levels, providing motivation for the modelling of hypoxic tumour growth and treatment response.

Chapter 3

A Review of Tumour Growth, Hypoxia and Radiotherapy Modelling

3.1. Introduction

Computer, or *in silico*, modelling involves the development of algorithms written in various programming languages to solve problems from a set of initial conditions and parameter values. Tumour growth algorithms are usually designed to simulate biological mechanisms on the microscopic scale, using input parameters and rules governing cell progression and propagation.

Computer models can be useful for analysing the changes in tumour individual cell properties through tumour evolution, as well as estimating the response of the tumour to different forms of treatment. Ideally, the parameter values and cellular data used should be experimentally determined before incorporation in models, and all results should be verified against experimental or clinical trial data for the cell type or disease studied to validate the model predictions.

In modern tumour models, the initial goal is usually to simulate the growth of a virtual tumour, up to a set size or cell number. Subsequent goals may then include the modelling of different treatment modalities and cellular response mechanisms, with the aim of analysing the efficiency and effectiveness of cell kill compared to standard treatment techniques. The treatment modality of interest in this work is fractionated radiotherapy, with modelling work aimed at investigating radiobiological mechanisms including reoxygenation of hypoxic tumours and accelerated repopulation.

The goals of tumour modelling vary among researchers, and may focus on one key biological/radiobiological mechanism, or explore mechanisms and ranges of parameter values. Many models aim to identify mechanisms at the cellular level (and parameter values) that are responsible for macroscopic tumour outcomes, e.g. the cell kinetic properties affecting the tumour growth or shrinkage rates. Modelling goals can include increasing the understanding of cellular proliferative hierarchy and differentiation processes, evolution of tumour cell genetic mutations, tumour morphology, tumour pressure gradients, capillary networks and oxygen distributions.

The modelling methodology employed to simulate a biological system may be mathematical or stochastic in nature. Stochastic methods use random number generation and probability distribution functions to simulate cell propagation and evolution of the tumour, e.g. Monte Carlo (MC) methodology. Analytical (mathematical) methodology is more traditional, utilising deterministic equations, usually in the form of a set equations incorporating multiple parameters, e.g. sets of differential equations.

Linear quadratic (LQ) theory (Equation 3.1) is a commonly used analytical method of predicting the impact of fractionated radiotherapy on a cell population;

$$SF = \frac{N}{N_0} = e^{-(\alpha d + \beta d^2)} \tag{3.1}$$

where SF is the surviving fraction of cells after a dose d of radiation (Gy), N_0 is the initial cell number, N is the surviving cell number, and where α/β (Gy) is a measure of fractionation sensitivity (α (Gy^{-1}) is a measure of single strand break radiosensitivity and β (Gy^{-2}) is a measure of double strand break radiosensitivity).

The modelling work described in this report involves the use of LQ theory; however, stochastic methodology is employed to predict treatment response at the cellular level. This approach is in contrast to the use of deterministic correction factors in purely analytical models.

This chapter includes a review of the MC modelling technique, followed by chronological reviews of hypoxic tumour and radiotherapy effect models from the literature. The review includes both analytical (commonly named mathematical or deterministic models) and stochastic models, with an emphasis on recent stochastic modelling developments from the 1980's to the present.

3.2. The Monte Carlo Modelling Technique

Monte Carlo methodology enables a system to be modelled from first principles. It is a form of computation using random sampling and iteration to simulate the evolution of a physical or biological system, and involves the use of probability distribution functions for decision making, e.g. for the allocation of parameter values from a range of possible values.

This technique is useful for modelling systems with a large number of coupled degrees of freedom, which are difficult to solve using equation based methods. Pseudo-random number generation is often used in MC models to provide a repeating number sequence (commonly 2^{32} number repeating sequence), initiated by a random "seed" number. Multiple iterations of the model may be performed to assess the statistical errors associated with the results or predictions generated.

Although computational MC methodology arose in the 20th century, it was as early as the 1770's when Buffon and later Laplace used the theories of iteration and random chance to calculate the value of π. This was achieved by counting the number of times the throw of a needle intersected a line on a horizontal plane ruled with parallel lines (Ramaley 1969).

Lord Kelvin then used random sampling techniques to solve integrals required for his kinetic theory of gases (Kelvin 1901). Courant, Friedrichs and Fermi were all integral to the development of probability theory in the lead up to the 20th century and the subsequent widespread use of the MC technique.

Modern MC methodology was first used in the 1940's by physicists such as Nick Metropolis, John von Neumann, Enrico Fermi and Hans Bethe and Richard Feynman to advance digital computer systems (MANIAC) for nuclear weapon projects at the Los Alamos National Laboratory (Anderson 1986). Their work was named after the relationship of the methodology with chance, gambling and the famous casinos in Monte Carlo, Monaco.

An early application of MC theory was the calculation of radiation shielding for neutrons during nuclear weapon design. The technique soon became useful and popular for other researchers including physicists of many specialities as well as chemists and operations researchers.

Use of MC methodology can assist in modelling the statistical nature of biological and radiobiological mechanisms involved in cell division and radiation induced cell death. This allows microscopic/cell-based parameters to be allocated (using probability distributions) and the subsequent macroscopic effect analysed. Examples of this include the macroscopic analysis of tumour doubling time (T_d), the sub-volume of hypoxia in tumours and the rate of tumour reoxygenation during treatment. MC methodology allows the user to explore average population response predictions using averaged parameter values, as well as individualised tumour responses using specific tumour parameter values.

The modelling of tumour hypoxia may be implemented using probability distributions for cellular oxygenation, commonly in the form of pO_2 histograms. MC methodology allows a range of oxygen levels to be simulated and provides flexibility for changing oxygen distributions in time. This technique may also be used to simulate random or chaotic blood vessel structures for spatial tumour models simulating oxygen diffusion.

The general limitations of stochastic tumour modelling include the availability of quantitative experimental data for the required parameter values and computer time and memory restrictions when modelling large numbers of cells ($>10^8$ or 10^9 cells). In some cases, it may not be possible or feasible to measure individualised tumour parameter values for input into a model (such as the time and rate of reoxygenation). However, one of the great advantages of MC modelling is that is it can be used to assess the influences

of changing a parameter value through a range of plausible values, or including distributions of values for a parameter within the same simulation. The model user can then analyse the relative importance of each parameter and obtain information about the inter-dependency of parameters when many processes and mechanisms are modelled simultaneously.

3.3. Model Outlines

3.3.1. Analytical Models

This section will outline many of the deterministic tumour models from the mid 20th century to the present, with an emphasis on models that have incorporated the effects of tumour oxygenation. As previously mentioned, the well studied LQ model of cell survival will not be reviewed in this work. However, a comparison of the extensions of the LQ model with the current MC model presented in this report will be discussed in Chapter 5.

Analytical tumour models are deterministic and use sets of equations to describe the behaviour of a system. Analytical tumour models often utilise differential equations to predict the rate of change of factors such as tumour radius and oxygen diffusion rate during growth or treatment. These models tend to be more generalised than stochastic methods, with functions controlling the whole cell population, although they may be extended to include ranges of parameter values. Models using a spatial approach with discrete mathematical functions are referred to as cellular automaton models, and simulate the growth of a tumour in time and space using discrete voxels/grid elements.

Thomlinson and Gray were the first to use the theories of simple geometry and diffusion (Hill 1928) to mathematically model and predict the existence and location of chronic hypoxia in bronchial tumour cord cells, and the implications of oxygen related tumour radioresistance (Gray 1953, Thomlinson 1955). Their modelling work was verified by experiments which revealed the absence of central necrosis in the bronchial tumour cords

less than 160 µm in diameter, and the presence of cellular necrosis for tumour cords with a diameter of greater than 200 µm.

Work progressed in the areas of modelling oxygen diffusion and radioresistance in the 1960's and 1970's, when Tannock and co-workers used results from experimental studies to model tissue oxygenation and the associated distribution of cellular radiosensitivies in tumours (Elkind 1965, Tannock 1968, 1972, Tannock 1970). The model utilised oxygen tension values based on the radial distances from blood vessels. Cell survival curves during radiotherapy were derived for hypoxic and oxic conditions, with results showing that a large number of cells have intermediate oxygenation levels in tumours, and that a simple 2-component model with cells either existing as oxic or hypoxic is inadequate to describe a tumour *in vivo*.

Brown's group then published experimental results verifying the presence of acutely as well as chronically hypoxic cells in mouse tumours, and drew attention to the limitations of reoxygenation as a means of re-sensitisation of tumours when acute hypoxia was present (Brown 1979).

McElwain published a model of vascular compression in tumours using mathematical methods to describe the oxygenation levels of cells in tumour spheroids (McElwain 1979). The group recognised the limitations of tumour spheroid systems because of the lack of natural angiogenesis of tumour *in vitro*. However, along with useful experimental work involving the growth of tumour spheroid systems, their model helped to achieve a better understanding of the processes of cellular migration from well nourished to necrotic regions of the tumour, and tumour pressure gradients due to cell proliferation and cell death for the cases of central or peripheral oxygen sources (McElwain 1993).

Smolle and Stettner introduced a 2D cellular automaton model in the early 1990's reporting that changing the microscopic properties of tumour cells as well as the surrounding stroma dramatically influenced tumour growth patterns (Smolle 1993). At each time step, an action was chosen for a random individual cell through set probabilities controlling proliferation, migration, death, and local paracrine and autocrine factor related effects. The total cell number achieved was in the order of thousands for

this qualitative and spatial based assessment of tumour growth, however no tumour oxygenation was considered.

In 1997, Wouters and Brown reported on a mathematical model using radial outward diffusion of oxygen from a simple geometrical array of blood vessels (Wouters 1997). Oxygen diffusion theory was based on the work of Tannock, while LQ and oxygen enhancement ratio (OER) theories (Alper 1956) used either a binary approach (e.g. 80% oxic and 20% hypoxic cells) or a range of pO_2 values between 0.5 and 20 mm Hg. Reoxygenation during tumour shrinkage was included in the model, with full tumour reoxygenation implemented between treatment fractions.

The model predicted large differences in surviving cell fractions when intermediately oxygenated cells were present in a tumour compared to well oxygenated cells.

For the case of 30 x 2 Gy irradiation of a tumour with oxygen diffusion modelled (using 60 mm Hg capillary wall oxygenation levels and a hypoxic fraction of 10%) there was a factor of 10^4 less cell kill compared to the use of a binary oxygenation approach. When using diffusion modelling, reoxygenation impacted in a less significant way upon cell kill than anticipated. It was concluded that hypoxia, especially for cells in the range of 0.5 to 20 mm Hg, plays a significant role in tumour radiosensitivity and treatment outcome, and that binary approach lacks the specific oxygenation information required to accurately predict tumour response to radiotherapy. In this equation based model, individual cell properties such as cell cycle time and proliferative capacity were not included.

A cellular automaton model investigating the diffusion of nutrients and the associated impact on tumour morphology and metastatic potential was in development in the 1990's (Pescarmona 1999). This was achieved by modelling the transport of iron in blood and assessing the number of viable cells at the tumour rim, the necrotic central volume and the number of cells entering the blood stream.

Nutrient consumption rate and the non-uniformity of the nutrient distribution were found to be critical parameters on tumour shape. This model used stochastic methods to model the ranges of some tumour parameters but restrained the cells to a 2D *slab* of tissue and concentrated more on the early stages of neoplastic development and deviation from

uniform spherical geometry. Treatment of the virtual tumour and the effects of treatment related parameters were not considered.

Although primarily concentrating only on epidermal cell kinetics, the experimental and modelling work of Aarnaes, Clausen and co-workers in the 1980's and 1990's provided the ground work for cell hierarchy and kinetics modelling for SCC. The cellular parameters investigated included cell cycle time, circadian rhythms of the cell cycle, cellular hierarchy and differentiation. Their research lead to models of tumour angiogenesis and the difference between avascular and vascular growth in solid tumours (Chaplain 1996, Anderson 2000).

From this work they were able described the response of the tumour to angiogenesis factors and the associated influences on secondary tumour growth/metastases, endothelial cell migration, branching and proliferation, as well as an explanation for the frequent clinical detection of secondary tumours shortly after surgical treatment of the primary tumour and the growth pattern of tumours in the pre- and post-angiogenic phases of development. There work however did not concentrate on radiotherapy treatment or the modelling of individual cells.

Further mathematical models have considered biological as aspects of tumour growth such as;

- the extent of chronic hypoxia in tissue segments based on spherical geometry using tissue respiration rate and the oxygen threshold for proliferation parameters (Maseide 2000),
- the early stages of tumour growth and subsequent tissue invasion, through vascular growth and anaerobic tumour cell metabolism processes (Patel 2001),
- tissue vascularature using micro-vascular density and heterogeneity using diffusion of oxygen and the oxygen consumption rate parameters and hypoxic regions that varied spatially (Nilsson 2002).

Analytical models have been the corner stone of tumour predictions, used for analysis of tumour growth patterns, responses to treatment, and the effects of oxygen deprivation. Many models simulating radiotherapy treatment use standard LQ theory for baseline cell kill predictions and incorporate oxygen effects through various mechanisms to adjust cell kill probability. This method has also been applied in many of the models described in the next section that reviews past stochastic modelling approaches.

Models based purely on mathematical equations can provide useful generalised predictions of tumour evolution and are well suited to systems that consider rates of change in parameters such as oxygen and nutrient consumption rates, oxygen diffusion rates and the changes of tumour diameter and mechanical pressure gradients. As we move forward into an era of fast computing, the goal of individualised radiotherapy treatment using specific patient imaging and cell/genetic parameters may soon be realised, if these parameters can be incorporated into models at the cellular level and handled using probabilistic methods.

Analytical models continue to assist researchers in understanding tumour behaviour and the mechanisms involved in growth and shrinkage during therapy, but lack the advantages of individual cell based Monte Carlo models, which have the flexibility to incorporate deterministic equations as well as probabilistic functions within their algorithms.

3.3.2. Stochastic Models

Stochastic methodology in biological models employs the use of functions describing the ranges of possible parameter values and their allocation probabilities, e.g. cell cycle time and cellular oxygenation. For tumour and radiotherapy modelling this general technique may be applied in a number of ways.

A spatial modelling approach requires the construction of a virtual lattice (similar in concept to mathematical cellular automaton methods) with defined geometrical properties for cells (or a number of cells) occupying one voxel of the lattice. A temporal modelling approach requires cellular information to be stored and updated in time as the cell population propagates, without the use of spatial cell coordinates. Often, spatial models use more computational resources, as each cell requires the storage of division related parameters as well as coordinates in the lattice.

3.3.2.1. Early Models

One of the first models to use stochastic methodology to model tumour cell propagation and radiotherapy was named "CELLSIM" and subsequently "CELLGROW" (Donaghey 1980, 1983). It was a temporal model dedicated to simulating cell population growth through the movement of cells through the phases of the cell cycle (time distributions used for each cell cycle phase). Tumour growth was initiated with a cohort of cells moving through the cell cycle and dividing at mitosis, where two new cell cohorts would emerge.

The growth fraction parameter controlled the number of mitotic cells entering the G0 phase instead of the G1 phase, controlling the tumour growth rate. Cell progression from the G1 to the S phase of the cell cycle could be halted to model the effects of phase blocking cytotoxic drugs. Due to the number of cells required, cells were grouped and their parameters averaged, with group size adapted throughout growth. Radiotherapy was incorporated into CELLGROW, using a lethal damage probability of 50% per cell (Donaghey 1983), however cellular oxygenation was not considered.

In the early 1980's Duchting and co-workers began developing the first 3D cell based algorithm to model tumour growth with individual cell growth and death considered (Duchting 1992, Duchting 1981, 1985, Duchting 1995). Nutrient levels were also modelled by diffusion from the surrounding medium into the spherical tumour mass. The model included four proliferative cell cycle phases; a G0 phase and cells in a necrotic state. Cells lacking in nutrients entered the G0 phase and were returned to the cell cycle if nutrients became available.

Tumour volumes up to 1 mm^3 were simulated using a 40x40x40 lattice, with 100 *cell-time units* taking 8 minutes to process. A critical radius of 100 µm was set for oxygen diffusion, producing an outer layer of proliferating cells, a middle layer containing only a few proliferating cells, and a central region of necrosis. Artificial capillaries were introduced to study the effects on the necrotic tumour core.

In the mid 1990's, the model was extended to consider basic cell repair of radiation damage and reoxygenation through G0 phase recruitment. Hypoxia was modelled using separate $\alpha_{hypoxic}$ and $\beta_{hypoxic}$ terms, with the same final α/β value as proliferative cells. Five alternate fractionation radiation schedules were modelled, with the hyperfractionated schedule found to be the most effective for tumour control for most simulations. Although individual cells were considered, computation time relatively slow and only single/constant terms were used to define the OER for hypoxic cells.

At the time, Qi's group were developing a 2D cellular automaton model to simulate Gompertzian type tumour growth rate characteristics (Qi 1993). In this model, a cell could only divide if there was an empty space in one of the four lateral or longitudinal directions for the second daughter cell to inhabit. Cell death was purely a stochastic process as was quiescent cell allocation, unlike other models considering nutrient diffusion. Mechanical pressure, cell density, proliferation rate and cytotoxic immune system parameters were used and their effects on tumour growth reported. Growth curves were in agreement with experimental data. Tumour hypoxia and treatment related results were not considered in this model.

In the late 1990's, a group lead by Kocher began developing a 3D model of solid and necrotic brain tumour behaviour with an emphasis on modelling tumour oxygen supply and the prediction of tumour control probability (TCP) based on post radiotherapy cell survival (Kocher 1997, Kocher 2000). Proliferating (constant cell cycle time of 5 days), non-proliferating (hypoxic) and necrotic cells were modelled using a lattice of 74^3 elements, where capillaries were placed at every 7^{th} lattice position.

An oxygen diffusion limit of 100 µm was used to define hypoxia and 140 µm to define necrosis. A constant OER value of 3.0 was used for hypoxic cells. New capillaries were placed at the original capillary lattice positions when the mean density dropped below 90% of the ordinal capillary density. This provided a hypoxic fraction of up to 2% and 25% for vascularised and non-vascularised tumours respectively. Vascular occlusion was considered and the impact of hypoxia on treatment outcome analysed.

Three radiotherapy schedules were simulated with a focus on radiosurgery. Accelerated radiotherapy schedules increased tumour control rates more effectively for fast growing tumours compared to slower growing tumours. Results confirmed the need for modelling neovascularisation, vascular occlusions and necrotic effects when comparing the results with clinical outcomes of 90 brain tumour patients. The model was refined to run in 40 hours for 100 cell layers (averaging over 100 simulations). Oxygen levels allocated to the $4x10^5$ cells in this model did not allow for the full range of possible pO_2 or OER values.

Concurrently, Kansal and group were developing a discrete brain tumour (glioblastoma) growth model, considering the tumour cells as well as the surrounding normal cells (Kansal 2000a, Kansal 2000b). Adaptive Voronoi tessellation techniques were employed to structure the cells in a 3D spherical space. The tumour started with 1000 cells, and grew to a clinically detectable size by increasing grid spacing during tumour growth. Cell loss at the tumour boundary as well as cell quiescence due to oxygen deprivation and spatial restriction were considered. Cellular oxygen levels were calculated using the distance from the tumour boundary.

The model produced an approximate spherical tumour mass, which grew in a Gompertzian manner according to input parameters including: probability of cell division, base necrotic thickness, proliferative shell thickness and maximum tumour radius. In this model, small number of automaton voxels represented 1000 individual cells and tumour hypoxia/necrosis was described in a broad fashion through a spherical rim of proliferative cells and inner core thickness of non proliferative cells. No tumour oxygen source was modelled, nor was the possibility of user defined oxygenation distributions. No treatment effects were considered in this model.

3.3.2.2. Recent Models

Dasu has reported simulations considering both acute chronic and hypoxia, that have used mathematical equations to describe oxygen diffusion and variable oxygen consumption rates (Dasu 2003, 2005). A 2D vascular network was modelled with a spatial distribution of inter-vascular distances characterised by the mean and coefficient of variation using Monte Carlo methods and log-normal probability distributions. This allowed the modelling of realistic blood vessel networks and the calculation of their associated pO_2 histograms. The average value of the inter-vascular distance gave an overall indication of tissue oxygenation, but the width/spread of the distribution was necessary to quantitatively assess the system. A wide distribution meant that a significant portion of the tissue had sparse vessel formation even if the mean inter-vascular distance were relatively small.

Modelling work by the group has continued, considering the effects of acute and chronic hypoxia on tumour control after radiotherapy. Using a threshold of 2.5 mm Hg to define cellular hypoxia, comparisons were made between oxic and hypoxic tumours using a single OER value approach versus a full OER curve approach.

Results yielded significant differences in cell survival using the two approaches and justified the need for a full description of tumour oxygenation to predict treatment outcomes. Results also showed that temporal oxygenation changes between treatment fractions are less important than the presence of perfusion limited (chronic) hypoxia, and that the presence of a small degree of hypoxia during every treatment fraction has an effect on tumour response, regardless of the changes in spatial hypoxia patterns in the tissue.

This model has provided evidence for the need to use the full oxygenation distribution for the allocation of pO_2 to cells in the tumour, and showed that chronic hypoxia is primarily responsible for tumour radioresistance during/after radiotherapy. Note that the *HYP-RT* model presented in this report uses a full pO_2 distribution to describe chronic tumour hypoxia.

During the past decade, a group led by Stamatakos, Dionysiou and co-workers has been developing Monte Carlo tumour growth and radiation response model for decision making and individualisation in treatment planning. Initial work began with a 3D discrete time step model (extending upon pioneering work by Duechting in the 1980's) with spatial visualisation and modelling *in vitro* tumour spheroids for small lung cell carcinoma (Stamatakos 2001).

The basic algorithm controlling tumour growth started with a single tumour cell at the centre of a 100^3 lattice. Cells progressed through the phases of the cell cycle, where at each hour of tumour time the time remaining in the current phase of the cell cycle was decreased for each cell. Cell cycle times were based on Gaussian probability distributions, and cells entered a G0 phase if more than 3 cell layers from the oxygen/nutrient medium food source (non-angiogenic model) and a hypoxic lifetime, *TG0*, of 25 hours. Cells could exit the G0 phase to simulate reoxygenation during tumour shrinkage.

A cell loss factor 1% was used, as were individual α and β values for S phase of the cell cycle compared to non-S phase cells and G0 cells, for determining the cell kill for each treatment fraction. A conventional and accelerated schedule were applied (2 Gy/day or 2x2 Gy/day, 5 days a week up to 60 Gy), with results showing reasonable agreement with *in vitro* clonogenic assay experiments using fractionated schedules.

Since 2004 the group has published work modelling *in vivo* tumour systems, concentrating on glioblastoma multiform, and the incorporation of experimental and clinical data (Antipas 2004, Dionysiou 2007, Dionysiou 2006, Dionysiou 2004, Stamatakos 2006). The model now uses the concept of a "geometrical cell" (GC) to average the properties of up to 10^6 tumour cells (depending on the tumour volume imaged), and uses a maximum grid size of 100^3 (later expanded to 120^3) for the spatial locations of the GC's.

In a GC, cells are considered synchronised at the time of irradiation, with the time register set to a random value between zero and the maximum phase duration for the cell cycle phase the GC was calculated to exist in. This process decreased the statistical significance of the results but assisted in computational limitations, but was not

considered a major limitation due to the limited resolution of the information input into the model obtained from tumour imaging.

PET imaging metabolic and proliferative activity data from real tumours was used to assign GC sub-volumes to proliferating, G0 phase or dead cell regions/rims of the tumour. Results from radiotherapy simulations (2 Gy/day or 2x1.2 Gy/day, 5 days/week), varying α and β values in the different cell phases as well as the total α/β, showed good agreement with clinical trials outcomes for hyperfractionated schedules and with general tumour control rates observed for this tumour type.

Further complexity was introduced by the group by modelling interphase as well as mitotic cell death mechanisms and the visualisation of blood vessel formation. Uniform OER values (range of 1 to 3 was applied in different simulations) were assigned to hypoxic cells, although separation of OER into $OER\alpha$ and OER_β parameters was performed. An OER_β value of 3.0 to 3.5 provided cell kill in agreement with cell culture survival curves and, as expected, low OER simulations resulted in the largest tumour shrinkage rate. GBM p53 mutated vs. wild type tumours were modelled by changing the α_{oxic} term in simulations.

A comparison between six radiotherapy fractionation schedules, including HART and CHART schedules was performed, varying parameters such as the cell loss factor, OER, OER_β, cell cycle time and mutated versus wild type p53 status. Results showed that accelerated schedules are beneficial and that wild type tumours (higher α/β) respond well compared to mutated tumours. In addition, the cell loss factor greatly impacted on overall cell number (varied between 0.04 and 0.9), and a reduction in cell cycle time (approximately 60 down to 50 or 40 hours) resulted in faster repopulation rates. The effect of a changing the OER for hypoxic cells was considered, but not considering a full range of OER values.

Popple has published work on a MC tumour model that aimed to predict tumour control probabilities after selective boosting of hypoxic sub-volumes within a tumour mass (Popple 2002). Emphasis was placed on developing the treatment algorithm and delivering different doses to different compartments based on oxygen status. Clonogenic cells were considered to be in well oxygenated, temporarily hypoxic, or permanently hypoxic states, where up to 20% of the total volume consisted of cells in a hypoxic state.

The tumour was initiated with a population of geometrically stable hypoxic (GSH) and oxic cells. Upon radiation treatment, a randomly selected proportion (which varied spatially for every treatment fraction) of the oxic cells formed a geometrically transient hypoxic (GTH) population. Reoxygenation was modelled based on random cell selection from the GSH population using a binomial distribution, assuming that the GTH percentage remained constant, and that the GSH fraction was constant in regions near a hypoxic sub-volume. Cells could only leave the GSH group to become oxic (upon reoxygenation) after a treatment fraction. Clonogenic cell survival for each fraction was calculated using binomial distributions and the standard LQ equation.

Tumour control was predicted through multiple simulations using the same input parameters, to obtain the average number of surviving clonogens for 10^9 cells. A 20% to 50% boost in dose delivered to a sub-population of cells increased TCP equal to that of an oxic tumour. When the majority of hypoxic cells were part of the GTH group, the boost dose had had little effect. However, with 20% GSH (and no GTH) a boost dose ranging from 0.2 to 1 Gy increased TCP from 50% to 80%, for a boost to the whole GSH. An OER of 2.0 for 2 Gy per fraction was used (α/β_{oxic} = 6 Gy, $\alpha/\beta_{hypoxic}$ = 12 Gy), producing SF_2 and $SF_{2.4}$ (2.4 Gy boost dose) values of 0.48 and 0.40 for oxic cells, and 0.73 and 0.67 for hypoxic cells. This model provided information of the benefits of boosting dose to stable hypoxic tumour regions. However, a distribution of OER values for a continuous range of cellular oxygenation levels was not applied and accelerated repopulation was not considered.

Sovik has published work on a cellular automaton model aimed at optimising TCP through re-distribution of delivered dose ("dose painting") (Sovik 2007). Up to $4x10^4$ cell groups (with $2.4x10^4$ cells per group) were modelled using experimentally verified pO_2 histograms to simulate varying oxygen distributions, ranging from 0 to 102.5 mm Hg in

2.5 mm Hg bins. Acute and chronic hypoxia was defined by a pO_2 threshold of 5.0 mm Hg. Reoxygenation was modelled by randomly shifting cell groups to the next highest oxygenation bin after each fraction. Heterogeneous cell density and cell propagation between treatment fractions were considered. Dose to regions of the tumour were re-distributed according to four pO_2 thresholds: 2.5, 5.0, 20.0, 102.5 mm Hg. OER values were calculated for these groups according to an OER versus pO_2 relationship, and an $OER_{\alpha,max}$ and $OER_{\beta,max}$ of 2.5 and 3.0 respectively, and a K_m value of 3.28 (Wouters 1997, Dale 2007).

The group concluded that prescribing varying doses to different parts of the tumour can significantly increase TCP although the rate of reoxygenation was found to be the crucial parameter. Tumours with no reoxygenation had the most benefit of dose re-distribution. The level of chronic hypoxia influenced TCP more than the level of acute hypoxia. Although averaging cells into large cells groups, this model used a continuous OER curve to describe hypoxic cell radioresistance, however no accelerated repopulation was modelled.

Marcu initiated the development of a stochastic individual cell model, to analyse the temporal aspects head and neck tumour growth and treatment outcome (Marcu 2006, Marcu 2005, Marcu 2003, 2004, Marcu 2002). Tumour growth was initiated from a single clonogenic (stem) cell, up to 10^6 cells, followed by radiotherapy and Cisplatin chemotherapy treatment. The aims of the modelling were to explore the biological mechanisms controlling tumour growth rate, repopulation and accelerated repopulation during and after treatment, and the optimal timing of chemotherapy administration.

The algorithm used a truncated Gaussian cell cycle time distribution (with an average cell cycle time of 33 hours) to propagate stem cells (infinitely proliferative) and proliferating cells (average of 3 generations). Non-proliferative G0 cells were modelled with an average cell loss factor of 85%. The choice of cell type for the second daughter cell upon stem cell division employed MC methods using a probability ratio of approximately 2:6:92 for stem, proliferative or non-proliferative cells respectively. This yielded a tumour cell population consisting of realistic cell type percentages and a growth rate consistent with literature reports for HNSCC. However, no tumour hypoxia was considered in the model.

Cell cycle phases were assigned individual radiosensitivity values of which the M and G2 phases were three times more sensitive than the S phase, and where the G0 phase was 1.1 times more sensitive than the S phase. The G1 phase was assigned the average radiosensitivity value based on an SF_2 of 54%. Mechanisms of accelerated repopulation were explored including the loss of asymmetrical stem cell division, accelerating cell cycle times and G0 phase cell recruitment.

Loss of asymmetrical division was modelled by increasing the probability of a stem cell dividing into two daughter stem cells, with an upper bound of 10%. Cell recruitment was modelled by selecting G0 cells to re-enter the cell cycle at the G1 phase. The timing of accelerated repopulation was investigated in an *in vitro* experimental study which indicated an immediate repopulation response after initiation of irradiation.

A conclusion drawn from the propagation and treatment of 10^5 cells, was that the loss of asymmetrical stem cell division was the dominant mechanism for accelerated repopulation, although all mechanisms impacted upon tumour re-growth to some degree when used in various degrees and combinations. It was also found that late onset of accelerated repopulation reduces the rate of tumour repopulation, and that only very small percentage of stem cells undergo asymmetry loss and contribute to the accelerated repopulation to achieve realistic rates of tumour re-growth.

Borkenstein and group considered angiogenesis in their modelling work and used an individual cell approach to spatially model tumour growth and radiotherapy treatment (Borkenstein 2004). Up to $5x10^6$ individual cells were modelled, taking approximately 1 day of computation. Tumour growth was initiated from a single cell which was assigned a radio-resistivity, oxygenation level, cell cycle time, and age related parameter. Random or linear (the latter, more time efficient however less accurate morphologically) displacement of cells towards the periphery created a free position for a new cell if necessary.

The number of cycling cells could be varied using parameters controlling the growth fraction and probability of spontaneous cell death. The probability of apoptosis could be modelled as volume dependent, ranging from 0% to 25%. Dead cells were assigned a re-absorption time described by a normal distribution. Capillaries were placed at intervals in a 3D lattice, with cellular oxygenation based on the distance to the nearest capillary cell. Cells in a hypoxic state secreted an angiogenesis factor in proportion to the number of hypoxic cells in the tumour. Diffusion of the angiogenesis factor was modelled using a step function (maximum diffusion distance of 240 µm), and angiogenesis was modelled through the division of capillary cells when the level of the factor reached a threshold level.

Radiotherapy and reoxygenation were modelled for up to $7x10^7$ cells (20 hours computation time) based on the LQ theory, with an average α/β value of 10 Gy. Individual α and β values were assigned to each cell using Gaussian distributions with capillary cells considered radioresistant. Accelerated repopulation was modelled by varying the growth fraction in time and/or the probability of apoptosis. Radiotherapy schedules of 2 Gy/day and 2x1.5 Gy/day were compared, using OER values of 3 and 2.5.

As expected, tumour growth rate increased with decreasing cell cycle time and tumour doubling time. An increase in capillary cell cycle time affected tumour doubling times, as did the inter-capillary distance. For example, with capillary spacing reduced from 7 to 6 cell layers, tumour doubling time decreased by 2 days. Total doses of 86 Gy *vs.* 78 Gy were required to control the simulated tumours for conventional and accelerated schedules respectively, using an end point of zero surviving clonogenic cells. These doses varied as cell kinetic and capillary parameters were varied.

Harting has extended this work by modelling a hypoxia induced angiogenesis factor excreted radially from hypoxic cells (Harting 2007). A steady-state diffusion equation involving a diffusion coefficient, the maximum diffusion radius, the radial distance from a capillary to a tumour cell, the radius of the capillary, enabled calculations of pO_2 for each cell as a function of distance from nearby capillaries.

OER calculated based on pO_2 using the formula by Alper and Howard Flanders (Alper 1979, Alper 1956). A virtual tumour containing $5x10^7$ was modelled using a Cartesian

grid. Cell kill during radiotherapy was calculated using LQ theory and altered for OER, and carried out by the dead cells being replaced by normal cells or being absorbed by neighbouring cells.

Results showed that hypoxic tumours were more radioresistant and, as expected, that inter-tumour variation in radiosensitivity flattens the dose response curve with the latter effect heightened when proliferation is modelled during treatment. Spatial intra-tumoural changes in radiosensitivity did not impact upon treatment outcomes. Specific oxygen distributions in the model were estimated using diffusion theory. This approach has merit but limits individualised pO_2 data input. All tumour cells were treated as clonogenic if oxic and cycling, i.e. no cellular differentiation mechanisms were modelled. The group expressed the intention to extend the model to propagate a larger cell population and a more heterogeneous distribution of proliferation and hypoxia.

A stochastic tumour simulation model using cell line specific parameters and functional pre-treatment PET/CT data was developed to investigate the effects of oxygenation on the radiation therapy outcome for HNSCC (Titz 2008). An average 36 hour cell cycle time and a five day cell death clearance rate were implemented. A 1D space was used for stochastic calculations and processes, with data imported from PET images to provide voxel based data on hypoxia levels and regions of proliferation. One voxel provided data for 10^6 cells.

Above a necrotic threshold of 1 mm Hg, the probability of cell division for each cell was determined using an exponential based equation. The OER for cells was calculated based on the Alper-Flanders formula, with a *K* value of 3.0 mm Hg. The LQ equation with OER modification was used to determine cell death probability for each radiation fraction. Individual phase radiosensitivities were used including G0 phase and hypoxic quiescent cell parameters. Chronic (but not acute) hypoxia and reoxygenation were considered in the model.

The results showed changing tumour responses and variability in radioresistance as tumour oxygenation levels decreased. Tissue growth curves followed *in vitro* cell line data for un-irradiated and irradiated cell lines (HNSCC-1), with an accurate time delay of tumour shrinkage predicted. This model included many important biological effects and

allowed for data to be entered for each 10^6 cell voxel. However, it did not consider the processes of cellular differentiation and accelerated repopulation of HNSCC during radiotherapy.

3.4. Summary

The models reviewed in this chapter represent a selection of models that have been, or are currently being, developed by radiobiologists and other medical scientists in the international scientific community. This chapter provides a representation of the various methods that enable cellular oxygenation to be incorporated into a computerised tumour model.

The modelling of hypoxic tumour propagation and subsequent radiotherapy has been approached in many different ways. Some groups have reported on the use of pre-determined distributions of cellular oxygenation based on pO_2 histogram data, while others have taken a spatial approach using a lattice of capillaries and the diffusion of nutrients from these capillaries to the tumour cells. Capillary growth has also been stimulated, and in one case, modelled through the excretion of angiogenesis factors by hypoxic cells.

The *HYP-RT* model described in this report is a temporal stochastic model, simulating individual tumour cell division and the effects of fractionated radiotherapy. The model is based on the proliferative hierarchy of epithelial tissue, to simulate head and neck squamous cell carcinoma growth. Tumour hypoxia is modelled using an oxygen distribution (pO_2 histogram) which is applied when the tumour has reached a 10^6 cell threshold. The model is capable of simulating the effects of reoxygenation of hypoxic tumours as well as more rapid growth onset during treatment. *HYP-RT* was designed to retain all necessary cell information, while retaining computational efficiency and minimal user input unless deviation away from the default parameters are required.

Chapters 4 and 5 of this report fully outline the *HYP-RT* algorithm development process and the parameters utilised to propagate and treat the tumour.

This method of hypoxia modelling differs from other recent stochastic modelling methods that have simulated individual cells or groups of cells (Harting 2007, Titz 2008, Dionysiou 2008). The lack of spatial coordinates for cells in the *HYP-RT* model has enabled efficient computation and memory usage. The temporal approach was considered justified for the modelling of relatively small tumours, considering immunohistochemical studies showing that hypoxic tumour cells are often spatially irregular and chaotic in small head and neck tumours down to the microscopic level (Ljungkvist 2006, Wijffels 2008). This is likely to be attributed to a large proportion of temporal (acute) hypoxia. Thus, for simulated treatment of uniform linear accelerated beam dose profiles, a non-spatial approach was deemed adequate.

Although *in vitro* experimental and retrospective clinical trial studies have been carried out regarding the effects of accelerated repopulation, there is a current lack of models in the literature simulating inter-fraction variable repopulation growth rates, as well as the simulation of $>10^6$ individual cells with individual cellular oxygenation levels.

Owing to the complexities and dynamic nature of tumour oxygen distributions and the reoxygenation process, MC methods remain the most efficient way of incorporating hypoxia into a tumour model. MC methods also allow for relatively simple statistical analyses of results on an individual cell basis, e.g. the analysis of tumour growth rate, cell type percentage, the rate of reoxygenation, the rate of tumour re-growth, and radiation induced cell kill efficiency. Moreover, these tumour properties may be recorded and assessed over the time course of tumour evolution. Model input parameters can be tailored to the individual or a population subset, providing estimates of the way in which tumour parameters influence tumour growth and responses to treatment.

The current trend towards the use of stochastic methods in tumour modelling has been influenced by increasing computer power, the value of statistical analyses and the level of individualisation made possible despite the large number of input parameters and variables. However, mathematical (continuous and automaton) methods still have a place in the recent tumour modelling literature.

In this relatively early era of Monte Carlo tumour modelling, it is proposed that the advantages of a simplistic and efficient tumour simulation tool, such as the *HYP-RT*, will be useful for the prediction and improvement of treatment outcomes for HNSCC patients after radiotherapy treatment, and also provide information about the consequences of unscheduled treatment breaks during a course of radiotherapy.

The current difficulties posed by biological modelling include the lack of accurate and specific biological data for the cell type/cell line being considered. In fact, there maybe no accurate single value for many tumour-related parameters because of the wide variation of tumour properties among different patients, even for the same disease site and pathology. This makes modelling useful for the prediction of individual tumour outcomes but difficult to validate against real patient data.

Chapter 4

Modelling Oxic and Hypoxic Tumour Growth

4.1. Introduction

A key aim of this research was to develop a Monte Carlo (MC) computer model of head and neck squamous cell carcinoma (HNSCC), to investigate the behaviour of this aggressive disease during growth and radiation treatment. As discussed in chapter 2, tumour hypoxia is a common occurrence in HNSCC which can affect cellular proliferative capacity and sensitivity to ionising radiation. Consequently, the modelling of a realistic oxygen distribution among the tumour cells has been a key focus of this work.

The model, named *HYP-RT*, was designed to propagate a cell population starting from a single stem cell, up to a tumour consisting of 10^8 cells. Each cell in the tumour was considered separately and allocated parameters such as cell cycle time (CCT), the type of cell (in terms of proliferative hierarchy), the number of divisions a cell would cycle though, and oxygenation level. Development of the model has enabled the study of the cellular mechanisms impacting on tumour growth rate and the percentages of cell types in the tumour cell population. Of particular interest in the tumour growth model were the effects of decreased oxygen levels (tumour hypoxia) and the division/differentiation characteristics of the tumour cells.

As discussed in Chapter 3, MC methodology has allowed for the relatively simple modelling of complex and dynamic processes, compared to analytical modelling methods. The current model allows for the input of individual tumour parameters that can be easily manipulated and studied for their effect on tumour growth and response treatment.

The following sections discuss programming methods (using FORTRAN 95), tumour growth algorithm design, the mechanisms used to model cell division, allocation and data storage of cellular parameters, e.g. cell cycle time and oxygenation, and the impact of these parameters on tumour growth rate, total growth time and the percentages of cycling and non-cycling cell types comprising the tumour.

4.2. Biological Mechanisms and Model Parameters in the Tumour Growth Algorithm

4.2.1. Modelling Cell Division and Epithelial Cell Hierarchy

In this model, a dividing cell is considered to be the "mother" cell and the products of division considered to be the "daughter" cells. Upon division, the mother cell ceases to exist and all information regarding this cell is deleted. The CCT time of the mother cell determines the future time (computational time) of division of the mother cell and consequently the time at which its one or two daughter cells are allocated cellular parameters and stored in computer memory.

Modelling the propagation of an epithelial cell population was the first step in developing the *HYP-RT* model. The cell types used to represent the proliferative hierarchy included: stem cells (*S* cells) which are infinitely dividing (i.e. clonogenic), transit cells (*T* cells) which cycle for a set number of divisions, as well as non-cycling cells including differentiating (*D1* or *D2* cells), fully differentiated (*D3* cells) and temporarily quiescent cells. The quiescent cell group consisted of stem cells in a "resting" G0 phase as well as any hypoxic cells with oxygen levels below the quiescent threshold ($pO_2 \leq 1$ mm Hg).

Stem cells were modelled to divide into at least one daughter stem cell and the second daughter cell which could be either a stem cell (*S*), a first generation transit cell (*T1*) or a "level 1" differentiating cell (*D1*). For the second daughter cell, cell type probability was labelled the *S:T1:D1* ratio. Before a new stem cell entered the cell cycle, it was modelled

to wait in the G0 phase (Wright 1984, Izquierdo 1972). The distinction between G0 phase stem cells and cycling stem cells was made because of reported differences in radiosensitivity, i.e. G0 non-cycling cells have a higher resistance to radiation than the average radioresistance value of cycling cell when averaging over the G1, S, G2 and M phases (Hall 2006, Aarnaes 1990).

In the model, the radiosensitivity of both cycling and non-cycling cells was decreased with decreasing oxygenation. However, non-cycling cells were assumed to be inherently more radioresistant by a factor of two. This inherent radioresistance factor was also applied to all differentiated and severely hypoxic non-cycling cells.

Transit cells (also named progenitor cells) were modelled to divide into two daughter transit cells for a set number of generations, allocated from a normal shaped probability distribution with a range of one to four generations. This range was selected according to reported experimental and modelling data regarding the turnover of epithelial tissue and the progression/differentiation rate of stem cells from the basal to the superficial layers of the epithelium (Wright 1984). In the model, when a last generation transit cell was due to divide, two differentiating cells (*D1* or *D2*) were produced.

Differentiating cells were modelled to pass through up to three phases, named the *D1*, *D2* and *D3* phases. The *D1* and *D2* phase cells could be produced from stem or transit cell division, with the *D1* cells representing those normally created in the basal layer of the epithelium (in healthy tissue) and *D2* cells representing cells normally created above the basal layer. Both the *D1* and *D2* cells eventually progressed into the *D3* phase. *D3* cells represented fully differentiated cells and existed for a finite period before being modelled to die through natural processes of apoptosis or sloughing of the superficial epithelium (Wright and Alison 1984, Aarnaes et al 1990, 1993).

Figure 4.1 summarises the cell types modelled, and the possible daughter cell products for each cell type.

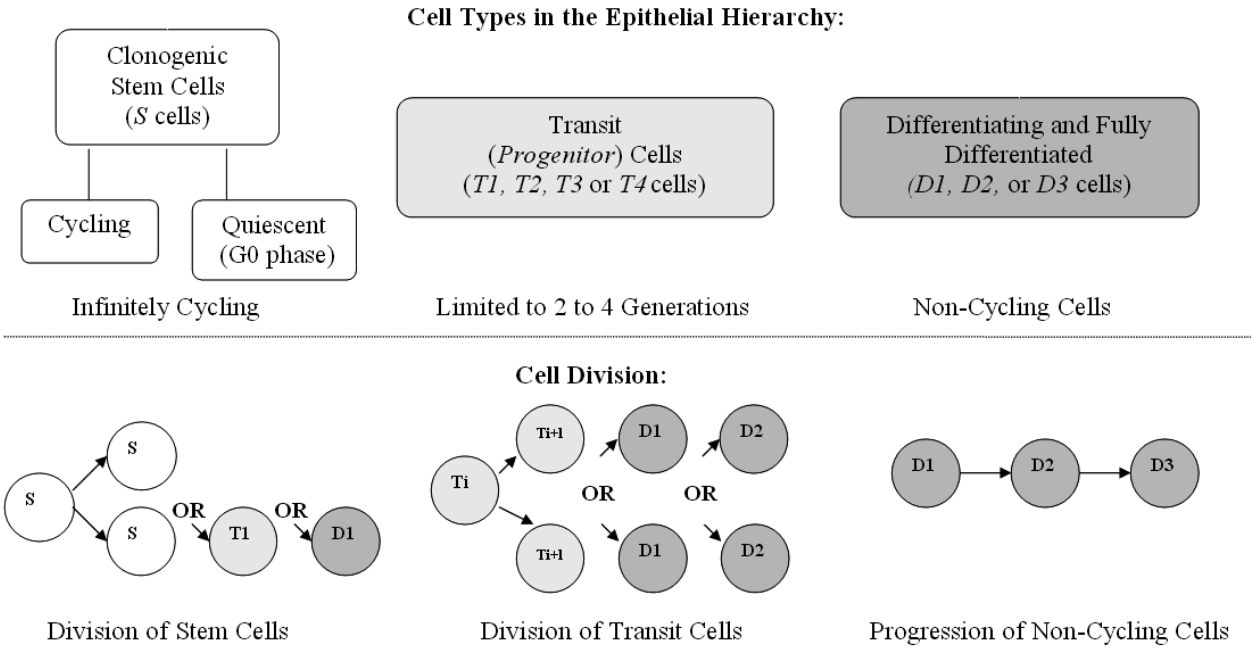

Figure 4.1. The epithelial cell proliferative hierarchy used in the model, outlining the different cell types modelled, and the daughter cell products of these cell types upon division.

Cycling cells were allocated CCT's from a truncated normal probability distribution, with a minimum possible CCT of 12 hours and a maximum CCT of 59 hours. The times allocated represented the period between cell creation and cell division. The mean and standard deviation of the cell cycle probability distribution were set considering the average CCT to be the length of the synthesis phase of the cell cycle multiplied by three and using data from published reports (Steel 2002, Aarnaes 1990, Begg 1990, Clausen 1981, Eschwege 1997, Hume 1990, Izquierdo 1972, Wilson 1988).

As previously discussed, all stem cells were modelled to experience an exponential stem cell G0 phase duration probability before entering the cell cycle. As the life span of a stem cell consisted of a G0 phase duration followed by duration in the cell cycle, the total life time was calculated as the convolution of the G0 phase exponential duration and the stem cell CCT probability distribution (normal). Figure 4.2 illustrates the stem and transit cell cycle time distributions.

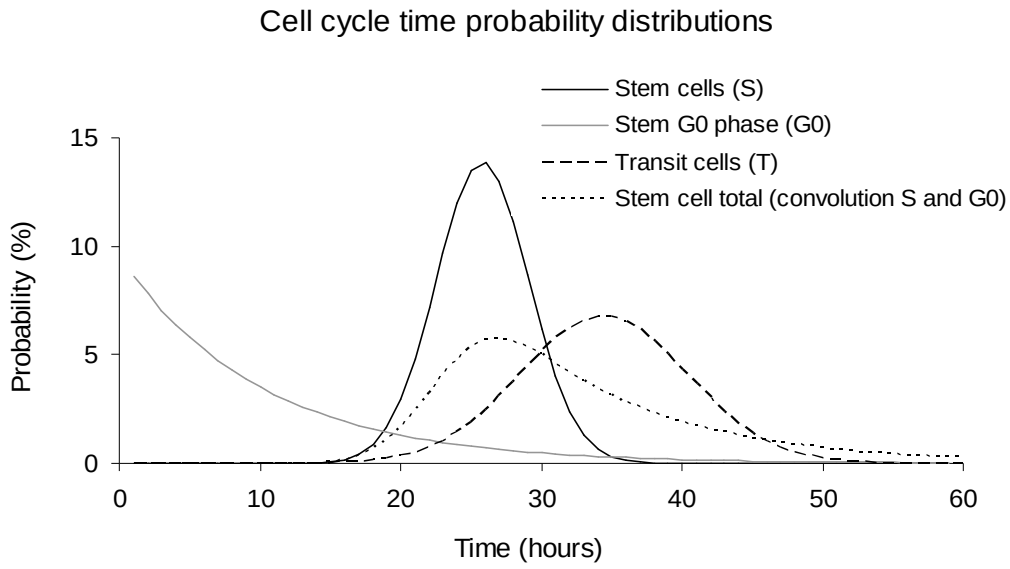

Figure 4.2. The probability distributions used for cell cycle time allocation in the model for transit and stem cells. The "Stem total" curve represents the overall lifetime probability of stem cells which first undergo a resting G0 phase followed by a cell cycle.

The differentiating cells were allocated durations according to a uniform distribution between 24 and 48 hours, and had 10% chance of apoptotic death. *D3* cells were modelled to have an 80% chance of dying to account for apoptotic as well as aging and sloughing of the epithelium. These death probabilities resulted in a biologically consistent cell population consisting of 60% to 70% *D3* cells and 80% to 90% *D1+D2+D3* cells. References and explanations regarding cell cycle times and differentiation phase durations are provided in the parameter overview section of this chapter (Table 4.2).

Although the layered structure of normal epithelial tissue is distorted in carcinomas compared to normal tissue, in this non-spatial model it has been assumed that the percentages of different cell types are approximately maintained. However, the modelled tumour cell population has an increased probability of symmetrical stem cell division, affecting the small (~1%) but critical percentage of stem cells in the tumour. This parameter is referred to as *Spercent* in this work and is equivalent to "*S*" in the *S:T1:D1* ratio for stem cell division, referred to at the beginning of this section.

Daughter cell type probabilities were determined based on published data reporting on the cell percentages present in epithelial tissue (Aarnaes 1990, Appleton 2002, Steel 2002, Wright 1984). Aarnaes and group investigated the percentages of proliferating and non-cycling cells in the basal layer of the epithelium, reporting a 12% to 50% *D1* cell population and an approximate 50% proliferating cell population. The group also estimated the percentage of cells in the G0/G1 phase awaiting migration to be approximately 20% in the basal layer. The total non-cycling population was assumed to be 80% to 90% for the total cell population, with the differentiated group of cells having a high probability of cell death. The data from Aarnaes and group was used in the current work to verify that the final percentages of different cell types were within biologically plausible ranges.

The approach of modelling the whole epithelial cell hierarchy, including non-cycling cells, assisted in more accurate modelling of epithelial tumour growth. As a result, the process of varying different tumour parameters to find their most accurate default values was made simpler, because the value could be set based on the impact it had on cell percentages within the tumour.

4.2.2. Cellular Oxygenation

4.2.2.1. The Distribution of Oxygen

To model realistic tumour oxygenation distributions, published HNSCC Eppendorf histogram data was used (and normalised) containing pO_2 values ranging from 0.0 to 100.0 mm Hg (Adam 1999, Lartigau 1998). Oxic tumours (with "normal" oxygenation) were assumed to have a uniform pO_2 distribution, with pO_2 values ranging from 5 to 100 mm Hg. The oxygen distribution for oxic tissue has been reported to have a normal-like shape, with a peak at 40 mm Hg (Petit 2009). However, the shape of the pO_2 distribution was not considered crucial in this model because the OER for the majority of the cells was well over 2.5 (corresponding to pO_2 values $\geq$ 15 mm Hg). The modelled pO_2 distributions along with two sets of published hypoxic tumour Eppendorf probe data sets are shown in Figure 4.3.

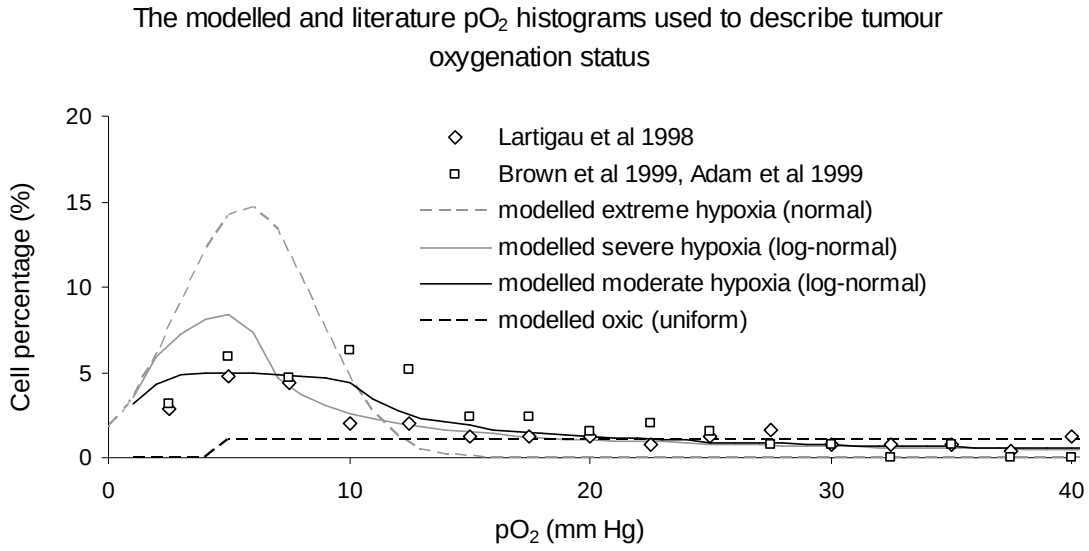

Figure 4.3. The distribution of oxygen levels used to simulate moderate and severe tumour hypoxia and oxic tumours, compared to published data. The modelled distributions represent the pO_2 histograms outputs from the model using a log-normal, normal or uniform random number probability distribution of pO_2 values to allocate cellular oxygenation.

Simulation results from the *HYP-RT* model focus on two hypoxic tumour types labelled "moderately hypoxic" and "severely hypoxic". The moderately hypoxic tumours were assigned log-normally shaped pO_2 distributions based on published data (Lartigau 1998), while the severely hypoxic tumours were assigned pO_2 distributions with an increase the number of cells in the low pO_2 range ($pO_2 \leq 10$ mm Hg), relative to the moderately hypoxic distribution (Figure 4.3). This increase was carried out while noting the impact on tumour growth rate and the percentage of cells being assigned to the quiescent phase due to very low oxygenation ($pO_2 \leq 1$ mm Hg).

Trial runs of the model for severe hypoxia with the percentage of hypoxia induced quiescent cells > 4% resulted in tumours with total growth times exceeding ten years or total cessation of growth, which was not considered reasonable due to the small size of the virtual tumour being grown (10^8 cells have a volume of approximately 0.8 cm^3 assuming spherical geometry and a cell diameter of 25 μm).

A fourth pO_2 distribution was later used to simulate an even more severely hypoxic tumour, labelled the extreme hypoxia distribution (used for treatment simulations,

presented in Chapter 5). The peak value of the *extreme* hypoxia distribution was kept the same as the other distributions; however the width was increased using a truncated normal function which substantially boosted the percentage of cells in the 0 to 10 mm Hg range (up to 95%).

Numeric pO_2 histogram data of the percentages of cells in various pO_2 ranges used in the model are presented in Table 4.1.

Table 4.1. The modelled percentages of cells in four commonly reported pO_2 ranges based on published tumour oxygenation histogram data.

pO_2 (mm Hg)	**Oxic (%)**	**Moderately hypoxic (%)**	**Severely hypoxic (%)**
0 to 1	0.0	3.1	3.5
0 to 2	0.0	7.3	9.4
0 to 5	1.0	22.1	33.2
0 to 10	5.2	45.6	54.5
0 to 20	15.6	65.4	69.6

The method of allocating cellular oxygenation levels from a pO_2 probability distribution is simple and unique compared to most recent models that simulate spatial oxygenation distributions by the diffusion of oxygen from uniformly or non-uniformly spaced capillary networks (Borkenstein 2004, Dasu 1998), or models that assume spherical geometry and use the radial distances of cells from the tumour periphery to determine oxygenation (Maseide 2000, McElwain 1993).

The current method has the advantages of simplicity and flexibility because the pO_2 distributions can be easily altered by the user and also varied during the growth or treatment in a single simulation, if required. The current method also enables a randomised method of assigning oxygen values to individual cells, which reflects the spatial and temporal irregularity of hypoxia observed within *in vivo* tumours (Ljungkvist 2002).

4.2.2.2. Applying Oxygen Values to the Cell Population

To implement tumour hypoxia in the model, pO_2 distributions were used to allocate a pO_2 value to each tumour cell, as explained in the previous section. The allocation

occurred at division of the mother cell. For a mother cell producing only one cell (e.g. when the second daughter cell was eliminated due to natural apoptosis), the pO_2 value of the mother cell was passed to the daughter cell.

When two daughter cells were produced, one cell was randomly chosen to retain the mother cell pO_2 value and the other received a new pO_2 value from the input pO_2 distribution. This method was chosen on the pretence that one daughter cell would replace the mother cell in terms of spatial location and that the other cell would move to a different (nearby or far away if migration occurred) location. For this work, a correlation between pO_2 values of "sister" cells was considered irrelevant, as only the overall tumour pO_2 distribution relevant to the model.

4.2.2.3. The Effect of Oxygen on the Cell Cycle

The duration of the cell cycle has been reported to increase with decreasing oxygenation, predominantly because of "arrest" or "delays" in the G2/M (and to a lesser extent G1 and S) phases of the cell cycle (Gardner 2001, Koritzinsky 2001, Webster 1998, Wilson 1995). The ability of tumour cells to survive in hypoxic conditions has been shown to be increased compared to normal cells due to phase delays, as well as the ability of the tumour cells to enter the G0 quiescent phase and survive for a number of days (Royds 1998). Survival mechanisms assisting the cell to adapt to hypoxic environment include the inducement of anaerobic metabolic processes and a reduced probability of apoptotic death.

To model this effect, CCT's for all cycling cells were adjusted based on pO_2 using a multiplicative "CCT adjustment factor" (Figure 4.4). Consequently, cells with the lowest oxygenation had CCT's 2.5 times longer than initially allocated.

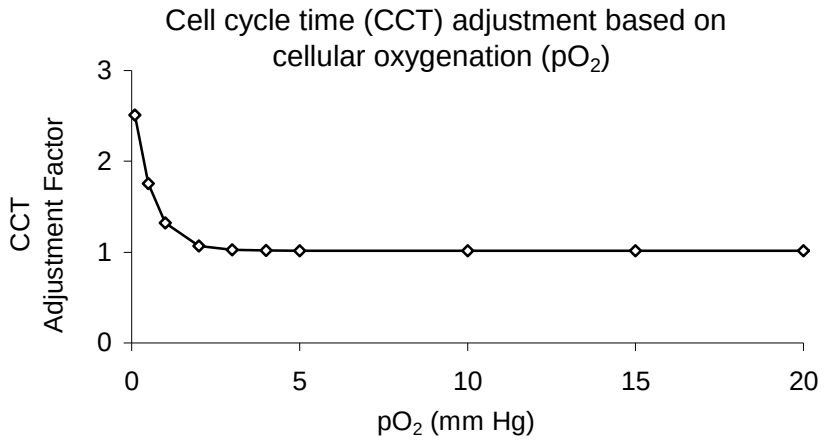

Figure 4.4. The CCT adjustment factor used to increase the duration of the cell cycle with decreasing pO_2, adapted from published data and fitted to an exponential curve (Alarcon 2004).

The CCT adjustment factor curve was derived from the work of Alarcon and group (Alarcon 2004), who formulated a relationship between CCT increase, *f*, and oxygenation, *x* (Equation 4.1) using constant values of y_0=33.27, a=58.88, b=1.73.

$$f = y_0 + a.e^{(-b*x)} \qquad (4.1)$$

In their modelling work, the CCT adjustment factor and pO_2 relationship was postulated based on a mathematical modelling. The curve plotted in Figure 4.4 was derived for the current work through normalisation of the curve postulated by Alarcon, such that the function had a value of 1 at 20 mm Hg.

Because of the need to increase CCT for cells with pO_2 levels < 20 mm Hg (and later decrease CCT if cells were reoxygenated), a *Time of Action* parameter was stored for each cell. This parameter provided information on the *global time* of division for the cell (with minute accuracy). In the event of a cellular pO_2 change, the CCT of a cell (or the time remaining the cell cycle) was adjusted according to the new pO_2 value. The time left remaining for the new CCT was then calculated, added to the current *global time* and then saved as the new *Time of Action* for the cell.

4.2.2.4. Hypoxia Induced Cell Quiescence and Death

A threshold value of 1 mm Hg was chosen for assigning cells to the hypoxia induced quiescent state, however the exact pO_2 is not clear from the literature, and is likely to vary for different cell lines. As such, only a percentage of cells (default of 50%) with pO_2 values $\leq$1 mm Hg were modelled to enter the quiescent phase. The default quiescent cell percentage was determined by trial and error, observing the total percentages of cycling and non-cycling cells with pO_2 levels $\leq$1 mm Hg. The aim was to keep the instantaneous pO_2 histogram of the modelled tumour that same as the original pO_2 distribution chosen by the user (e.g. for moderate hypoxia, a total cell population of 3% with pO_2 values $\leq$1 mm Hg). Cells in a hypoxia induced quiescent state were eliminated using a half life parameter with a default value of 4 days (Durand 1998).

To save computer memory, hypoxia induced quiescent cells did not have cellular attribute data saved. Rather, counter parameters was used to monitor the total number of cells of each type assigned to be quiescent (in the same way that *D3* cells were counted). If a quiescent cell was reoxygenated, the associated quiescent cell counter was decreased by one cell, and a new cycling or differentiating cell was inserted into the *Cellarray*. A quiescent hypoxic cell *half life* was implemented to kill a percentage of the cells in this group at regular intervals (5 hourly) to model cell necrosis. This was equivalent to halving the cell number every 4 days (default half life) but allowed for more frequent updates of total cell numbers.

4.2.3. Limitations and Assumptions

HYP-RT is a temporal model, implying that cellular properties relate only to cell kinetics and oxygenation, and not to spatial locations or coordinates. A temporal approach was taken to increase computational efficiency, as less data is required per cell. The model in its current state can propagate up to 10^8 cells. A cell population beyond this number is currently difficult to model due to the limitations of most off-the-shelf computers considering the amount of data storage required per cell.

Although the total cell number in the model is lower than the cell number found in most clinically detectable tumours (>10^9 cells (Hall 2006)) it was considered sufficient considering the stability of the statistical error of the model results (cell type percentage and tumour growth rate) for a cell population >10^7 cells, and the initiation of hypoxia at 10^6 cells.

Hypoxia has been reported to affect the rate of cellular differentiation (Chou 2004) and the radiosensitivity of newly reoxygenated cells compared to continually oxic cells (Bindra 2004, Koritzinsky 2001). However, these effects have not been considered in the current model. It should also be noted that no DNA or gene mutation mechanisms have been modelled in this work. Rather, cells are modelled as single entities, with no internal components. Only tumour cells have been considered in this work, and consequently no directly normal tissue effects (NTCP) could be predicted. However, Chapter 6 will outline a method of ranking altered fractionation schedules based on the biological effective doses (BED's) to normal tissues, assuming that they received 100% of the tumour dose.

4.2.4. Parameter Summary

In the tumour growth algorithm, there were four attributes used to describe a cell: the C*ell Type* (incorporating the generation number parameter for transit cells), *CCT* (minutes), *Time of Action* (the global time of cell division, in tumour hours) and pO_2 (mm Hg). Many other parameters were included in the model to control cell cycle division and radiotherapy related processes. These have been based on literature data where possible, including the necrotic cell death rate, the differentiated cell death rate and the threshold for hypoxic cell quiescence.

All relevant tumour growth algorithm parameters are outlined in Table 4.2, including default parameter values/ ranges and comments regarding the use of the parameter. Note that in some cases, the references given in Table 4.2 provide reports on methodology or a macroscopic parameter value which was then considered in simulations while setting the default microscopic/cellular parameter. Quantitative values for some model parameters,

such as the oxygenation threshold for cell quiescence and the length of time spent in the differentiating phases, are difficult to measure experimentally. Consequently these parameters were set through trial and error by analysing the impact on macroscopic tumour outcomes such as tumour growth rate and cell types in the population.

Table 4.2. The key parameters in the tumour growth algorithm of the HYP-RT model.

Parameter	Default	Parameter Range	References	Comments
celltotal	10^8	1 to 10^8	N/A	The fully grown tumour cell limit.
Spercent and subsequent $S{:}T_1{:}D_1$ ratio	S =3% T1 = 87% D1 = 10%	*Spercent* : 1 to 30%	(Steel 2002)	The symmetrical stem cell division probability, set to produce an approximate 1% total stem cell population in the tumour.
G0 stem cell phase duration (hrs)	5 hrs	Exponential, mean= 5 hrs	(Izquierdo 1972) Indirect: (Potten 1986, Wright 1984, Tannock 1998)	Total average Cell cycle time (CCT) (G0 and cycling phases) is ~ 33 hrs, with a small number of cells remaining in G0 for a relatively long time.
CCT (*S* cells) (hrs)	27 hrs	Normal, sigma = 3 hrs	Indirect: (Potten 1986, Wright 1984, Tannock 1998, Begg 1999, Mantel 2001)	The G0 phase adds to the length of time before stem cell division.
CCT (*T* cells) (hrs)	33 hrs	Normal, sigma = 6 hrs	Indirect: (Potten 1986, Wright 1984, Aarnaes 1990)	With 2 to 4 generations of division.
Differentiating time: *D1 & D2* cells	D1: 36 hrs D2: 36 hrs	Uniform: range of 24 to 48 hrs	Indirect: (Potten 1986, Wright 1984)	Estimate based on 1-2 week cell turnover in epithelial tissue based on 3 transit cell divisions.
Transit cell division in *D1 or D2* cells	D1: 80% D2: 20%	Constant	Indirect: (Potten 1986, Wright 1984, Aarnaes 1990)	This was set to produce a plausible differentiating cell population in the tumour.
Fully differentiated cell natural death rate (%)	D3: 80%	Constant	Indirect: (Steel 2002)	The cell loss rate (apoptosis and aging/sloughing) to achieve a total aver age cell loss of 85% for the whole population and the correct ratio of cell types.
Differentiating cell apoptotic death rate (%)	D1: 10% D2: 10%	Constant	Indirect: (Steel 2002)	Aging and spontaneous apoptotic death considered.
Oxygen distribution – moderate hypoxia	5 mm Hg	Log-normal	(Adam 1999, Lartigau 1998)	A log-normal describes the literature data using Eppendorf electrodes. Values range between 1 and 100 mm Hg.
Low oxygen limit for cell cycle arrest (mm Hg)	1 mm Hg	Constant	Indirect: (Alarcon 2004, Ljungkvist 2002)	At this pO_2 level hypoxia induced quiescence may be initiated.
Percentage of cells exiting the cell cycle (with pO_2 < 1 mm Hg)	50%	10 to 100%	N/A	With this percentage, the total number of hypoxia induced quiescent cells (< 1 mm Hg) = 3% of the total population, which agrees with the pO_2 histogram used.
Tumour cell number threshold for hypoxia	10^6	Constant	(Chin 2003, Conti 2002, McElwain 1979, Stanley 1977)	Hypoxia is implemented in the model after the cell number has reached this number, by initialising pO_2 allocation from the selected pO_2 histogram.
Hypoxic cell half life (due to necrosis: pO_2 < 1-2 mm Hg) (days)	4 days	Constant	(Durand 1998, Ljungkvist 2005)	Set due to the 4 to 10 day hypoxic cell lifetime in human colon carcinoma spheroids, and 2 days in xenograft HNSCC.

4.3. Algorithm Design and Analysis Methods

4.3.1. Programming Methods

4.3.1.1. Monte Carlo based Parameter Assignment

The Ziggurat *random number generation* algorithm (Marsaglia 2000) was utilised in the model to generate a random 32-bit integer sequence and convert the sequences into a set of random floating point numbers between 0 and 1. With this algorithm, numbers could be generated with a uniform or normal shaped distribution. For exponential distributions the Ziggurat algorithm was once again used but with the uniform outputs converted using a formula (logarithmic) to obtain the correct final distribution. For log-normal distributions, a different algorithm was used, written by J. J. Filliben (Modules *UNIRAN* and *LOGRAN* v82.6 1982).

Attributes were allocated to cells, or to parameters used for decision making in the model, based on the values of random numbers. For example, in the process of stem cell division, the second daughter cell was chosen using a single random number (linear distribution) and allocating the cell to be a stem cell if the random number was ≤ 0.029, a differentiating cell if between 0.030 and 0.13, and a transit cell if ≥ 0.14. This process created the desired ratio used in the model for the *S:T1:D1* ratio.

4.3.1.2. Programming Tools

The FORTRAN 95 programming language (complier v7.1.0, *Lahey Computer Systems Inc.)* was used to write the *HYP_RT* source code, within the *Visual Studio* framework (2003, *Microsoft Corporation*). The Java programming language (Java SE Development kit 6.17) and *NetBeans IDE* (v6.8 2009, *Oracle Corporation*) were used to develop the graphical user interfaces.

FORTRAN 95 was chosen for this project because of the computational speed achievable through the use of basic functions and commands. Early in development, the tumour growth algorithm was written in the MATLAB programming language and compared to

FORTRAN 95, using similar basic functions and programming styles. MATLAB proved to have more than a five fold decrease in computational efficiency compared to FORTRAN 95. Use of the 1995 edition of FORTRAN allowed each cell in the model to be declared and accessed as an *object*. Each *object* could have multiple attributes assigned and stored with data types ensuring a compact representation.

4.3.1.3. The Linked List Method of Data Management and Model Efficiency

Cell data was stored in a vector, called the *Cellarray,* with each element (or *object*) in the vector representing one cell. Six bytes were required per cell to store cellular attributes, with an additional four bytes required to store a *pointer index* value. The *pointer index* linked a cell to the location of the next cell due to divide (within the same hour of tumour time) within the *Cellarray*. Effectively, this process formed *hourly lists* of cells for the algorithm to process through in chronological order. Sixty separate *list pointer* elements were also used, one for each *hourly list* that a cell could be allocated (maximum CCT of 59 hours). The *list pointer* was required to locate the first cell in each *hourly list*.

Using this method, the *hourly lists* in the *Cellarray* provided maximum flexibility for the number of cells assigned to each hour of tumour time, while making use of all elements in the pre-allocated *Cellarray*. Furthermore, this arrangement met the random access requirement for efficient data access upon cell division and cell death. Alternative cell attribute storage methods were trialled for time and memory efficiency, e.g. a 2D matrix (with one column for each list of cells due to divide in the same hour) and a 3D matrix, using the third dimension to describe each cell attribute instead declaring cells as *objects*. These methods both increased data access time and increased memory usage because of the large number of matrix elements required.

Care was taken to develop a time and memory efficient tumour growth algorithm. This was assisted by coding the algorithm at a basic level with minimal use of libraries and in-built functions. Model results have been presented based on the growth of a 10^8 cell tumour. This cell number was chosen to limit the time taken to produce useful results, whilst propagating a sufficient cell population to model the initiation of tumour hypoxia at 10^6 cells. Computer memory requirements were are issue when exceeding 10^8 on a 2 to 4 GB RAM computer, considering the 10 bytes of memory required per cell. For oxic

tumour growth simulations, the average computation time was under fifteen minutes. For hypoxic tumours this extended to fifteen or thirty minutes because of the extra cell death occurring throughout growth. Increasing the *Spercent* parameter decreased computation time because of the higher proportion of cycling cells compared with non-cycling cells, and hence reduced cellular differentiation and cell death.

4.3.2. The Tumour Growth Algorithm Work Flow

The main processes involved in the tumour growth algorithm are shown in a flow diagram (Figure 4.5), where tumour growth is initiated by the division of one oxic stem cell. As cells divide, new daughter cells are created and all cell data for cycling and differentiating cells is stored in the *Cellarray*. The time increment used (*T*) was 1 hour. Tumour growth simulations are finished when the cell population reaches the maximum cell number set by the user (*cellmax).*

4.3.3. Tumour Growth Model Implementation

4.3.3.1. Parameter Input

A graphical user interface (GUI) (Figure 4.6) was developed to enable convenient input of key parameter values which were often varied during tumour growth and treatment simulations, as well as the running of multiple of simulations (batches), iterating over ranges of parameter values.

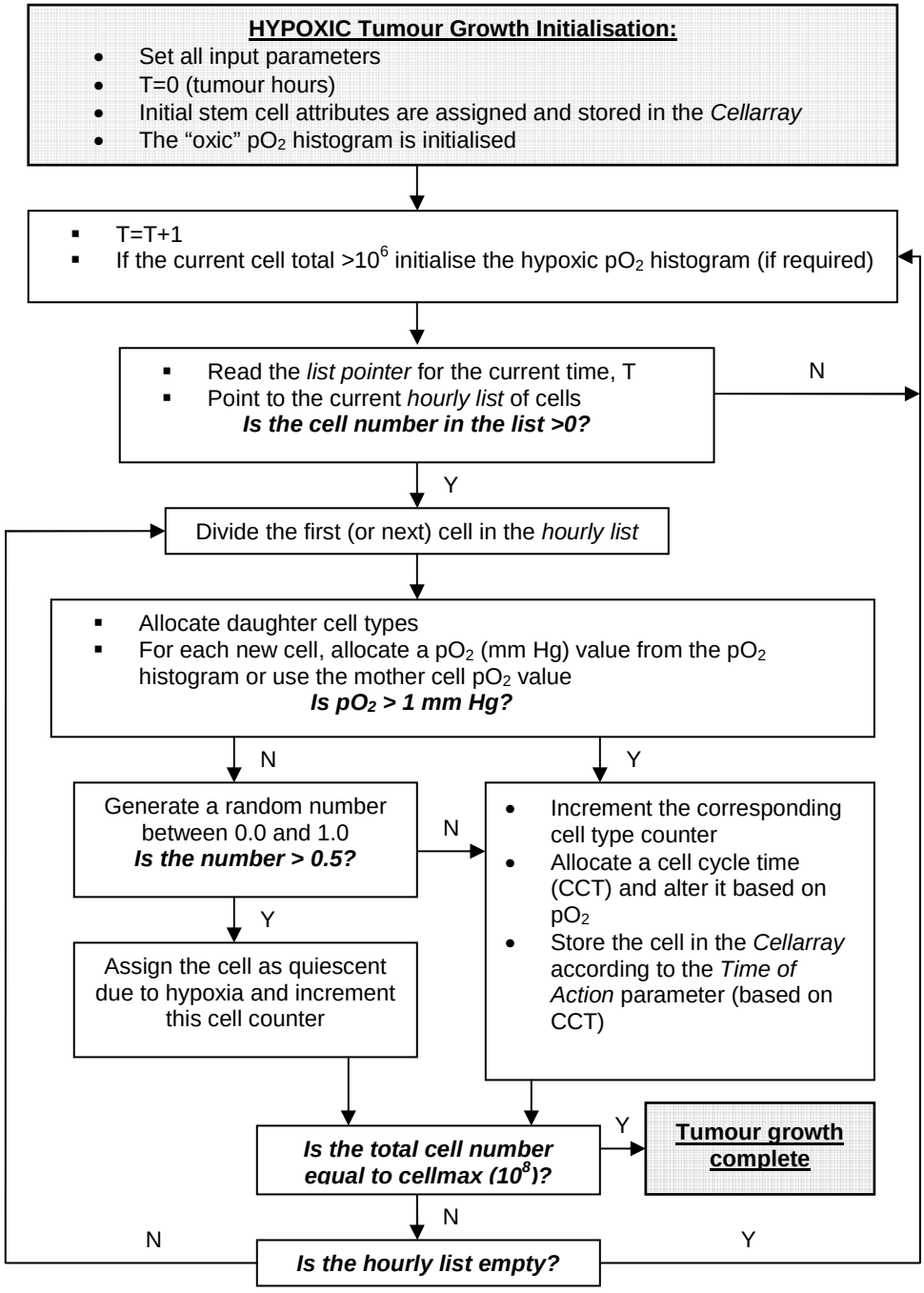

Figure 4.5. An outline of the HYP-RT tumour growth algorithm, where a single stem cell is propagated up to tumour consisting of 10^8 cells. The "Cellarray" is the cell storage vector and "cellmax" is the final number of cells.

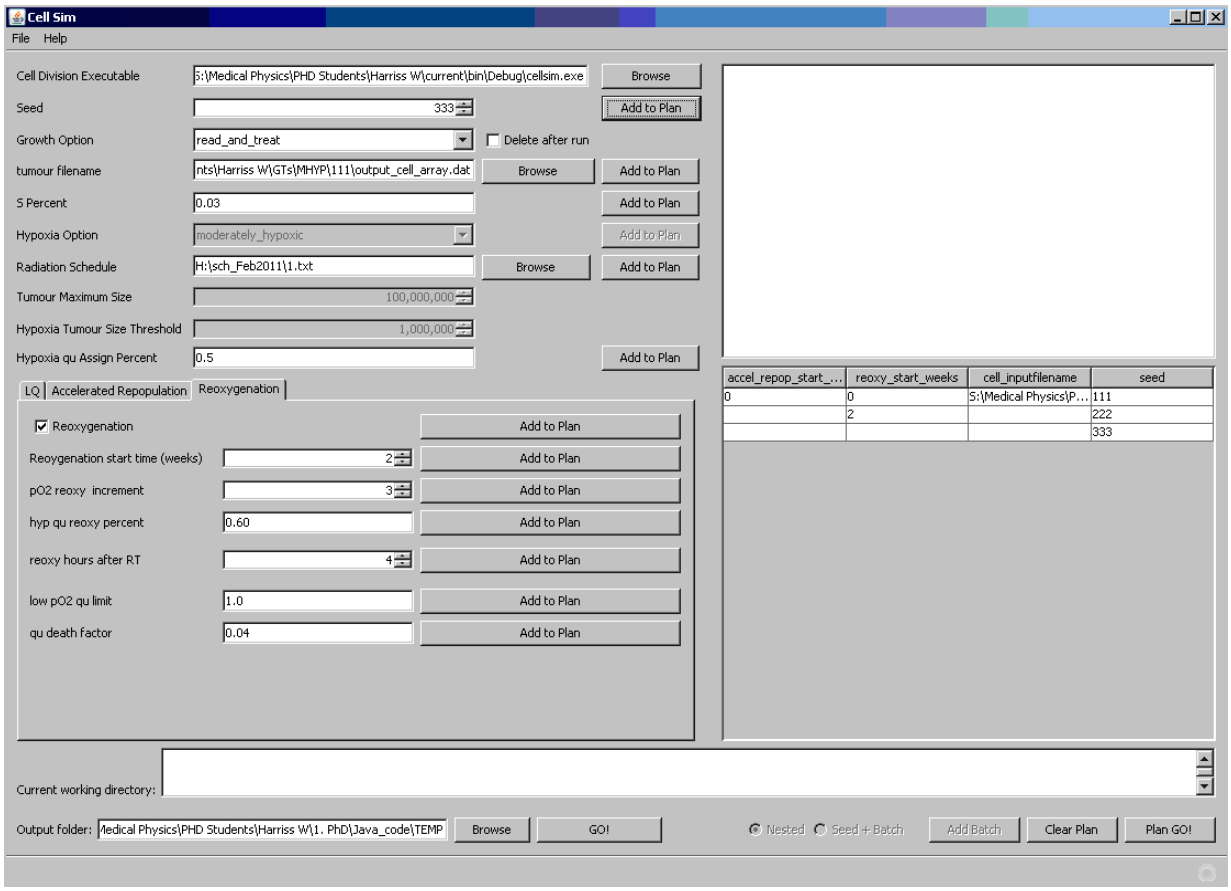

Figure 4.6. The graphical user interface, developed in the Java programming language to enable simple tumour and treatment related parameter value setting, and the initiation of multiple "batch" runs iterating over different random seed numbers and parameter values.

4.3.3.2. Simulation Output Analysis

After a tumour growth simulation, the *Cellarray* vector and a number of other real and integer parameters values were written out to file. A separate program and GUI was designed to access these files and report data such as the number and percentage of tumour cells of each type in the *Cellarray*, the number and percentage of quiescent hypoxic and differentiated cells and the tumour doubling time (T_D) when approaching the end of growth (10^8 cells).

The files also contained information including the oxygenation status, the *global time* when the total cell number (*cellmax)* was reached, and information regarding the pointer indexes/start position for the *hourly lists* in the *Cellarray*. As such, when virtual radiotherapy was required (immediately or at a later time), multiple simulations could be

run for the same tumour, using different treatment schedules or treatment response related parameters. This saved computation time considerably because the tumour growth simulations only had to be run once for each random seed number and oxygenation status.

4.3.3.3. Computer System Requirements

The *HYP-RT* model was designed to run on a computer with a Microsoft Windows operating system, with a minimum random access memory (RAM) of 2 GB. Simulations require the installation of a FORTRAN 95 and Java source code complier.

Future plans for the model include re-writing the model source code in the C++ programming language, to enable simpler GUI programming and interfacing, and for more simple extension of the model in terms of other potential users/researchers and for the use of additional modules which are already written in (or easily converted into) C++.

4.3.4. Statistical Methods

The statistical software package *Prism 5* (v5.02, *GraphPad Software Inc.* CA, USA) and the *Excel* (*Microsoft Office* 2003) were used for data analysis. Reported errors in this work correspond to one standard deviation in the results from five tumour growth simulations (reported on in this chapter) and nine radiotherapy simulations (three growth simulations and three treatment simulations per tumour), unless otherwise indicated.

Statistical significance between two data sets was assessed using a two-tailed t-test method (paired where indicated) using a confidence interval of 95% (significant for $p<0.05$). Correlation was calculated using linear regression (Pearson) with a confidence interval of 95%. Linear fit gradients and Pearson r values are presented with standard deviations and 95% confidence intervals respectively.

4.4. Tumour Growth Algorithm Parameter Analysis

An analysis of the growth algorithm was performed to deduce the influence of cellular parameters such as the symmetrical stem cell division probability (*Spercent)* and CCT, on aspects such as tumour doubling time (T_D) and the percentage of different cell types in the cell population. The results and discussion below relate to the effects of varying model parameters and the justification for setting of the default values used in the model.

4.4.1. Cell Kinetics of Oxic and Hypoxic Tumours

4.4.1.1. Stem Cell Division

The *Spercent* parameter had a large impact on the percentages of different cells types in the cell population, shown in Figures 4.7 a). The default *Spercent* value of 3% resulted in the most plausible distribution of cells and tumour growth rate (Aarnaes 1993, Aarnaes 1990) and a biologically plausible stem cell population of approximately 1% (Steel 2002).

Note that the hypoxia related default parameters were set to ensure that the percentages of cell types were consistent with the percentages from oxic tumour simulations (Figure 4.7 b). Some reports have suggested that a decreasing non-proliferative cell population due to spatially selective (locations away from blood vessels) hypoxia causes an increase in the stem cell percentage and contributes to the accelerated repopulation phenomenon (Steel 2002). However, quantitative data suitable for input into tumours models is difficult to find in the literature and more research is required before this issue can be tested in models, whether they are spatial and/or temporal in nature.

The T_D results from the model were in good agreement with head and neck clinical data (Steel 2002, Withers 1988). The tumour growth characteristics for simulated oxic and hypoxic tumours for *Spercent* values in the range of 2% to 30% averaged over 5 simulations are displayed in Figures 4.8. a) and b).The difference between oxic and moderately hypoxic tumour growth was significant for *Spercent* values $\geq$ 3%. On average, T_D increased from 37 days to 64 days for oxic versus hypoxic tumours using an

Spercent value of 3%, which agreed well with published HNSCC doubling time data (57 days, 95% CI 43-75 days) (Steel 2002). A value of 3% was therefore used for the default value of the *Spercent* parameter for all further simulations.

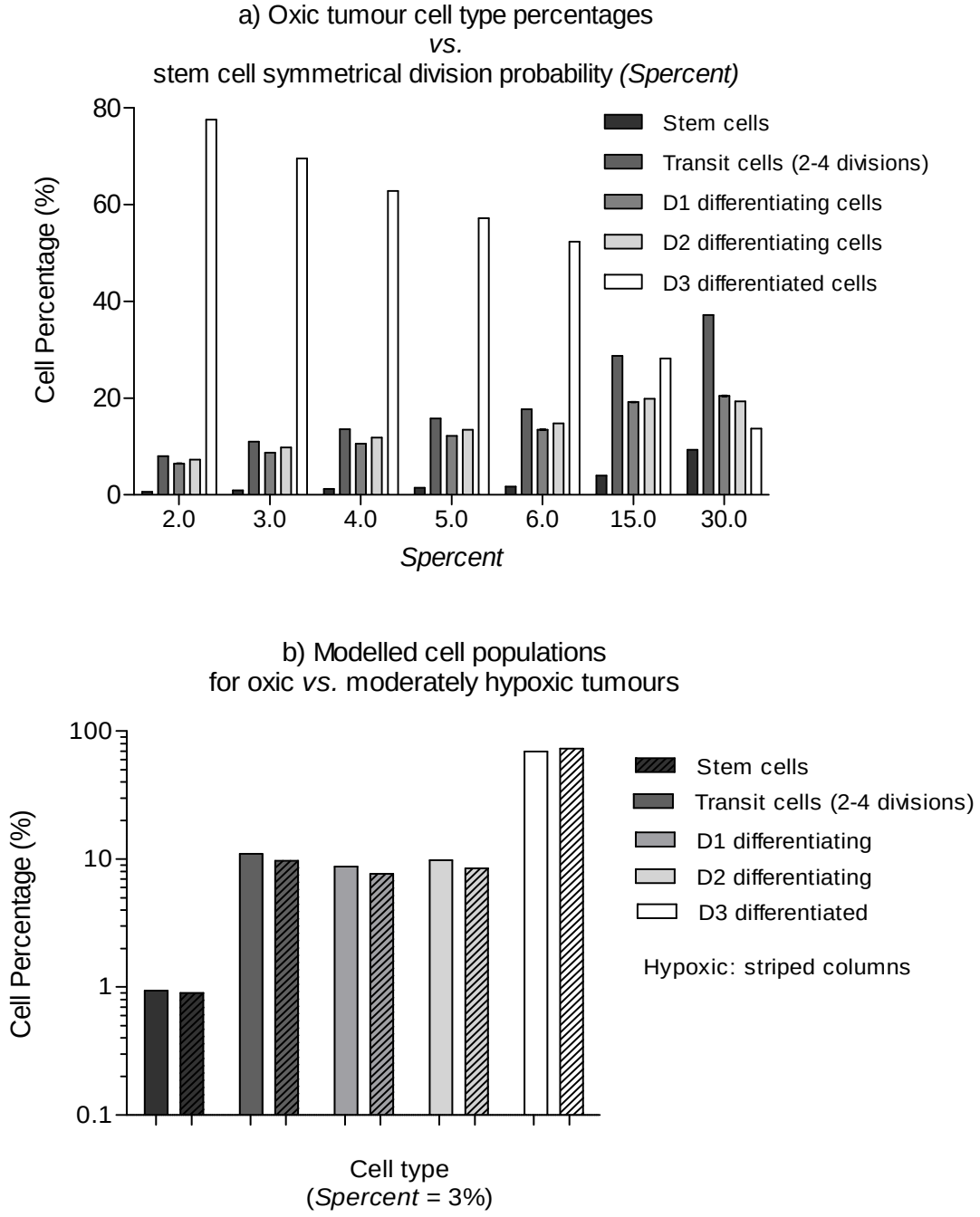

Figure 4.7. a) The average percentages of cell types within simulated tumours of 10^8 cells for a variety of Spercent values between 2% and 30% , and b) oxic versus moderately hypoxic tumour cell types in the population using an Spercent value of 3%.

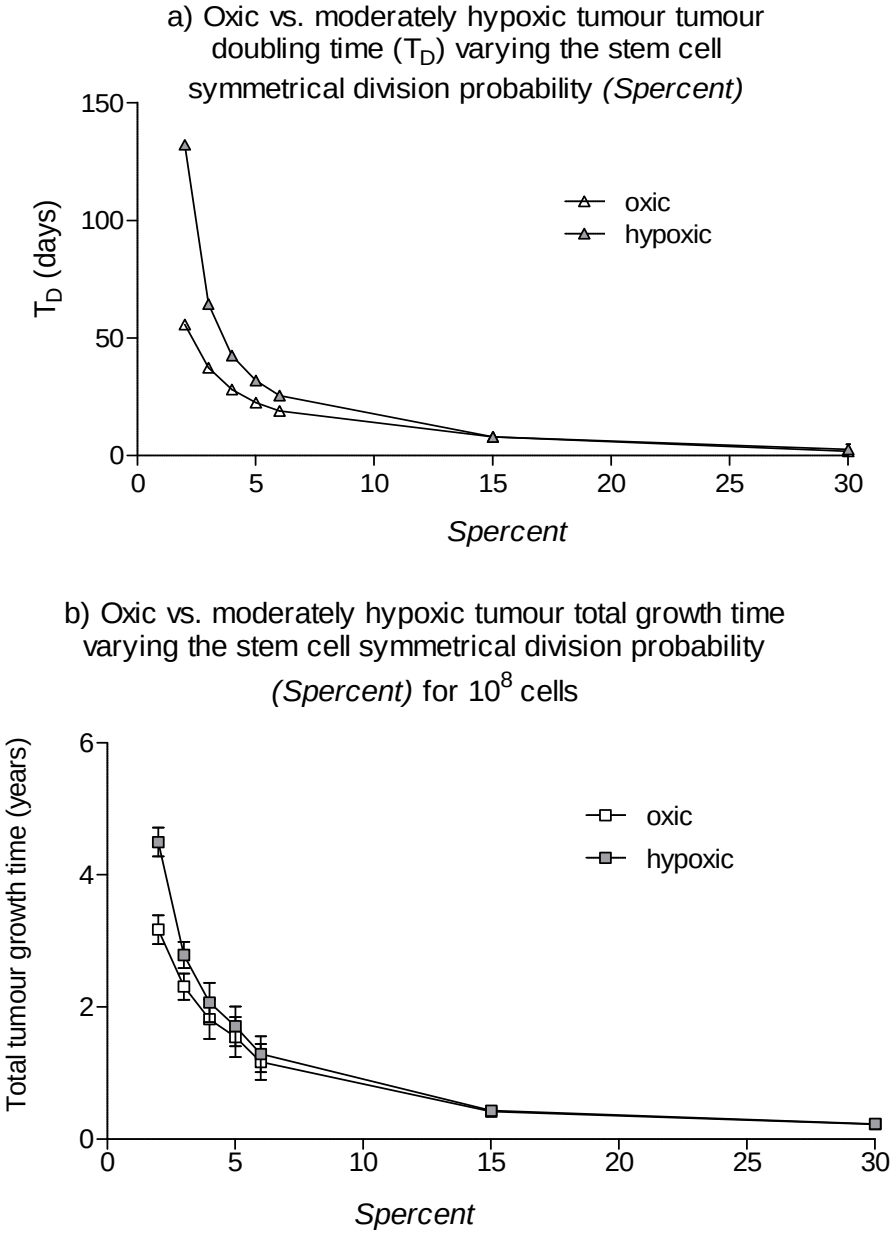

Figure 4.8. Simulation results of a) tumour doubling times (T_D), and b) total tumour growth times, varying the stem cell symmetrical division probability (Spercent) for oxic and moderately hypoxic tumours up to 10^8 cells. Note that the error bars in a) were smaller than the scale used.

Figures 4.9 and 4.10 show the tumour growth curves from oxic and moderately hypoxic tumour simulations for a range of *Spercent* values. Note that it is the initial difference in cell growth that dominates the total growth time, not the shape of the curve. For an *Spercent* value of 1%, cell death exceeded cell division, and therefore a cell number of 10^8 was not achieved for hypoxic tumours, and using an *Spercent* value of 3%, average

tumour growth time increased by 6 months for hypoxic tumours compared to oxic tumours.

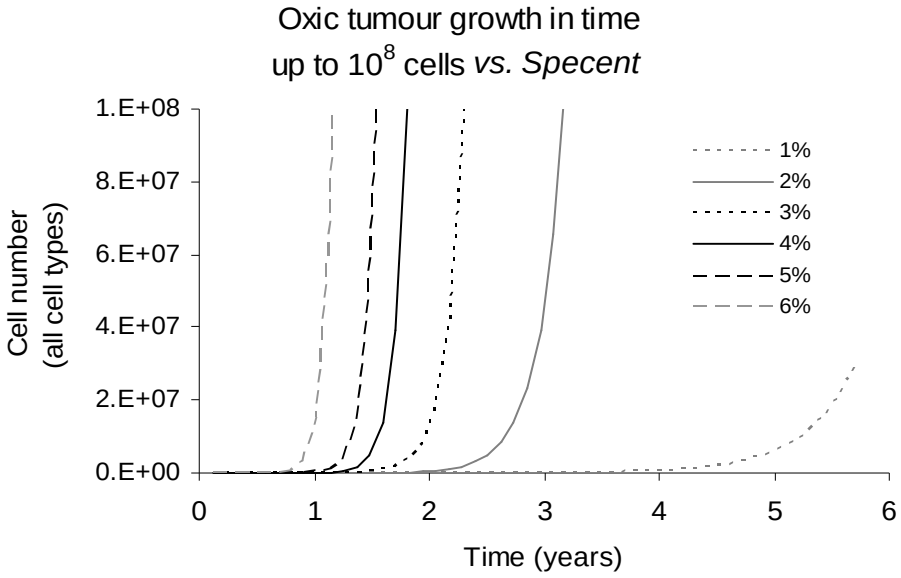

Figure 4.9. Oxic tumour growth curves for a range of stem cell symmetrical division probabilities (Spercent).

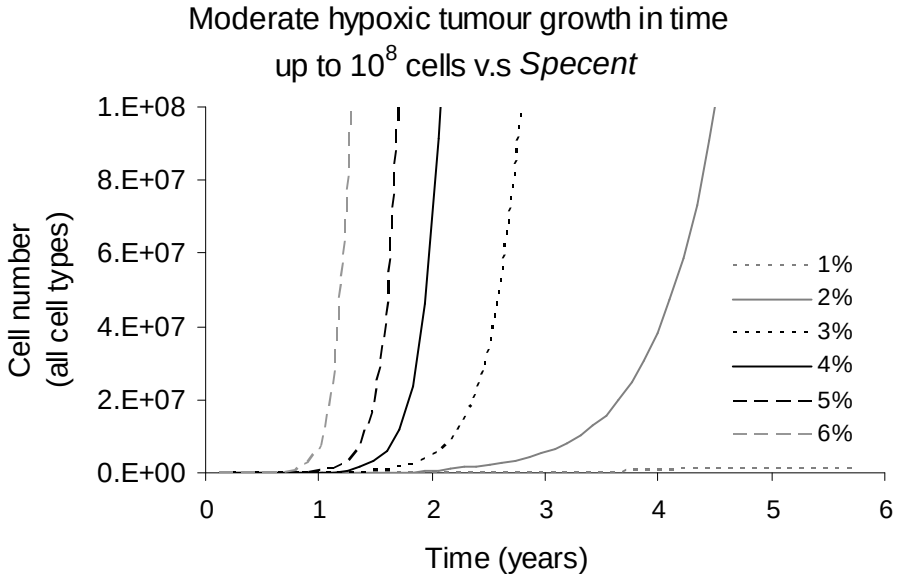

Figure 4.10. Hypoxic tumour growth curves for a range of stem cell symmetrical division probabilities (Spercent).

In Figures 4.11 and 4.12, the change and eventual plateau of T_D results for a range of *Spercent* values are displayed (from simulations using the same random seed number). The initial fluctuations in T_D in these figures highlight the instability of the tumour growth rate at small cell numbers.

At small cell numbers, the influence of the initial, however small, statistical variation in stem cell percentage dominates growth. This was apparent in both hypoxic and oxic tumour simulations.

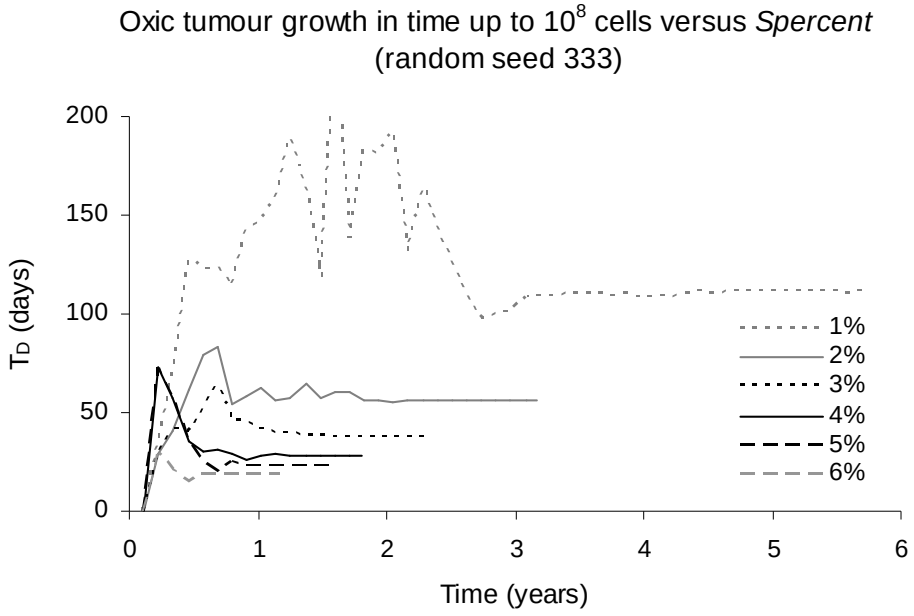

Figure 4.11. Oxic tumour doubling times (T_D) throughout growth, varying the stem cell symmetrical division probability (Spercent).

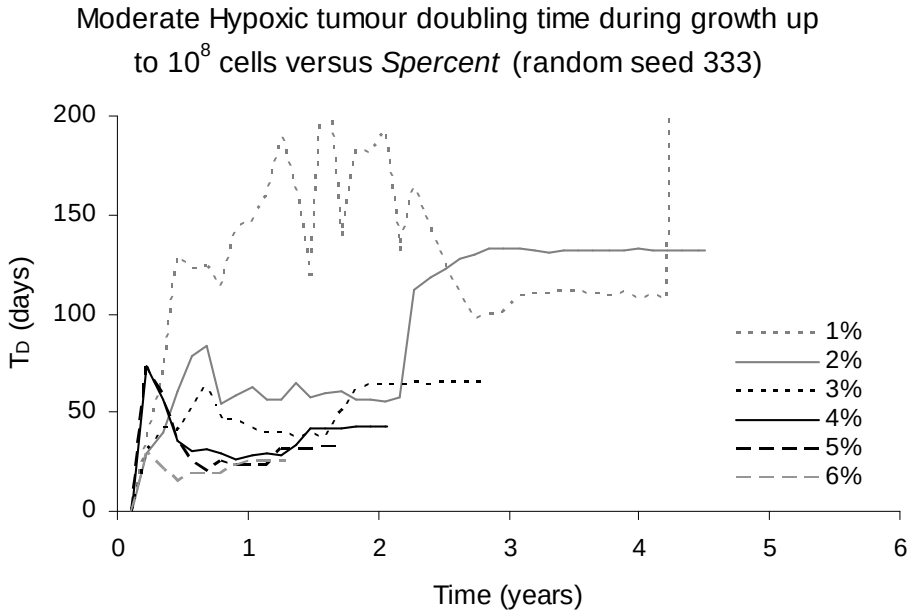

Figure 4.12. Hypoxic tumour doubling times (T_D) throughout growth, varying the stem cell symmetrical division probability (Spercent).

4.4.1.2. Transit Cell Division

Varying the number of generations of transit cells from a single value of three, to a distribution with an average of three, did not have a significant impact on tumour growth simulations. Further, varying the average generation value in the distribution (from 2 to 4) did not impact significantly upon tumour growth rate, but did slightly alter the percentage of transit versus differentiating cells in the population**.** A distribution of generation numbers with an average of three was used for all other simulations in this work.

Varying the probability for a final generation transit cell differentiating into either a *D1* or *D2* cell (default ratio for *D1:D2* = 80:20) also did not impact significantly upon tumour growth rate. This was expected as these cells were non-proliferating.

4.4.1.3. Cell Cycle Time and Cell Death

An analysis was performed to deduce whether the use of a normal distribution rather than a single value (equal to the peak value) had an impact on tumour growth rate. Using a single random seed number, simulations were run with stem cells and transit cells having both a distribution of CCT's and a constant CCT equal to the average value of the distribution. No significant differences in tumour growth rate were found for oxic or hypoxic tumour simulations. Despite this finding, the CCT's allocated to cells for the remaining simulations in this work utilised the normal CCT probability distribution, because a range in CCT's more closely resembles the kinetics of a real cell population.

Decreasing the *D3* cell death probability (representing losses due to aging and sloughing) did not influence the final tumour growth rate, but did decrease total growth time. Growth time decreased because on average the *D3* cells took longer to die, and hence the cell population reached the maximum size in a shorter period of time. However, as these were non-cycling cells, the instantaneous growth rate remained the same. The *D3* cell death probability parameter was held at the default value of 80% for all other simulations.

4.4.2. Oxygen Distribution Effects

In the previous section, the influences of full oxygenation and moderate hypoxia on tumour growth rate were discussed. In this section, the tumour growth characteristics for severe hypoxia are reported and compared to oxic and moderate hypoxia, as are the effects of varying other hypoxia related parameters. Severe hypoxia simulations used the same default parameters as previously mentioned for moderate hypoxia, e.g. the pO_2 threshold for quiescence and quiescent cell half life.

These parameters once again maintained the relative percentages of cells in the population, with the exception of a slight deduction in the stem cell percentage for *Spercent* values of 2% and 3% (Figure 4.13). However, this reduction had no significant impact on tumour growth time or growth rate for moderately compared to severely hypoxic tumours (Figure 4.14).

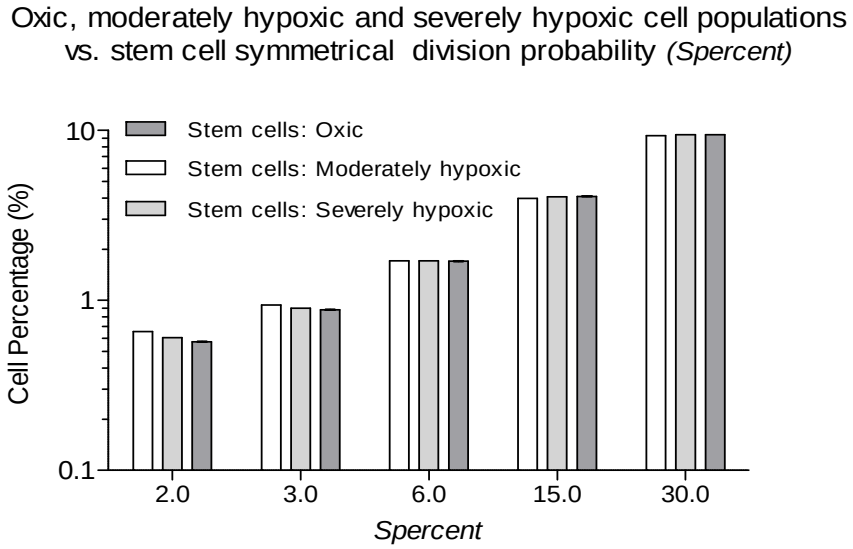

Figure 4.13. The stem cell percentages in simulated tumours of three oxygenation levels, varying the stem cell symmetrical division probability (Spercent) from 2%, up to the maximum possible value of 30% (the latter is applicable during accelerated repopulation). Note that the standard deviations are not visible on this scale.

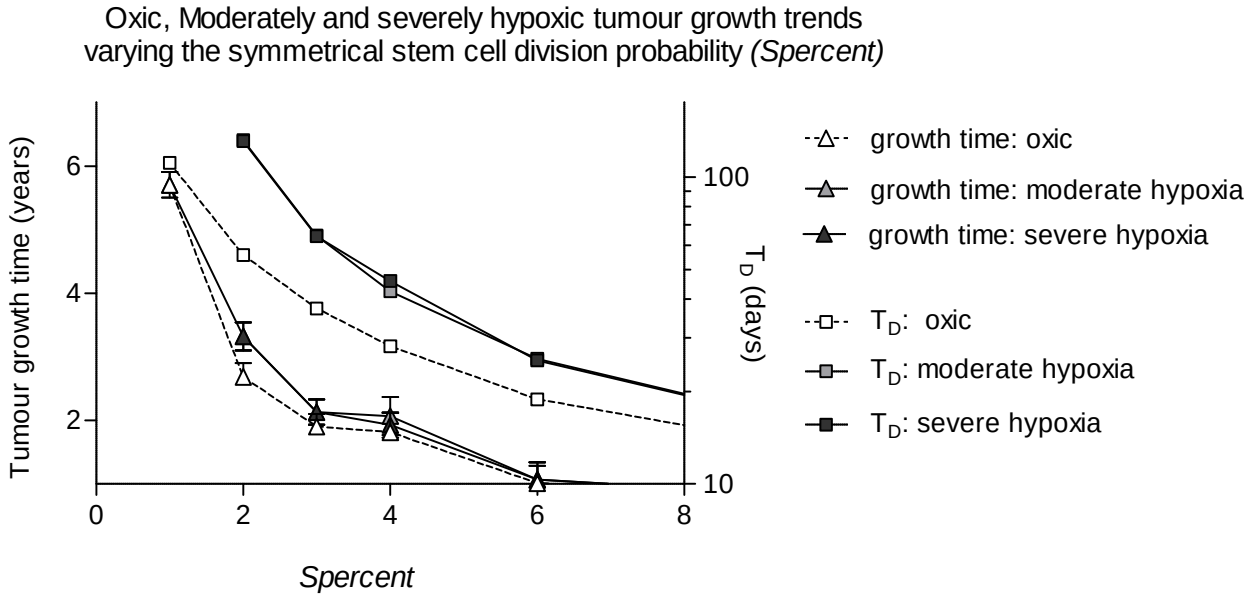

Figure 4.14. Tumour growth and doubling times (T_D) for three different tumour oxygenation levels. Note that there is no data for hypoxic tumours for Spercent = 1% because of a lack of tumour growth using this value.

When altering the percentage of hypoxia induced quiescent cells (allocated quiescent if $pO_2 \leq 1$ mm Hg) away from the default value of T_D was affected, however total tumour growth times did not change significantly (Figure 4.15). As previously discussed, the default value (50%) for this parameter was set to achieve a final percentage of cells with $pO_2 \leq 1$ mm Hg (3%), corresponding to the pO_2 histogram data shown in previously in Figure 4.3.

The half life of hypoxia induced quiescent cells also did not impact significantly on tumour growth rate, as this group of cells formed a very small percentage of the total cell population. However, it did have an impact on the proportion of cycling versus non-cycling cells (Table 4.3) when varied from 2 to 6 days. The default half life of 4 days resulted in the desired 3% population of cells with $pO_2 \leq 1$ mm Hg.

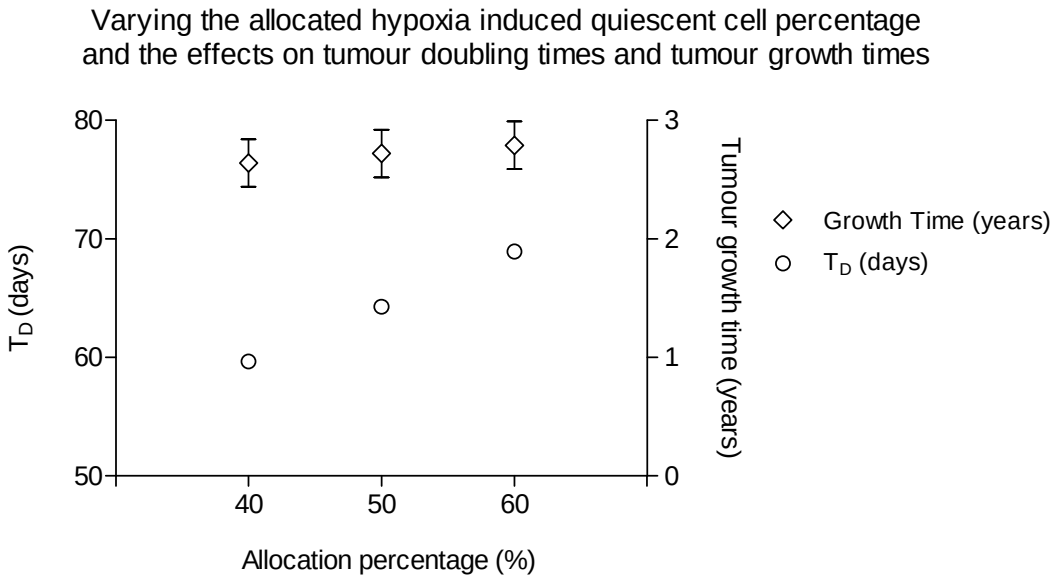

Figure 4.15. The impact of the hypoxia induced quiescent cell percentage on tumour doubling times (T_D), controlling the number of cells that cease to cycle when their pO_2 value fall to 1 mm Hg.

Table 4.3. The impact of the hypoxia induced quiescent cell half life on tumour growth and stem cell percentage.

Cell half life of hypoxia induced quiescent cells	Tumour growth time (years)	Tumour doubling time (days)	Stem cell (cycling) number	Stem cell (quiescent) number with $pO_2 \leq 1$ mm Hg	Stem cell (quiescent) percentage with $pO_2 \leq 1$ mm Hg (%)
6 days	2.363	63.95	8.56×10^5	4.91×10^4	3.6
4 days	2.368	63.95	8.74×10^5	2.62×10^4	**2.9**
2 days	2.371	63.95	8.82×10^5	1.56×10^4	1.7

4.4.3. Random Seed Number Effects

To quantify the impact of the random number seed on tumour growth time and rate, five different seeds were initially used in simulations for oxic and hypoxic tumours (Figures 4.16 and 4.17). The increase in T_D at approximately 1.5 years for hypoxic tumours was due to the initialisation of hypoxia which slowed the growth of the tumour because of increased cell cycle times and necrotic cell death.

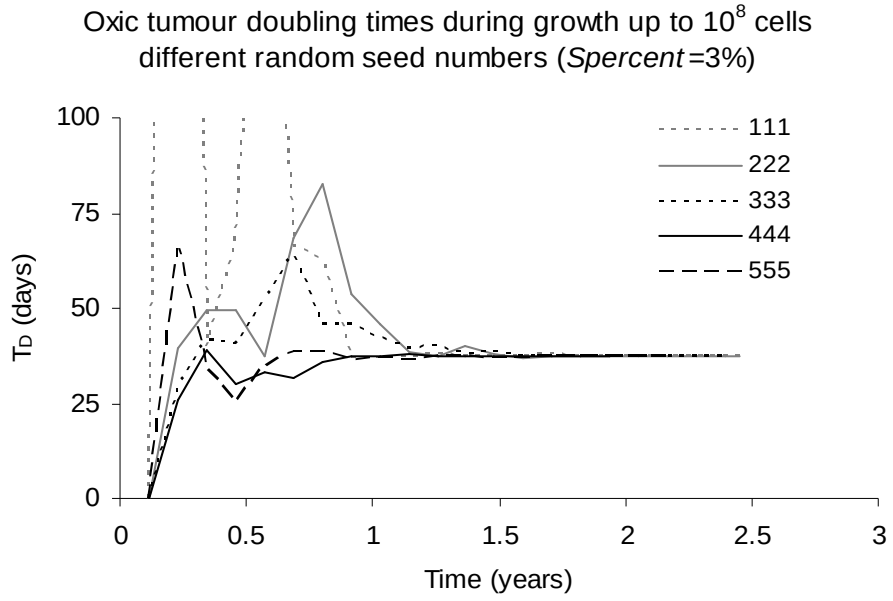

Figure 4.16. Oxic tumour doubling times (T_D) for five different random seed numbers, showing the change in T_D over the entire period of growth. The Spercent stem cell parameter was held constant at 3%.

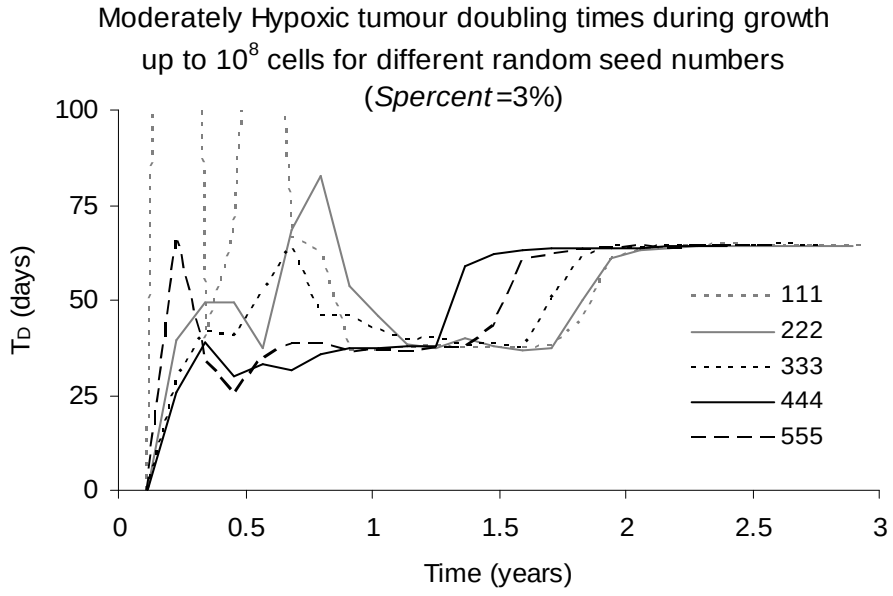

Figure 4.17. Hypoxic tumour doubling times (T_D) for five different tumour random seed numbers, showing the change in T_D over the entire period of growth. The Spercent stem cell parameter was held constant at 3%.

After the stem cell population exceeded 10^5 cells (after one year of tumour time), the T_D for all simulations remained steady regardless of the choice of random seed number. Fluctuations in T_D decreased to less than one day for small *Spercent* values and a few days for *Spercent* values greater than 3%. For the case of random seed "111" in Figure 4.16, the initial high stem cell number had a large impact on tumour growth, reducing total growth time but not the growth rate as the tumour approached 10^8 cells.

As the percentages of different cell types, and consequently the final tumour growth rates, were the same within statistical error using different seed numbers in the tumour growth algorithm, a limited set of three tumours were used in the majority of the fractionated radiotherapy simulations discussed in Chapters 5 to 7 of this report.

4.5. Tumour Growth Algorithm Conclusions

A tumour growth algorithm was successfully developed for the simulation of oxic and hypoxic tumour cell proliferation. The algorithm used Monte Carlo methods to propagate and store individual cells of various proliferative capacities according to epithelial cell hierarchy, starting from one infinitely proliferative stem cell. Other cell types included transit cells, differentiating cells, fully differentiated cells, G0 phase quiescent stem cells and hypoxia induced quiescent cells.

Cell data was stored in a pre-allocated 1D vector array of object elements (the *Cellarray*), with each element corresponding to a single cell and requiring 10 bytes of memory. Linked list methods allowed for efficiency and chronological division of cells, which were sorted into *hourly lists* within the Cellarray, according to the hour at which the cells were due to divide (based on their cell cycle time).

Oxygenation probability distributions (pO_2 histograms) were utilised to assign cellular oxygenation values to cells upon division. In the model, reduced oxygenation slowed down the cell cycle of stem and transit cells, and induced cell quiescence for a proportion of cells with $pO_2 \leq 1$ mm Hg. Hypoxia induced quiescent cells died of necrosis with a half life of 4 days.

The parameter dominating tumour growth rate was the *Spercent* parameter, which controlled the probability of stem cell symmetrical division. This parameter was set to a default value of 3% which resulted in plausible tumour growth doubling times of 37 days for hypoxic tumours and 65 days for oxic tumours, and realistic percentages of different cell types comprising the tumour (1% stem cells and 80% to 90% non-cycling cells).

Model parameters were set ensuring that the relative percentages of cell types were maintained when simulating tumour hypoxia. Tumour growth time (in years) and growth rate in terms of doubling time (in days) were analysed for tumours of three oxygenation levels (oxic, moderately hypoxic and severely hypoxic). Hypoxia slowed tumour growth considerably because of cell cycle slowing and cell necrosis, with hypoxia affecting all cell types equally.

There were no significant changes in tumour growth properties when modelling *moderate* versus *severe* hypoxia in the model, as defined in Figure 4.3. Therefore it was deduced that an even more severe pO_2 distribution, with a higher percentage of cells in the lower pO_2 range, must be required to slow growth beyond a doubling time of approximately 65 days (discussed further in Chapter 5, for radiotherapy of virtual tumours with *extreme* hypoxia). This however would slow the growth well beyond the average doubling times for HNSCC reported in the literature of approximately 40 to 60 days (Steel 2002).

The tumour growth algorithm has the advantage of being intuitive for the input of initial parameters and being computationally efficient, while tracking the propagation of up to 10^8 cells with a biologically realistic epithelial cell hierarchy. Further, the distribution of oxygen among the cells may be easily varied by changing the input pO_2 histogram, allowing the user to explore the effects of hypoxia on tumour growth. All results presented in this chapter are the average outcomes from five simulations, varying the random seed number in the tumour growth algorithm.

Chapter 5

Modelling of the Effects of Conventionally Fractionated Radiotherapy

5.1. Introduction

Following successful modelling of oxic and hypoxic tumour growth up to 10^8 cells, the next goal was to develop an algorithm to model the effects of ionising radiation on the tumour, taking into account the radiosensitivity of each tumour cell during a fractionated course of radiotherapy treatment.

The key features of the radiation effect model include the modelling of accelerated repopulation (AR), gradual tumour reoxygenation (ROx), and oxygen enhancement ratio (OER) curves encompassing a large range of oxygen values (pO_2). Further, the OER curves were modelled to be dependent on dose per fraction.

The model was designed to predict the number of treatment fractions required to kill all tumour cells with potential to grow back the tumour, i.e. the fraction number required to achieve 100% tumour control probability (TCP). For user convenience, the entire cell population history throughout tumour evolution could be saved to file after each simulation, allowing details such as the instantaneous pO_2 histograms and the number of hypoxic, quiescent and cycling cells, to be analysed at any desired time point during treatment.

The initial radiotherapy schedule modelled was the 5x2 Gy per week conventional fractionation schedule, the results of which will be presented in this chapter. The 5x2 Gy schedule is still the most commonly used schedule in Radiation Oncology worldwide for many tumour sites, including the head and neck. It was therefore chosen when performing comparisons between the *HYP-RT* model and the control arms of clinical

trials. The model allows for the simulation of any desired fractionation schedule, with discussions regarding altered fractionation schedules included in Chapters 6 and 7 of this report.

This chapter will first discuss the development of the radiation effect algorithm, and outline the parameters and mechanisms used to model cell death, cellular oxygenation and reoxygenation, as well as cell propagation during treatment. A description of the methods used to model AR and explanation on the *AR boost factor* parameter used to control the stem cell symmetrical division probability are provided, as this parameter heavily influenced simulation outcomes. Experimental work performed to validate the range of biologically plausible tumour ROx onset times (murine xenograft oxygenation experiment) to use in the model will be also be outlined.

After analysing the parameters employed to model radiotherapy, results are presented from radiotherapy simulations using different combinations of oxic and hypoxic tumour AR and ROx onset times, with the number of 2 Gy fractions (or total dose) required to achieve tumour control reported. Conclusions are drawn about the validity of the model through comparison of the total dose results with the doses usually prescribed for real human tumours as well as comparisons of the model with linear quadratic (LQ) theory.

5.2. Mechanisms and Parameters in the Radiation Effect Algorithm

5.2.1. Modelling of Radiation Induced Cell Death

The radiotherapy algorithm was developed to simulate the effects of fractionated therapy, assuming that a uniform dose is delivered to all cells. The model requires information from the user including the fractionated schedule desired, the α/β ratio, and the onset times of AR and ROx (in weeks). If no information is provided, the default model parameters are used for the simulation. Selection of a treatment schedule involves choosing a schedule from the list of eleven pre-defined clinical trial schedules or creating

a new schedule through the development of a basic data file (containing all necessary dose and fraction scheduling data). This section outlines the mechanisms used to model cell kill and the way in which oxygen related radioresistance has been incorporated in the model. This is discussed in terms of the theory behind the mechanisms used and the programming techniques employed to apply the mechanism into the radiation effect algorithm.

5.2.1.1. Linear Quadratic Cell Kill

The LQ theory of cell survival, previously outlined in chapter 2, was used to calculate the average cell survival probability for cycling oxic cells. The surviving fraction was then converted to a *cell death probability* value between 0.0 and 1.0, for use in the model. This was calculated for each cell, for each dose fraction in the schedule. The default α and β values used were 0.3 and 0.03 respectively were used (α/β = 10 Gy). Consequently, for a standard 2 Gy treatment schedule the SF_2 (for oxic cycling cells) was 48.7%. Results discussed in Chapter 6 extend on results presented in this chapter, and concern altered fractionation schedule outcomes using doses per fraction, *d*, as low as 1.1 Gy, with SF_d values also calculated using LQ theory.

5.2.1.2. Oxygenation Dependent Cell Kill

For each treatment fraction, cells were assessed chronologically within the *Cellarray* vector (discussed in chapter 4) to determine whether they were to survive or die for each dose fraction. For cycling cells, final *cell death probability* was calculated using the SF_d as well as a dose per fraction dependent OER factor (Figure 5.1a) (Denekamp 1998, Dasu 1999, 1998, Joiner 1988).

The OER function was used in a normalised form (Figure 5.1b); with the final function representing the factor applied to the calculated SF_d value to reduce cell death probability with decreasing pO_2 (if $\leq$ 40 mm Hg). Dose per fraction effects were implemented in the model in preparation for the simulation of hyperfractionated radiotherapy schedules.

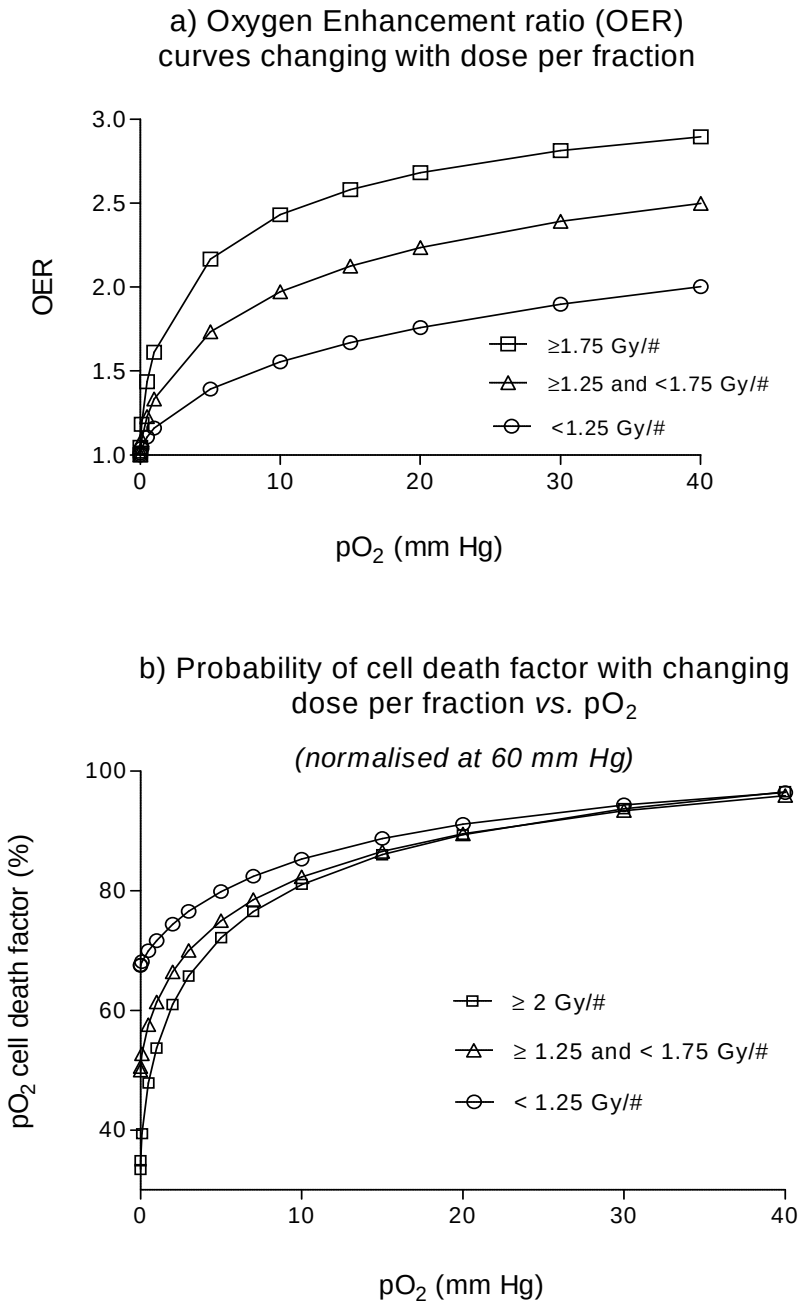

Figure 5.1. a) Oxygen enhancement ratio (OER) curves implemented in the model for adjusting the radiosensitivity of cells during radiotherapy, based on cellular pO_2 and dose per fraction (Dasu 1998, 1999, Kirkpatrick 2004), and b) conversion of the OER curves into a cell death probability function.

Results from investigations into the differing radiosensitivities of hypoxic cells that are hypoxic because of acute compared to chronic hypoxia have been reported (Brown 1979, Spiro 1984) with differences attributed to the way that energy from the radiation exposure is deposited, differences in gene expression, DNA repair capacity and cellular kinetics (Wilson 2007). However, these effects were not model in the current work.

Quiescent cells, with pO_2 levels ≤1 mm Hg, were also eliminated by radiation induced cell death using a multiplicative death factor. The default death factor for these cells was set to 0.41, corresponding to an average pO_2 value of 0.5 mm Hg for this cell group. The number of surviving quiescent hypoxic cells after each dose fraction was set reducing the original number of cells, C_0, by the cell number to be eliminated, $C_0SF_d0.41$.

5.2.2. Modelling Reoxygenation

Reoxygenation of tumours during treatment has the potential to re-sensitise previously resistant tumour cells to subsequent doses of radiation and hence improve TCP. However, to quantify the improvement in cell kill in a temporal model such as *HYP-RT*, information regarding the dynamics of reoxygenation is required, including the level of pO_2 increase to apply to the tumour cells and the frequency and timing of the pO_2 increases during the treatment schedule.

5.2.2.1. Reoxygenation Algorithm Development

The gradual rise in tumour oxygenation levels during radiotherapy was simulated by the allocation of small pO_2 increments to a percentage of randomly chosen cells in the population. These increments (default size of 3 mm Hg) were applied as a series of discrete “events”, occurring at a set interval (default of 4 hours) after each dose fraction. During the ROx events, the randomly selected cells had their pO_2 attributes increased by one or more pO_2 increments (i.e. by 0, 3, 6, 9 or 12 mm Hg) and their CCT’s decreased accordingly.

The number of cells randomly chosen to receive increases in pO_2 were based on Binomial theory (Equation 5.1);

$$P_k = \binom{n}{k} p^k (1-p)^{n-k} \tag{5.1}$$

where n is the total number of oxygen increments (equal to the number of cells in the population at the current time), k is the number of pO_2 increments applied to a cell, and P_k is the probability of a cell receiving a kx3 mm Hg increase in pO_2. Values of k ranging from 0 to 4 were used in the model, with the corresponding percentages of cells receiving k increments shown in Table 5.1. The probability of five or more increments was below 0.5% and regarded as negligible.

Table 5.1. The percentages of cells, P_k, affected during reoxygenation "events" in the model, where k is the number of increments of 3 mm Hg allocated to the cells to increase their oxygenation attributes based on Binomial theory.

Number pO_2 of increments (k)	**Cell percentage affected (P_k) (%)**
0	36.6
1	37.0
2	18.5
3	6.1
4	1.5

The default oxygen increment size of 3 mm Hg was chosen based on trial and error, observing the timing and tumour size at which full oxygenation of the tumour occurred. The goal was to achieve full tumour oxygenation when the tumour had shrunk to a cell number between 10^5 to 10^6 cells (corresponding to a tumour diameter of 1 to 2 mm, assuming spherical geometry and an average cellular diameter of 25 µm). An initially hypoxic tumour was defined as "oxic" during a radiotherapy simulation, when all hypoxia induced quiescent cells had been eliminated and all cellular pO_2 values were ≥ 5 mm Hg.

Cells previously assigned to the quiescent phase also had a probability of having their pO_2 level increased, and consequently re-entering the cell cycle. This was modelled using a parameter to control the percentage of cells retrieved from the quiescent cell group, after which they could be allocated parameters and re-entered into the *Cellarray*.

ROx information required for the model included the onset time of ROx (in weeks) and the delay time to implement ROx "events" after individual dose fractions. This was investigated using an experimental study involving *in vivo* tumour xenografts in a mouse model and the FaDu HNSCC cell line. The aim was to quantitatively investigate tumour oxygenation levels using a fibre optic probe system during an accelerated course of radiotherapy (OxyLab System, *Oxford Optronix* Pty. Ltd.).

Hypoxia was also visually confirmed in this experiment, using the biological marker *Pimonidazole* and subsequent immunohistochemical analysis. Experimental results led to the conclusion of a late average ROx onset time of 2 weeks in the accelerated radiation schedule applied to the xenografts (40 Gy in 12 days). Due to limited animal numbers and technical issues, data relating to the timing of ROx after each radiotherapy fraction could not be obtained and therefore a default value of four hours was used in the *HYP-RT* model (Ljungkvist 2002). The section below provides a summary of the experimental study, based on a published report (Harriss 2010).

5.2.2.2. Onset Time of Tumour Reoxygenation: An Experimental Study

5.2.2.2.1. Experimental Design and Methods

An immuno-deficient mouse model was used to develop tumour xenografts derived from a human head and neck pharyngeal squamous cell carcinoma cell line (FaDu). *In vivo* pO_2 measurements were performed, with the aim of assessing pre-treatment and inter-fraction oxygenation levels during a course of radiotherapy. The information of interest was the timing of onset of ROx, as well as the degree and timing of pO_2 increases during radiotherapy. Measurements of pO_2 were made in six animal groups after increasing numbers of daily radiation fractions. Measurements utilised a fibre optic probe system (*Oxford Optronix* Pty. Ltd.) using fluorescence quenching and feedback signalling to report tissue oxygenation (Collingridge 1997, Young 2006). Tumours received radiation

doses ranging from 0 to 40 Gy (3 or 5 Gy per fraction), with dose delivered once per day for a maximum of 12 days.

Cell and Animal Preparation

The FaDu human pharyngeal squamous cell carcinoma cell line (donated by the Peter MacCallum Cancer Centre, Melbourne) was plated with Roswell Park Memorial Institute (RPMI) media solution and foetal bovine serum (10%). A total of seventy 6 to 8 week old Balb/c nu/nu female mice (University of Adelaide, Waite Campus) received a subcutaneous injection of $2x10^6$ cells in 50 µL to the right hind flank. Tumours up to 7 to 8 mm in diameter were established (15 days of growth), at which diameter hypoxic areas were demonstrable, without the use of clamps to artificially induce hypoxia (Petersen 2003). Tumour volume (*volume=length.width*^{2}*/2*), and weight records were kept daily.

Irradiation and Oxygenation Measurement

Preliminary studies to observe the welfare and tolerance of the animals to the irradiation and oxygen measurement procedures under anaesthetised conditions, as well as to observe tumour response to daily irradiation were performed. In the main experiment the tumours were exposed to 3 Gy per day up to a maximum dose of 40 Gy (later accelerated to 5 Gy per day, see discussion). The original schedule consisted of 15x3 Gy over 19 days. Both the planned and delivered schedules provided a similar biological effective dose (BED) (Fowler 2003) compared to the conventional 5x2 Gy per week schedule (±5%), using the standard BED formula (Equation 6.2, outlined in the next chapter ???) with a kick off time T_k of 21 days, a T_{pot} of 3 days, an α value of 0.3 Gy^{-1} and an α/β of 10 Gy. The flow chart shown in Figure 5.2 outlines the timing of the procedures performed on the groups of mice.

Mice were caged in groups of five, forming eight experimental groups. Mice were selected for these groups based on tumour size, to ensure that an even range of tumour diameters (between 2 to 6 mm) were allocated to each group. Two mice were kept as control animals to observe non-irradiated tumour growth.

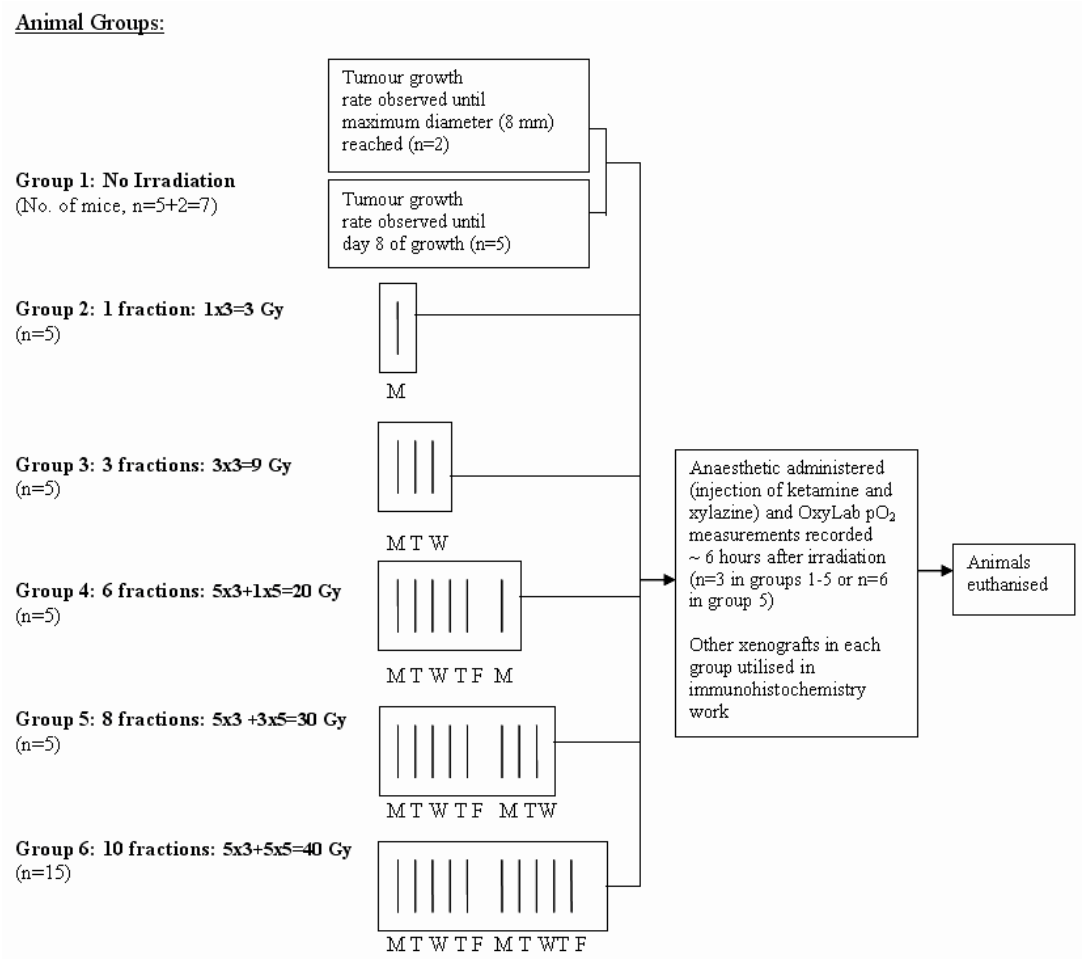

Figure 5.2. ***The irradiation and pO_2 measurement schedule for the tumour xenografts (n=42), where pO_2 measurements were performed after 0, 3, 9, 20, 30 or 40 Gy in 20 mice, with the remaining xenografts used in immunohistochemical hypoxia staining work.***

To irradiate the tumours to therapeutic doses using x-ray radiation (6 MV radiation beam from a 6/100 Varian linear accelerator) and to minimise acute normal tissue reactions, a technique was developed to restrain the animals during dose delivery. The restraining technique greatly reduced the extent of irradiation outside of the tumour mass and meant that the mice could be irradiated unanaesthetised. Daily administration of anaesthetic during irradiation was avoided because of the effects on blood flow and tissue oxygenation (Baudelet 2004), however it was necessary during pO_2 measurement. The effects of anaesthetic on pO_2 measurements using the OxyLab system have been reported as having minimal impact on the measurements on the minute time scale (Urano 2002).

A radiation field size of 2 x 35 cm^2 was used, with the field covering the lower abdomen, hind legs, and base of the tail of each of the 5 mice in each group. Wax bolus (*Jelonet*

paraffin gauze) 9 x 3 x 1 cm^3 was fitted between each animal to provide radiation scatter conditions (Figure 5.3 a). Individual conical shaped bags were made to restrain the mice during irradiation (Figure 5.3 b).

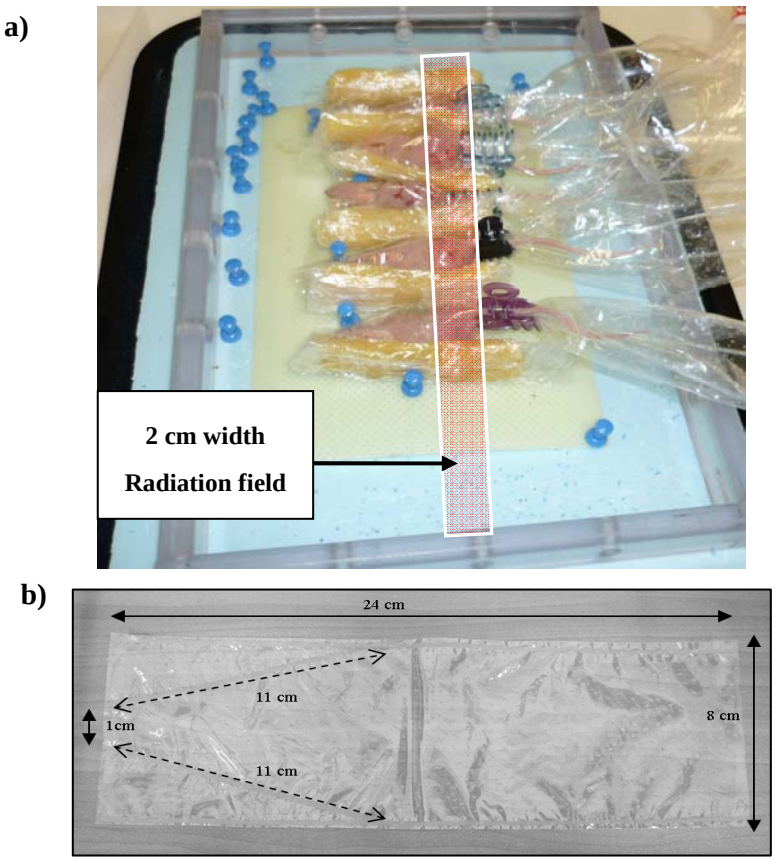

Figure 5.3. ***a) the animal irradiation tray and a 2 x 35 cm^2 radiation field aligned over the pelvis and hind leg, for a group of mice in restraining bags with adjacent wax bolus, and b) the plastic heat pressed bag used for animal restraint during radiotherapy. The plastic was perforated to prevent perspiration build up and overheating, and pinned to the tray during irradiation.***

The OxyLab pO_2 system (on loan courtesy of the Austen Health Centre, VIC) was used to measure pO_2 levels in the tumour xenografts. This system was chosen because of the advantages relating to real-time pO_2 tissue oxygenation readings. These include the small sampling volume (approximately three cell layers, or 0.25 to 0.35 mm^3), the use of relatively thin probes to minimize tissue disturbance, and the fluorescence signalling design of the system which does not consume oxygen during the measurement process. The system is thus particularly useful for tissues with small volumes and very low oxygenation.

The measurements of oxygenation in the OxyLab system are based on illumination and excitation of a fluorophore with light pulses from a blue light emitting diode (LED). The fluorophore is platinum based and located 2 mm back from the probe tip. The fluorescent light emitted from the probe radiates into the surrounding medium, where the presence of oxygen molecules quenches the signal proportionally to the oxygen concentration.

The instrument measures the reduced lifetime of fluorescence of the reflected signal and displays a value for pO_2 (in mm Hg or kPa) according to the Stern-Volmer equation (Equation 5.2), where T_0 is the fluorescence lifetime in the absence of O_2, T is the fluorescence lifetime at the given O_2, I_0 is the fluorescence intensity in the absence of O_2, I is the fluorescence intensity at the given oxygen level and k is the Stern-Volmer quenching constant.

$$\frac{T_0}{T} = \frac{I_0}{I} = 1 + k[O_2] \qquad (5.2)$$

The instrument uses phase-modulation to determine fluorescence lifetime: both the excitation and the emission light are phase-modulated and the phase-angle is used in the calculation. The fluorescence technique has the advantage of being more sensitive at lower pO_2 levels (<60 mm Hg) due to the longer fluorescence lifetimes compared to methods relying on redox reactions within the tissue (polarographic electrodes), thus making the system particularly useful for tissues with low oxygenation, as discussed earlier.

Pre-calibrated bare fibre optical probes (BF/O/E) with a 230 µm width shaft and 280 µm tip diameter were used with the OxyLab system (Figure 5.4). Oxygen measurements were recorded in units of mm Hg and were displayed along with the current thermocouple temperature in continuous mode on the unit, and with a chosen output range of 0 to 100 mm Hg (resolution of 0.1 mmHg and accuracy of 0.7 mm Hg).

Figure 5.4. The OxyLab system fibre optic probe manufactured Oxford Optronix Ltd (230 µm width shaft and 280 um tip diameter) used for in vivo pO_2 measurement.

To measure tumour pO_2 using the OxyLab system, animals were anaesthetised to restrict movement and minimize discomfort during the invasive procedure. Xenografts from each fractionation group were analysed for tumour oxygenation (pO_2), with a single calibrated probe, and with the use of an animal heating pad and lamp. A delay of 4 to 6 hours post-irradiation was waited before commencing pO_2 measurement. This delay corresponded to limited data of the likely ROx time of tumour tissues of head and neck origin. (Lartigau 1998, Ljungkvist 2006).

A micromanipulator was used to hold and drive the probe along two perpendicular tracks for each tumour (Figure 5.5). Various measurement positions along the tumour track were achieved by slowly pulling the probe back out of the tumour along the track. Measurements of pO_2 were recorded point by point from the data display on the OxyLab unit, along with animal temperature. Automatic adjustment of pO_2 with temperature was enabled by positioning a 100 µm copper thermocouple wire under the animal. Temperature monitoring was necessary to verify animal welfare and because of the dependence of pO_2 on temperature. Light anaesthetic proved effective for up to 30 minutes.

To complement the OxyLab tumour oxygenation measurements, immunohiochemical staining was performed to visualise the hypoxic areas in the total cell population in a subset of the xenografts (n=2 per dose group). The aim was to verify the presence of hypoxia and to observe the spatial distribution of hypoxia in the tumours before treatment, after treatment, and when no treatment was delivered (larger control tumours).

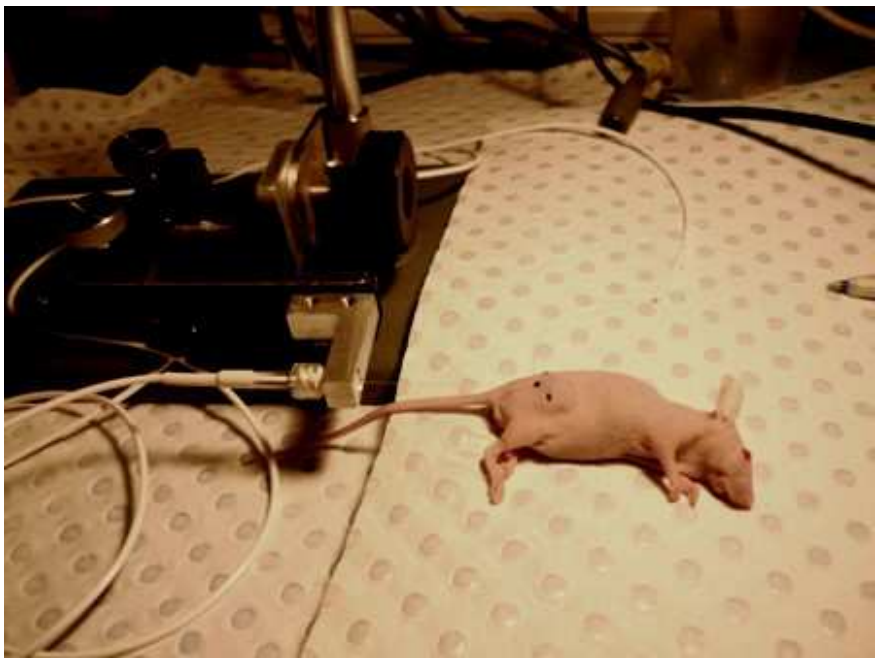

Figure 5.5. The set up of the mouse and hind leg FaDu xenograft for OxyLab pO_2 probe measurements using a micromanipulator, with the probe entering the tissue in the inferior to superior direction.

The hypoxia marker *Pimonidazole* (Hypoxyprobe^{TM}, HPI, Inc.) was injected before excise of the tumour, to bind to the hypoxic tumour cells. Tumours were then excised, frozen in liquid nitrogen and shipped in dry ice for analysis (Department of Radiology, Radboud University Nijmegen Medical Center, Nijmegen, The Netherlands, with the kind assistance of Professor A. van der Kogel and his team gratefully acknowledged).

Frozen sections (5 µm) were fixed in acetone and the Hoechst 33342 profusion marker signal recorded on air-dried tissue sections. After rehydration, consecutive tumor sections were triple-stained using the methods below, for Pimonidazole (green), Hoechst 33342 (red) and the BrdUrd proliferation marker (blue) [Adapted from Ljungkvist et al 2006]. Pimonidazole was detected with a polyclonal rabbit anti-Pimonidazole (a gift from J. A. Raleigh) and donkey anti-rabbit F(ab9)2Alexa488 (Molecular Probes, Eugene, OR).

For the staining of the blood vessels, undiluted 9F1 supernatant [rat monoclonal to mouse endothelium, (Department of Pathology, Radboud University Nijmegen Medical Centre, Nijmegen, The Netherlands)] and chicken anti-rat ALEXA647 (*Molecular Pro*bes) were used. For BrdUrd staining, the tumor sections were first denatured in 0.2N HCl for 10 min followed by neutralization for 10 min in 0.1 *M* borax. BrdUrd was visualized with

sheep anti-BrdU IgG (*Abcam* Ltd., Cambridge, UK) and donkey anti-sheep F(ab9)2-Cy3 (Jackson Immuno Research). For analysis of the BrdUrd labeling index, all nuclei were stained with propidium iodide (Molecular Probes).The tumor sections were mounted with Fluorostab (ICN Pharmaceuticals, Inc.) and analysed quantitatively with a semi-automatic image recording system, as routinely used by the Nijmegen group (Ljungkvist 2005, Rijken 2000, Rijken 2002).

Dosimetry

Verification of surface dose delivery was performed using thermo luminescent dosimetry (TLD) using lithium fluoride (LiF TLD-100) in 1 x 1 cm^2 sachets, which were compared to TLD capsules irradiated under reference conditions. Results indicated that the correct surface dose (within 5%) was delivered to the tumours. A Pinnacle (*Philips Medical Systems*) treatment planning system verification was performed, through calculation of dose using an imported CT image of three mice in the treatment position and a single 6 MV modelled beam.

Figure 5.6 shows the Pinnacle^3 isodose curves for a transverse CT slice of 3 mouse set-up for irradiation, and the approximate positions of the tumours. The isodose curves show that the tumours receive approximately 100% of the desired dose at the surface and 95% or more at or near the tumour centre.

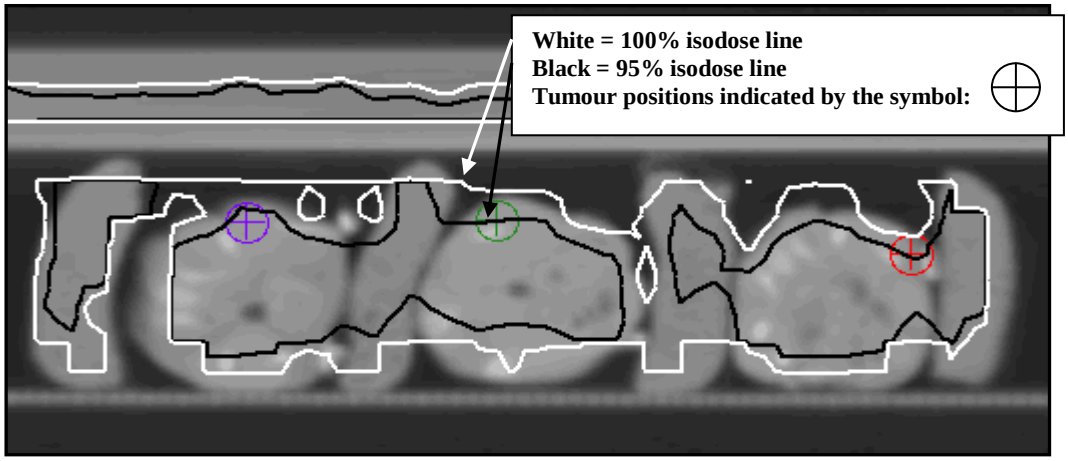

Figure 5.6. A transverse slice and Pinnacle^3 TPS isodose curves (6 MV x-ray beam from a 6/100 Varian linear accelerator) for 3 mice, set up in the irradiation position, indicating the 95% and 100% isodose curves and the approximate tumour positions.

Data Analysis

Individual pO_2 data was recorded from the OxyLab device for each tumour, along with the history of tumour length and width (±0.01 mm) to calculate the volume. The measured pO_2 values for each tumour were analysed considering the volume at the time of probing and for the total dose received, where measurements were taken directly after the last daily fraction of radiation for each mouse group. The hypoxic fraction of cells was calculated using the Software program *Image J* (v1.42q, NIH, USA) by analyzing the relative number of green (hypoxic) pixels, representing the number/area of cells having oxygenation less than ~10 mm Hg compared to the red (vessels) or blue (proliferating) cell areas.

Statistical Analysis

All data was processed using the statistical software package Prism 5 (v5.02, GraphPad Prism Software Inc.). Statistical significance between two data sets was assessed using a 2-tailed t-test (paired where indicated) ($p<0.05$, together with a 95% confidence interval). Linear regression gradients and *r* values and 95% confidence intervals were used to examine relationships between pO2 measurements at 2 and 5 minutes after OxyLab probe insertion and relationships among hypoxic proliferating and vessel cells with tumour volume and radiation dose.

Ethics Approval

This experimental study was approved by the IMVS and University of Adelaide animal ethics committees, and was carried out in collaboration with the Hanson Institutive of South Australia, the laboratories of Bionomics Ltd, and at the Department of Radiation Oncology at the Royal Adelaide Hospital.

5.2.2.2.2. Experimental Results

Error bars presented in the graphs below (Figures 5.7, 5.8 and 5.11b) for the measurement of oxygenation and tumour diameter/volume represent the standard deviation of the data. The box and whisker plots (Figure 5.7, 5.8 and 5.9a) show the mean value of the data set as a cross, and the quartile, median and third quartile levels with horizontal lines and all outlying data beyond the 10 and 90% percentile bars are also shown.

Preliminary Study

Preliminary tests showed that the FaDu cell line grew well in the hind flanks of all animals. The average width and length measurements increased up to 8.7±0.2 mm (with a range of 7.2 to 11.5 mm) from day 1 to 15 of tumour growth pre-irradiation or no irradiation, corresponding to a diameter and volume increase of approximately 0.6 mm and 21 mm^3 per day respectively.

A single anaesthetic dose of 200 μL/20gm of ketamine and xylazine (injected intra peritoneal) was sufficient to achieve tolerable sedation in most animals. In view of the 30 minute time restriction for oxygenation measurements, 4 peripheral and 2 central pO_2 readings only were recorded per tumour for the main study. In addition, for the main study, each measurement was recorded after 2 minutes and then repeated after 5 minutes to ensure stability of the readings before moving the probe to the next measurement point within the tumour. Thus, the readings were derived from a total of six tumour points and twelve individual readings per tumour.

Variations in initial pO_2 measurement were relatively large, fluctuating by approximately 5 to 10 mm Hg at a single point over 5 minutes in some tumours. The majority of the oxygenation measurements were relatively low and in the range of 0.1 to 0.5 mm Hg consistent with previous reports (Adam 1999, Nordsmark 2005), with no apparent difference in pO_2 between the tumour periphery and tumour centre.

Immobilisation was well tolerated by all mice, and animal movement was sufficiently restricted in the longitudinal direction (from mouse head to tail) to ensure that the tumours were kept within the radiation field for the duration of the treatment. The average tumour growth rate during the radiation schedule continues to increase initially, but reduced after the fourth fraction compared to pre-irradiation growth rates resulting in shrinkage of the tumours (Figure 5.7).

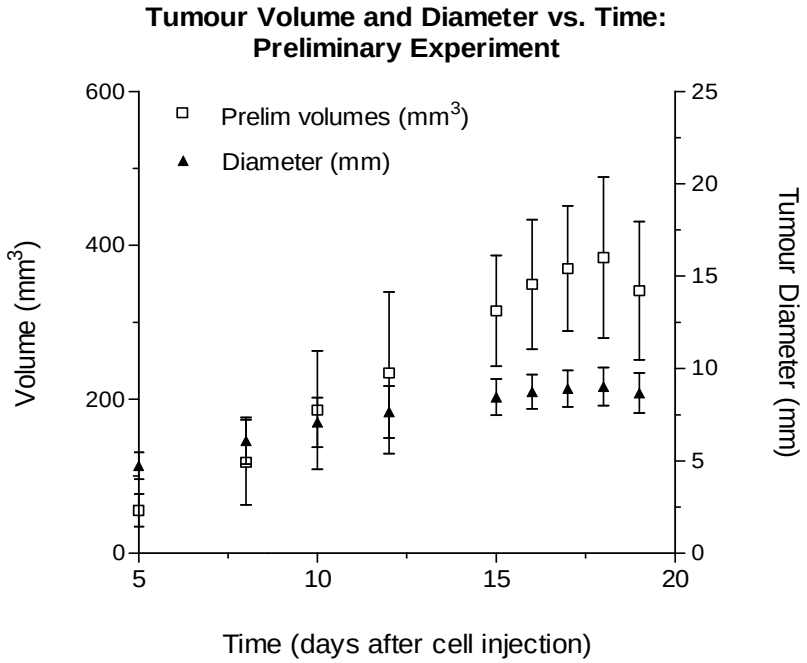

Figure 5.7. Preliminary experiment tumour diameter and volume, during 15 days of tumour growth (grey, n=12, 2 diameter measurements per tumour), followed by five daily fractions of 3 Gy irradiation starting at day 15 (n=9).

Owing to the continual increase in tumour volume during the first 4 days of treatment, many tumours grew to exceed 8 mm in diameter, at which point tumour ulceration occurred and risk of infection threatened the welfare of the animals. Pre-treatment diameter limits were accordingly adjusted from 7 to 8 mm to 4 to 5 mm in the main experiment.

Results from the Main Experiment

All 42 animals had visible tumours, with an average diameter of 5.3±0.2 mm, corresponding to an average volume of 78 mm^3, seven days post injection. Radiotherapy commenced with tumour diameters measured daily and the associated volume calculated (n=40). A dose of 3 Gy per fraction was used for the first week of the main study (on day 8 to 12). However, from fraction 6 onwards (from day 15), the schedule was accelerated and used 5 Gy daily fractions. Thus the total time of treatment was reduced from three to two weeks.

This change was made due to the observation of continual tumour growth during the first week of treatment, which if not abated with a higher dose schedule would have resulted in tumours reaching the 8 mm ulceration threshold.

As Figure 5.8 highlights, the average tumour volume increased during the first week of treatment (as expected from the preliminary tumour group response), and began to decrease after 12 days (15 Gy). Tumour volume increased on average by 70% between days 8 and 12 (from 80.6±7.2 mm at fraction 1 to 137.4±14.9 mm at fraction 5) with an average total reduction of 66% by day 19 (27.4±4.2 mm) corresponding to an increase in average tumour diameter from 5.3±1.2 to 6.3±1.5 mm between fraction 1 and 5, followed by a reduction to 3.6±0.9 mm by fraction 10 (40 Gy).

The average rate of growth of the 40 irradiated tumours was, as expected, greatly reduced compared to the control tumours, which by day 12 were increasing in volume by approximately 100% per day. The control mice were euthanised at day 15 due to tumour size limitations.

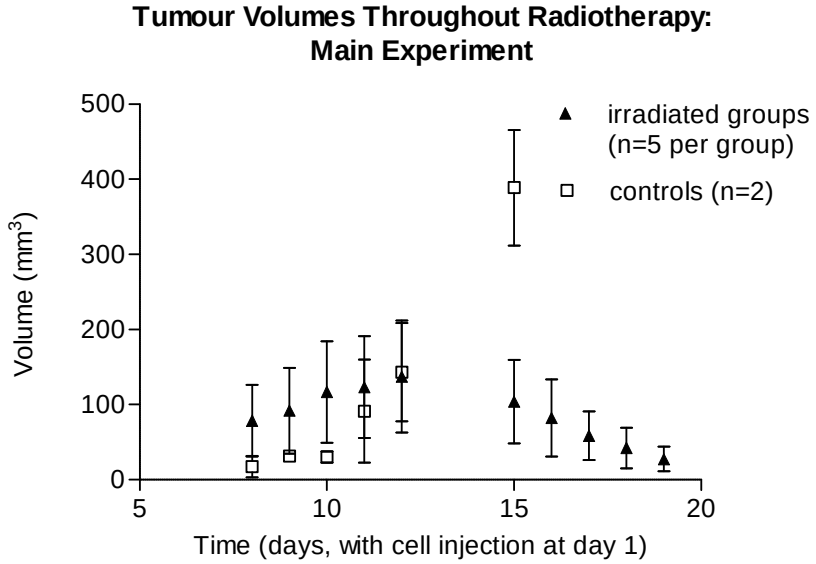

Figure 5.8. Average change in tumour volume (n=40) during radiotherapy starting 8 days after xenograft cell injection (note that animal numbers reduced to 10 by day 19 due to elimination of mice proceeding pO_2 measurements). Two control tumours received no irradiation and were left to grow until day 15. No treatment occurred on days 13 and 14 because of the weekend break.

Data for each dose point in the main study relating to measured pO_2 is shown in Table 5.2, with the range in pO_2 values observed at each dose point being relatively large. The standard deviation in pO_2 over the 6 tumour points (and up to twelve individual measurements) analysed for each tumour, had a mean value of 4.84 ± 3.18 mm Hg when averaging this standard deviation over all twenty one tumours. This figure provides a value for the observed variation in pO_2 data per tumour (coefficient of variation of 65.7%).

Tumour pO_2 levels remained relatively low during the first 8 fractions of therapy, corresponding to doses between 0 and 30 Gy. This was followed by an increase in average pO_2 at 40 Gy. Analysis comparing all 155 data points in the 0 to 30 Gy dose range and all 38 data points at 40 Gy showed a significant difference ($p<0.05$, 95% CI 5.8-15.8) as is shown in Figure 5.9 a). Central versus tumour periphery pO_2 differences were non-significant for all dose points (Figure 5.9 b).

Table 5.2. OxyLab pO_2 measurement data for all tumour points analysed. Up to 6 pointes were analysed per tumour, with data recorded at 2 and 5 minutes after probe insertion, per point. The total mouse number used was 20 and the total number of readings recorded was 193.

Dose (Gy)	**No. of pO_2 measurements**	**pO_2 (mm Hg)**						
		Min	**Median**	Max	Mean	10^{th} Percentile	90^{th} Percentile	Std. Dev.
0 Gy	35	0.00	**0.75**	20.00	1.95	0.50	4.95	3.77
3 Gy	29	0.00	**0.75**	25.50	3.71	0.00	9.25	6.26
9 Gy	32	0.00	**0.00**	8.60	0.65	0.00	2.29	2.00
20 Gy	28	0.00	**0.73**	37.00	6.19	0.00	21.55	9.86
30 Gy	32	0.65	**1.48**	14.25	3.10	0.74	9.35	3.43
40 Gy	38	0.15	**5.63**	45.00	12.81	0.40	37.75	14.07
Control: 0 Gy (day 12)	*12*	*0.45*	*1.95*	*20.5*	*4.99*	*0.47*	*20.50*	*7.38*

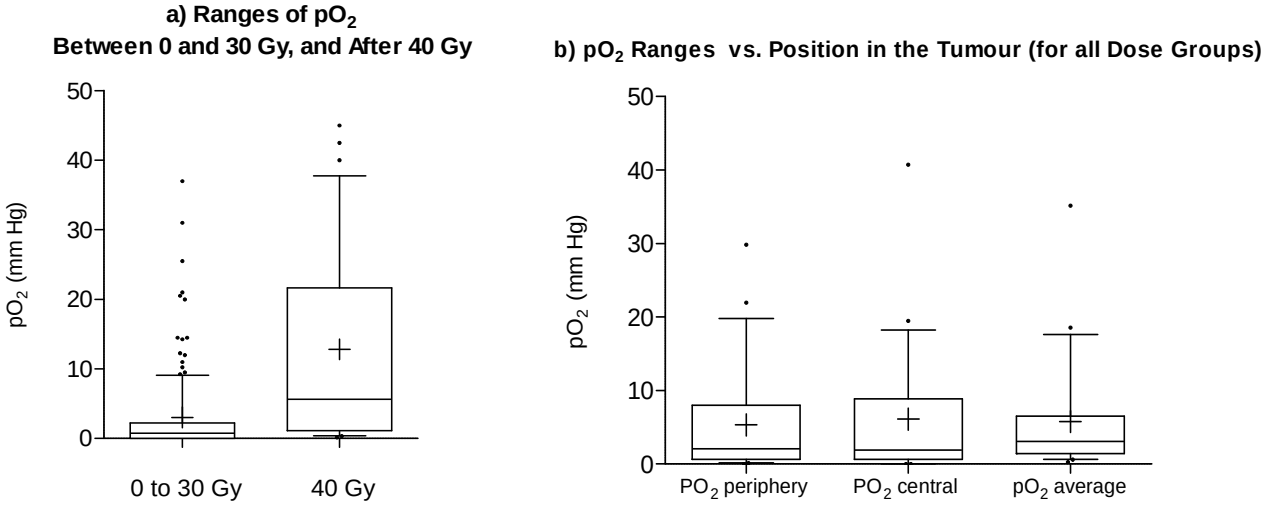

Figure 5.9. Oxygenation measurements indicating, a) a significant increase in pO_2 with increasing dose of fractionated radiotherapy from 0 to 30 Gy to 40 Gy ($p<0.05$), and b) no significant difference between the periphery, centre and total average pO_2 of the tumours.

Tumours with the smallest final volumes (measured just prior to pO_2 measurement) were, as expected, those that received the highest accumulated dose. Two very small tumours (<50 mm^3) were in the group analysed after only 0 or 3 Gy, however, the remainder of the very small tumours received 30 Gy or higher. Oxygenation data from all tumours is plotted against tumour volume (volume on the day of pO_2 measurement), separated into groups of small, medium and large tumours (Figure 5.10 a).

The ranges of tumour volumes in each group are shown in Figure 5.10 b). There was a significant difference between mean pO_2 and volume for tumour groups having volumes less than or greater than 100 mm^3 ($p<0.01$, CI 95% 1.2-6.2). A linear regression analysis using all pO_2 and tumour volume data resulted in a significant correlation between these oxygenation measurements and tumour volume ($p<0.01$, $r^2=0.15$, 95% CI (-0.5)-(-0.26), for the Pearson *r* value).

Four of the mice receiving the full 40 Gy dose were not used to measure pO_2 because the radiation therapy had reduced the visible tumour diameters and were too small to be discerned as a discrete tumour under dry skin of the animals.

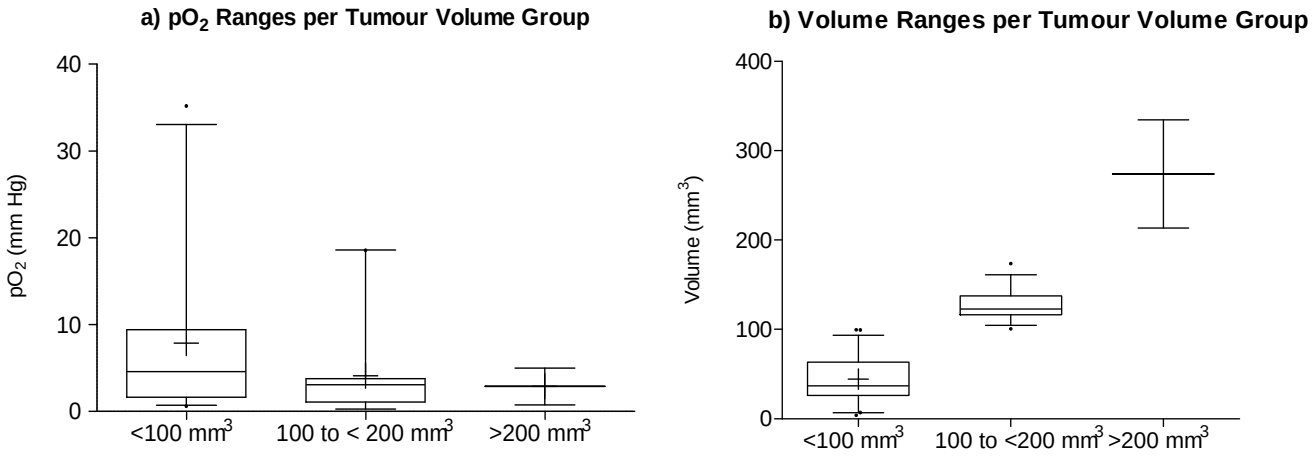

Figure 5.10. Plots for a) oxygenation data (pO_2) for small, medium and large tumours (n=10, n=9, n=1, with up to 12 points measured per tumour), b) the ranges of tumour volumes within each volume group.

Two pO_2 were recorded per tumour point. Although the purpose of the two measurements was to allow for changes of pO_2 with time, no significant difference between the 2 and 5 minute readings were observed, for any of the tumour dose groups (p=0.67, CI 95% (-1.99) -3.08) (Figure 5.11 a).

Furthermore, linear regression analysis of the pO_2 measurements 2 and 5 minutes after probe insertion showed gradient close to one (0.93 ±0.03, r^2 = 0.91, 95% CI 0.93-0.97, p<0.01) (Figure 5.11 b). For all statistical analyses of the data, pO_2 readings for the 2 and 5 minute time point from the same tumour point more than 10 mm Hg apart, were disregarded, as a change of this magnitude would be most unlikely on the minute time scale of the measurements (Brurberg 2005, Kirkpatrick 2004) and would be more likely to be attributed to blockage of the probe with blood or animal movement.

The existence of hypoxic regions in a selection of the xenografts was verified by immunohistochemical staining followed by analysis of fluorescence imaging (Figures 5.12a to 5.12f).

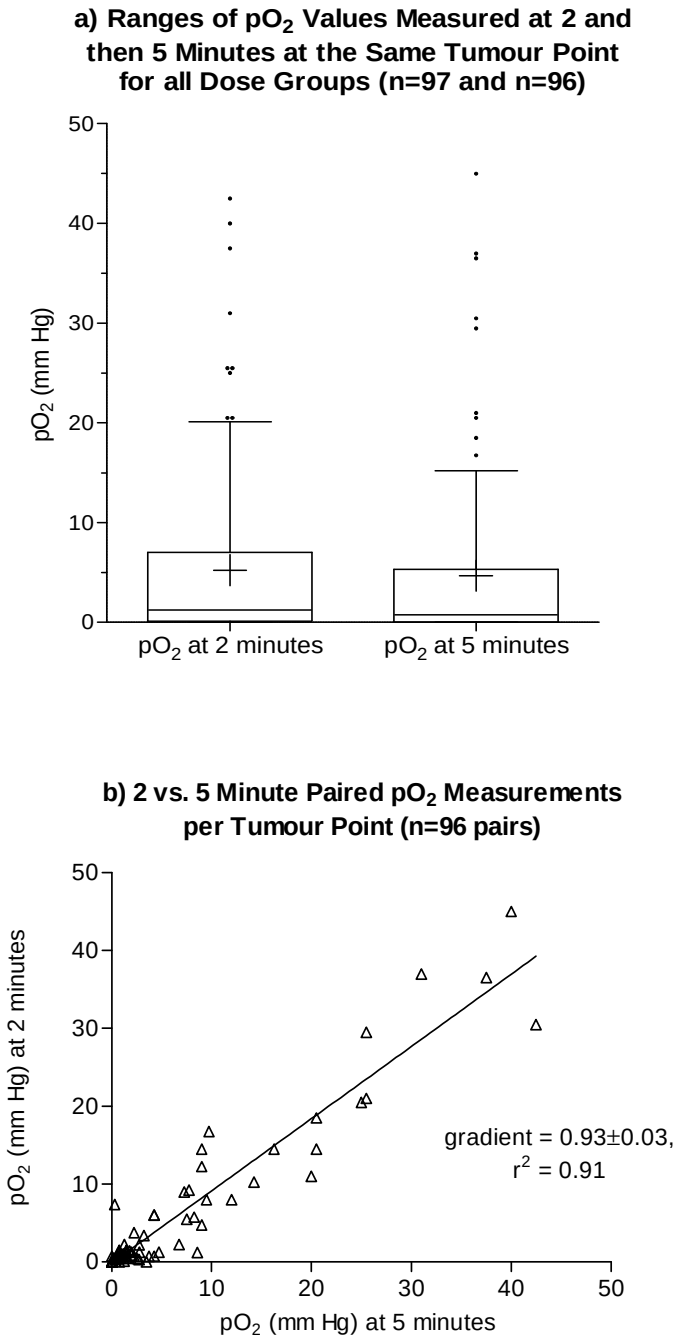

Figure 5.11. A comparison of the pO_2 readings after 2 and 5 minutes, for all mice involved in the OxyLab procedure (n=20), with an average of 6 points measured per tumour and 3 tumours per dose group from 0 to 40 Gy, for a) all 2 minute data compared to all 5 minute data, and b) the plot of the 2 minute vs. the 5 minute measurements corresponding to each tumour point (96 pairs of measurements).

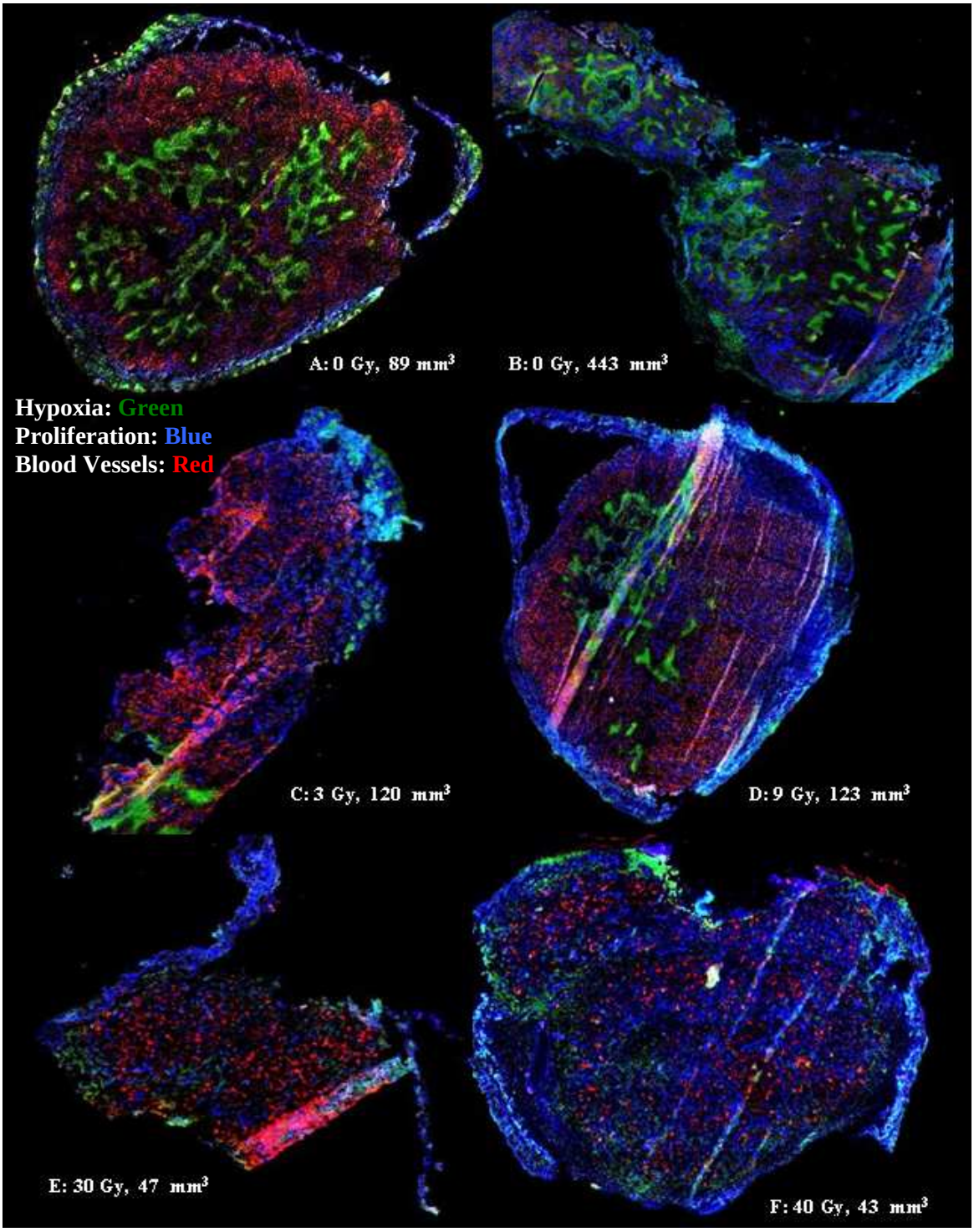

Figure 5.12. Analysis of a selection of immunohistochemical cross sections of a sample of tumours receiving, a) 0 Gy, b) 0 Gy, c) 1x3 Gy, d) 3x3 Gy, e) 5x3+3x5 =30 Gy, and f)5x3+5x5 = 40 Gy. Fluoroscopic imaging shows the hypoxic green cells (Pimonidazole hypoxia marker), red endothelial/vessel cells and blue proliferating cells. Note that xenograft B grew for an extended 15 day period before excision of the tumour, hence the larger volume of the tumour.

There was a direct relationship between the increase in the number of hypoxic cells in the tumour cross sections with an increasing tumour volume (linear regression gradient 0.04±0.02, r^2=0.26, 95% CI 0.04-0.8, p=0.04) (Figure 5.13a), and decreasing dose (linear regression gradient -0.23±0.10, r^2=0.28, 95% CI -0.8-(-0.06), p=0.03) (Figure 5.13b). The tumour with the highest hypoxic cell number by relative green pixel percentage was the control tumour (15 days of growth with no irradiation).

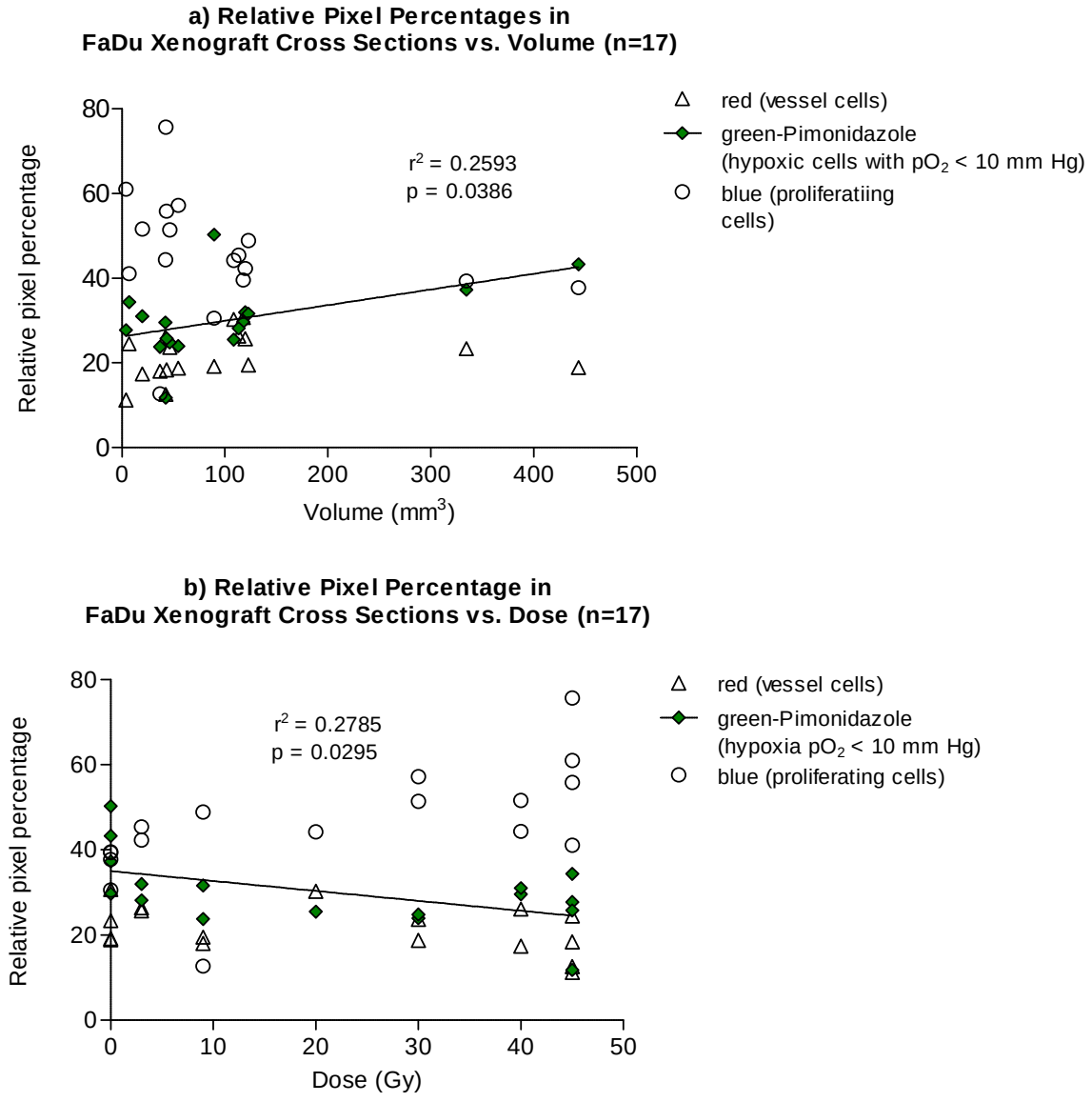

Figure 5.13. The relative percentage of green hypoxic cells using Pimonidazole compared to all stained cell pixels (including red vessel and blue proliferating cell pixels, based on the Immunohistochemical staining tumour cross sectional images of 17 tumours receiving between 0 and 40 Gy, plotted against a) tumour volume, and b) total dose.

Although no strong relationships existed among the coloured pixels, the largest correlations were of an increase in green (hypoxic cell) pixels with a decrease in blue pixels (proliferating cells), green pixels with an increase in tumour volume, green pixels with increasing dose, and the correlations involving the tumour volume and dose (Figure 5.14).

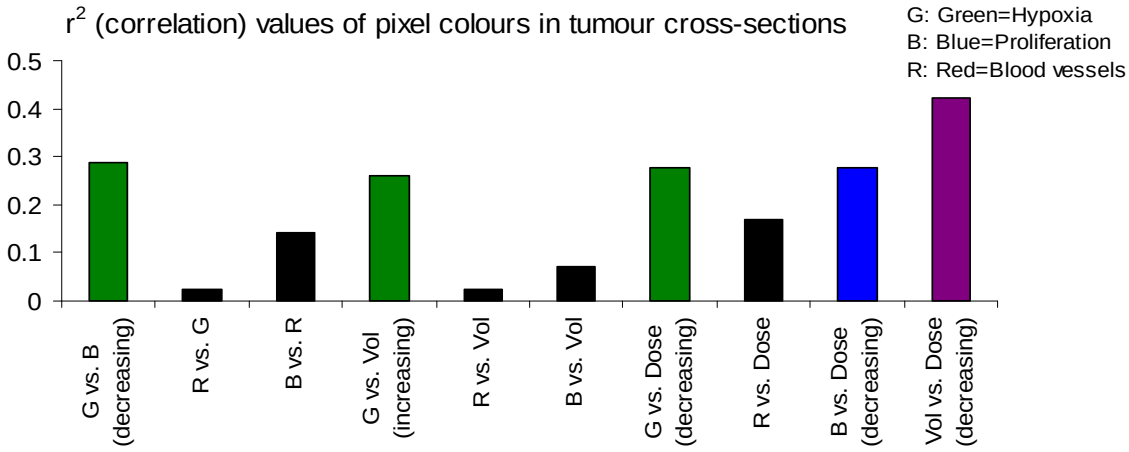

Figure 5.14. The relationships among the relative percentage of the green hypoxic cells, red vessel cells and blue proliferating cells and pixel count with total dose or tumour volume, in 17 immunohistochemically stained xenografts cross-sections.

Figure 5.15 further shows the changing percentages of green, red and blue coloured pixels, for a range of xenografts, with the columns of the chart ordered for increasing tumour volume from left to right in each section.

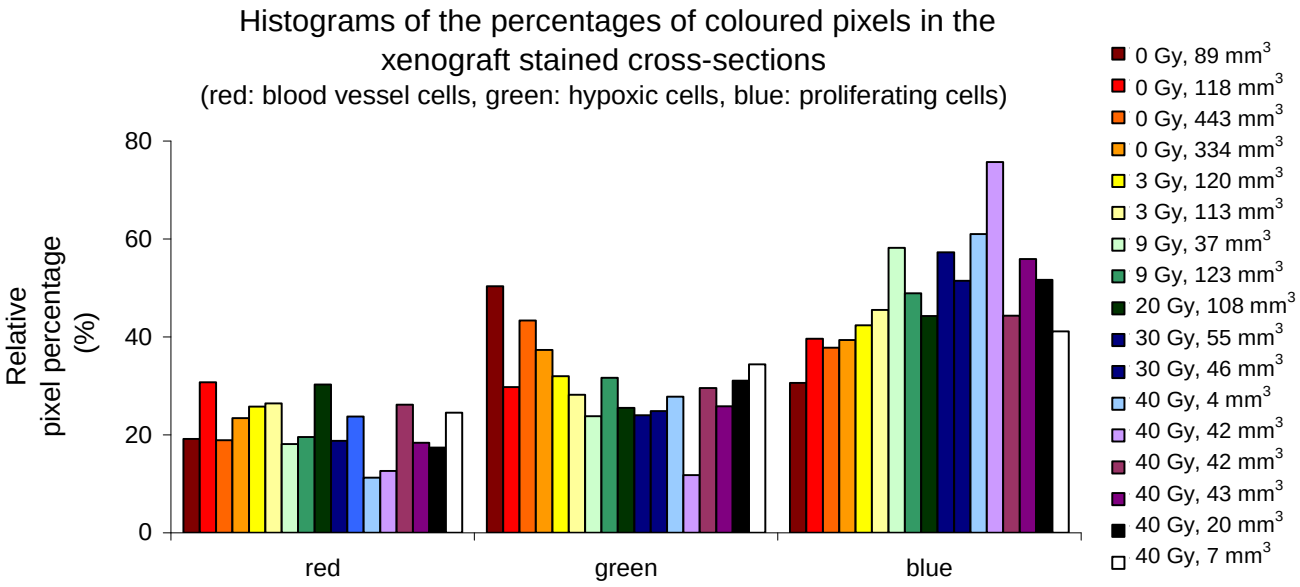

Figure 5.15. The percentages of red, green and blue pixels (representing vessel cells, hypoxic cells and proliferating cells) in order of smallest to largest tumour volume (tumour received between 0 and 45 Gy) in 17 immunohistochemically stained xenograft cross sections, excluding tumours with folding artefacts in the 7 µm and with tumour volumes less than 15 mm^3.

5.2.2.2.3. Experimental Study Discussion

The aims of the experiment were to determine the timing and degree of ROx onset in a HNSCC mouse model during an accelerated radiotherapy schedule. The results of the study indicate that an increase in tumour oxygenation occurs relatively late (2 weeks) in an accelerated schedule in the HNSCC xenografts, despite the well documented early response of this cell line (average surviving fraction after 2 Gy of 45 to 50%) (Bjork-Eriksson 2000, Eschwege 1997, Steel 2002).

The relatively late reoxygenation in the mice here contrast with other studies involving alternative carcinoma cell line xenografts or in vivo tumour measurements using a variety of techniques including the OxyLab, Eppendorf or immunohistochemical staining (Kitakabu 1991, Ljungkvist 2006, Nordsmark 2005). However, the results here are consistent with those reported by Petersen *et al*, who found that ROx occurred after a time delay of 12 days following clamp hypoxia (Petersen 2003).

The complementary immunohistochemical staining analysis in the experiment here verified that ROx was induced by irradiation and not a spontaneous occurrence over time. Hypoxia was present in all of the tumours in the immunohistochemical study (n=17), with extent increasing with tumour volume. The fluoroscopic imaging results are consistent with measurements which increased with decreasing tumour volume. Data from the two oxygenation analyses cannot be directly compared because of the different methodology including the approximate 10 mm Hg pO_2 threshold that applied to the immunohistochemical staining technique.

It should also be noted that the hypoxia detected by the OxyLab system and immunohistochemical staining techniques is not specific for the mechanism of hypoxia, i.e. acute or chronic. Based on the similarity of pO_2 data measured at different time points (Figure 5.11), it is likely that chronic hypoxia was the dominant mechanism observed by the OxyLab system. The results of the pO_2 measurements in the experiment are based on the minute time scale rather than the hourly scale.

It is possible that some of the variation in pO_2 readings in individual tumours and between tumours in the same dose group could be accounted for by slowly varying acute hypoxia. However, with up to 6 tumour points assessed in each tumour and with 3 to 4 tumours per dose group, it is probable that changes in pO_2 due to acute hypoxia would statistically cancel out, and represent a mean pO_2 value which primarily reflects chronic hypoxia.

5.2.2.2.4. Experimental Study Conclusions

Tumour oxygenation was analysed before and during fractionated radiotherapy in HNSCC xenografts. The average pO_2 level measured with the OxyLab system increased significantly only after the delivery of the last daily fraction which corresponded to a total dose of 40 Gy delivered in 10 fractions. This was later in the treatment course than anticipated based on the observed tumour shrinkage which began after fraction 5.

The increase in oxygenation resulted in a mean pO_2 of less than 6.2 mm Hg for doses between 0 and 30 Gy, rising to a mean of 12.8 mm Hg at 40 Gy. There was a direct relationship between tumour volume above or below 100 mm^3 and oxygenation. The

presence of tumour hypoxia was verified using immunohistochemical analysis and no ROx occurred in the absence of treatment.

5.2.3. Modelling of Accelerated Repopulation during Radiotherapy

Accelerated repopulation (AR) was modelled by increasing the *Spercent* variable (defined in chapter 4) controlling the probability of stem cell symmetrical division, i.e. the chance of a stem cell dividing into two daughter stem cells. This increase in *Spercent* was implemented using a multiplicative factor, the *AR boost factor*. Onset of AR in the model was made flexible so that the user could define the number of weeks into treatment that the AR boost factor would apply.

The default *AR boost factor* value (10) was validated during an analysis of the increase in the dose per fraction that was required to kill the extra cells that had propagated after the onset of AR due to the accelerated growth response, as this has been reported as approximately 0.5 to 1.0 Gy from HNSCC clinical trials (Armpilia 2004, Maciejewski 1989, Tucker 1999, Withers 1988, Fowler 2000).

With no AR effects modelled, 30x2 Gy was required to control the virtual tumours. In an analysis to determine the value for the default *AR boost factor*, simulations using various combinations of onset times of AR and ROx were modelled to obtain the total treatment lengths and doses. This was followed by calculations of the increase in dose per fraction that was required (after onset of AR) to reduce the total treatment time despite the presence of AR back to the standard 6 weeks (60 Gy).

The dose per fraction required was calculated by solving for the dose per fraction, *d*, in the biological effective dose (BED) formula (Equation 5.3, Dale 2007), with *BED* as the total dose required in simulations (after onset of AR only) to achieve tumour control, an α/β value of 10 Gy, and with *n* as the number of fractions simulated after the onset of AR.

$$BED = nd(1+\frac{d\alpha}{\beta}) \tag{5.3}$$

5.2.4. Radiation Effect Model Parameter Summary

5.2.4.1. Parameters Values and Ranges

The key parameters used in the radiotherapy effect algorithm are presented in Table 5.3. Where possible published reports have been used to set default parameter values. Where no specific data was applicable, suitable ranges for the values were used.

Table 5.3. Modelling parameters used in the fractionated radiotherapy effect algorithm, including parameter values/ ranges and literature references where applicable.

Parameter	Default	User input?	Input limits tested	References	Comments
Accelerated repopulation (AR) – time of onset after initialisation during RT (weeks)	No AR	yes	0, 1, 2, 3	(Marcu 2004, Withers 1988, Maciejewski 1989, Trott 1991, Kummermehr 1992, Peters 1997, Trott 1999, Terhaard 2005)	The no. weeks into RT for onset of AR, 2-4 are values reported in the literature; however in the model 0 week onset has been made possible for modelling microscopic response in a small tumour system.
Reoxygenation (ROx) – time of onset after initialisation during RT (weeks)	No ROx	yes	0, 1, 2, 3		An extremely variable parameter and open to user input.
Time of ROx after a particular RT fraction (weeks)	4 hours	yes	4 to 48	(Ljungkvist 2002)	
AR boost factor	10	yes	3 to 15	(Marcu 2004, Marcu 2002, Steel 2002)	The factor applied to increase the symmetrical stem cell division probability during AR.
ROx induced incremental increases in pO_2 (mm Hg)	3 mm Hg	yes	N/A		The pO_2 increment size during randomised reoxygenation after a RT fraction (linear SF dependent), set to obtain full oxygenation by ~ 1 to 2 mm tumour diameter.
ROx percentage of the very low oxygenated cell population	60%	yes	0 to 100%	N/A	The percentage of hypoxia induced quiescent cells brought back into the cell cycle upon ROx after a RT fraction (linearly SF dependent); set to achieve full tumour oxygenation when the tumour has reduced down to between 10^5 and 10^6 cells (from 10^8 initial cells).
Alpha (Gy^{-1})	0.30	yes	N/A	(Stuschke 1997, Horiot 1994)	Constant values used only for SF calculations. In this study apla was held constant and beta was varied from 0.1 to 0.015 in LQ calculations, to compare *HYP-RT* out comes with the LQ model
Beta (Gy^{-2})	0.03	yes	0.1 to 0.015		
Non-cycling cell radiosensitivity compared to oxic cycling cells	0.5	no	N/A	(Hall 2006, Potten 1981)	Factor for the decreased radiosensitivity of non-cycling cells, based on the likely increase in resistance of cells in resting phase (transit cells and stems cells however assumed to be equally radiosensitive in tumour cells).

5.2.4.2. Assumptions and Limitations

The current method of modelling based on temporal cellular properties was deemed suitable in this work which studied the effects of tumours with randomly distributed cellular oxygenation values. The temporal nature of the model restricted the model to simulations modelling radiotherapy treatment that aimed for uniform dose coverage to the tumour. However, for future simulations there is scope within this temporal model to simulate altered probabilities of cell death for percentages of cells based on random allocation or based on cell type (i.e. stem, transit cells).

Accelerated repopulation was modelled using a single mechanism, i.e. increasing the stem cell symmetrical division probability. Other possible mechanisms include reducing cell cycle times and the recruitment of differentiated cells back to the cell cycle; however these were not applied in the current work. However, note that the *HYP-RT* model does simulate the ROx of hypoxic tumours which is a form of tumour repopulation because of the associated recruitment of very hypoxic quiescent cells back into cycle when they reach pO_2 levels greater than 1 mm Hg.

The modelling of tumour ROx was based on achieving full oxygenation (zero quiescent hypoxic cells) and a uniform pO_2 distribution among the tumour cells at a time at which the tumour had reduced to a diameter of 10^5 to 10^6 cells (1 to 2 mm diameter) (McElwain 1979). In human tumours, inter- and intra-tumour reoxygenation rates are likely to vary during tumour shrinkage, resulting in full reoxygenation at a range of different tumour diameters. Moreover, in some human tumours full oxygenation may never be achieved. This could be partially accounted for in the model in future versions by modelling a reoxygenation rate based on the instantaneous tumour diameter, with the option to completely reoxygenate the tumour (or not) depending on knowledge of the real tumour system being modelled and its blood supply (using imaging modalities such as PET and MRI).

The radiotherapy effect algorithm reported here does not take into account repair of radiation induced cell damage, however the modelling of repair will be considered in future work. A minimum time of six hours between treatment fractions has been implemented in all simulated hyperfractionated schedules. Therefore, the current version

of the model, whereby cells either survive or die after each dose fraction, adequately reflects the clinical situation whereby treatment fractions are separated by more than six hours.

As previously mentioned, no normal (healthy) cells have been modelled and therefore no detailed effects of treatment on normal tissues have been made in this work. However, in Chapter 6 altered fractionation schedules are discussed in terms of their calculated biological effective doses (BED) for acute and late normal tissue effects. BED was calculated assuming that the normal tissues received the same total dose delivered to the tumour, which this chapter as well as chapters 6 and 7 show varies greatly with different schedules and onset times of AR and ROx.

Features such as "gradual cell death" and abortive cell divisions were not modelled in this work, but could be considered in future versions of the model (Dorr 1997, Stamatakos 2006). Such cell death mechanisms could an impact on tumour oxygenation in future model versions which may link the pO_2 distribution and ROx dynamics to the shrinking tumour volume.

It should be noted that in the hours to days proceeding a dose fraction (corresponding to several cell cycle times), the number of cells in the tumour may not directly correlate with the proliferative capacity of the cell population. This is because it takes time for dead cell matter to be cleared from the tumour and also because of the effect of abortive stem cell divisions whereby cells may be appear to be successfully dividing and but their cell lines have a high probability of dying out after a few generations (Steel 2002, Joiner 2009).

5.3. **Radiation Effect Algorithm Development**

5.3.1. Implementing Efficient Randomised Cell Kill

In the model, cell death is assessed for each cell in the *Cellarray*, for each dose fraction. Cell death probability is based on the *SF* that has been pre-calculated for the average oxic

cycling cell population, and adjusted for oxygenation (using the relevant dose dependent OER curve), as previously discussed. In the algorithm, this involves the use of random number generation to decide whether a cell either survives the dose fraction or alternatively dies, resulting in elimination from the *Cellarray*. After cell death, links in the *Cellarray* are updated to maintain the chronological order of the cells in the relevant *hourly list*, and counters parameters are updated to keep track of the number of living cells of each type.

Automatic re-use of emptied *Cellarray* elements after cell death enables efficient computer memory usage. Efficiency of the algorithm was monitored during the development process, with the final version of the algorithm having the capability to treat a 10^8 cell tumour with fractionated radiotherapy in approximately 1 to 2 minutes. With AR simulated, more dose fractions were required to control the tumour and hence the total simulation time increased slightly.

The treatment data files containing information defining the simulated fractionation schedules were written as a basic text file containing lists of integer values describing the time (in hours) between each consecutive treatment fraction and the dose to be delivered for each treatment fraction. Up to 200 fractions were allowed for in these files to enable analysis of very resistant and rapidly repopulating tumours.

5.3.2. Algorithm Workflow

The radiation effect algorithm begins with either the growth (or the reading in of information from stored file) of a virtual tumour containing up to 10^8 cells with a pre-defined hypoxic status. During simulated radiotherapy cells continue to divide between fractions, with ROx "events" and the onset of AR implemented when required. Fractionated treatment continues until all cells with have been eliminated, or the desired number of treatment fractions has been delivered. A work flow diagram, outlining key steps of the radiation effect algorithm is displayed in Figure 5.16.

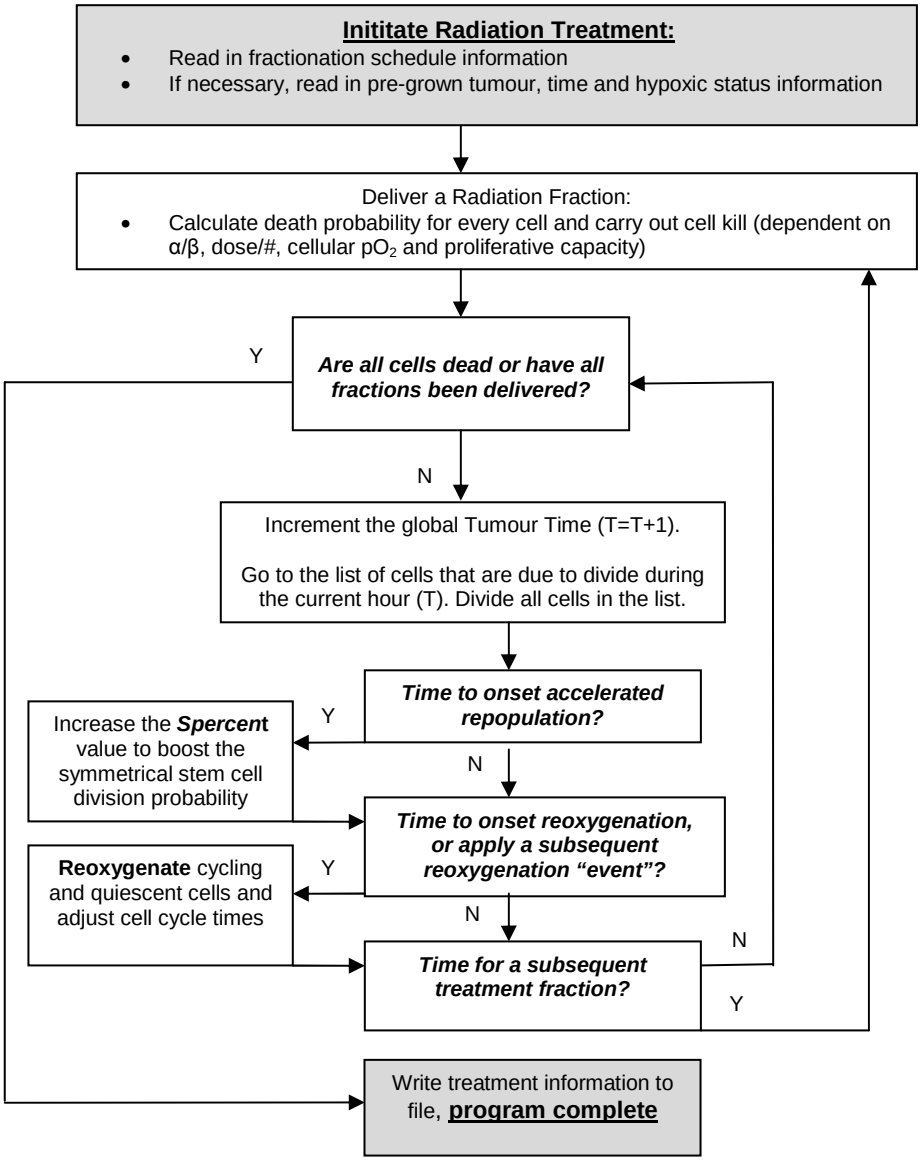

Figure 5.16. A flow diagram of the radiation effect algorithm, where initiation of treatment is followed by continual cell growth between subsequent treatment fractions. Accelerated repopulation is initiated once, and reoxygenation "events" are initiated and then repeated until the tumour is fully oxygenated. Treatment is complete when either the number of desired fractions has been delivered or total cell death has occurred.

5.3.3. Radiotherapy Outcome Analysis Methods

5.3.3.1. Output Results Format

Traditionally, clonogenic stems cells are thought to be the cells responsible for local treatment failure in radiotherapy, however in this work the number of fractions required to kill all oxic as well as hypoxic cells usually existing in the basal layer of the epithelium (stem, transit and level one differentiating cells, as defined in Chapter 2) were analysed, unless otherwise specified. This approach was taken because it is possible that tumour cells avoid radio-induced cell kill due to hypoxia, and reoxygenate after treatment completion contributing to local tumour recurrence. Moreover, hypoxia may cause genetic mutations in hypoxic cells due to the altered environmental conditions, promoting the de-differentiation of cells (to become more "stem-like") which may threaten tumour control (Axelson 2005, Chou 2004, Azuma 2003). For comparison however, for some of the data presented in this chapter, the analysis of stem cell death only has also been presented.

The graphical user interface (GUI) of the model was used for the selection of parameters relating to ROx and AR and for initialising the simulations of fractionated radiotherapy. Using the GUI, the model could be run multiple times, delivering treatment to a tumour using different random seed numbers in the treatment algorithm, and/or for delivering a radiation course to a set of tumours grown using different random seed numbers. The GUI also enables retrospective analyses of files written and stored during simulations to obtain information such as the fraction number at which full reoxygenation occurred and the percentages of cells of a particular cell type present after each dose fraction.

5.3.3.2. Data and Statistical Analysis Methods

In analysis of the model, various combinations of cellular and treatment based model parameters were compared in terms their impact on the number of 2 Gy fractions required to control a virtual tumour. The ranges of values applicable for each parameter are provided in Table 5.3. In the text and figures of this report, results are presented as the

mean and standard deviations of the data for nine simulations per parameter set, using the same programs as mentioned in Chapter 4.

5.3.3.3. Model Validation Methods

In the model development process, values for cellular parameters were chosen based on their influence on macroscopic tumour effects that could be compared to real tumour data, such as tumour doubling time and the stem cell population. For example, the symmetrical stem cell division probability parameter (*Spercent*) was set to 3% which created a 1% stem cell population in the virtual tumours (Steel 2002).

Clinical data from the control arms of randomised clinical trials were used to compare the TCP results from the model, using the number surviving cells and the Poisson equation. In clinical trials a set number of fractions are prescribed and the resulting average LC rates for the patient group (sometimes further stratified) are reported. In the model however, the total number of treatment fractions required to control an individual tumour are predicted. The model can be used to retrospectively analyse the effectiveness of a particular treatment schedule that uses a fixed total dose, using information stored in the model output files regarding the level of cell kill achieved at a particular dose threshold.

Linear quadratic theory was used to determine the number of fractions required to reduce the cell number to less than one cell (the first fraction number achieving less than 1.000 cells remaining) for comparison with *HYP-RT* model results. The aim of the comparison was to validate the *HYP-RT* model for the basic case of oxic tumour irradiation, against a simple and well recognised mathematical model. An analysis of the *HYP-RT* model against the LQ model and more complex forms of the LQ equation (incorporating AR and tumour hypoxia) was then performed. The methods and formulas used in this analysis are discussed below.

To incorporate AR into the standard LQ equation, a "time factor" adjustment was used (Equation 5.4) which incorporated a kick off time variable, T_k, the potential doubling time, T_{pot}, and the total treatment time, t, (where N_0 represents the initial number of cells and N represents the remaining number of cells) (Dale 2007). An initial cell number of

10^8 were used for all calculations, and the T_K and T_{pot} parameters assigned values of 2 to 3 weeks, and 4 days respectively.

$$\frac{N}{N_0} = e^{-[\alpha d + \beta d^2 - \frac{\log_e 2(t-T_K)}{T_{pot}}]} \tag{5.4}$$

Use of the LQ equation with OER modification (Equation 5.5 and 5.6) was included in the comparison between LQ theory and the *HYP-RT* model below (Dale 2007). LQ calculations were performed assuming a uniform hypoxic cell population represented by a single *q* value used to modify the radiosensitivity for hypoxic cells.

$$\begin{gathered} q = r_{max}/r \\ \text{where } r = (r_{max}.pO_2 + k)/(pO_2 + k),\ k = 3 \text{ and } r_{max} = 3 \end{gathered} \tag{5.5}$$

$$\frac{N}{N_0} = e^{-[\frac{\alpha d}{q} + \frac{\beta d^2}{q^2}]} \tag{5.6}$$

The LQ equation with an AR time-factor as well as OER modification was also used (Equation 5.7), applying the same range of *q* and T_k values as stated above.

$$\frac{N}{N_0} = e^{-[\frac{\alpha d}{q} + \frac{\beta d^2}{q^2} - \frac{\log_e 2(t-T_K)}{T_{pot}}]} \tag{5.7}$$

To compare *HYP-RT* model results to the LQ model, a 3% hypoxic population (representing cells with pO_2 levels between 0 and 1 mm H) was used in the LQ calculations (Equation 5.8) where *h* is the percentage of cells in the 0 to1 mm Hg range and with a relatively high *q* value of 2.0. No further LQ model comparisons were made in this work in terms of applying ROx modifying factors and functions, as too many assumptions about the parameters involved would have been required.

$$\frac{N}{N_0} = (1-h)e^{-[\alpha d + \beta d^2 - \frac{\log_e 2(t-T_K)}{T_{pot}}]} + (h)e^{-[\frac{\alpha d}{q} + \frac{\beta d^2}{q^2} - \frac{\log_e 2(t-T_K)}{T_{pot}}]} \tag{5.8}$$

5.4. Radiation Effect Algorithm Results and Discussion

Results of tumour growth and radiotherapy simulations using the *HYP-RT* model are presented below. Results predominantly refer to the number dose fractions required to achieve tumour control, considering all "basal" cells as cells that could potentially re-grow the tumour. All results in this chapter correspond to simulated conventional 2 Gy per day fractionated radiotherapy for virtual tumours consisting of 10^8 cells.

5.4.1. Results Interpretation and Parameter Analysis

5.4.1.1. Results Interpretation Based on Cell Type

The trend in model results observed for a set of moderately hypoxic tumour simulations with varying onset times of AR and ROx showed that the average difference between defining tumour control by elimination of all "basal" cells compared to all stem cells was only 2.2 fractions. However, this increase in fraction number to kill any remaining transit and level 1 differentiating cells after all stem cells had been eliminated was non-significant because of the wide standard deviation in the results (4.6 fractions).

5.4.1.2. The Level of Cell Kill Required for Tumour Control

Using standard Poisson theory (Equation 2.1 in Chapter 2), TCP is reduced from 100% to 37% if, on average, one clonogenic cell remains after completion of treatment. This assumes treatment on a set of identical tumours. Further, TCP is reduced to below 1% if five or more clonogenic cells remain after treatment. In the *HYP-RT* model, the average number of fractions required to eliminate all but one or all but five cells was assessed and was significantly lower, compared to eliminating all cells (Table 5.4).

The results in Table 5.4 above provide evidence so show that although cell kill during the last 1 to 5 fractions is minimal, these last fractions are vital for achieving a high TCP. On average in the model, only an extra 1 to 2 fractions were required to eliminate the last cell, but 3 to 5 fractions were required to eliminate the last five cells.

Table 5.4. The number of fractions difference required in simulations to eliminate <u>all cells compared to 1 cell remaining</u> and <u>all cells compared to 5 cells remaining</u> (killing all stem+transit+level 1 differentiating "basal" cells or all stem cells only), averaged over multiple simulations of moderately hypoxic tumours with different onset times of accelerated repopulation and reoxygenation.

	0 cells remaining compared to 1 cell remaining		**0 cells remaining compared to 5 cells remaining**	
	# Fractions	Dose (Gy)	# Fractions	Dose (Gy)
All Stem, transit, level 1 differentiating cells	0.7 ± 0.4	1.4 ± 0.7	3.0 ± 1.2	6.0 ± 2.3
Stem cells only	2.1 ± 0.7	4.3 ± 1.4	5.7 ± 1.2	11.3 ± 2.5

5.4.1.3. Statistical Variations due to the Random Seed Number

Statistical variations are inherent in the MC modelling process. The statistical variation observed in the fraction number required for 100% TCP, when treating the same virtual tumour with different random seed numbers, was small (consistently between 1% to 3%) for a set of nine simulations (three tumour growth and three treatment simulations). Initially, 25 simulations (five growth and five treatment simulations) were performed for each parameter set combination. However, it was found that the standard deviations in the results were statistically the same as only nine simulations.

The influence of the random seed number in the radiation effect algorithm had a smaller influence on radiotherapy outcomes compared to tumour growth outcomes. The larger variations observed due to random seed in during modelled tumour growth were attributed to the small but significant statistical variations in stem cell percentages early in tumour development, as this percentage was extremely influential on tumour growth rate and hence total growth time.

5.4.1.4. Oxic Tumour Model Outcomes

5.4.1.4.1. α/β Ratio Variation

The default *α/β* value used for the modelled tumours was 10 Gy. However, results for a range of *α/β* values were used to verify that the *HYP-RT* model predicted the same level of cell kill as LQ theory for oxic tumours (Figure 5.17). In LQ calculations, *α* values were held constant (0.3 Gy^{-1}) while the beta value was varied (from 0.1 to 0.015 Gy^{-2}), producing *α/β* values in the range of 3 to 20 Gy. For this analysis "basal" cell elimination as well as the elimination of only the tumour stem cells were considered.

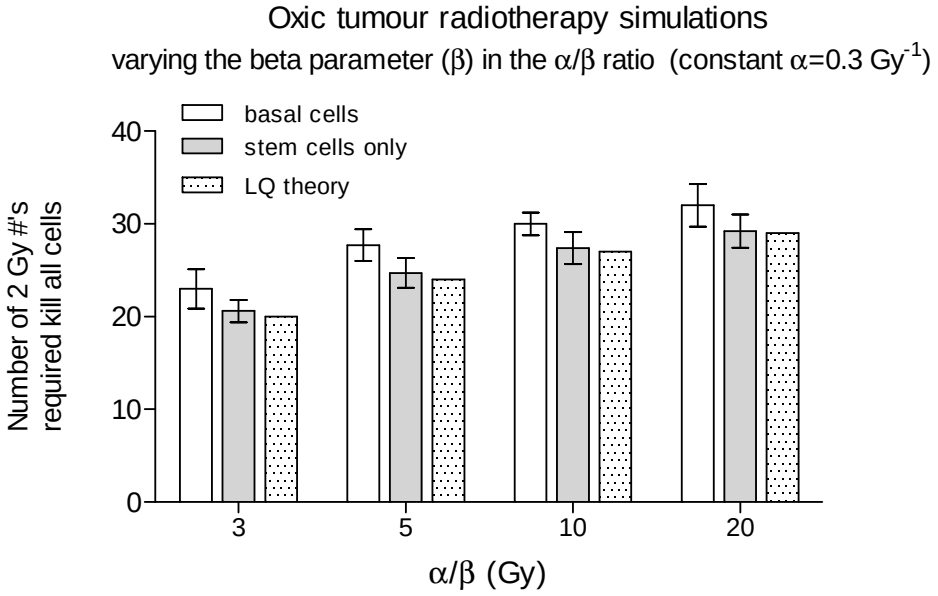

Figure 5.17. Comparison of the number of 2 Gy fractions required in the HYP-RT model to kill all "basal" or all "stem" cells compared to the linear quadratic (LQ) model in which the cell population is reduced to less than 1 cell (the first fraction that achieves <1.000 cells remaining), for oxic tumour conventional radiotherapy.

The stem cell simulation results were in good agreement with the LQ results, whilst the results involving the cell kill of all "basal" cells, averaged to 2 to 3 fractions higher. This comparison assisted in validation of the model, in that it was following LQ theory for the basic case of conventional oxic tumour radiotherapy.

5.4.1.4.2. The Oxic Tumour "*AR boost Factor*" Study

Using a factor to increase the stem cell symmetrical division probability to model accelerated repopulation (the *AR boost factor*) required a study to determine the effect of this parameter value on treatment response. In this study, the *AR boost factor* and onset times of AR were varied from 3% to 15% and from 0 to 3 weeks respectively, and the consequential extra dose per fraction required to account for the accelerated cell growth calculated (Figure 5.18). Note that the increases in doses per fraction shown in Figure 5.18 apply *during* the period of AR and not from the beginning of the schedule (unless AR was initiated at 0 weeks) and as such the week on AR onset was not a critical parameter.

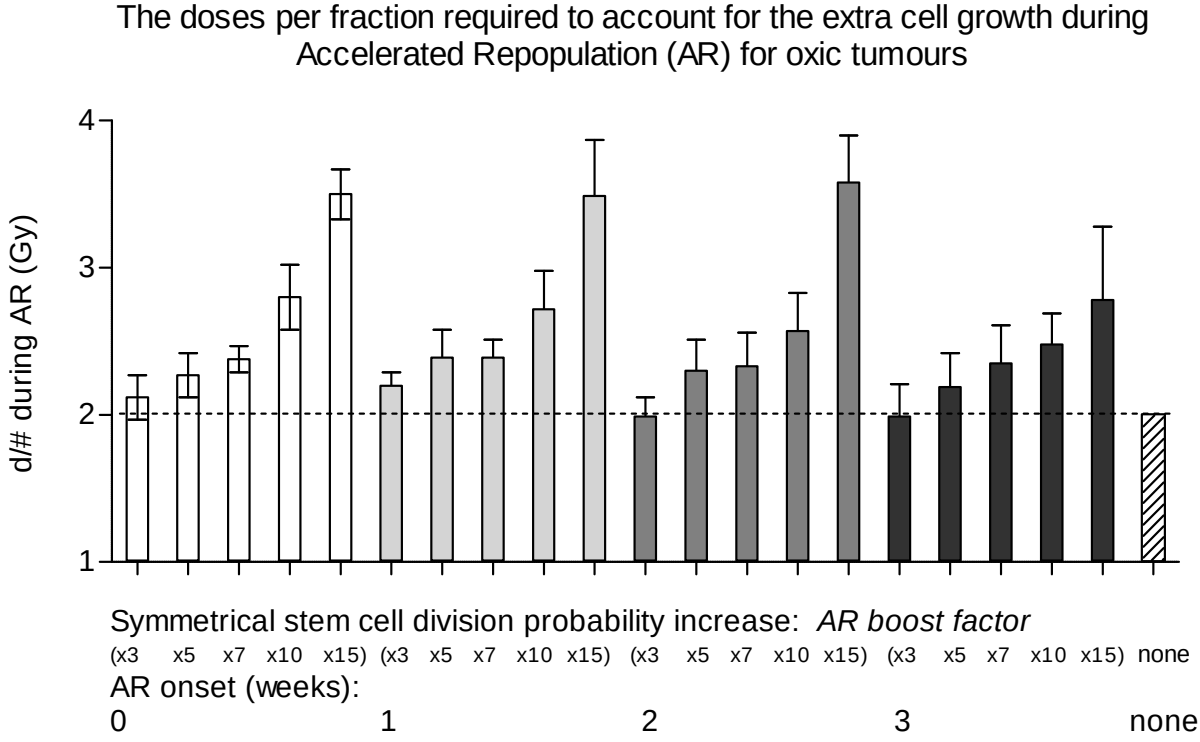

Figure 5.18. The increased doses per fraction (d/#) required during conventional radiotherapy of oxic tumours to account for accelerated repopulation (AR), assuming a fixed total treatment time of 6 weeks and the increase in d/# coinciding with the onset of AR, for various onset times of AR and AR boost factors . A dotted line is shown at the standard 2 Gy per fraction level.

An *AR boost factor* value of 10 resulted in an extra dose per fraction of between 0.5 and 0.8 Gy per fraction, which is consistent with clinical trial reports (Armpilia 2004,

Maciejewski 1989, Tucker 1999, Withers 1988, Fowler 2000). An *AR boost factor* less than 10 increased the dose per fraction by 0.3 Gy or less, and an *AR boost factor* more than 10 resulted in an extra dose per fraction above 1.0 Gy.

As AR has been reported to increase the tumour growth rate by up to 10 times [reducing the potential doubling time ($T_{pot)}$ of the tumour from around 10 to 20 days down to as low as 2 days and approaching the stem cell division time (Begg 1991, Withers 1988)], an *AR boost factor* of 10 was intuitively expected to impact on tumour response in a biologically plausible manner.

Modelling an *AR boost factor* of 10 was also supported by model results showing that the decrease in tumour doubling time was approximately 10 to 15 times after the onset of AR. For example, for moderately hypoxic tumours the tumour doubling time decreased in simulations from approximately 65 days before onset of AR to approximately 4.4 days after onset of AR. Similarly for oxic tumours, tumour doubling time decreased from approximately 37 days before onset of AR down to 3.7 days after the onset of AR (all standard division errors less than 1 day). For moderately hypoxic tumours these doubling times have very good agreement with HNSCC published data (Withers 1988).

5.4.1.4.3. The Effects of Accelerated Repopulation on Tumour Control

To analyse the effects of AR on cell kill, the *AR boost factor* was varied in simulations from 3 to 15. Figure 5.19 a) illustrates the change in the number of fractions required for tumour control, for onset times of AR ranging from 0 weeks (immediate onset) to 3 weeks.

For a AR boost factor of 10 there was a strong linear relationship between the number of fractions and onset time of AR (Pearson r^2 value of 0.93) corresponding to a 2.4±0.4 average reduction in the number of fractions required for tumour control for each week that onset of AR was delayed (Figure 5.19 b).

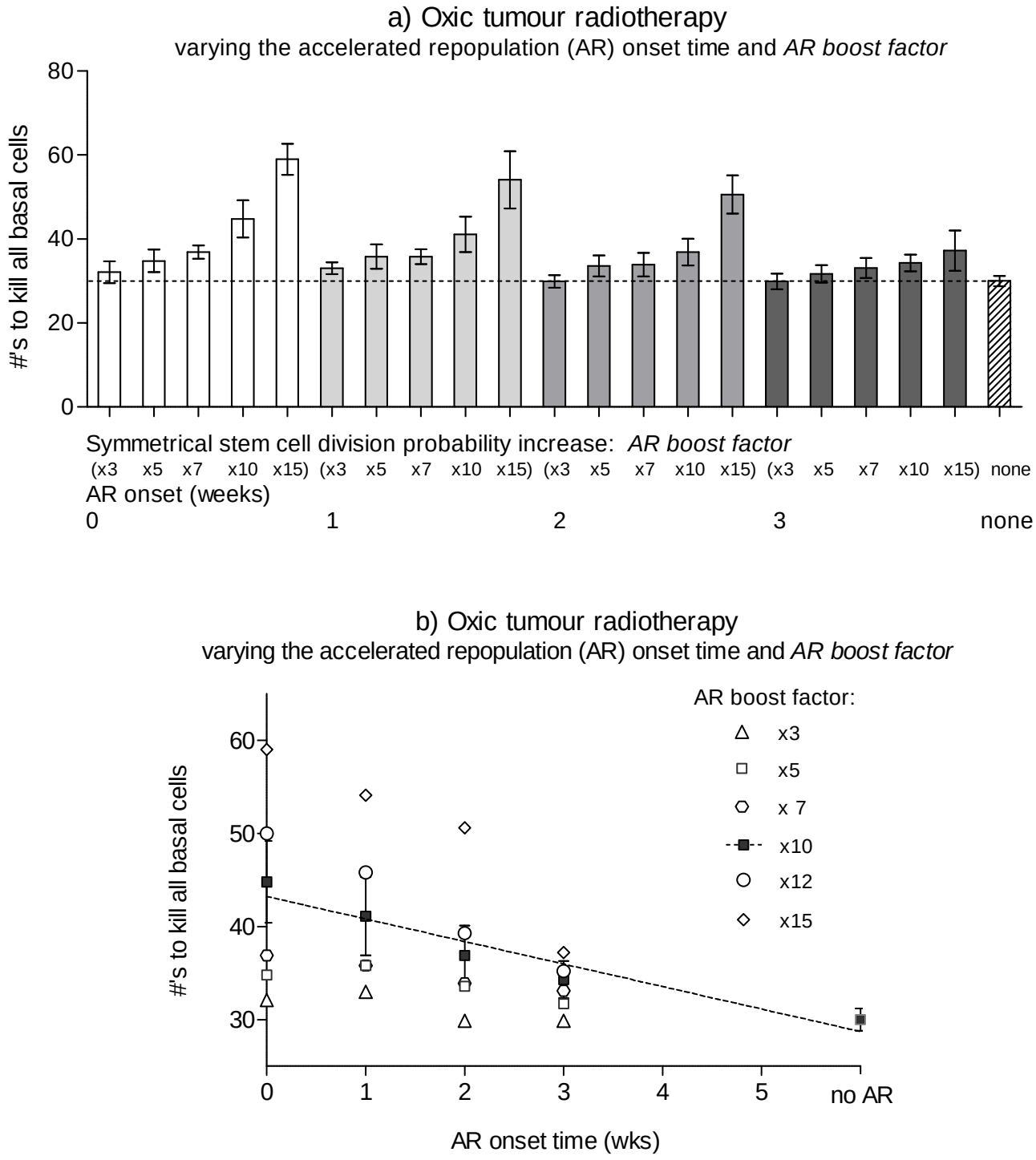

Figure 5.19. The number of conventional radiotherapy fractions required to model 100% TCP in oxic tumours, varying the AR boost factor from 3 to 15 in a) a column graph, and b) in a plot of fraction number versus AR onset time. Note that treatment simulations with no AR considered took 6 weeks of tumour time (30 fractions).

A cell survival curve from an example simulation is shown below (Figure 5.20) for conventionally fractionated radiotherapy. Note that the spacing of the data points is extended during the weekend gap periods.

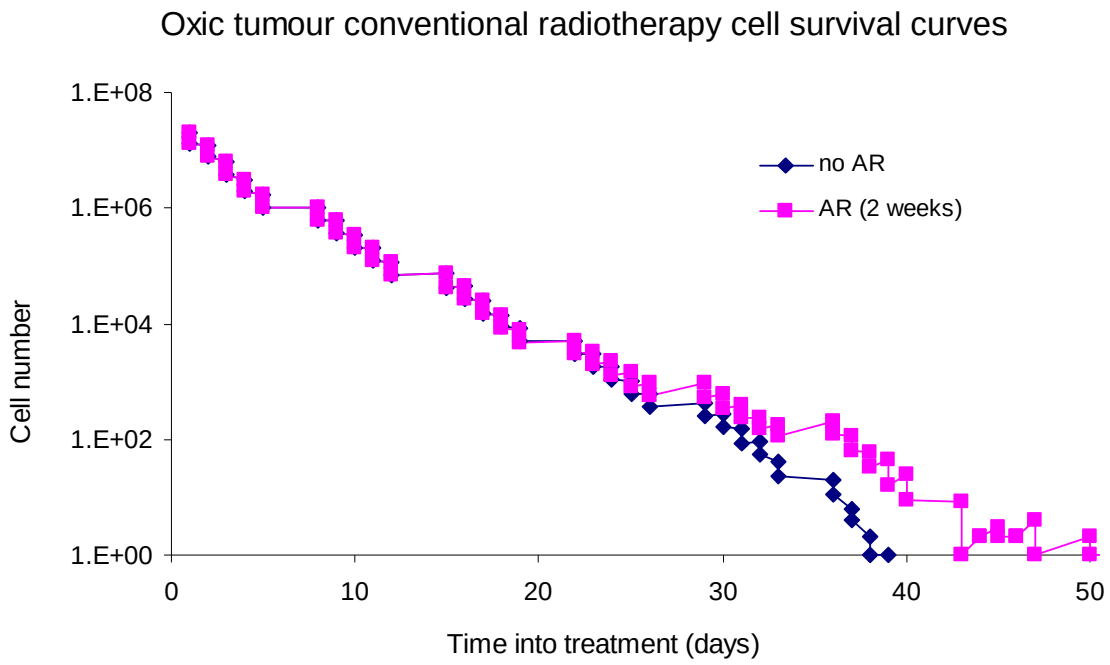

Figure 5.20. Cell survival curves of two oxic virtual tumours undergoing conventional radiotherapy, simulating no onset or AR and onset of AR at 2 weeks into treatment.

For an *AR boost factor* ≥10, AR onset times of ≤2 weeks significantly affected the number of fractions required for tumour control, compared to the no AR case. For an *AR boost factor* <10, no statistical significant difference was found in the number of required fractions. An *AR boost factor* of 15 was ruled out because of the extreme doses (80 to 120 Gy in 8 to 12 weeks) required for tumour control, even for oxic tumours. Such doses would not only be deemed clinically intolerable but also outside of the estimated plausible range for the control of oxic head and neck tumours which tend respond well to standard doses of approximately 70 Gy (Begg 1999, Nordsmark 2005).

The value of 10 for the *AR boost factor* is consistent with results from previous studies (Tuckwell 2008, Armpilia 2004, Fowler 2000, Maciejewski 1989, Tucker 1990, Withers 1988) including the "*AR boost factor* study" discussed earlier in this chapter. Note that radiotherapy treatment with concomitant chemotherapy treatment may delay accelerated tumour repopulation, but this effect has not considered for this report.

The total doses required to achieve 100% tumour control using the *HYP-RT* model ranged from 62 Gy to 108 Gy for moderately hypoxic tumours (depending on onset of ROx and AR). These doses were considered reasonable, considering that 70 Gy if often prescribed in conventional radiation schedules and also considering that the 2 Gy equivalent doses (EQD_2) and the biological effective doses (BEDs) were in the ranges of 54 to 82 Gy (α/β = 10 Gy) without time correction and 63 to 75 Gy (α/β = 10 Gy, α = 0.35 Gy^{-1}, T_{pot} = 4 days) with time correction, respectively. These BED values are in agreement with the doses prescribed in randomised HNSCC clinical trials that have reported improvements in the therapeutic ratio (Dische 1997, Fu 2000, Hliniak 2002, Pinto 1991, Overgaard 2000, Bourhis 2006).

For AR onset times of more than 3 weeks and an *AR boost factor* of 10, no significant difference from the absence of AR was observed during simulations. The exponential shape of the cell kill results for a fixed AR onset time (figure 5.19a) was somewhat expected because of the exponential cell growth caused by the increasing *Spercent* parameter value controlling stem cell symmetrical division probability.

5.4.1.5. Hypoxic Tumour Outcomes

An *AR boost factor* of 10 was also relevant for hypoxic tumour simulations. Results below correspond to a dose per fraction study similar to that performed for oxic tumours (with the added mechanism of ROx) and the results of the number of 2 Gy fractions required to control hypoxic tumours for various onset times of AR and ROx. The more hypoxic, "severe" and "extreme" hypoxia pO_2 distributions (shown previously in Figure 4.3) was used to obtain simulation results for very hypoxic tumours, and compare to oxic and moderate hypoxia results.

5.4.1.5.1. The Hypoxic Tumour "*AR boost Factor"* Study

The AR dose per fraction study described in the previous section was expanded for simulations of moderately hypoxic tumours. During calculations of the dose per fraction the only difference here compared to the oxic tumour study was the use of 8 weeks as the standard treatment time, as this was the treatment time required in hypoxic tumour

simulations with no AR considered. The increases in dose per fraction found in this study were 0.5 to 0.9 Gy using an *AR boost factor* of 10 (Figure 5.21). This increase agreed with oxic tumour simulations and further validated a value of 10 as the most plausible default *AR boost factor*.

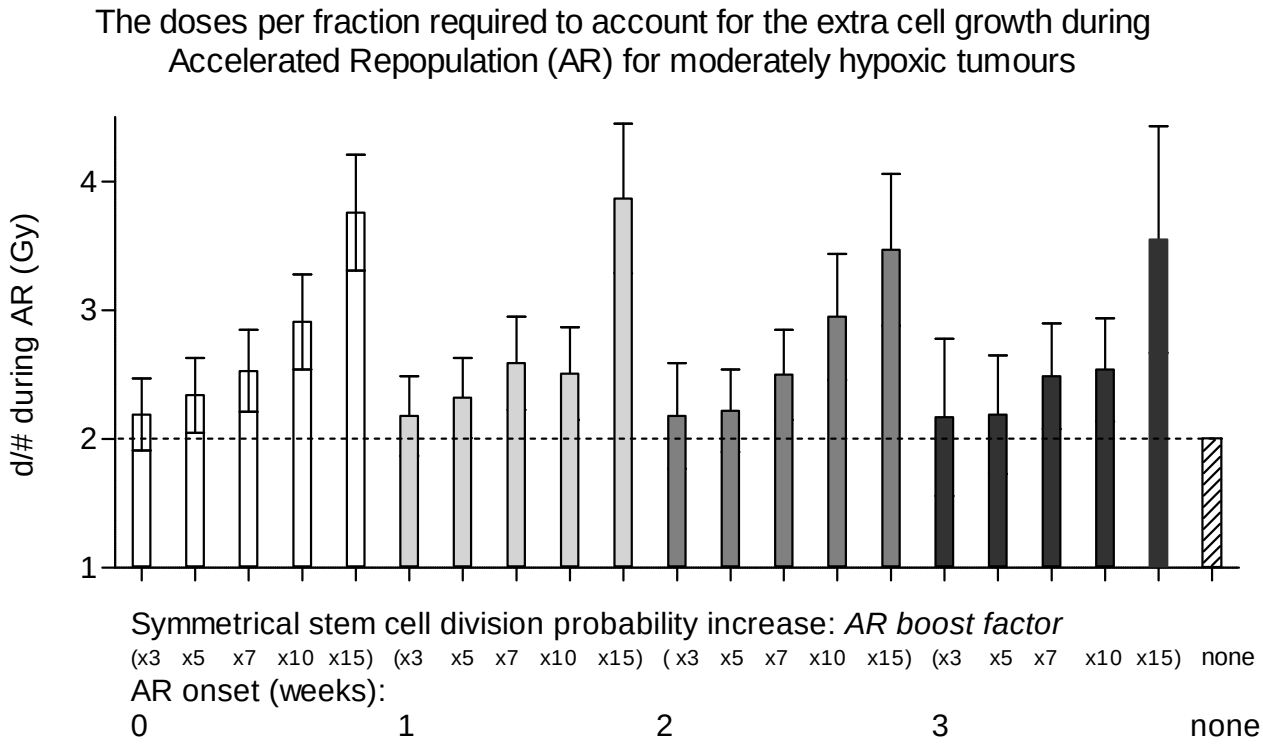

Figure 5.21. The increased doses per fraction (d/#) required during conventional radiotherapy of hypoxic tumours to account for accelerated repopulation (AR), assuming a fixed total treatment time of 8 weeks and the increase in d/# coinciding with the onset of AR, for various onset times of AR and AR boost factor values . A dotted line is shown at the standard 2 Gy per fraction level.

The dose per fraction required during AR to control the extra cell growth was relatively consistent for different AR onset times, because the dose increase only applied *after* AR onset. With ROx also considered the dose per fraction reduced slightly but was still approximately an extra 0.5 Gy per fraction (Figure 5.22).

An AR boost factor of 10 was again concluded as the most valid value based not only on the dose per fraction study, but also according to the decrease in tumour doubling times predicted by the model. For example, the tumour doubling time reduced down to 1 to 5

days after onset of AR compared with 35 to 65 days before onset of AR, with the range depending on the tumours oxygenation status.

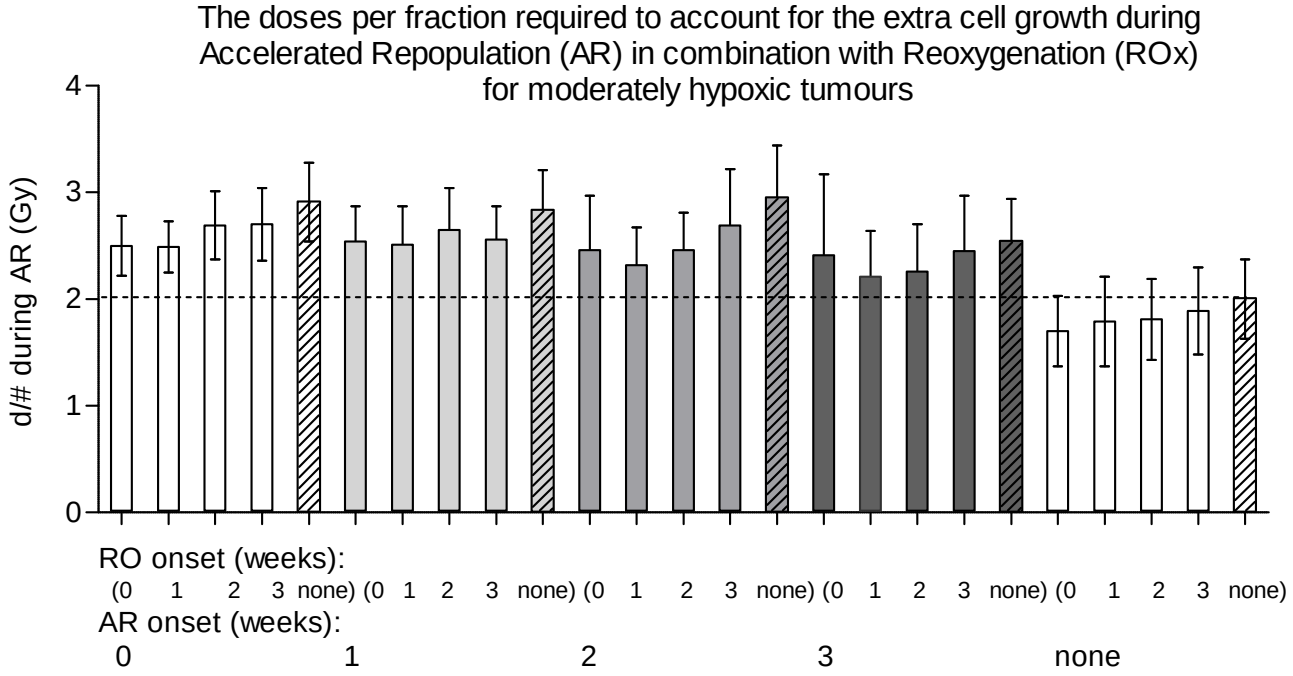

Figure 5.22. The increased doses per fraction (d/#) required during conventional radiotherapy of hypoxic tumours to account for accelerated repopulation (AR), assuming a fixed total treatment time of 8 weeks and the increase in d/# coinciding with the onset of AR, for various onset times of AR and ROx. A dotted line is shown at the standard 2 Gy per fraction level.

From this data it was deduced that the onset time of AR is likely to be ≤2 weeks if ROx occurs at <3 weeks, however the onset of AR could >2 weeks if ROx occurs late or not at all (based on dose per fraction increases of 0.5 to 1.0 Gy per fraction).

5.4.1.5.2. The Effects of Accelerated Repopulation on Tumour Control

For moderately hypoxic tumours, time of the onset of AR influenced cell kill rates for conventional radiotherapy in a similar but lesser extent compared to oxic tumours. The results shown in Figure 5.23a), are for varying the *AR boost factor* from 3 to 15. The linear relationship between the required number of fractions versus onset time for an *AR boost factor* of 10 compared to the oxic tumours was not as strong (Pearson r^2 value of 0.9), as shown in Figure 5.23b). For each week that onset of AR was prolonged the

number of fractions reduced by 2.4 ± 0.5 (approximately 5.0 Gy/week) in accordance with oxic tumour simulations.

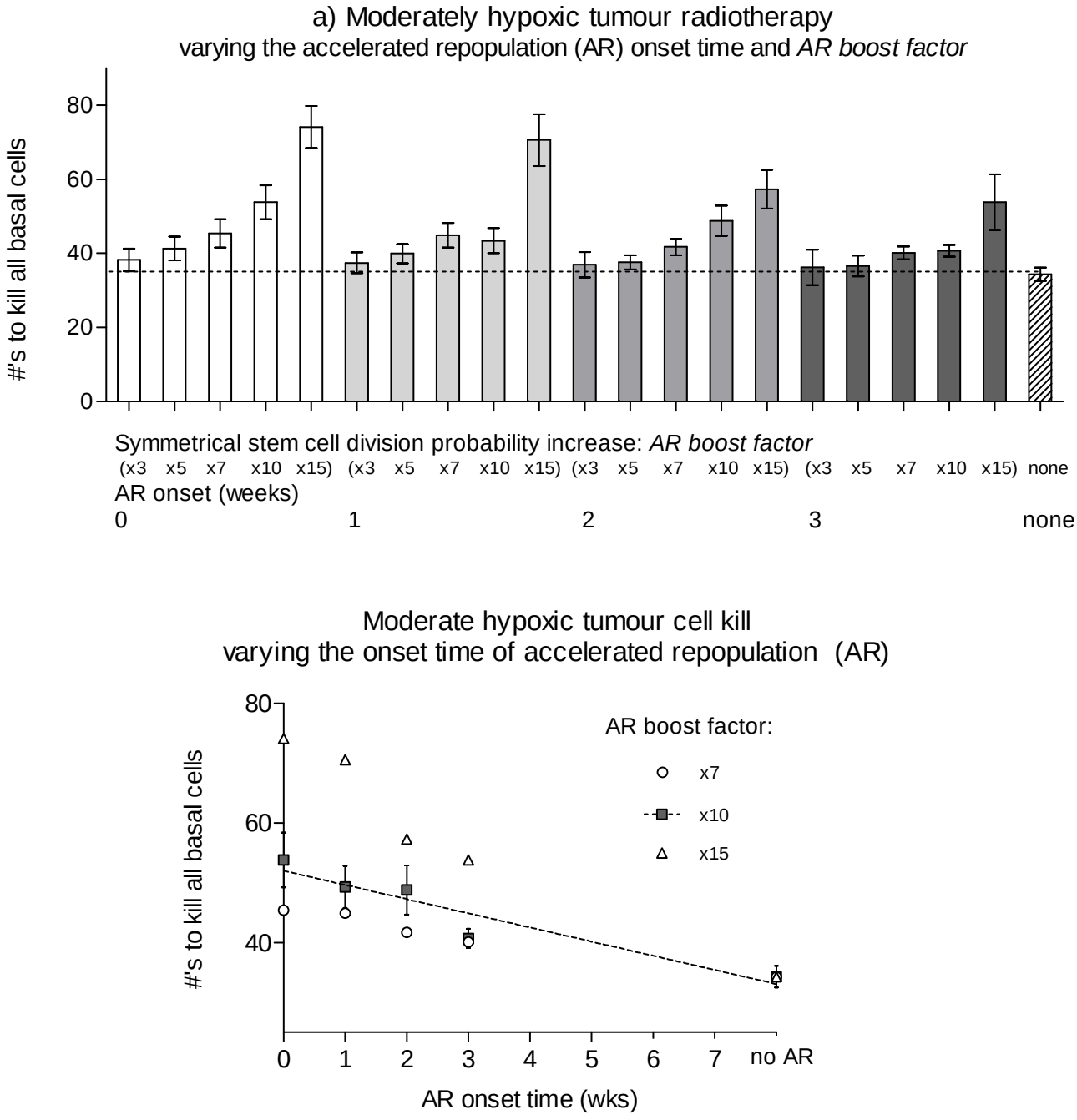

Figure 5.23. A comparison of the average number of conventional radiotherapy fractions required for moderately hypoxic tumours with no reoxygenation (ROx), varying the onset of accelerated repopulation (AR) and AR boost factor from a) 3 to 15, and b) from 7 to 15 in a plot of fraction number vs. AR onset time. A dotted line represents the standard number of fractions for the case of no AR and no ROx.

5.4.1.5.3. The Effects of Hypoxia Induced Cell Quiescence

A small change in the half life of hypoxic quiescent cells did not impact greatly on total cell kill results. Figure 5.24 shows the impact of the hypoxic cell half life on total cell kill and the timing of full tumour ROx, varied from 2 to 6 days. The default half life of 4 days was based on published data (Durand 1998) and used for all other simulations.

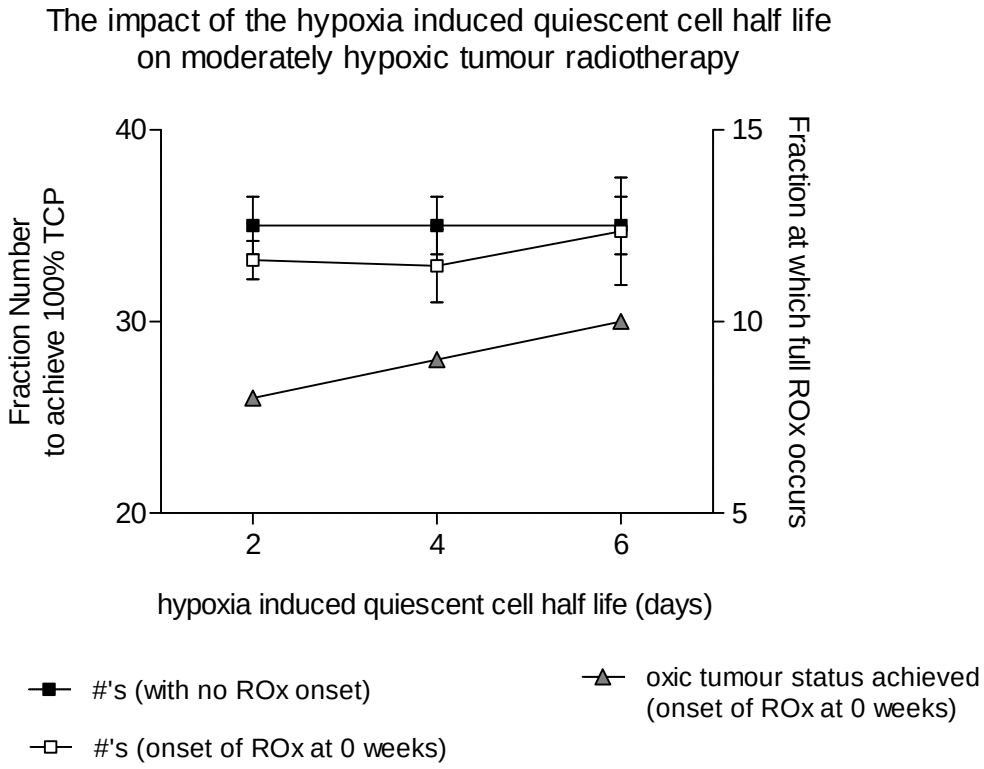

Figure 5.24. A comparison of the average number of conventional (2 Gy) radiotherapy fractions required for cell kill and the timing of full tumour reoxygenation (ROx) for moderately hypoxic tumours, varying the half life of hypoxia induced cell quiescence, with ROx onset at the start of treatment.

5.4.1.5.4. The Effects of Reoxygenation during Radiotherapy

Examples of simulation output pO_2 histograms for a reoxygenating tumour are shown in Figure 5.25. ROx was initiated after each fraction of conventional radiotherapy with full ROx occurring by fraction 11, (when a uniform pO_2 distribution was achieved). The length of time between a treatment fraction and a modelled ROx "event" was set to the

default time of four hours (Ljungkvist 2002). The model smoothly moved the peak of the histogram curve to the right hand side, resulting in gradual average oxygenation level increases to the cell population during treatment.

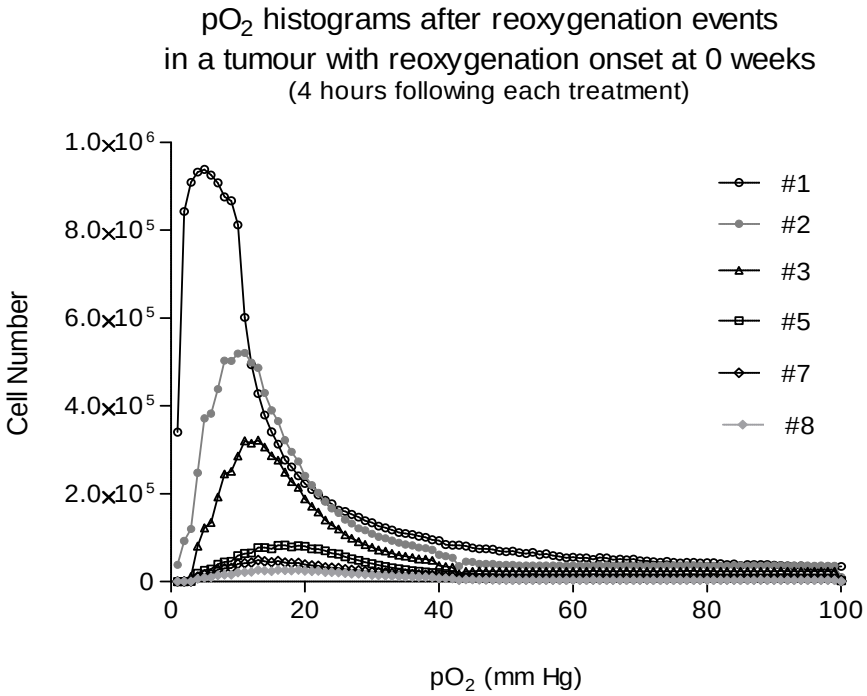

Figure 5.25. Oxygenation histograms after fractions of conventional radiotherapy (fraction 1 to 8 only) for a moderately hypoxic tumour, with ROx initiated four hours after each dose fraction.

Reoxygenation had a radiosensitising effect on hypoxic tumours, decreasing the number of fractions required to achieve 100% TCP (Figure 5.26), as expected. The fraction number increase was linear with ROx onset time, with a Pearson r^2 factor of 0.91. The total dose increased by 6.6 ± 3.6 Gy (11%), comparing the 0 week (immediate) onset and no onset of ROx. On average, for each week that ROx onset was delayed the number of required fractions increased by 0.4 ± 0.1 (approximately 1.0 Gy/week). This dose per week result is difficult to quantitatively compare with clinical data. For example, data from the Seattle group (Koh 1995) report on a reoxygenation related PET study in terms of the fractional hypoxic volume (FHV) of tumours throughout radiotherapy. This data informs us of the percentage of the tumour experiencing pO_2 values of approximately <10 mm Hg, but not the exact time course of reoxygenation or the impact of different reoxygenation times on patient outcome.

The timing of ROx "events" after each dose fraction was analysed for the impact on tumour control. No significant differences were found when ROx events were onset 4, 12, 24 or 48 hours after treatment fractions. This finding was expected as only conventional treatments were simulated for the results in this chapter, with 24 hours between treatment fractions, and therefore the ROx "events" occurred in the model before the next fraction was due and hence there were no sequencing issues between dose delivery and ROx occurred for any simulations.

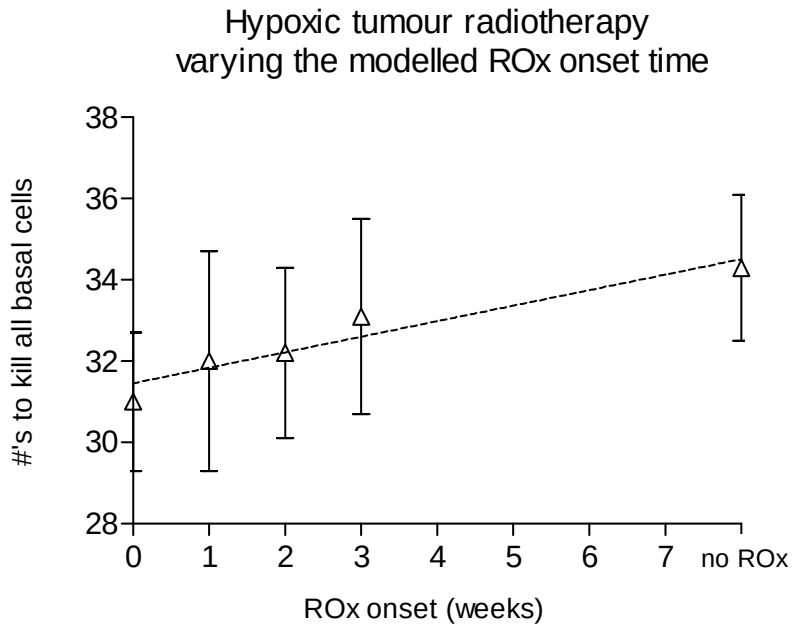

Figure 5.26. A comparison of the average number of conventional radiotherapy fractions required for moderately hypoxic tumours, with increasing reoxygenation (ROx) onset times, with no accelerated repopulation considered.

As clinical outcomes for hypoxic tumours have been reported as relatively poor in a number of HNSCC phase II and III clinical trials, the question arises as to whether these outcomes (LC) results can be potentially attributed to accelerated repopulation or the late onset of reoxygenation. One explanation, based on this modelling study, is that AR rather than ROx is the dominant factor decreasing LC, although ROx can decrease the negative impact of AR to some extent. Simulation results show the large differences in total doses required for tumour control (up to 40 Gy) that apply for tumours depending on their individual properties and responses to treatment, and outline the importance of obtaining or estimating these properties for the prediction of treatment response.

5.4.1.5.5. The Combined Effects of Accelerated Repopulation and Reoxygenation

For simultaneous modelling of AR *and* ROx for hypoxic tumours, the number of dose fractions required for 100% TCP reduced compared to modelling no ROx, as expected. Figure 5.27 presents all combinations of onset times of AR and ROx ranging from 0 to 3 weeks including the cases of no AR and no ROx.

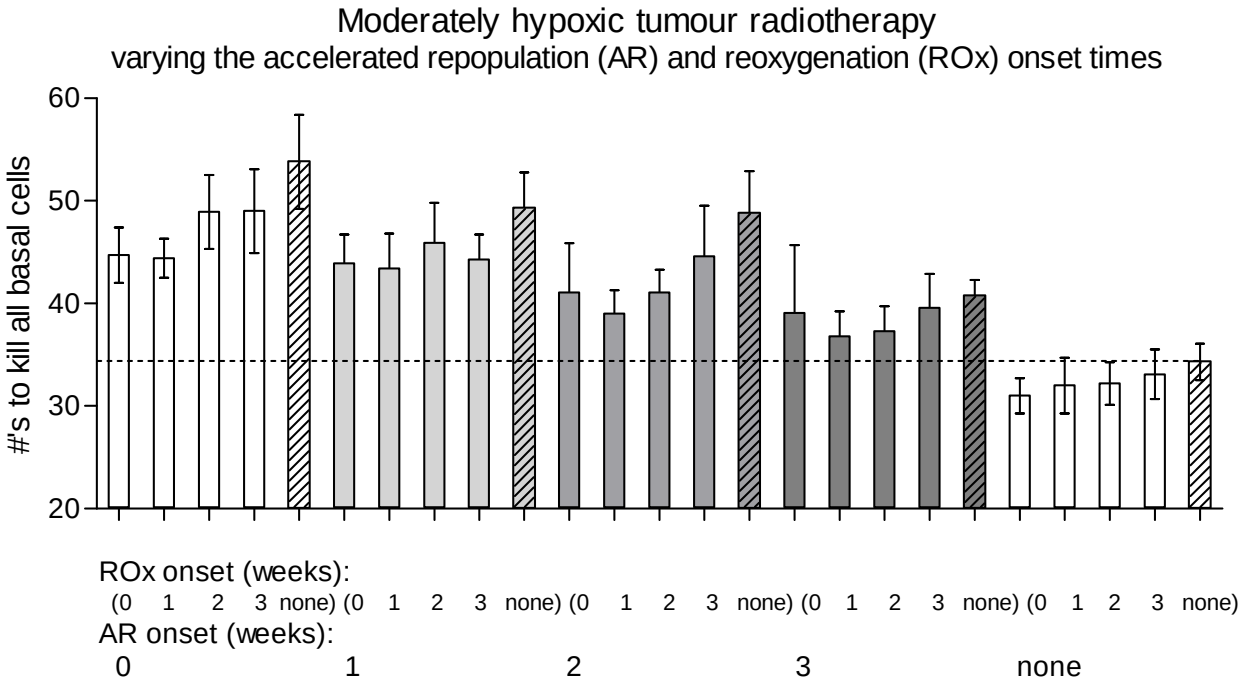

Figure 5.27. The number of treatment fraction required to model 100% TCP for moderately hypoxic tumour conventional radiotherapy, varying the onset times of accelerated repopulation (AR) and reoxygenation (ROx). A dotted line represents the standard number of fractions for the case of no AR and no ROx.

Example cell survival curves are presented for moderately hypoxic tumours with 1) no onset of AR or ROx, 2) onset of AR at 2 weeks with no ROx, and 3) onset of AR at 2 weeks and onset of ROx at 0 weeks (Figure 5.28).

When AR and ROx were modelled together, the number of fractions required to achieve 100% TCP for hypoxic tumours always increased compared to the case of no AR (in a similar trend to the case of oxic tumours). The maximum dose increase attributable solely to AR in hypoxic tumours was approximately 55% compared to the no AR case. This dose increase was much larger than the effect of ROx.

For example;

i) with AR onset at 0 weeks compared to ROx onset at 0 weeks, and each effect modelled separately, there was a **+20** versus a **-3** difference in the number of fractions required to achieve 100% TCP,

ii) with AR onset at 2 weeks compared to ROx onset at 2 weeks there was a **+15** compared to **-2** difference in the number of fractions required to achieve 100% TCP.

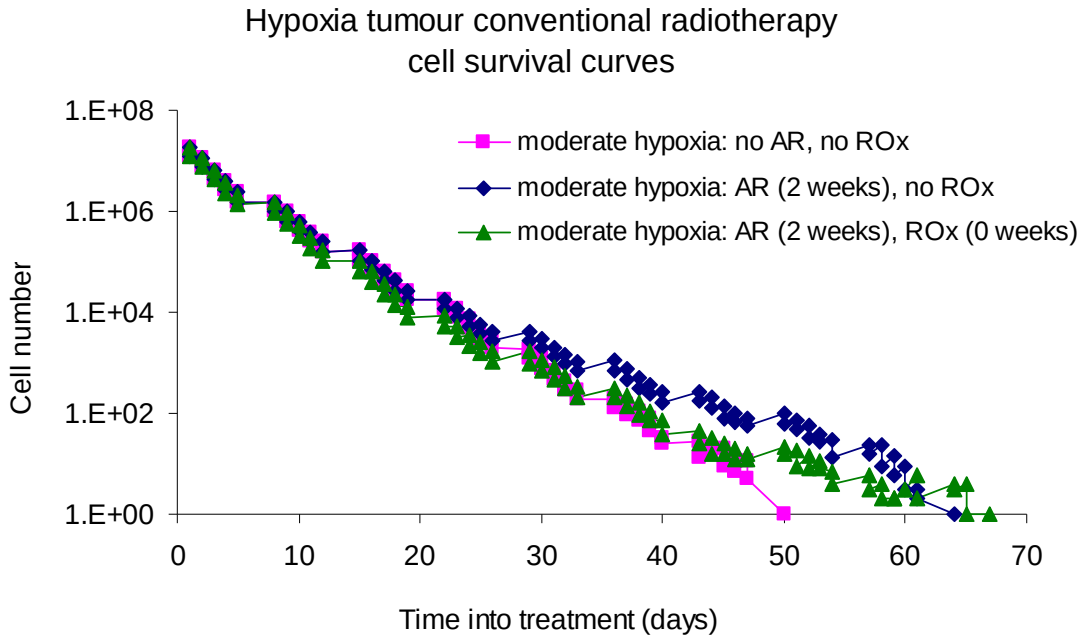

Figure 5.28. Cell survival curves from simulations of conventional radiotherapy of moderately hypoxic tumours, varying the onset times of AR and ROx.

ROx could only offset the extra cell growth caused by AR, for an onset of AR at 3 weeks or later together with simultaneous early onset of ROx. An overall dose reduction advantage for ROx occurred only for the case of ROx onset at week 0 or 1 and with no AR onset.

The effects of the onset of AR and ROx when simulated together could not be estimated through separate simulations of these two phenomena (i.e. non-additive effects). With the onset of both AR and ROx at 0 weeks, the required number of fractions increased by **11,** compared to an increase of **20** and a decrease of **3** when AR and ROx were simulated individually.

A consequence of early onset of both AR and ROx was an increase in the oxic stem cell population. This occurred because quiescent cells were re-entering the cell cycle due to ROx, and CCT's were decreasing. These changes lead to a greater number of stem cells available for symmetrical division and therefore an increase in the percentage of cells with the ability to repopulate the tumour. Studies which report AR to be of no great consequence when ROx is occurring (Scott 1990) have not used Monte Carlo modelling, without which the two dependent effects of AR and ROx cannot be independently predicted.

As the total dose required to control moderately hypoxic tumours was over 100 Gy for the case of immediate onset of AR and no onset of ROx, this combination of effects was not considered plausible (as good *average* LC rates have been achieved with prescription doses less than **80 Gy** in clinical trials, further discussed in Chapter 6). However, in tumours that experience early AR and limited ROx, it is conceivable that radiation doses up to 100 Gy may be necessary to achieve total cell kill. Verification of this dose prescription in the clinical setting would require a specific clinical trial with oxygenation measurements carried out for a carefully selected cohort of patients with hypoxic disease.

5.4.1.6. Comparison of Oxic and Hypoxic Tumour Results

On average it took an extra 16±6 Gy to kill moderately hypoxic tumours (4 to 12 fractions) compared to oxic tumours (Figure 5.29). This dose difference was attributed to the high proportion of cells (50%) that had low oxygenation levels (below 10 mm Hg) and therefore an increased radioresistance (OER values in the range of 1.0 to 2.0).

For hypoxic tumours, the required number of fractions to achieve 100% TCP increased from **34 to 41** for no (or late) onset of AR, and up to **54** fractions for early onset of AR. This translated into a dose increase of up to **40 ± 8 Gy** above the standard 60 to 70 Gy total dose.

This increase was slightly larger than the dose increase found for oxic tumours experiencing AR, however overall the difference was statistically non-significant. It was therefore concluded that the effects of AR were <u>not influenced by tumour oxygenation</u> in

the model, which can be observed from the parallel lines of the linear fits to the data in Figure 5.29.

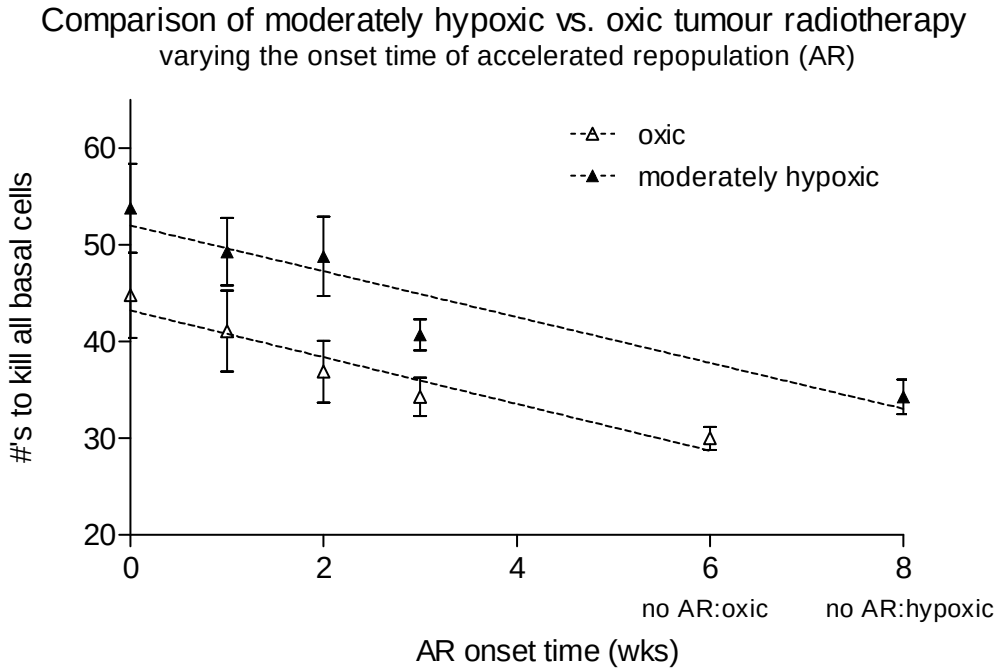

Figure 5.29. The relative influences of AR on oxic and moderately hypoxic tumour simulations, for various onset times of AR and using the default AR boost factor of 10.

When modelling severe hypoxia, no significant differences were found between moderately and severely hypoxic tumour simulation results for all AR and ROx onset times (Figure 5.30). This was unexpected considering the increased number of cells in the lower region of the severe hypoxia pO_2 histogram compared to the moderate hypoxia case (approximately 10% higher cell number in the 0 to 5 mm Hg and 0 to 10 mm Hg pO_2 ranges. These results show that an even more severe pO_2 histogram must be required in order to significantly impact on cell kill rates during simulated radiotherapy.

Similar AR and ROx onset trends were observed for the severely hypoxic tumours compared to moderately hypoxic tumours. For example, there was an inverse linear relationship between onset time of AR and the required number of fractions, and a linear relationship between the onset time of ROx and the number of required fractions.

To model even more severe tumour hypoxia, an "extreme hypoxia" pO_2 histogram, with an increased percentage of cells in the low pO_2 range, was modelled using a normal shaped pO_2 distribution (shown previously in Figure 4.3).

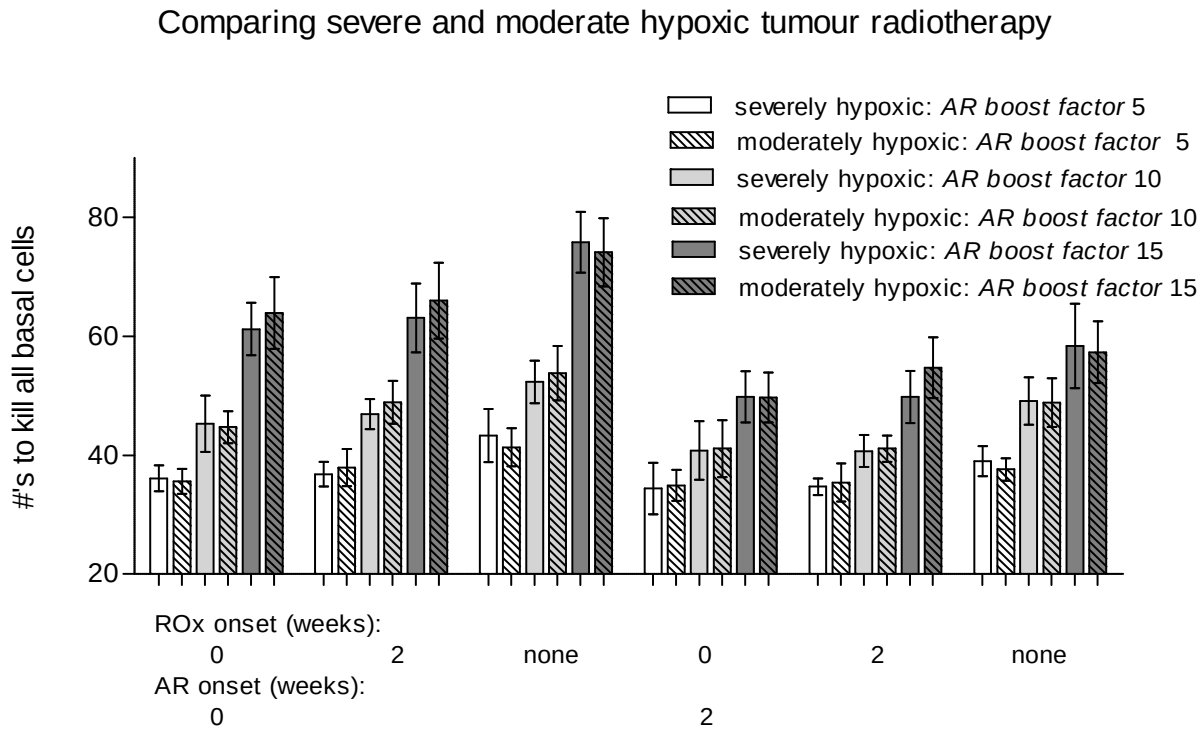

Figure 5.30. A comparison of the average number of radiotherapy fractions required for severely hypoxic and moderately hypoxic tumours for onset times of accelerated repopulation (AR) and reoxygenation (ROx) of between 0 to 2 weeks.

While manipulating and testing the effects of the normal shaped histogram in the model, it was found that increasing the percentage of cells above 3% in the very low pO_2 range of 0 to 1 mm Hg, caused tumour growth to cease. Growth ceased because of the increased percentage of hypoxia induced quiescent cells which had a finite life span (half life of 4 days).

Interestingly, the use of the extreme pO_2 histogram did not always impact on the dose required for 100% TCP. The only significant increase in required total dose occurred for the case of AR in the absence of ROx (Figure 5.31). This could not be accounted for by the natural necrotic death of the hypoxic cells because the number of cells induced to the quiescent state by hypoxia was maintained from moderate hypoxia simulations (3%).

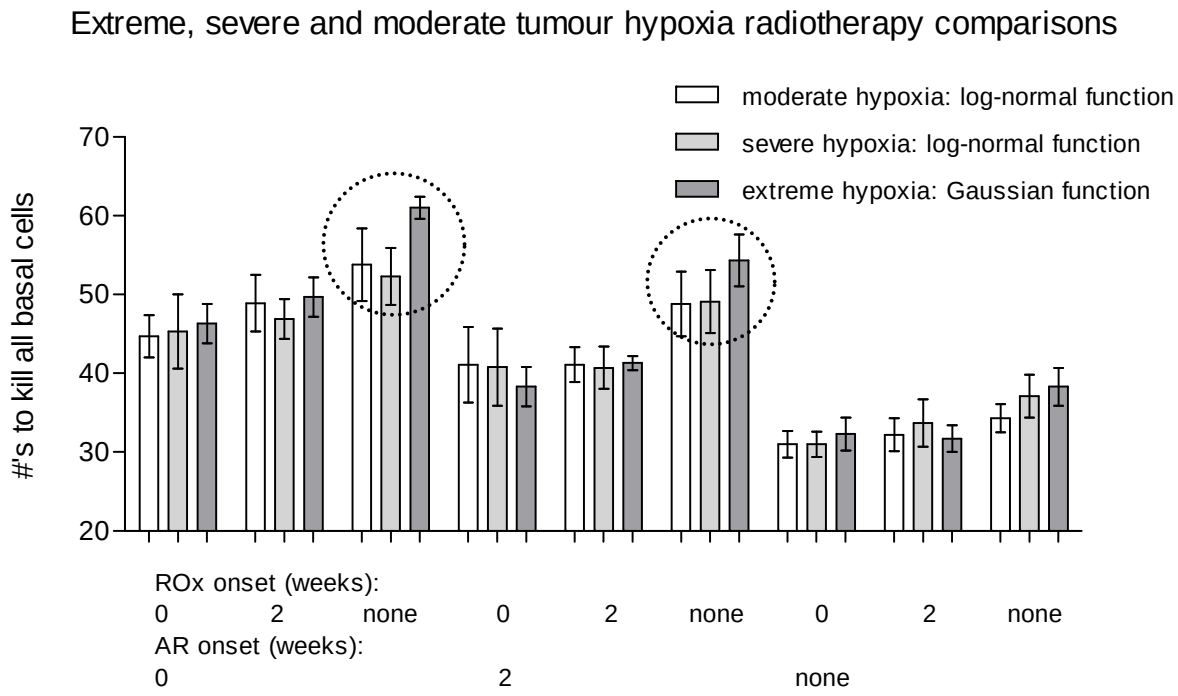

Figure 5.31. The effects of moderate, severe and extreme hypoxia on tumour control, varying the onset times of accelerated repopulation (AR) and reoxygenation (ROx), outlining the combination for which extreme hypoxia required an increased dose.

It was thus concluded that the degree of hypoxia, defined by the shape of the pO_2 distribution, was not critical in this work (compared to the onset of AR) for the prediction of the dose required for 100% TCP, when more than 50% of the cell population have pO_2 levels $\leq$ 10 mm Hg. In future work, even *more extreme* hypoxia will be investigated, to see if the tumour can be grown successfully without cessation of growth, while having more detrimental effects tumour control, compared to the hypoxia distributions used to obtain the current results.

5.4.1.7. Results Summary

On average, the final **1 to 2 fractions** accounted for the elimination of the very last tumour cell in conventional radiotherapy simulations, while the last **3 to 6 fractions** accounted for the elimination of the last five cells. The final fractions are therefore paramount for the achievement of tumour control.

In oxic as well as hypoxic tumours, AR dominated tumour regression rates during conventionally fractionated radiotherapy. An increase of **0.5 to 1.0 Gy per fraction** was required to kill the extra cells propagated during AR (with a default *AR boost factor* of 10), equating to an additional average dose of **2.4 Gy** for each week that onset of AR was brought towards the start of treatment. ROx however, required only an additional **0.4 Gy** for every week that is was delayed after the start of treatment.

The difference in the total dose required to control moderately hypoxic tumours versus oxic tumours was approximately **16 Gy**, regardless of AR onset time. Varying the onset times of AR and ROx for hypoxic tumours meant that the total dose required for 100% TCP varied by up to 40±10 Gy, which is a very considering the conventional 70 Gy prescription dose for HNSCC. The results from severely hypoxic versus moderately hypoxic tumour simulations were not significantly different for the pO_2 distributions modelled. The half life of quiescent hypoxic cells did not significantly impact upon cell kill, although it did affect the time at which full reoxygenation occurred.

5.4.2. Validation of the *HYP-RT* Model

5.4.2.1. Comparison to Linear Quadratic Theory

The standard LQ model predicted the need for **26** fractions to reduce a tumour of 10^8 cells down to less than 1 cell, using 2 Gy per fraction and an α/β value of 10 Gy. The LQ model with an onset time of AR of 2 to 3 weeks predicted the need for **31 to 34** fractions for the same tumour, using a T_{pot} value of 4 days.

The results of the LQ and HYP-RT comparison are shown in Table 5.5. For oxic tumours, there was a close correlation between the LQ and HYP-RT models both for no AR and onset of AR at 2 to 3 weeks. For hypoxic tumour comparisons the use of an average q value in the LQ model for the cases of no AR (no time factor) as well as onset of AR at 2 to 3 weeks, resulted in a good agreement between the two models. Adjusting the q value had a very large impact on the LQ model results, as shown in the lower section of Table 5.5. For example, using a q value of 2.0 in the LQ equation to model a

small hypoxic sub-volume (3% used to best match the cell population in the 0 to 1 mm Hg pO_2 range used in the *HYP-RT* model) resulted in **93 to 100** (2 Gy) fractions, with the two models no longer in agreement.

Table 5.5. Comparison of the HYP-RT and linear quadratic (LQ) models in terms of the number of 2 Gy fractions required for 100% tumour control probability (TCP) or the first occurrence of less than 1.000 cell survival, respectively, including the effects of accelerated repopulation (AR) and with a "q" value representing the dose modification factor due to low oxygenation in the LQ model.

		The number of 2 Gy Fractions required per 10^8 cell tumour to achieve:	
		1. 100% TCP in the *HYP-RT* model: *for the oxic or moderately hypoxic pO_2 distribution*	**2. Cell kill down to less than 1.000 cells in the LQ model:** *the first fraction achieving this level of cell kill*
	Time Factor settings *for AR:*	**OXIC TUMOURS**	
1.	No time factor	27±2	26
2.	No AR time factor (2 to 3 weeks **AR** onset)	33 to 35±3	31 to 34
	Time Factor settings *for AR:*	**HYPOXIC TUMOURS**	
1.	No AR time factor	33±3 OR 29 to 32±3 (if ROx is onset at 0 to 2 weeks)	32 (LQ: **q=1.182***)
2.	With AR time factor (2 to 3 weeks **AR** onset)	41 to 49 ±3 OR 37 to 41±3 (if ROx is onset at 0 to 2 weeks)	42 to 45 (LQ: **q=1.182***)
3.	No AR time factor		32 (LQ: **q=1.2**)
4.	No AR time factor		38 (LQ: **q=1.4**)
5.	No AR time factor		44 (LQ: **q=1.6**)
6.	No AR time factor		50 (LQ: **q=1.8**)
7.	No AR time factor		56 (LQ: **q=2.0**)
8.	No AR time factor		46 (LQ: **3% q=2.0, 97% q=1,** to represent the ~3% cell population in the ≤1 mm Hg range)
9.	AR time factor (onset of **AR at** 2 to 3 weeks)		93 to 100 (LQ: **3% q=2.0, 97% q=1,** to represent the ~3% cell population in the ≤1 mm Hg range)

* an average equivalent *q* value of 1.182 corresponds to the average pO_2 value in the moderately hypoxic tumour pO_2 histogram.

Compared to patients in the convention schedule arms of clinical trials and basic LQ theory, the number fractions required in simulations for 100% TCP was in good agreement for the oxic tumours. For hypoxic tumours, the *HYP-RT* model, LQ theory and clinical trial data were not always in agreement. The LQ theory used was basic in terms of a single *q* value representing the hypoxic cell population radiosensitivity, which resulted in an extremely sharp increase in the required fraction number with increasing *q* beyond reasonable fraction numbers for HNSCC.

The data would suggest that a hypoxic cell percentage of less than 10% is likely to exist clinically when considering very low oxygenation levels (with *q* values of approximately 2). To account for this situation, either a smaller percentage of hypoxic cells must exist in real tumours or else there must be a wide spread of oxygenation levels in tumours with only a very small percentage of cells within the very low (0 to 1 mm Hg) pO_2 range. The second explanation is considered valid as a large range in pO_2 values in HNSCC has been verified experimentally in human tumours on many occasions using the Eppendorf probe (Adam 1999, Lartigau 1998).

In addition, tumour reoxygenation which is likely to occur at some stage of tumour shrinkage in most real tumours decreases the average *q* value of the cell population with time and hence the fraction number required for tumour control (as indicated by the results in this work). An accurate estimate of this reduction would necessitate *in vivo* pre and inter-fraction oxygenation data.

The LQ model predicted the need for approximately **100** 2 Gy fractions for moderately hypoxic tumour control when an AR time factor was considered. It also predicted a relatively small (3%) hypoxic cell population when a *q* value of 2.0 was used. For comparison, the *HYP-RT* model predicted **40** fractions for moderately hypoxic tumours, up to **45** fractions with an onset time of AR time of 2 weeks, and **55** fractions for immediate onset of AR if no ROx was modelled (using a pO_2 histogram with 3% of cells in the 0 to 1 mm Hg range, and 7% in 0 to 2 mm Hg range) which more closely match HNSCC clinical prescriptions.

5.4.2.2. Comparison of the Model with Clinical Trial Data

In a selection of results from large clinical trials reports published between 1990 and 2004, the average LC rate for HNSCC was between 40% and 50% at 2 to 5 years for the conventional 5x2 Gy per week schedule delivered in 6.5 to 8 weeks. In many studies, LC has been reported to decrease significantly for advanced stage tumours which were of larger size and with a faster proliferating cell population. (Antognoni 1996, Begg 1991, Fu 2000, Horiot 1994, Horiot 1997, Selek 2004).

The total doses required to achieve 100% TCP in the *HYP-RT* model ranged from **62 to 108 Gy** for hypoxic tumours depending on onset times of ROx and AR. These doses are reasonable considering the **70 Gy** often prescribed for conventional radiotherapy schedules and the equivalent 2 Gy per fraction doses (EQD_2) of **54 to 82 Gy** (α/β = 10 Gy) and biological effective doses of **63 to 75 Gy** (α/β = 10 Gy, α = 0.35 Gy^{-1}, T_{pot} = 4 days) from advanced stage HNSCC altered fractionation clinical trials (Dische 1997, Fu 2000, Hliniak 2002, Pinto 1991, Overgaard 2000, Bourhis 2006).

An unavoidable limitation of the comparison of the model results from this work with human data is the heterogeneous tumour oxygenation levels present in the real tumour groups, even in similarly selected patients in clinical trials. There are also large variations in total cell numbers in different real tumours. Further, the exact number of fractions required to kill all tumour cells can not be readily obtained from clinical trials LC outcomes (only LC rates at 2 to 5 years), to compare with the model.

The reported average LC percentages in clinical trials are the closest matching data that can be used to compare human data with model predictions. The average LC percentages can be roughly equated to the average remaining tumour cell numbers using the Poisson model, with 50% corresponding to 0.7 cells remaining, or alternatively 70% of tumours having one cell remaining to potentially regrow the tumour. According to Poisson theory, it is thus reasonable to expect a higher number of required fractions to control tumours in a clinical trial patient group if a significant proportion of the tumours had some degree of hypoxia present.

A small number of clinical trials have been specifically aimed at analysing tumour properties such as oxygenation and the associated impact on tumour control. These trial reports provide the initial evidence of the significant negative impact of low oxygenation in HNSCC's on LC (Gatenby 1988, Lehtio 2004, Nordsmark 2004, Nordsmark 1996, Rischin 2006). Unfortunately however, averaging these trial results and equating this difference to the number of fractions required to kill all cells in the *HYP-RT* model (or the LQ model) is very difficult, particularly as clinical studies report upon the impact of hypoxia on LC in different ways. For example, some reports state the difference in outcome for tumours above or below a mean/median pO_2 level, while others correlate LC with the percentage of cells below a pO_2 threshold (e.g. 2.5 mm Hg) or correlate LC with the presence of any hypoxia at all (using imaging modalities such as PET).

A clinical trial report by Rischin *et al* presented LC results that were based on dividing patients into groups above and below the median percentage of cells of 2.5 mm Hg (median of 15%) (Rischin 2006). The 35 patients received 70 Gy in 2 Gy fractions, which resulted in a 33% versus 77% LC rate (Rischin 2006). Using Poisson theory, the average remaining cell number in each of the LC groups would have been approximately 1 and 0.3 cells for the 33% and 77% LC groups respectively.

This LC difference is a very large difference in clinical outcome, with LQ theory predicting an extra **2 to 3** fractions being required to bring the remaining cell number in the 33% group equal to that in the 77% group. Moreover, the fraction number required could be up to 3 times greater (**6 to 9** fractions) if the last remaining cells were hypoxic, equating to a **4 to 6 Gy** increase for oxic remaining cells and up to a **12 to 18 Gy** increase for hypoxic remaining cells (an increase of **8 to 12 Gy**). In contrast to these LQ model predictions, the *HYP-RT* model predicted the need to increase the required dose by **20 Gy** to achieve LC in hypoxic compared to oxic tumours hypoxic tumours (which would reduce if ROx was also modelled).

Chapter 6 will extend the *HYP-RT* model versus clinical trial comparison for a selection of relatively successful as well as unsuccessful altered fractionation clinical trial schedules (in terms of improvements to the therapeutic ratio) for advanced stage HNSCC.

5.5. Radiation Effect Algorithm Conclusions

The *HYP-RT* model includes a radiotherapy effect algorithm, to simulate fractionated radiation induced cell kill for oxic and hypoxic tumours. The algorithm was designed to achieve convenient computational and temporal efficiency (1 to 2 minutes), while maintaining an individual cell approach.

Due to the random nature of radiation beam energy deposition and the complexities and dynamic nature of the parameters required in the model (e.g. the cellular oxygen distribution and the processes of tumour reoxygenation and repopulation), MC modelling methods were used to model radiation induced cell death and the response of the surviving cells throughout the treatment course.

Four different tumour oxygenation levels were included this work, to analyse the effects of tumour hypoxia on tumour control after conventional radiotherapy, with the degree of oxygenation defined as oxic, moderately hypoxic, severely hypoxic and extremely hypoxic.

Key results are summarised here in dot point:

- The ROx algorithm provided a method of manipulating cellular oxygen levels throughout treatment to model the gradual increase of tumour reoxygenation in moderately, severely or extremely hypoxic virtual tumours to a fully oxygenated (oxic) tumour.

- The AR algorithm provided a method of increasing the cell propagation rate using a parameter controlling the stem cell symmetrical division probability (the *AR boost factor*). An *AR boost factor* of **10** was concluded to be most biologically relevant value, which was validated by the increase in the dose per fraction (from 2.0 Gy up to **2.5-3.0 Gy** per fraction after AR onset) required in simulations to kill the extra cell growth, while maintaining 100% TCP for the same length treatment course.

- AR was the most dominant effect during treatment, requiring up to **40±10 Gy** increased in the total dose to achieve 100% TCP. ROx effects were less dominant but were significant for hypoxic tumours when the onset at 2 weeks or earlier after the start of treatment.

- On average, moderately hypoxic tumours required an extra **16±6 Gy** compared to oxic tumours to achieve 100% TCP, but in general no significant dose increase was necessary when modelling severe or extreme hypoxia (unless AR was modelled in combination with no ROx).

- The effects of AR and ROx were not independent in the model. Therefore, separate simulations for each combination of onset time of AR and ROx were required in simulations to explore the effects of these two phenomena.

- Oxic tumour simulation results agreed well with the LQ model with modifications for oxygenation and AR. Hypoxic tumour simulation results were difficult to compare to the LQ model, but gave overall more clinically realistic total dose predictions than LQ theory for hypoxic tumours (**62 to 108 Gy** depending on the onset times of ROx and AR).

This model has provided an efficient and reproducible analysis tool to investigate the effects of AR and ROx on cell kill during conventionally fractionated radiotherapy. Results in this report will now proceed to explore altered clinical trial fractionation schedules and compare model results with published reports and further be used to explore newly devised altered fractionation schedules.

Chapter 6

Modelling Altered Fractionation Radiotherapy

6.1. Introduction

It is well established that some patients with advanced HNSCC receiving radiotherapy can benefit from an altered fractionation schedule, compared to the conventional schedule of 2 Gy delivered 5 times per week. This benefit has been demonstrated in randomised clinical trials, based on the so called *time-factor* principle, for radiotherapy of head and neck cancers (Withers 1988). This principle was proposed to apply predominantly to fast growing tumours with relatively high α/β ratios (fractionation independent according to the LQ model) that trigger the tumour cell population to grow at an accelerated rate sometime after commencement of radiotherapy treatment. Thus, shortening results in elimination of all or most of the clonogenic cells in the tumour before the accelerated cell repopulation is initiated.

Ten different clinical trial schedules were simulated using the *HYP-RT*, to investigate the potential of the model in accurately predicting the level of cell kill achieved in altered fractionation radiotherapy schedules for HNSCC. The aim of simulating these schedules was to validate the *HYP-RT* model with real patient data and to investigate the variations in total doses required for 100% TCP when altering specific tumour characteristics such as the onset time of reoxygenation and accelerated repopulation.

Owing to the well recognised heterogeneity of tumour characteristics including response to treatment, even in randomised trials of altered fractionation, it is still very difficult to predict whether individual patients will benefit from the use of a particular schedule.

Model predictions and clinical trial results were compared in the current work in a number of ways. Firstly, the total delivered doses and total times of treatment were compared, while modelling 100% TCP. Secondly, two methods were devised to compare model cell kill predictions with clinical trial local control (LC) rate outcomes. Radiotherapy clinical trial outcomes are commonly reported in the form of the average patient LC percentage or survival percentage after 2 to 5 years. In this work, clinical LC percentages were compared to model results by converting cell survival into TCP using, 1) the Poisson equation, or 2) directly counting the number of controlled tumours having all cells eliminated while varying the random seed number in the model.

The model and clinical trial results comparisons were performed for various onset times of accelerated repopulation (AR) and reoxygenation (ROx), with conclusions drawn regarding the most likely combinations of AR and ROx onset times. When comparing the model TCP results with clinical trial LC percentages in the later part of this chapter, model results were based only on the elimination of tumour stem cells. This approach was chosen to be consistent with other computer model reports of TCP versus clinical local control (Harting 2007). In any case, the final results presented in this chapter did not have any significant differences when considering stem cells alone or all "basal" cells (discussed in section 6.3.1) because of the statistical errors involved.

To extend the analysis and compare individual modelled fractionation schedules, simulation results were also ranked in terms of the calculated biological effective doses (BEDs) to normal tissues. The normal tissue parameters chosen in this chapter correlate with late onset effects, representing reactions such as tissue fibrosis and telangiectasia, and acute onset effects (or early effects) such as oral mucositis.

Although normal tissue cells were not simulated with the model, BED equations were used with published parameter values for acute and late reacting tissue reactions, and assuming that the normal tissue received 100% of the tumour dose (outlined in Tables 6.2 and 6.3). The aim of the BED analysis was to find the most efficient schedule from a set of simulations in which 100% TCP had been achieved, by finding the schedule with the lowest relative BED's to normal tissues.

6.2. Modelling Altered Fractionation Schedules

The altered schedule *HYP-RT* results in this chapter are reported in terms of the total doses and treatment times that were required to achieve 100% tumour control. For these results, tumour control has been defined in a similar way as the previous chapter, i.e. the dose at which all stem cells, transit cells, level 1 differentiating cells and *all* hypoxic quiescent cells are eliminated (unless otherwise indicated).

6.2.1. Radiotherapy Schedule Selection

A selection of seven clinical trial altered fractionation schedules which have been reported to improve the therapeutic ratio in the treatment of locally advanced HNSCC were simulated with the *HYP-RT* model. Clinical trial fractionation schedules were deemed to improve the therapeutic ratio if there was an increase in LC compared to the conventional fractionation treatment arm. (Bourhis 2006, Dische 1997, Fu 2000, Hliniak 2002, Horiot 1997, Overgaard 2000).

For a more comprehensive comparison, a further two schedules were also simulated that had provided a decrease in LC or a significant increase in acute or late toxicity (Horiot 1997, Skladowski 2000), as well as a schedule with a introduced after 2 weeks of treatment to analyse the effects of the break on overall cell kill (Fu 2000). Thus, eleven radiation schedules (including the conventional schedule) were simulated in total (Table 6.1) for oxic and moderately hypoxic virtual tumours of 10^8 cells.

Table 6.1: The 11 HNSCC clinical trial schedules simulated with the HYP-RT model. Schedules 2 to 8 are from therapeutically beneficial trials, schedules 9 to 10 are from trials with no therapeutic gain, and schedule 11 is one in which a two week break has been inserted to simulate patient recovery time due to acute effects.

	Clinical Trial Simulated:	**Fractionation Category:**	**Fractionation Scheme: M T W Th F S Su M T W Th F (repeating)**	**Dose / # (Gy)**	**#'s / day**	**Days/ wk**	**Total Dose (Gy)**	**Total #'s**	**Total Time (wks)**	**Trial LC (%) at 2-5 years (vs. conv. RT)**	**Late toxicity compared to the conventional schedule arm of the trial, BED_{late}:**
1.	Conventional	Standard 2 Gy per Fraction	**I I I I I I I I I I …..**	**2.0**	**1**	**5**	70.0	35	7.0	49 (average)	N/A, BED_3 = 70 Gy
2.	RTOG: Fu et al 2000	Hyperfractionated	**II II II II II II II II II II …..**	**1.2**	**2**	**5**	81.6	68	6.8	54 (vs. 46)	Late –slight increase, but not significant, BED_3 = 114 Gy
3.	Pinto et al 1991	Hyperfractionated	**II II II II II II II II II II …..**	**1.1**	**2**	**5**	70.4	64	6.4	62 (vs. 52)	Late – no increase, BED_3 = 96 Gy
4.	Hliniak et al 2000	Accelerated	**I I I II I I I I II I …..**	**2.0**	**1** or 2	**5**	66.0	33	5.5	81 (vs. 85)	Late – no increase, BED_3 =110 Gy
5.	DAHANCA: Overgaard et al 2000	Accelerated	**I I I I I I I I I I I I …..**	**2.0**	**1**	**6**	66.0	33	6.5	76 (vs. 64)	Late – no increase, BED_3 =110 Gy
6.	GORTEC: Bourhis et al 2000	Hyper Accelerated	**II II II II II II II II II II …..**	**1.8**	**2**	**5**	63.0	35	3.3	58 (vs. 34)	Late – no increase, BED_3 =101 Gy
7.	UK (CHART): Dische et al 1997	Continuous Hyper Accelerated	**III III III III III III III III III III III III**	**1.5**	**3**	**7**	54.0	36	1.7	52 (vs. same)	Late – reduced, BED_3 =81 Gy
8.	RTOG: Fu et al 2000	Concomitant Boost (after 5 weeks)	**I I I I I I I I I I (for 3.6 wks)** **II II II II II II II II II II …..**	**1.8** 1.5 Gy boosts	**1** 2 during boosts	**5**	72.0	42	6	55 (vs. 46)	Late – no increase, BED_3 =113 Gy
9.	EORTC spilt course 22851, Horiot et al 1997	Split Course Hyper Accelerated (2 week break after 8 days)	**III III III III III III (1.8 wk break)** **III III III III III III III III III III ……**	**1.6**	**3**	**5**	72.0	45	5.8	59 (vs. 46)	Late – increased, BED_3 =110 Gy
10.	Polish (CAIR): Skladowski et al 2000	Continuous Accelerated	**I I I I I I I I I I I I I I …..**	**2.0**	**1**	**7**	64.0	32	4.6	82 (vs. 35)	Late – slight increase, but not significant , BED_3 =107 Gy
11.	RTOG: with a treatment break	Split Course HyperAccelerat-ed (2 wk break after 2 wks)	**II II II II II II (break)** **II II II II II II II II II II …..**	**1.2**	**2**	**5**	81.6	68	8.8	N/A	N/A

= fractions of radiotherapy, BED_3 = Calculated value of the Biological Effective Dose using an α/β value of 3 Gy.

6.2.2. Simulation Methods

Results in this chapter relating to the simulation of the schedules in Table 6.1, were modelled using the 3 different OER curves dependent on the dose per fraction (previously shown in Figure 2.7). Thus, hyperfractionated schedules for which the dose per fraction was in the range of 1.25 to 1.75 Gy the maximum OER in the OER curve used in the model was reduced from 3.0 to 2.5, and for schedules with a dose per fraction less than 1.25 Gy the maximum OER was reduced to 2.0. The impact of modelling reduced OER's will be discussed from a comparison of simulations performed with and without the dose per fraction dependency applied in the model.

A range of AR and ROx onset times of between 0 and 3 weeks were also simulated for the altered schedules, as reported in chapter 5 for the conventional schedule. The majority of the results in the current chapter will be limited to onset times of 0 (immediately after treatment commencement) and 2 weeks for AR and ROx, unless indicated otherwise. All tumour cell kill results in this chapter relate to the use of constant alpha and beta LQ values of 0.3 Gy^{-1} and 0.03 Gy^{-2}.

Text files were developed for each of the 11 fractionation schedules to be simulated, containing information about the timing between each fraction and the dose per fraction desired. A batch run facility was implemented for the convenience and efficiency of iterating simulations over multiple random number seeds, different pre-grown virtual tumours, different schedules and various onset times of AR and ROx, among other varying parameters.

6.2.3. Model Outcome Analysis Methods

The irradiation of virtual tumours was simulated using the 11 fractionation schedules until the tumours were controlled (100% TCP). This meant that the total number of fractions differed from that reported from clinical trials. The total number of fractions and the total doses required to control the tumours have been plotted for onset times of

AR of 0, 1, 2, or 3 weeks for oxic tumours, and various combinations of onset times of AR and ROx for moderately hypoxic tumours.

All results in this chapter are the averaged results from nine simulations using the same virtual tumour and treatment related parameter sets. The nine simulations were the result of importing data from three virtual tumours generated using three different random seeds and a further three simulations for each virtual tumour of using different random seeds.

Results have identified schedules requiring the highest total dose and longest treatment times. However, as 100% TCP was achieved in all simulations, comparisons of the relative efficacy of the schedules was extended to consider acute and late reacting normal tissues toxicities using calculated Biological Effective Doses (BED's). Corresponding BED's were calculated for each schedule using the model results of total dose, time and fraction number, and Equations 6.1 and 6.2 below (Dale 2007, Fowler 2007, Fowler 2010).

$$BED_{late} = nd'(1+\frac{d'}{\alpha/\beta}) \tag{6.1}$$

$$BED_{early} = nd'(1+\frac{d'}{\alpha/\beta}) - \frac{\ln(2)(t-T_k)}{\alpha T_p} \tag{6.2}$$

where d is the standard dose per fraction (2 Gy), d' is the altered dose per fraction, n is the number of fractions, T_k is the repopulation kick off time (2 weeks), T_p is the potential doubling time (2.5 days), and α/β is the alpha beta ratio for acute effects e.g. acute oral mucosa effects (10 Gy) or late normal tissue effects (3 Gy) (Fowler 2004).

As normal tissue was not modelled in the *HYP-RT* simulations, acute and late reacting tissues were assumed to have received the same total dose as the virtual tumour. The 11 simulated fractionation schedules were ranked according to acute and late normal tissue toxicities using BED equations 6.1 and 6.2 above, with the lowest BED result indicating the schedule with the lowest predicted rates of acute and late normal tissue effects (and hence the highest therapeutic ratio).

Model cell kill results were also compared to reported clinical trial LC percentages. Note that LC rates at 2 to 5 years for the seven therapeutically beneficial trials are presented in Table 6.1. Consequently, the comparison of the total doses required for tumour control in simulations (100% TCP) versus the clinically delivered doses had limitations.

To overcome some of the limitations two methods were devised thoroughly compare the model results with clinical LC data. These methods which enabled conversion of model results in terms of stem cell survival to a percentage of locally controlled (LC) tumours involved:

1. Running simulations for nine random seeds and reporting the modelled TCP or LC% as the percentage of tumours out of these nine runs which were controlled after delivery of the **same number of fractions as the clinical trial**, using a control threshold of:
    - *0 cells remaining*
    - *less than 5 cells remaining*
2. Running simulations for nine random seeds and reporting the modelled TCP or LC% using the average cell number remaining and Poisson theory [TCP=exp(-a), where a is the remaining cell number after RT], after delivery of the **same number of fractions as the clinical trial**

The decision analyse the control threshold in method 1 to be 0 cells was not trivial. Traditionally, tumour control has been considered to be a certainty if zero tumour cells remain after treatment. However, according to Poisson theory there is also a chance of tumour control if more than 0 cells remain after treatment, e.g. one cell remaining equates to a 37% chance of control. In addition, the clinical trial dose prescriptions in Table 6.1 did not result in local tumour control for 100% of patients (on average approximately 40 to 60% LC).

The five cell threshold was an estimate considering other issues in the result of clinical trials including the presence of a tumour of a non-detectable size at follow up and the elimination of tumour cells by natural immunological mechanisms which vary in effectiveness in patient to patient. Method two was investigated as an alternative to method one using the average number of cells remaining from simulations and Poisson theory, rather than the number of tumours (out of nine) that were controlled.

The data required from the model for both methods of TCP calculation, predominantly comprised of the number of remaining tumour stem cells after simulated delivery of the same number of dose fractions as the clinical trial. To avoid repeating simulations to obtain this data, a separate program was developed to search the output data files from the simulations which were left to run until all cells were killed to find the data required. This program performed the role of finding the fraction at which all stem cells had reached zero or less than five cells. In additions, it was extended to produce a list of cell numbers and the types of cells remaining at any desired fraction number and report on the percentage of tumours that had less than a particular cell number remaining at that point in time.

6.3. Altered Fractionation Results and Discussions

6.3.1. Total Dose, Fraction Number and Treatment Time Outcomes

Simulations of 11 different fractionation schedules were run using the *HYP-RT* model. These were performed for oxic and moderately hypoxic tumours, as defined in section 4.4.2, and for AR and ROx onset times ranging from 0 to 3 weeks. Results herein will present limited data because of the large number of combinations of parameters simulated.

The full range of tabulated results for onset times of AR and ROx of up to 3 weeks for the conventional schedule and up to 2 weeks for all schedules are found in Appendices B and C. Data relating to the total fraction numbers, total treatment times and acute and late BED's are also tabulated in Appendix C for all schedules.

6.3.1.1. Hypoxic Tumours

The results for the schedules comparing fraction numbers required for 100% TCP for moderately hypoxic tumours and the schedules from clinical trials outlined in Table 6.1 are presented below (Figure 6.1).

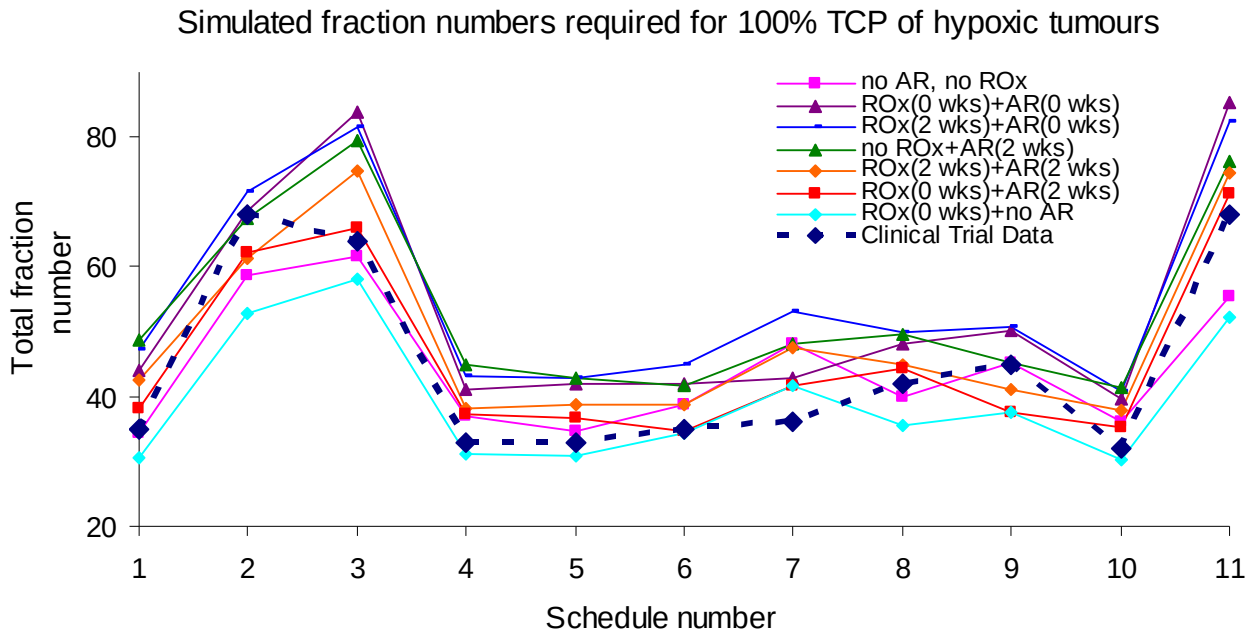

Figure 6.1. The number of fractions simulated to achieve 100% tumour control probability (TCP) in the model for hypoxic tumours for 11 fractionation schedules (Table 6.1), compared to the number of fractions delivered in clinical trials.

The ranges in results for each of the schedules in Figure 6.1 were relatively large (average of 18±9 fractions) when varying the onset times of AR and ROx. The largest range applied to the schedules with the smallest dose per fraction (schedules 2, 3 and 11) of up to 34 fractions. These results show that the onset times of AR and ROx should be of concern when prescribing fraction number and therefore total doses for fractionated schedules, and that this importance becomes more critical as the total number of fractions increases.

The values and ranges in the number of fractions shown in Figure 6.1 from simulations were in good agreement with the fraction numbers that were prescribed in clinical trials, except for the most accelerated clinical trial schedule (CHART: 3x1.5 Gy/day).

The results of the simulations in Figure 6.1 are presented below as the total doses required for 100% TCP (Figure 6.2).

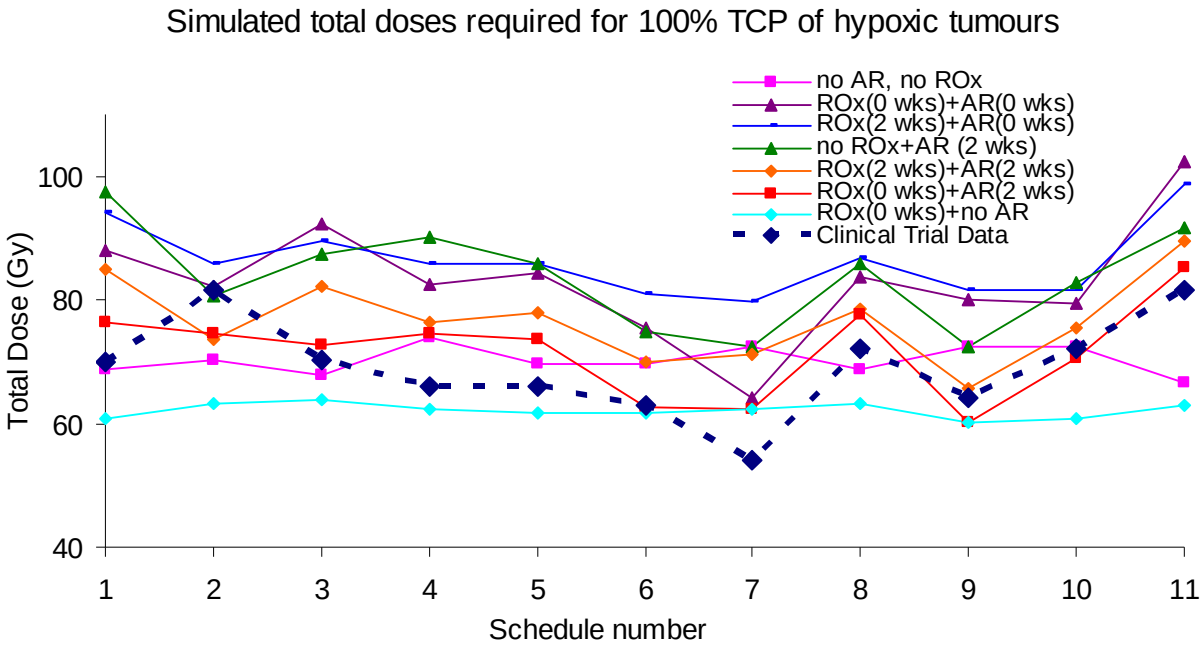

Figure 6.2. The total doses simulated to achieve 100% tumour control probability (TCP) in the model for hypoxic tumours for 11 fractionation schedules (Table 6.1), compared to the number of fractions delivered in clinical trials.

Based on data shown in Figures 6.1 and 6.2 for moderately hypoxic tumours, the combination of onset of ROx 0 weeks and onset of AR after 2 weeks (red data line) provided the closest overall match to clinical data, whereas the onset of ROx and 0 weeks and no onset of AR (purple data line) gave the poorest match to clinical data.

The general comparison of model results of the number of fractions and total doses required for 100% TCP was considered to be important but limited because the tumours represented in the clinical trial results were not all controlled (see Table 6.1 for published clinical trial outcomes) and would have consisted of tumours that may or may not have experienced the effects of AR and ROx.

However, the comparison was deemed beneficial in this work because modelling a range of AR and ROx onset times provided a good estimate of the doses and fraction numbers required in real tumours (for 10 out of the 11 schedules modelled) and provided evidence that the clinically plausible combination of onset times of AR at 2 weeks and immediate onset of ROx is close to the average patient response.

The results in Figure 6.1 and 6.2 relate to "basal" cell elimination to achieve tumour control. Figure 6.3 shows the total dose results from the model relating to the total eradication of stem cells only.

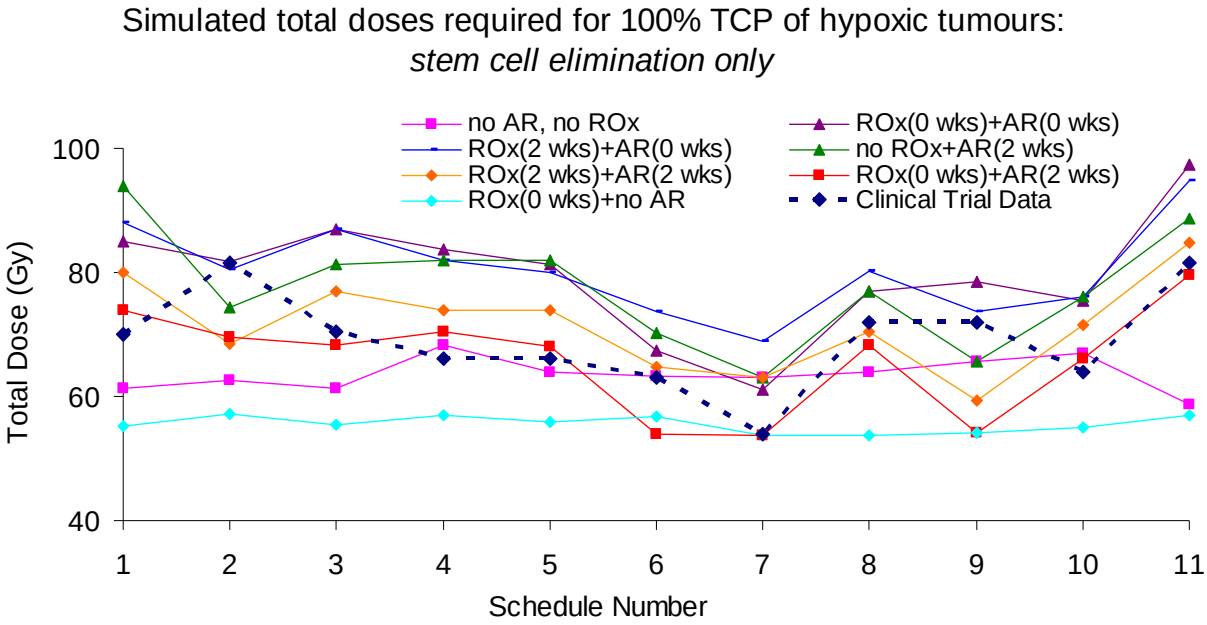

Figure 6.3. The total doses simulated to achieve 100% tumour control probability (TCP) in the model, based on stem cell elimination only for hypoxic tumours for 11 fractionation schedules (Table 6.1), compared to the number of fractions delivered in clinical trials.

As shown in Figure 6.3, the clinically delivered doses still fell within the simulated range of doses that resulted in 100% TCP considering stem cell alone. Averaging over all eleven schedules and eight combinations of AR and ROx onset times, "basal" cell elimination took an extra 2 to 10 Gy (average of 5 Gy) compared to stem cells only (Figure 6.4). However considering statistical errors of 4 to 8 Gy in most simulations, these differences were not significant.

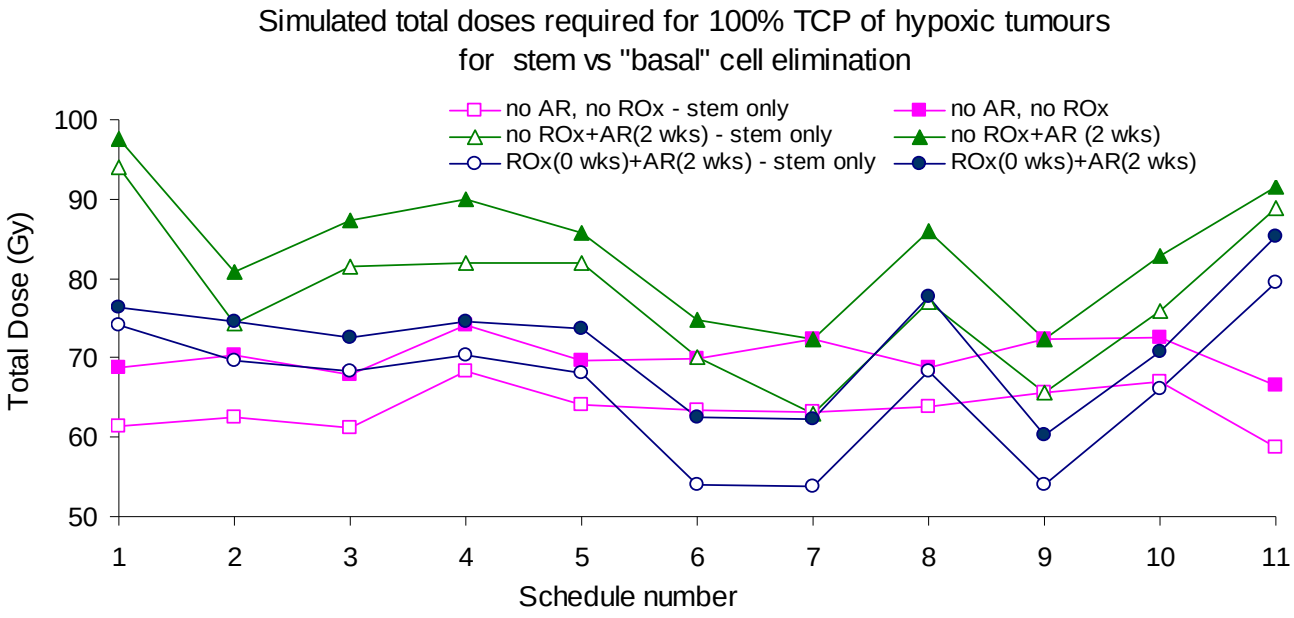

Figure 6.4. Total dose requirements in the model to achieve 100% TCP, for the elimination of all stem cells vs. the elimination of all "basal" cells which includes all stem, transit and level 1 differentiating cells, for 11 fractionations schedules (Table 6.1).

Note that results in Chapter 5 show that when tumour control was defined based on stem cell elimination alone, the total dose required for 100% TCP was reduced, on average, by 2.2 fractions (4.4 Gy).

The cell survival curves from simulations of onset of AR at 2 weeks and ROx at 0 weeks for schedules 1 to 8 allow the differences in cell kill throughout the duration of the different schedules to be observed (Figure 6.5). From these cell survival curves, the effect of the weekend gaps in the schedules, except for the CHART schedule (no. 7) can be observed, whereby cell numbers increase due to stem cell proliferation, although in some cases a decrease because of losses of differentiated cells occurs despite continuous division of the small but important proportion of stem cells in the tumour (e.g. schedule no. 5 with a break on Sundays).

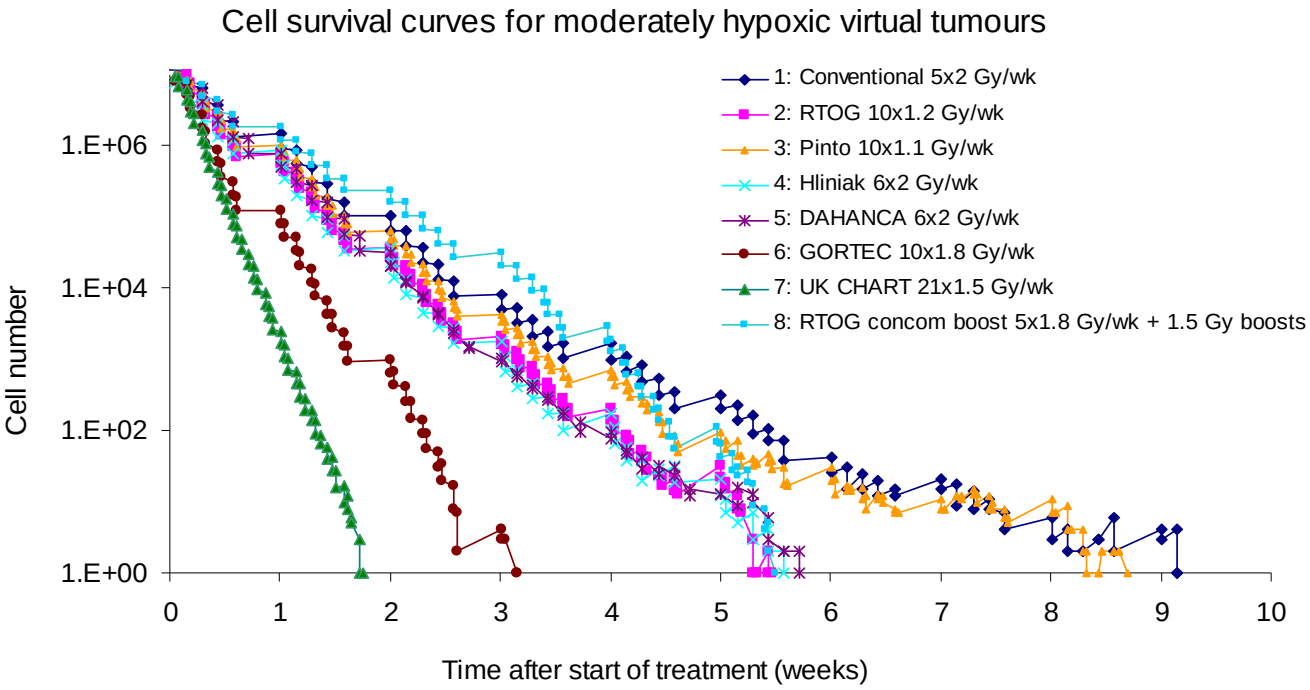

Figure 6.5. Cell survival curves throughout treatment from simulations of 8 different fractionation schedules (Table 6.1), with onset of accelerated repopulation (AR) onset at 2 weeks and onset of reoxygenation (ROx) at 0 weeks.

6.3.1.2. Oxic Tumours

The simulation results for oxic tumours for the 11 schedules also showed an approximate 20 fraction range when varying onset the times of AR (Figure 6.6).

The AR onset times of 2 weeks for oxic tumours best matched clinical trial dose data, for schedules 1, 2, 3, 5, 6, 8, 10 and 11. A strong correlation with a specific onset time of AR for all schedules was not expected as it is very likely that most tumours in the clinical trials had at least some degree of hypoxia present at the start of treatment given the advanced stage of the disease and the likely presence of sub-hypoxic volumes, as discussed in Chapter 2.

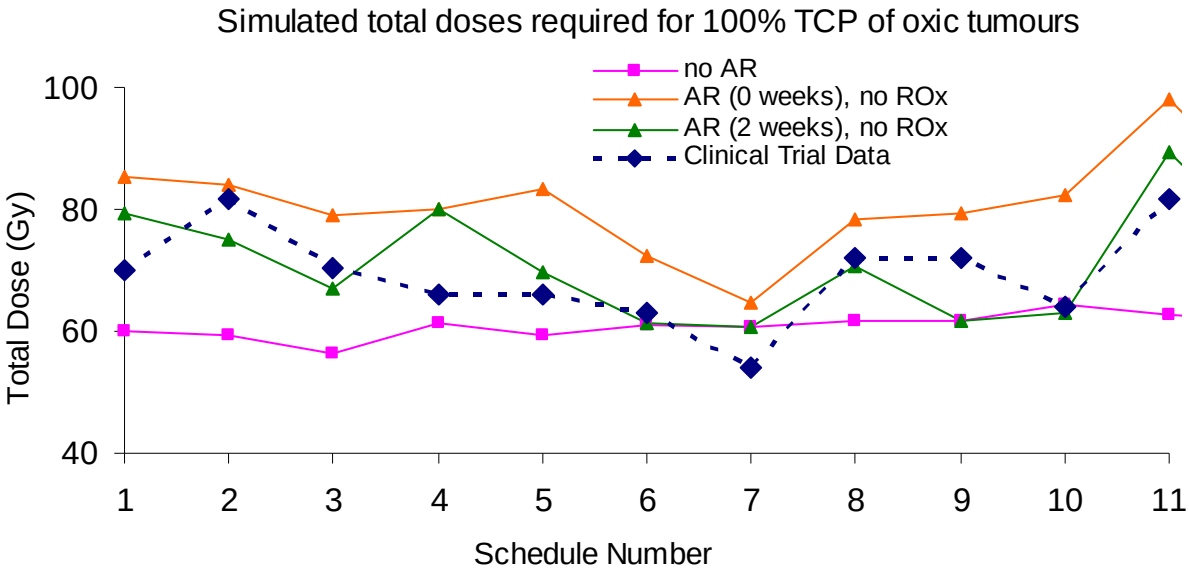

Figure 6.6. The total doses simulated to achieve 100% TCP in the model for oxic tumours for 11 fractionation schedules (Table 6.1), compared to the number of fractions delivered in clinical trials.

6.3.1.3. Comparison of Oxic and Hypoxic Tumours

As expected it was found that oxic tumours required less total dose compared to hypoxic tumours in simulations (Figure 6.7). For the 11 schedules it took on average an extra 16±4% extra dose to control hypoxic tumours for the example of no AR onset.

Schedule 1 (conventional) and schedule 4 (6x2 Gy/wk), followed by schedules 2, 3, 5 and 11, show the largest difference in required total dose for hypoxic compared to oxic tumours. Note that for these results the OER was modelled to change based on dose per fraction, meaning that the impact of hypoxia on cell kill was decreased as dose per fraction decreased. Despite this, most of the simulated hyperfractionated schedules (no. 2 and 3) have large total dose differences for oxic versus hypoxic tumours in Figure 6.7.

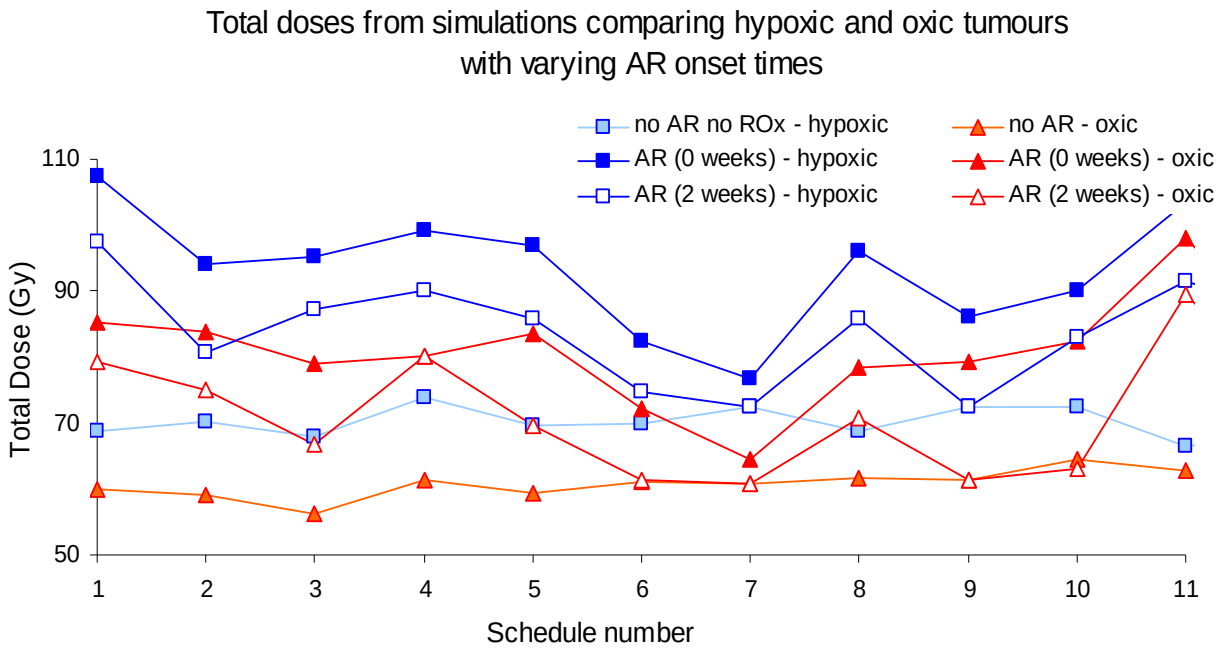

Figure 6.7. The total doses simulated to achieve 100% TCP in the model for oxic versus hypoxic tumours, varying the onset of AR for 11 fractionation schedules. No reoxygenation (ROx) was implemented during these simulations.

To supplement the total dose and fraction number data shown above, plots of total treatment times for the 11 schedules are presented below (Figures 6.8a and 6.8b), where it can be observed that schedules 1, 2, 3, followed closely by 5 and 8, have the longest overall treatment times according to the model. Schedule 11 with the 2 week break also had a long treatment time as expected.

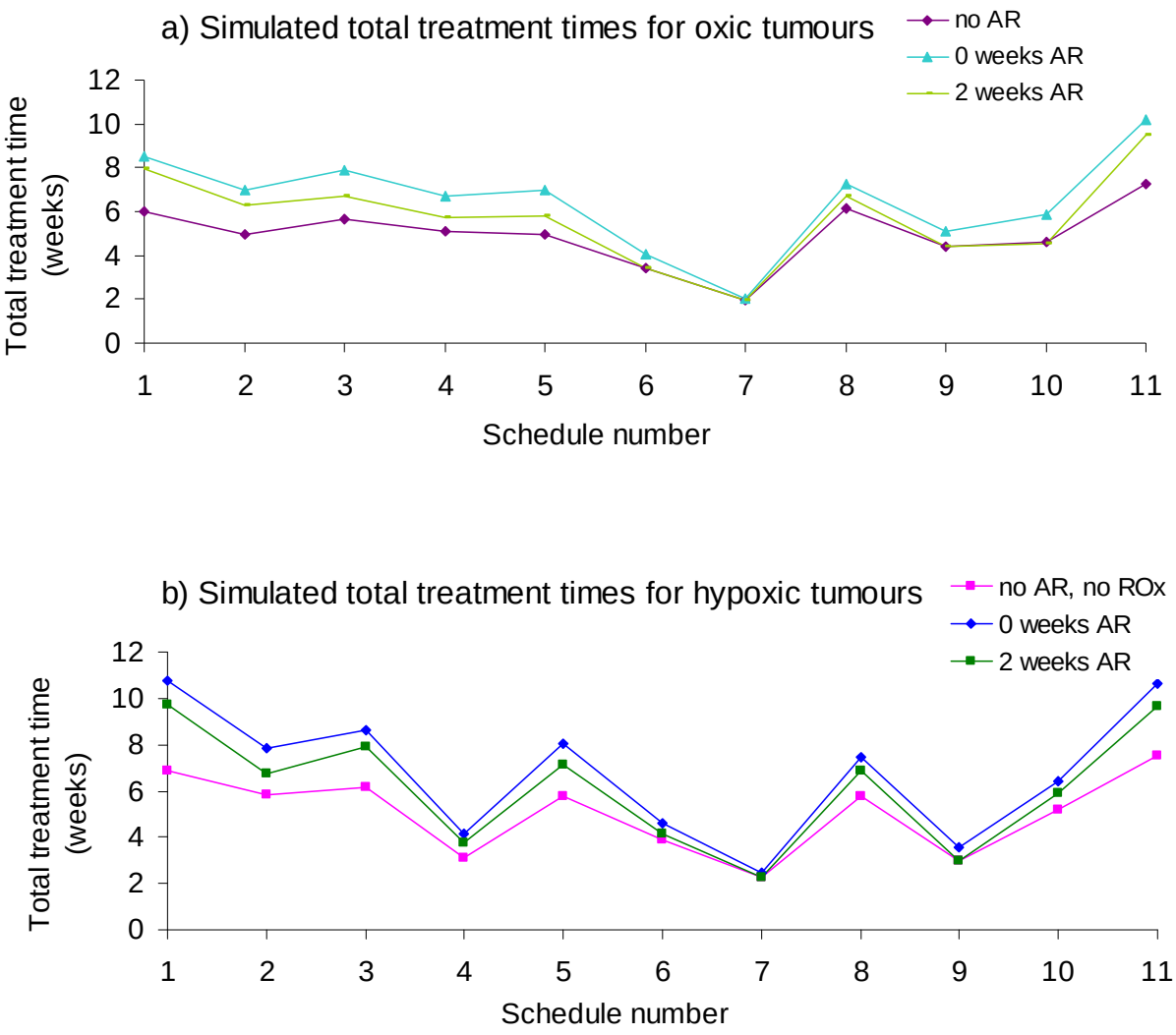

Figure 6.8. Total treatment times required to achieve 100% TCP in the model for 11 fractionation schedules with various onset times of accelerated repopulation (AR), for a) oxic tumours, and b) hypoxic tumour simulations. No reoxygenation (ROx) was implemented for these simulations.

6.3.1.4. The Impact of Using Dose per Fraction Dependent OER Curves

When reducing the OER for hyperfractionated schedules (<1.75 Gy), a small but significant effect on the total doses required for tumour control was observed compared to using the standard OER curve with a maximum value of 3.0 for all schedules (Figure 6.9).

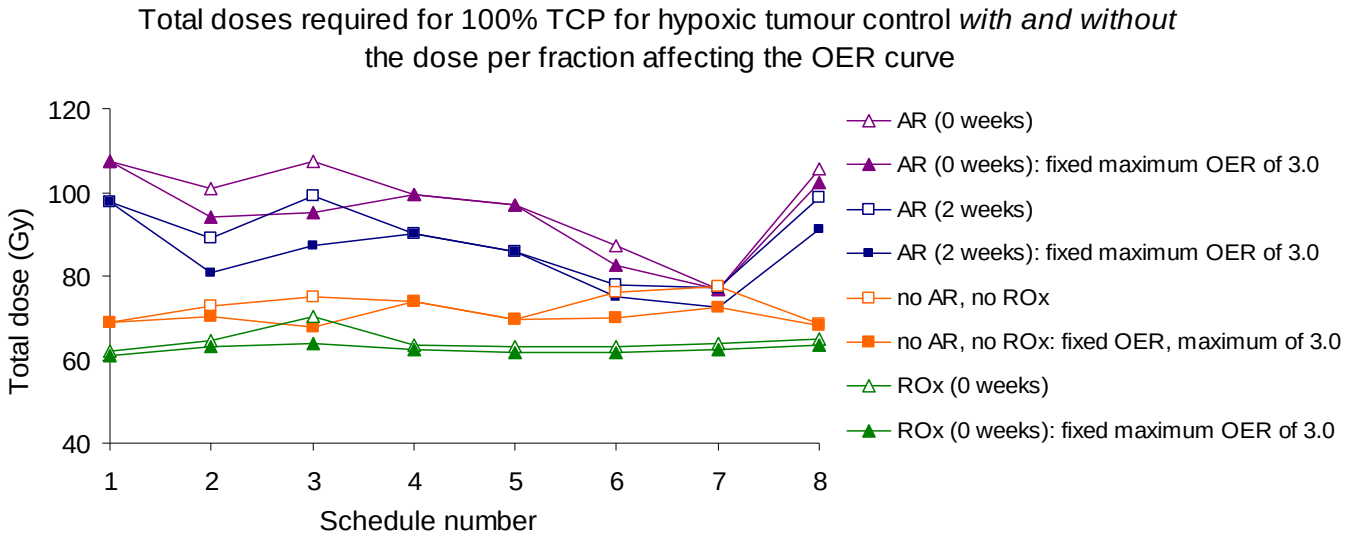

Figure 6.9. The effects on total dose required for 100% TCP when modifying the OER curve with dose per fraction compared to modelling one fixed OER curve with a maximum value of 3.0, during simulations of 8 various fractionation schedules (Table 6.1) for various onset times of AR and ROx.

The use of a reduced OER curve had the most impact on hyperfractionated schedules with a dose per fraction ≤1.25 Gy, and therefore the largest drop in maximum OER (from 3.0 to 2.0). Schedules 2 and 3 which were the most hyperfractionated had total dose requirements in the range of 5 to 10 Gy, although this only applied for simulations with AR and hence larger overall total doses.

For schedules with a dose per fraction lower than 1.75 Gy but higher than 1.25 Gy, there was no significant difference in required total doses when altering the OER curve, and hence no predicted beneficial effect for the treatment of hyperfractionation alone compared to the conventional schedule for hypoxic tumours. The use of a single versus dose per fraction dependent OER curve in the model will be discussed further in the next chapter of this report.

6.3.2. Ranking of Normal Tissue Effects Based on Calculated BED

Ranking oxic tumour simulation results was performed in terms of the calculated BED's for acute and late normal tissue effects. Rankings were based on the assumption that normal tissue received the total dose required for tumour control in the model and normalised to a ranking ranging from 0.0 to 10.0. A score of/near 0.0 indicated a very beneficial (low) predicted rate of normal tissue toxicity, while a score of/near 10.0 indicated a very poor (high) predicted rate of normal tissue toxicity. Rankings were designed to maintain the relative differences in BED values between the schedules, rather than simply assigning schedules an integer ranking value based on lowest to highest BED outcomes.

6.3.2.1. Oxic and Hypoxic Tumour BED Rankings

6.3.2.1.1. Acute Normal Tissue Effects

The acute effect BED rankings observed from the model for the 11 simulated schedules were similar for hypoxic versus oxic tumours (Figures 6.10a and 6.10b).

The results show that schedules 1 (conventional), 2, 3 (hyperfractionated) and 11 (2 week break) were predicted to be optimal for acute normal tissue effects for most combinations of AR and ROx onset times for both hypoxic and oxic tumours. However, for different AR and ROx onset times there were wide variations in the rankings for individual schedules, providing evidence of the importance of individualisation of treatments for HNSCC patients.

The most accelerated schedule (no. 7, CHART), ranked high (poorly) for acute normal tissue effects for oxic as well as some combinations of onset times of AR and ROx for hypoxic tumours. However, schedule 7 ranked well for the specific cases of acute onset of AR in hypoxic tumours because it had the shortest overall time of treatment.

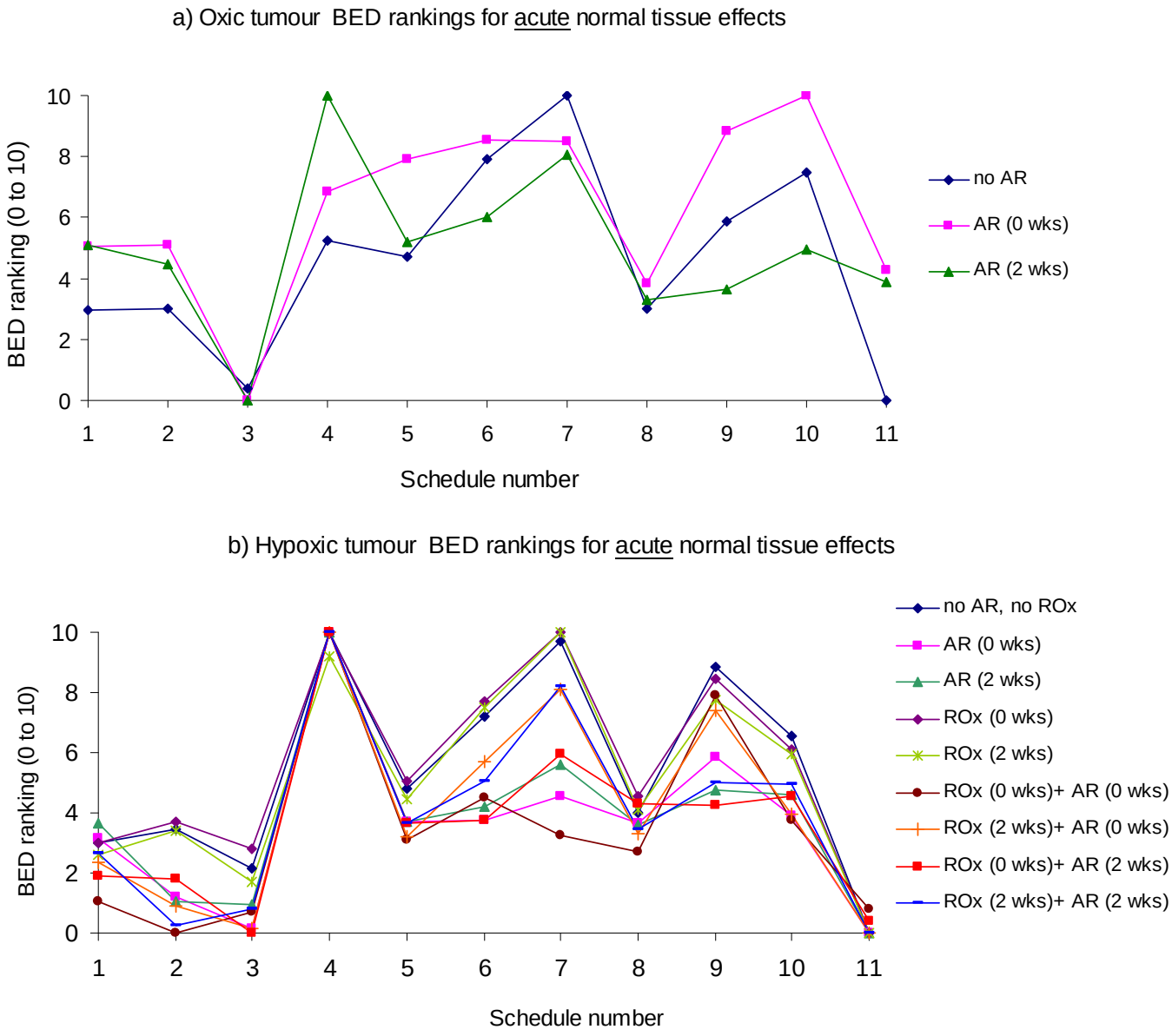

Figure 6.10. Rankings of acute normal tissue biological effective doses (BED) based on the total dose required for 100% for 11 fractionation schedules in a) oxic tumours, and b) hypoxic tumour simulations (in both cases the lowest BED ranking is optimal for acute normal tissue effects).

6.3.2.1.2. Late Normal Tissue Effects

The rankings for predication of late normal tissue toxicities based on BED are also presented below (Figures 6.11a and 6.11b). The plots show that schedules 2, 3, 9 (hyperfractionated) and 7 (CHART) ranked low (well) for most combinations of AR and ROx onset times for both hypoxic and oxic tumours.

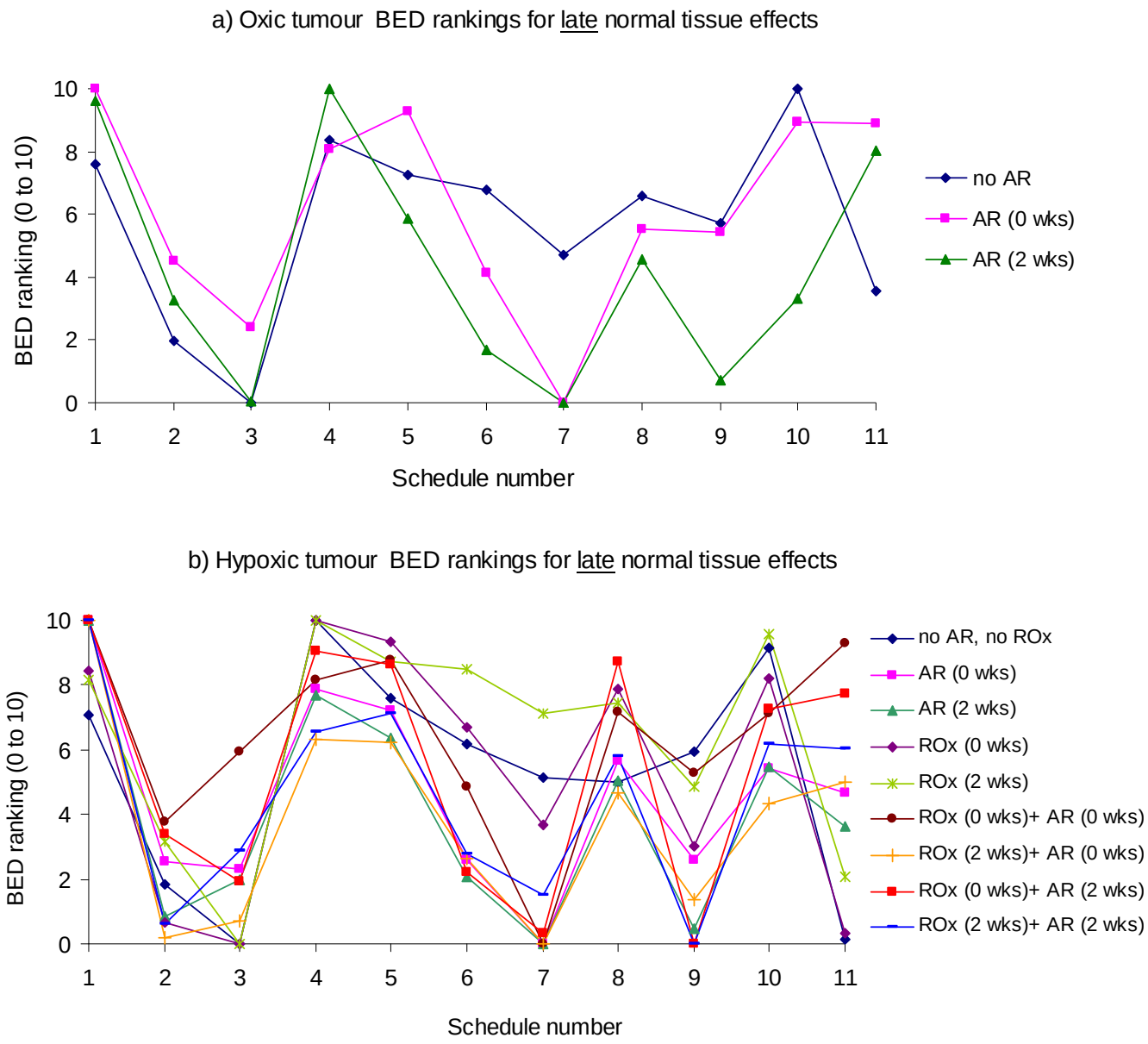

Figure 6.11. Late reacting normal tissue biological effective dose (BED) rankings based on the total dose required for 100% TCP for 11 fractionation schedules (Table 6.1), for a) oxic tumours, and b) hypoxic tumour simulations (in both cases the lowest ranking is optimal for late normal tissue effects).

The range in the late effect BED rankings with different onset times of AR were relatively large compared to the range in the data relating to acute effects in Figure 6.10. Schedules 4, 5, and 10 (followed by 9 and then 6) ranked highest (poorly) for late normal tissue effects. These three schedules were all accelerated schedules. The conventional schedule had an average ranking, sharing overall 4th position with two other schedules.

6.3.2.1.3. Summary of Normal Tissue Toxicity BED Ranking Results

BED rankings between values of 0.0 and 10.0 are shown in Tables 6.2 and 6.3 for oxic and hypoxic tumour simulations, with the relatively more beneficial schedules highlighted in green (a low ranking ≤ 3.0) and poorer schedules highlighted in red (a high ranking ≥ 7.0). Note that the specific parameters used in the associated BED equations (Equations 6.1 and 6.2) used to obtain the BED values are shown in the respective tables.

Table 6.2: Rankings of calculated BBED acute and late normal tissue effects of 11 fractionation schedules for oxic tumour simulations, where a high number indicates a worse ranking and a low number indicates a better ranking of predicted normal tissue toxicity levels.

Acute normal tissue effects: BED formula - T_k = 7 days, α = 0.35 Gy^{-1}, α/β = 10 Gy, T_p = 2.5 days					
	Sch #	no AR, no RO	AR (0 weeks)	AR (2 weeks)	d/#
Oxic Tumours	1	3.0	5.0	5.1	2.0
	2	3.0	5.1	4.5	1.2
	3	0.4	0.0	0.0	1.1
	4	5.2	6.8	10.0	2.0
	5	4.7	7.9	5.2	2.0
	6	7.9	8.5	6.0	1.8
	7	10.0	8.5	8.1	1.5
	8	3.0	3.8	3.3	1.8
	9	5.9	8.8	3.7	1.6
	10	7.5	10.0	5.0	2.0
	11	0.0	4.3	3.9	1.2
Late normal tissue effects: BED formula - α/β = 3 Gy					
	Sch #	no AR, no RO	AR (0 weeks)	AR (2 weeks)	d/#
Oxic Tumours	1	7.6	10.0	9.6	2.0
	2	2.0	4.5	3.3	1.2
	3	0.0	2.4	0.1	1.1
	4	8.4	8.1	10.0	2.0
	5	7.3	9.3	5.9	2.0
	6	6.8	4.1	1.7	1.8
	7	4.7	0.0	0.0	1.5
	8	6.6	5.5	4.6	1.8
	9	5.7	5.4	0.7	1.6
	10	10.0	8.9	3.3	2.0
	11	3.6	8.9	8.0	1.2

Table 6.3: Rankings of calculated BED acute and late normal tissue effects of 11 fractionation schedules for hypoxic tumour simulations, where a high number indicates a worse ranking and a low number indicates better ranking for predicted normal tissue toxicity levels.

B **Acute normal tissue effects**: BED formula - T_k = 7 days, α = 0.35 Gy^{-1}, α/β = 10 Gy, T_p = 2.5 days

	Sch #	no AR, no ROx	AR (0 wks)	AR (2 wks)	ROx (0 wks)	ROx (2 wks)	ROx (0 wks)+ AR(0 wks)	ROx (2 wks)+ AR(0 wks)	ROx (0 wks)+ AR(2 wks)	ROx (2wks)+ AR(2wks)	d/#
Hypoxic Tumours	1	3.0	3.2	3.6	3.0	2.6	1.0	2.3	1.9	2.7	2.0
	2	3.5	1.2	1.0	3.7	3.4	0.0	0.9	1.8	0.2	1.2
	3	2.2	0.1	1.0	2.8	1.7	0.7	0.1	0.0	0.8	1.1
	4	10.0	10.0	10.0	9.9	9.2	10.0	10.0	10.0	10.0	2.0
	5	4.8	3.7	3.7	5.0	4.5	3.1	3.2	3.7	3.7	2.0
	6	7.2	3.8	4.2	7.7	7.5	4.5	5.7	3.8	5.0	1.8
	7	9.7	4.5	5.6	10.0	10.0	3.3	8.1	5.9	8.2	1.5
	8	4.0	3.7	3.6	4.5	4.1	2.7	3.3	4.3	3.4	1.8
	9	8.8	5.8	4.7	8.4	7.7	7.9	7.4	4.3	5.0	1.5
	10	6.5	3.9	4.6	6.1	6.0	3.7	4.0	4.6	4.9	2.0
	11	0.0	0.0	0.0	0.0	0.0	0.8	0.0	0.4	0.0	1.2

Late normal tissue effects: BED formula - α/β = 3 Gy

	Sch #	no AR, no ROx	AR (0 wks)	AR (2 wks)	ROx (0 wks)	ROx (2 wks)	ROx (0 wks)+ AR(0 wks)	ROx (2 wks)+ AR(0 wks)	ROx (0 wks)+ AR(2 wks)	ROx (2wks)+ AR(2wks)	d/#
Hypoxic Tumours	1	7.1	10.0	10.0	8.4	8.2	10.0	10.0	10.0	10.0	2.0
	2	1.9	2.6	0.9	0.7	3.2	3.8	0.2	3.4	0.6	1.2
	3	0.0	2.3	2.0	0.0	0.0	5.9	0.7	1.9	2.9	1.1
	4	10.0	7.9	7.7	10.0	10.0	8.2	6.3	9.0	6.6	2.0
	5	7.6	7.2	6.4	9.3	8.7	8.8	6.2	8.6	7.1	2.0
	6	6.2	2.6	2.1	6.7	8.5	4.8	2.6	2.2	2.8	1.8
	7	5.2	0.0	0.0	3.7	7.1	0.0	0.0	0.3	1.5	1.5
	8	5.0	5.7	5.0	7.9	7.4	7.2	4.7	8.7	5.8	1.8
	9	6.0	2.6	0.5	3.0	4.9	5.3	1.4	0.0	0.0	1.5
	10	9.2	5.4	5.5	8.2	9.6	7.1	4.3	7.2	6.2	2.0
	11	0.1	4.7	3.6	0.3	2.1	9.3	5.0	7.7	6.0	1.2

For oxic tumours, **schedule 3** followed by **1, 2, 8, and 11** ranked well in terms of acute normal tissue effects, while **schedule 3** followed by **7, 2, 6, and 9** ranked well for late normal tissue effects. For both acute and late normal tissues, 2.0 Gy per fraction **schedules 4, 5 and 10** ranked poorly.

For hypoxic tumours, **schedule 3** followed by **11, 1, 2, and 8** ranked well for acute normal tissue effects, while **schedules 3 and 2** also ranked well for late normal tissue effects. For both acute and late normal tissues, **schedules 4, 6, 7 and 8** ranked poorly for most combinations of onset times of AR and ROx.

When onset times of AR and ROx were set to 2 and 0 weeks respectively, the better schedules included **2, 3, 9 and 6.** For these simulations, the **conventional** schedule was worst for late normal tissue effects and **schedule 4** was the worst for acute normal tissue effects. The low BED results for **schedules 2 and 3** are in agreement with clinical trial reports of the benefits of *b.i.d.* hyperfractionated schedules for treatment of HNSCC (Fu 2000).

Schedule 11 (with the 2 week break after the initial 2 weeks of treatment) ranked very well for acute normal tissue effects because of the extended treatment time, and average to well for late normal tissue effects for most simulations. However, **schedule 11** did rank poorly for simulations involving AR because of proliferation during the break, as expected.

Based on the data presented in the above sections, the *HYP-RT* model predicted **schedule 3** (10x1.1 Gy/wk, Pinto *et al*.) to be the most beneficial schedule considering both acute and late normal tissue effects. **Schedule 2** (10x1.2 Gy/wk, Fu *et al*.) was the next best overall schedule for both acute and late normal tissue effects. The worst overall schedules for late normal tissue effects were **schedules 4, 5 and 10** which were all 2.0 Gy per fraction accelerated schedules.

Table 6.4 summarises the overall order of the most beneficial to the least beneficial schedule in terms of normal tissue toxicity for the 11 schedules. The order was based on a scoring system utilising the early and late normal tissue effect BED rankings previously presented in Tables 6.2 and 6.3.

Table 6.4: Summary of the overall order of schedules predicted to have to the lowest to highest normal tissue toxicity for acute and late effects for 11 fractionation schedules, averaged over a range of onset times of accelerated repopulation (AR) and reoxygenation (ROx).

Schedules ordered from the most beneficial (1) to the least beneficial (7) for normal tissue toxicity Scoring for each acute/late effect: 1 = good averaged BED ranking, 2 = intermediate/mixed BED ranking, 3= bad averaged BED ranking						
Schedules: as detailed in Table 6.1	Oxic tumours: acute effects	Oxic tumours: late effects	Hypoxic tumours: acute effects	Hypoxic tumours: late effects	**Sum of the four scores:**	**Overall order:**
1: Conventional	2	3	1	3	9	**4**
2: RTOG: 10x1.2 Gy/wk	2	1	1	1	5	**2**
3: Pinto: 10x1.1 Gy/wk	1	1	1	1	4	**1 – Best schedule**
4: Hliniak: 6x2 Gy/wk	3	3	3	3	12	**7 – Worst schedule**
5: DAHANCA: 6x2 Gy/wk	3	3	2	3	11	**6**
6: GORTEC: 10x1.8 Gy/wk	3	2	3	2	10	**5**
7: UK CHART: 21x1.5 Gy/wk	3	1	3	2	9	**4**
8: RTOG: concom. boost	2	2	2	3	9	**4**
9: EORTC: split course	3	2	3	2	10	**5**
10: EORTC: 2x7 Gy/wk	3	3	2	3	11	**6**
11: RTOG: with 2 week break	2	3	1	2	8	**3**

The results summarised in Table 6.4 are consistent with published clinical trial data, which have reported high toxicity levels for purely accelerated schedules (Skladowski 2000). It should be stressed here that the order of the schedules was from oxic and hypoxic tumour simulations with many combinations on onset times of AR and ROx. Although useful for comparisons with clinical trial data, the exercise deviates from the goal of the model which is to predict the utility of a particular radiation dose schedule on an individual patient basis.

6.3.2.2. Calculated BED versus Clinical Trial Toxicities

The overall scores for normal tissue toxicity for the 11 schedules in Table 6.4 were compared with reported clinical toxicity data for acute (mucosa effects, if available) and late normal tissue effects at 2 to 5 years.

Clinical trial reports often publish toxicity data in terms of the increase or decrease in effects compared to the conventional 5x2 Gy per week schedule. Some reports add further levels of detail with a breakdown of the percentage increases in toxicities according to the grade and stage or other groups; however this level of data is not always accessible. Thus, for this work, only a general comparison between the rankings/over all scores and the toxicities reported from clinical trials was possible.

Direct correlations between the predicted BED's for acute and late normal tissue effects from the model and clinical trial data relating to increased or decreased rates of normal tissue toxicity were not found. This was not unexpected, as there are a large number of factors affecting normal tissue toxicity in the patient population and unknown variations in the radiation doses delivered to the normal tissues in patients participating in the trials.

However, for the specific case of onset of AR and ROx onset at 2 weeks and 0 weeks respectively, **schedule 3** outcomes compared favourably with clinical data showing a clear benefit for acute normal tissue effects, while **schedule 7** outcomes compared well with clinical reports of high rates and increased severity of acute normal tissue effects.

6.3.3. Comparison of Model Predictions with Clinical Trial LC Data

The *HYP-RT* model has been developed with the goal of predicting the response of tumours with varying onset times of AR and ROx, tumour cell radiosensitivities, and oxygenation levels to fractionated radiotherapy. This is a positive step forward towards the goal of individualisation of radiotherapy planning in the discipline of radiation oncology. However, newly developed models are challenging to verify against actual patient data because of differences in reporting treatment outcomes and the properties of the tumours in the clinical trial patient groups as discussed above.

Results in this section report on the predictions for moderately hypoxic tumours in terms of modelled TCP compared with clinical trial LC data. Two methods were devised to transform model data and enable valid model and clinical trial comparisons. Stem cell survival results were obtained from the model by setting a threshold fraction number

equal to that delivered in the associated clinical trial. This method differs from previous results where simulations were left to run and deliver as many fractions as were required to achieve 100% TCP. A limited set of six combinations of onset times for AR and ROx were used in this data analysis.

6.3.3.1. Method 1: Assessing the Percentage of Controlled Tumours while varying the Random Number Seed

Using a zero stem cell threshold, simulations of the 11 fractionation schedules using the exact number of fractions reported in the clinical trials resulted in a large range of tumour control outcomes (Figure 6.12a). Owing to the large range in TCP results observed for each treatment schedule with varying onset times of AR and ROx no significant correlation between clinical trial LC and model TCP were found.

This lack of correlation was because of the variation in individual simulation runs with different random seed numbers which resulted in standard deviations of total doses required for 100% TCP ranging from 0 to 12 Gy. Thus, the cell kill statistics at set fraction numbers differed considerably for the 9 simulations considered for each schedule and created the spread in model TCP data points for each schedule. Increasing the threshold stem cell number to five cells also did not result in any correlations between model TCP and clinical trial LC data (Figure 6.12b).

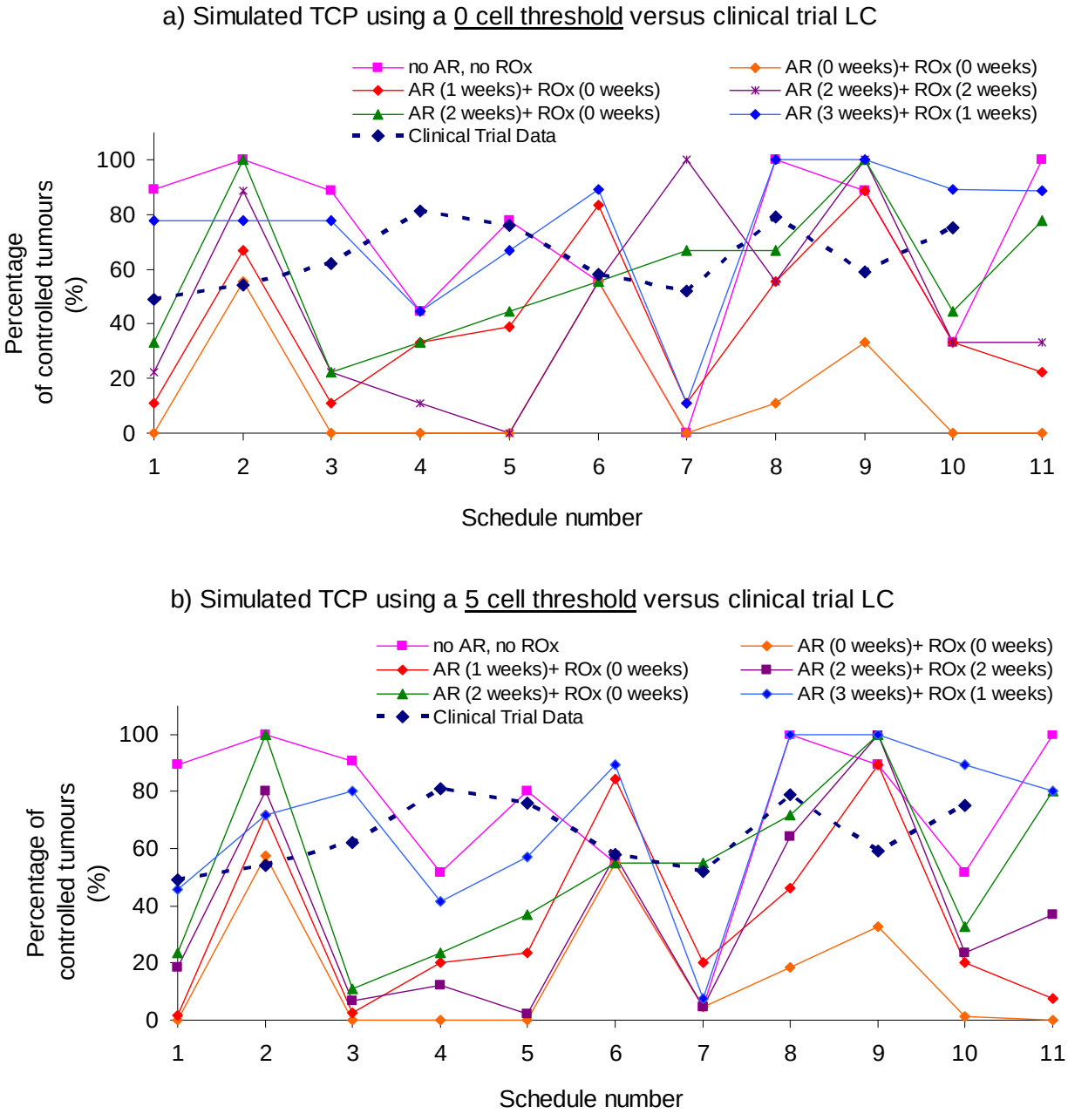

Figure 6.12. Comparisons of tumour control probability (TCP) using a) a zero cell threshold and b) a five cell threshold with varying accelerated repopulation (AR) and reoxygenation (ROx) onset times and corresponding clinical trial fraction numbers for 11 schedules with reported clinical trial local control (LC) percentages.

6.3.3.2. Method 2: Using Poisson Theory to Calculate TCP from Averaged Cell Survival

The results calculated using exponential Poisson theory (using the average remaining cell number after nine simulations) show similar large variations in TCP results (Figure 6.13) compared to the first method (Figure 6.12).

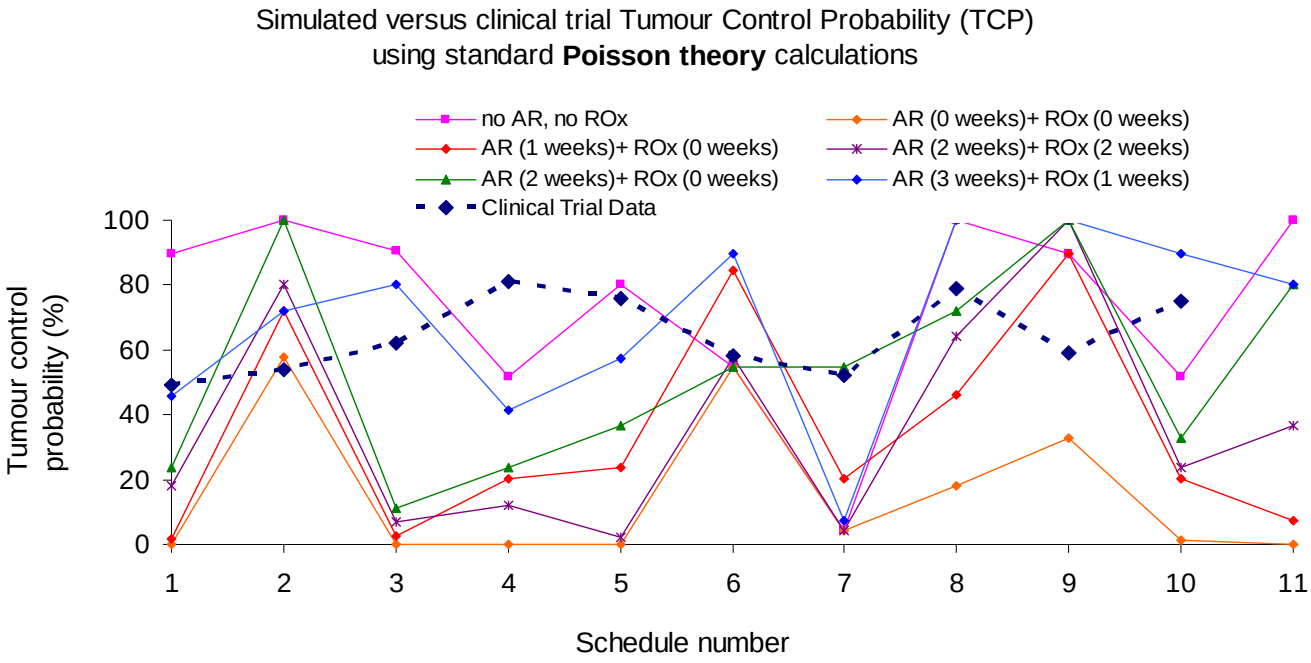

Figure 6.13. Comparisons of tumour control probability (TCP) using modelled cell kill data and Poisson theory for varying AR and ROx onset times and corresponding clinical trial fraction numbers for 11 schedules with reported clinical trial local control (LC) percentages.

This type of data analysis can therefore not provide meaningful results unless the variances of the outcomes are much lower using different random seed numbers. Even so, it is likely that the modelling results would be different from reported clinical data since the clinical data are not directly cell number related and the absence of clinical evidence of tumour recurrence does not rule out the presence of sub-clinical levels of tumour stem cells. For these reasons the best method of model verification is in the comparison of total doses to required achieve 100% TCP, discussed in section 6.3.1.

Although the ideal way of validating model TCP percentages is to correlate data with clinical trial LC percentages, it is currently not achievable because of heterogeneity of

tumour data, even in randomised clinical trials. This once again highlights the need for specific models to predict individual patient outcomes, rather than relying on extrapolated clinical trial results which are based on the average values of large numbers of patients.

6.4. Conclusions

The *HYP-RT* model was developed to simulate a wide range of clinically relevant fractionation schedules for evaluation of tumour cell kill and control probability and comparison of these outcomes with published HNSCC clinical trial data.

However, it has not been possible to obtain clinical trial data with the specific tumour parameters chosen for the model. Therefore comparisons between the specific virtual tumours simulations in the model and the average clinical trial outcomes have been limited. Even though attempts have been made to group/stratify patients by cellular sensitivity and initial tumour cell numbers, large variations in individual responses for radiotherapy (by means of both TCP and NTCP) have been observed which provides evidence of the need for more specific individualised patient data in the radiotherapy planning process (Bentzen 1993, Dobbs 1999).

Cell kill outcomes from the model have been discussed in this chapter in terms of the fraction numbers and total doses required to achieve total cell kill and hence 100% TCP. Outcomes were further investigated in terms of BED, where standard BED equations were used with parameters relating to acute and late normal tissue effects and assuming that the normal tissues received the same dose as the virtual tumour. Finally, cell kill outcomes from the model were converted to TCP using two different methods to compare model outcomes with clinical trial data.

Key results from this work are summarised in the dot points below:

- Comparisons between the average model predictions of fraction number and total dose required for 100% TCP, found good agreement with the prescriptions used in clinical trials, supporting the utility of the *HYP-RT* model.

- Biological effective dose rankings for acute and late normal tissue effects for the eleven fractionation schedules tested confirmed that the lowest dose per fraction schedules were the most favourable (low BED rankings), assuming that all treatment schedules eventually controlled the tumour, i.e. with no restriction on the number of fractions.

- The conventional schedule of 5x2 Gy per week was predicted with the model to be relatively good in terms of acute normal tissue effects, but had one of the poorest BED rankings late normal tissue effects. This fact is interesting and indicates that altered schedules have the potential to decrease late toxicity rates in hypoxic and oxic tumours for most combination of onset times of AR and ROx.

- Schedule number 11 (10x1.2 Gy/week with a 2 week break after 2 weeks of treatment) did not rank as poorly as anticipated, with an overall late normal tissue BED ranking of third place behind the hyperfractionated schedules 2 and 3. However, for the simulations where onset of AR was applied it ranked poorly for late normal tissue effects because of accelerated repopulation and the associated extended treatment time and total dose. For acute normal tissue effects schedule 11 ranked well due to the long total treatment time as anticipated.

- The model showed that the combination of a 0 week (immediate) onset time of ROx and a 2 weeks onset time AR was the most likely match to the “average” real tumour scenario based on the clinical trial dose data and the total doses required for hypoxic tumour control in the model.

- For the most likely (average) onset times of AR and ROx mentioned above, schedules 3, 11, 2 and then 1 (conventional) ranked most favourably for minimisation of acute normal tissue effects, while schedules 9, 7, 3 and 6 ranked most favourably for minimisation of late normal tissue effects.

- Comparing the model in terms of TCP using a number of methods involving the percentages of controlled tumours (by varying the random number seed) and Poisson theory was not sufficient for validating the model against published (averaged) patient LC percentage data from clinical trials. This was because of the large variation of the specific tumour parameters used in the model in the patients involved in the clinical trials.

- Despite the poor correlation of the model with the clinical trial LC percentage data the *HYP-RT* model has merit because of the good agreement in predicted total required doses (for 100% TCP) compared to that required in human tumours and also because it can be used to predict results for individual patients with specific tumour parameters for onset times of AR and ROx.

Chapter 7

Modelling New Altered Fractionation Radiotherapy Schedules

7.1. Introduction

In the previous chapter, the *HYP-RT* model was used to simulate altered fractionation radiotherapy based on head and neck cancer clinical trials. Simulation outcomes predicting the total dose required for 100% tumour control probability (TCP) agreed well with the prescribed doses reported in the clinical trials. The model has now been applied associated biological effective doses (BED's) to normal tissues, for four new fractionation schedules. The new schedules were developed in an attempt to reduce normal tissue toxicity (i.e. minimise BED) while maintaining 100% TCP.

7.2. New Fractionation Schedules

7.2.1. Fractionation Design

The four new fractionation schedules (no. 12 to 15) represent modifications of clinical trial schedules discussed in Chapter 6, with the adjustment of one parameter, e.g. the dose per fraction (Table 7.1). Adjustment of single parameter was not a model restriction, rather it was planned to assist in the analysis process of the existing versus the new fractionation schedules.

Table 7.1. The four new altered fractionation schedules developed for analysis with the HYP-RT model.

	Schedule Number and Description:	Fractionation Scheme: M T W Th F S Su M T W Th F (repeating)	Dose / # (Gy)	#'s / day	Days/ wk	Justification for Modelling the Schedule:
12.	Concomitant boost (during *first* 2 weeks) radiotherapy	II II II II II II II II II II I I I I I I I I I I	**1.8** 1.5 boost at beginning	**1** 2 during boost	**5**	To compare with boosting at the end of the treatment course.
13.	Continuous hyperfractionated accelerated radiotherapy (CHART)	III III III III III III III III III III III III	**1.2**	**3**	**7**	A less aggressive version of the 21x1.5 Gy/wk UK CHART schedule.
14.	Hyperfractionated accelerated radiotherapy	II II II II II II II II II II	**1.5**	**2**	**5**	A more accelerated version of RTOG *b.i.d* schedule by increasing the dose per fraction.
15.	Hyperfractionated accelerated radiotherapy	II II II II II II II II II II II II	**1.2**	**2**	**6**	A more accelerated version of RTOG b.i.d schedule by increasing the number of fractions per week

= number of fractions of radiotherapy.
For schedules **1 to 11** see Table 6.1 in Chapter 6 of this report.

[NB: The four new schedules were developed for analysis in the *HYP-RT* model and are not based on clinical trials; therefore no treatment outcomes are reported.]

7.2.2. Schedule Implementation and Analysis Methods

The four new schedules were implemented using text files that were developed for the model to read-in before treatment simulation. These files contained all of the necessary fractionation information, including the doses per fraction and the hours between each dose fraction in the schedule (the same method as text files for schedules 1 to 11 from Chapter 6).

Results were analysed in terms of the total doses required for tumour control based on the elimination of all stem, transit and level 1 differentiating cells ("basal" cells) and the calculated BED's to acute and late responding normal tissues. Total dose and BED results were compared to five clinical trial schedules (schedule 1: conventional, schedules 2 and 3: *b.i.d.* hyperfractionated, schedule 7: UK CHART and schedule 8: concomitant or "concom" boost). These five schedules were those most similar to the new schedules.

BED analysis results have been presented as the *raw* BED calculation values, and have not been converted into a 0 to 10 ranking, as done for Chapter 6. This method enabled a more direct "new" versus "clinical trial" schedule comparison. Note that the equations and assumptions made in the BED analysis are the same as those discussed in section 6.2.2 of this report.

Statistical analysis was performed in the same way and with the same software as the results from Chapters 5 and 6, with a total of nine simulations run per parameter set and with the error bars in the figures representing the one standard deviation of the data.

7.3. New Schedule Modelling Results and Discussions

7.3.1. Total Doses required for Tumour Control

The data in this section relates to simulations of oxic and moderately hypoxic virtual tumours, with model outcomes presented as the total doses from the *HYP-RT* model that were required to achieve 100% TCP.

7.3.1.1. Oxic Tumour Simulations

The total doses required in oxic tumour simulations for the four new schedules (no. 12 to 15) are shown in Figure 7.1 along with five clinical trial schedules (no. 1, 2, 3, 7 and 8).

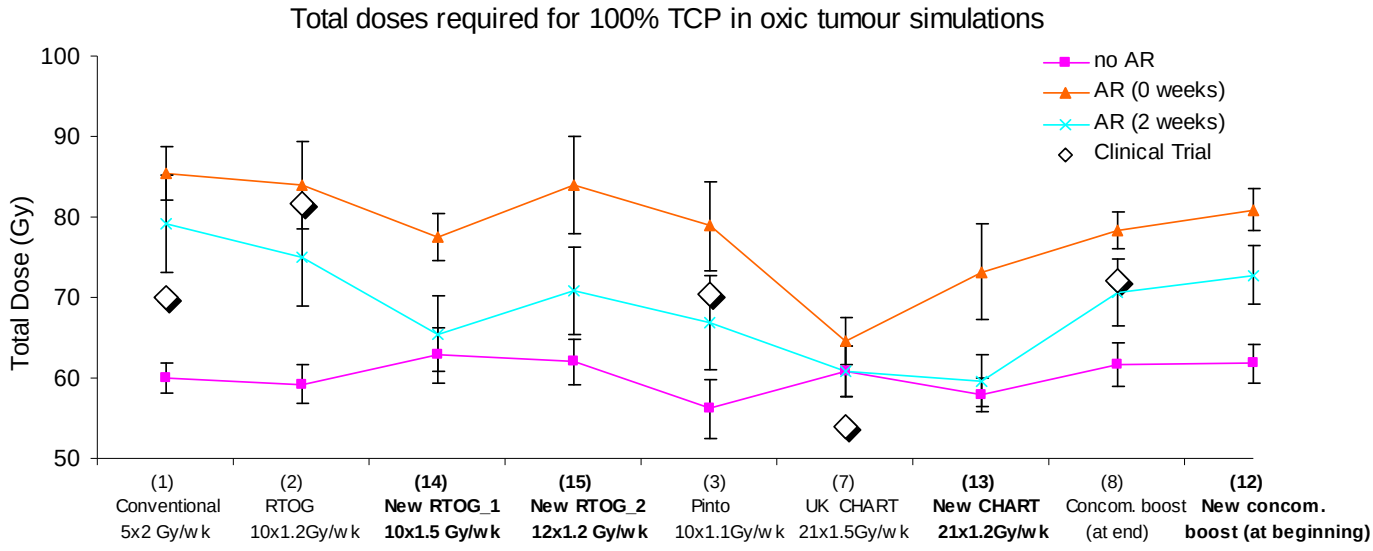

Figure 7.1. Oxic tumour simulations with varying onset times of AR comparing the total doses required for 100% tumour control probability (TCP) for four new altered fractionation schedules and five clinical trial schedules.

Oxic tumour simulations revealed that the two variations of the *b.i.d.* RTOG schedule (no.14 and no. 15) had similar rates of cell kill compared to the original schedule (no. 2). The 1.5 Gy per fraction schedule (no. 14) required the **least total delivered dose**, except when no AR was simulated. For the most clinically likely (on average) onset of time of AR (2 weeks, as discussed in Chapter 6), the total dose difference for schedule no. 14 compared to schedule no. 2 was **-9.5±6.2 Gy**. This was a significant dose decrease.

Schedule no. 15 was not significantly different from the original RTOG schedule (no. 2) for any AR onset times.

On average, the new CHART schedule (no.13) required **more total delivered dose (+8.6±6.7 Gy)** compared to the UK CHART schedule (no.7) for onset of AR at 0 weeks. However, for the other onset times of AR the dose differences were not significant. The new concomitant boost schedule (no.15), with the boost at the beginning of treatment, required approximately the **same total delivered dose** to achieve 100% TCP, compared to the original schedule (no. 8).

7.3.1.2. Hypoxic Tumour Simulations

The total dose predictions for the hypoxic tumour simulations for the four new and five clinically trialled schedules are presented in Figure 7.2.

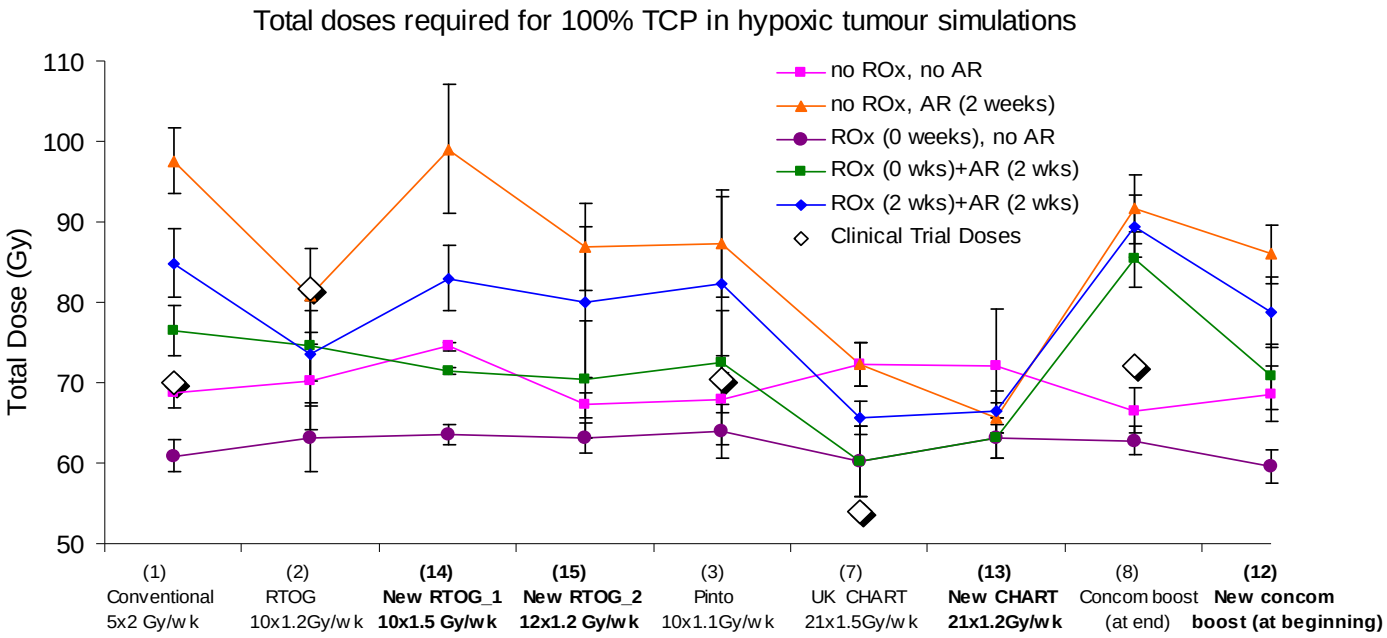

Figure 7.2. Hypoxic tumour simulations varying the onset times of AR and ROx comparing the dose required for 100% tumour control probability (TCP) for four new altered fractionation schedules and five clinical trial schedules.

Overall, the new CHART schedule (no. 13) required the same range of total delivered doses to achieve 100% TCP, using various onset times of AR and ROx, compared to the UK CHART schedule (no. 7). This occurred despite the lower of the dose per fraction in

schedule no. 13. This was attributed to the shallower OER curve for doses per fraction of <1.25 Gy.

The two hyperfractionated schedules (no. 14 and 15) required **more total delivered dose** on average compared to the original RTOG schedule (no. 2), in the range of 1 to 20 Gy. For onset of AR at 2 weeks and ROx at 0 weeks there was a small dose reduction of **6±5 Gy** when using schedule no.14 compared to no 2.

Boosting at the beginning of treatment (no. 12) required **less total delivered dose (-3 to -15 Gy)** compared to boosting at the end of treatment (no.8), except for specific simulations with no AR and no ROx.

7.3.2. Normal Tissue Effect Predictions Based on Calculated BED

The data presented in this chapter has involved the total delivered doses required in the model for 100% TCP. To compare the therapeutic ratio of the new schedules against clinical trial schedules, a normal tissue BED analysis was performed (using Equations 6.1 and 6.2 from Chapter 6).

Note that the error bars in the BED results figures of this chapter have been omitted for simplification purposes, but are in the range of **3 to 15 Gy** for acute effect BED predictions and **4 to 20 Gy** for late effect BED predictions, depending on the onset times of AR and ROx. These errors were calculated using Equations 6.1 and 6.2, inputting the total dose results shown Figure 7.5, plus or minus the standard deviation in the total dose data (i.e. $D \pm \Delta D$), to obtain the upper and lower limits of BED for each data point. BED errors are however included in Figures 7.5, 7.6a and 7.6b, when discussing the effects of a variable versus constant OER curve.

7.3.2.1. Oxic Tumour BED Results

Oxic tumour BED calculation results for the four new schedules and five clinical trial schedules are shown in Figure 7.3 a). Almost all BED results for the new schedules had

mid-ranged acute effect BED results, compared with the eleven schedules presented Chapter 6. The only exception to this was the new "less aggressive" CHART schedule (no. 13) which had relatively high BED results for the cases of no onset of AR and onset of AR at 0 weeks. However, the BED for onset of AR at 2 weeks of the new CHART schedule was mid-ranged.

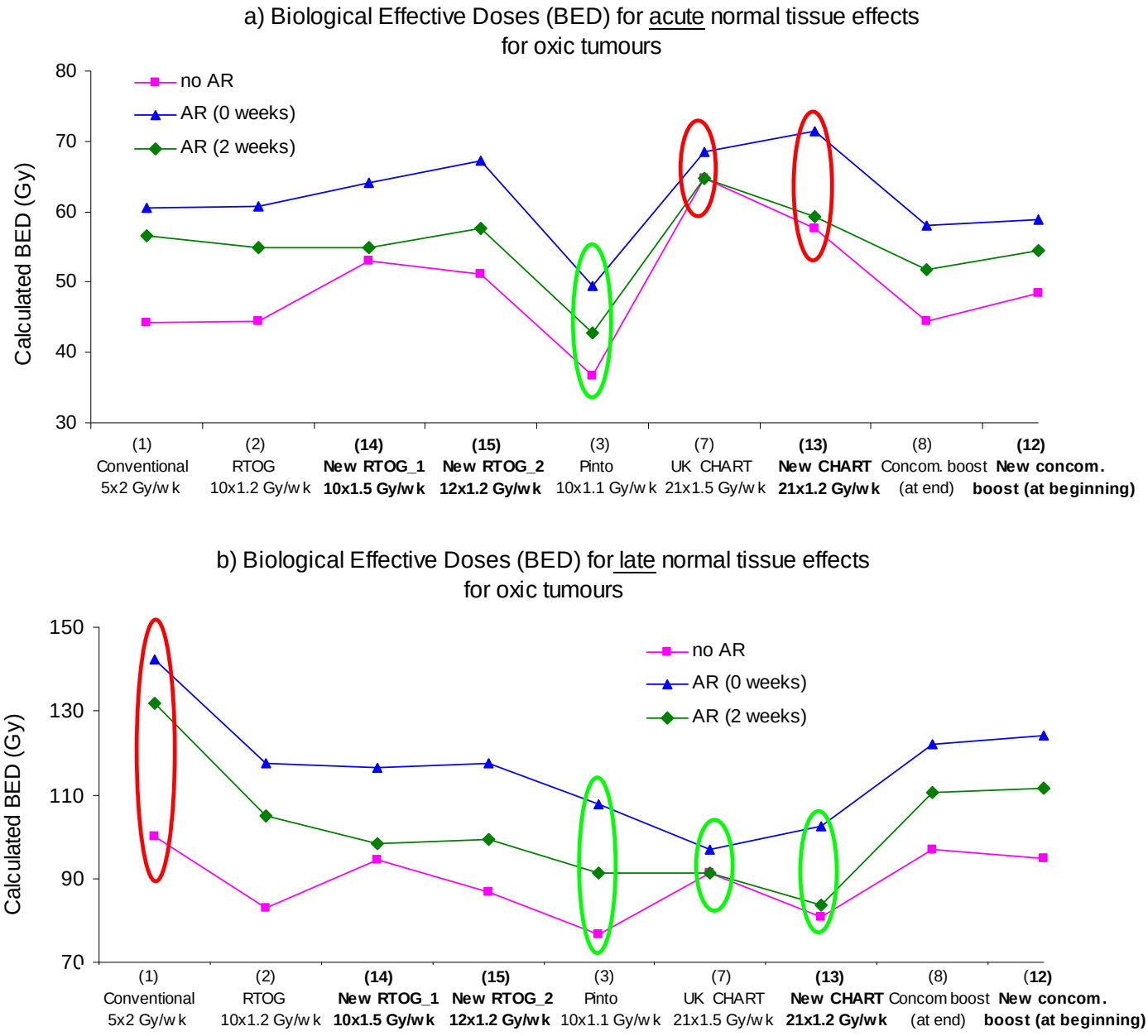

Figure 7.3. BED calculations based on the modelled 100% TCP dose, for predictions of a) acute normal tissue effects and b) late normal tissues effects in oxic tumour simulations for four new and five clinically trialled schedules and various onset times of AR. The red circles indicate the worst schedules and the green circles the most beneficial schedules in terms of the predicted a) acute and b) late normal tissue tolerances.

Considering acute effects in all of the simulated clinical trial *and* new schedules, the Pinto *et al.* 10x1.1 Gy per week schedule (no. 3) was found to be most beneficial, having the overall lowest BED values for early onset AR in oxic tumours. However, for later onset AR (≥2 weeks) the new CHART schedule of 21x1.2 Gy/wk had the overall lowest BED values.

For late normal tissue effects, all BED results for the four new schedules were mid-ranged, except for the new CHART schedule (no. 13) which had relatively low BED values. Consequently, the new CHART schedule was the overall most beneficial schedule for late normal tissue effects, having BED values that were marginally lower than the Pinto *et al.* schedule (no. 3) for both the 0 and 2 weeks onset times of AR (Figure 7.3 b).

7.3.2.2. Hypoxic Tumour BED Results

Similar predictions, based on BED calculations, for acute and late normal tissue toxicity during hypoxic tumour treatment simulations were found for the four new schedules versus five clinical trial schedules.

The results for the hypoxic tumour simulations (Figure 7.4 a) show that the clinical trial schedules 1, 2, and 3 had relatively low BED's for acute normal tissues. The new schedule with a boost at the beginning of treatment (no. 12) had marginally lower acute normal tissue BED results compared with its clinical trial counterpart (no.8) (between 1 and 8 Gy), which was significant only for the case of onset of AR at 2 weeks and ROx at 0 weeks.

The two new hyperfractionated schedules (no. 14 and no. 15) had relatively high BED's for acute normal tissues. The concomitant boost schedule (no. 12) improved upon its clinical counterpart, but only for onset of AR at 2 weeks and onset of ROx at 0 weeks (BED reduced by 8 Gy). Overall, none of the four new schedules had acute normal tissue BED's as low, and hence beneficial, as the Pinto *et al.* schedule (no.3).

For late normal tissue effects in hypoxic tumour simulations (Figure 7.4 b), the conventional schedule was predicted to be poorly tolerated (high BED's), while the

hyperfractionated schedules (no. 2, 3, 14 and 15) and the two CHART schedules (no. 7 and 13) were all predicted to be well tolerated (low BED's).

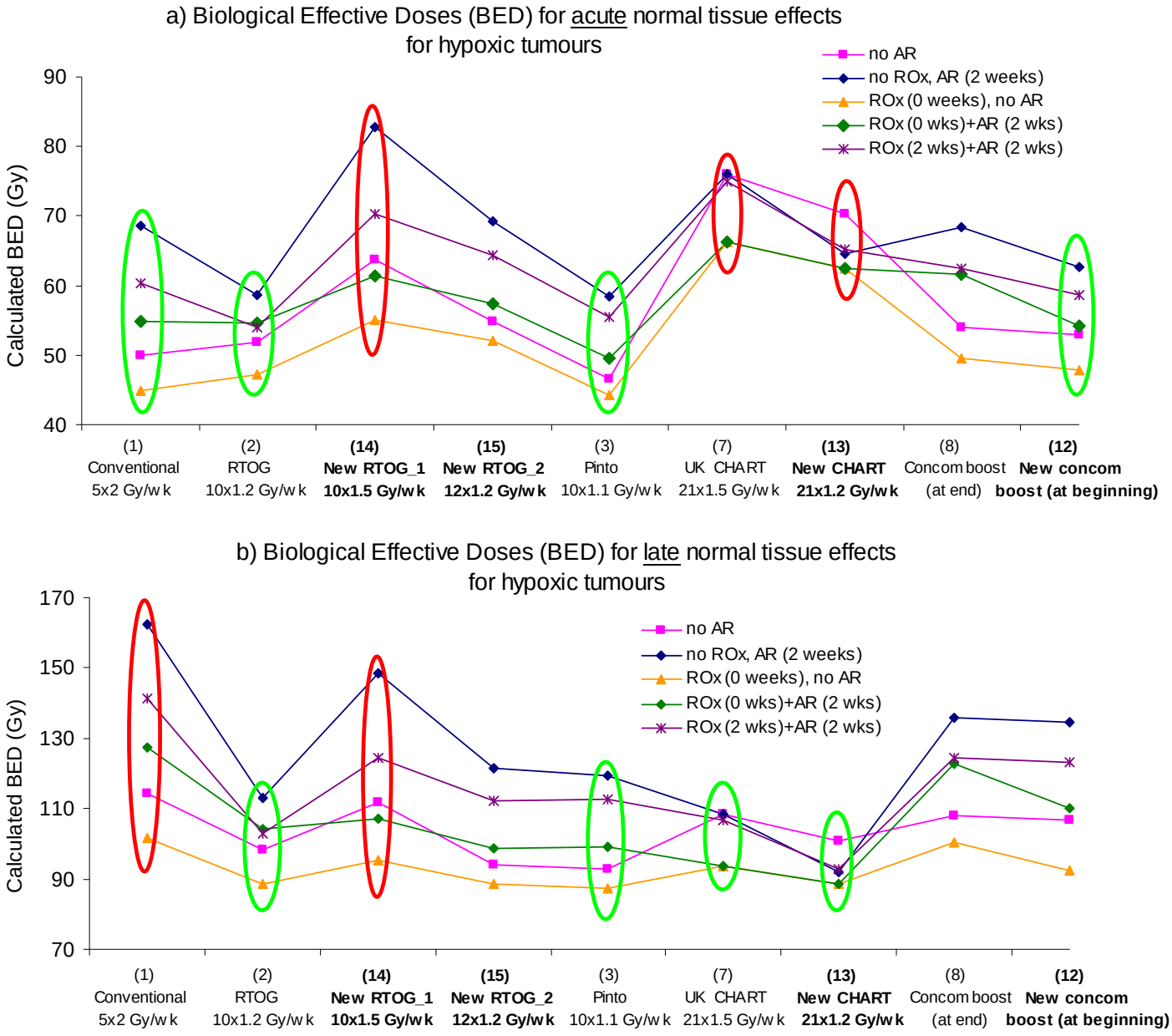

Figure 7.4. BED calculations based on the modelled 100% TCP dose, for predictions of a) acute normal tissue effects and b) late normal tissues effects in moderately hypoxic tumour simulations for four new and five clinically trialled schedules and various onset times of accelerated repopulation (AR) and reoxygenation (ROx). The red circles indicate the worst schedules and the green circles the most beneficial schedules in terms of the predicted a) acute and b) late normal tissue tolerances.

The two new hyperfractionated schedule (no. 14 and 15) and the schedule boosting at the beginning of treatment (no. 12) did not have statistically significant reductions in late normal tissue BED's compared to the original clinical trial schedules, except for the boost schedule (no.12 vs. no. 8) for the case of onset of AR at 2 weeks and onset of ROx at 0 weeks (12 Gy). The new CHART schedule (no. 13) was found to be the new overall **most beneficial schedule** for late normal tissue effects.

In summary, assuming that that normal tissues receiving the 100% TCP dose in *HYP-RT* simulations, the **Pinto *et al.* schedule** (1.1 x10 Gy/wk) was overall the most beneficial schedule simulated (very advantageous for early normal tissue effects), while the **new CHART schedule** (21x1.2 Gy/wk) was the next most beneficial schedule (advantageous for late normal tissue effects).

Regarding the four new schedules, it was found that the **new CHART schedule** and **new concomitant boost schedule** may have some advantages in reducing late and acute normal tissue toxicity for various combinations of onset times of AR and ROx. However, the two new RTOG derived hyperfractionated schedules did not provide any advantages in terms of normal tissue toxicity reduction.

See Appendix C for a tabulated summary of the total doses, fraction numbers and calculated BED results obtained from the model, relating to all oxic and hypoxic tumour simulations for the eleven schedules discussed in Chapter 6 and the four new schedules discussed in this chapter.

7.3.2.3. The Effects of Modelling a Constant versus. Variable OER Curve

The results presented in the chapter thus far have related to the modelling of an OER curve that was dependent on dose per fraction. However, when modelling a fixed OER curve, with a maximum OER value of 3.0, the total doses required for tumour control were generally increased for hypoxic tumours, as expected.

Figure 7.5 shows examples of total dose predictions for the specific case of onset of AR at 2 weeks and ROx at 0 weeks, for simulations involving a fixed versus variable (dose per fraction dependent) OER curve.

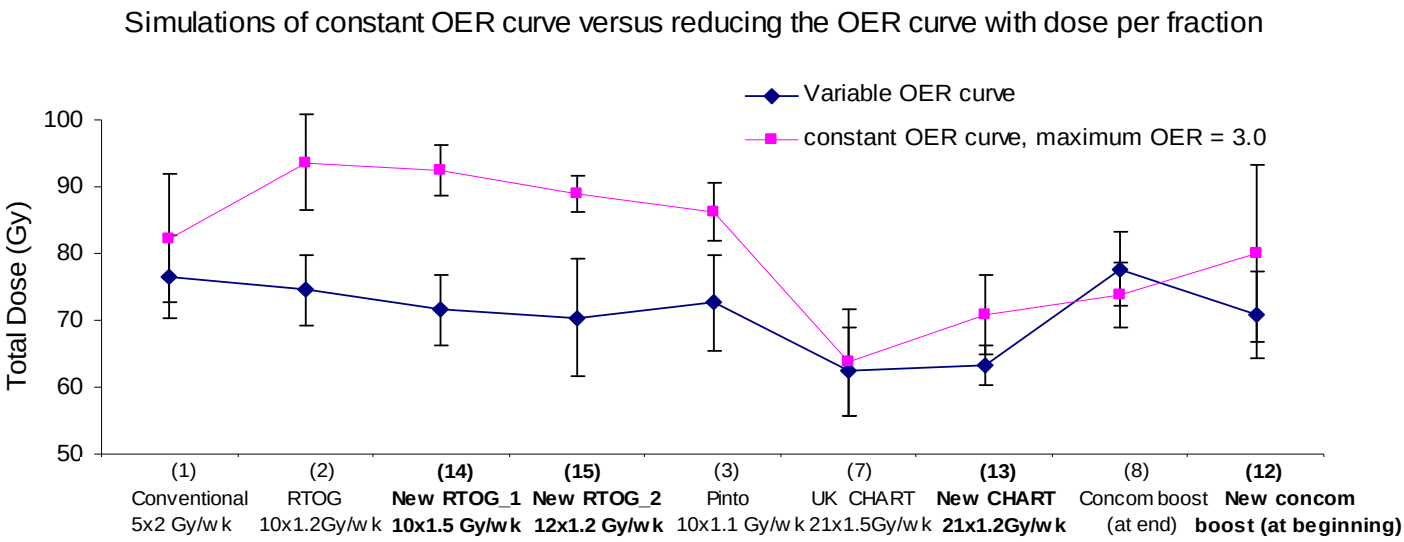

Figure 7.5. Total doses for the specific case of onset of accelerated repopulation (AR) at 2 weeks and onset of reoxygenation (ROx) at 0 weeks, for hypoxic tumour simulations for four new and five clinically trialled schedules modelling a fixed versus variable OER curve (dependent on dose per fraction).

Simulations involving a constant OER curve predicted total doses that were increased by approximately 20±10% for the hyperfractionated schedules, excluding the CHART schedule (no. 7). Schedules involving doses per fraction above 1.75 Gy were not affected because the OER curve with a maximum of 3.0 was used for all the simulations.

As a consequence of the increases in total dose using a fixed OER curve, the calculated BED values for normal tissue effects increased. Figure 7.6 shows some example BED calculation results, again for the specific case of onset of AR at 2 weeks and ROx at 0 weeks, comparing results using a fixed versus variable (dose per fraction dependent) OER curve.

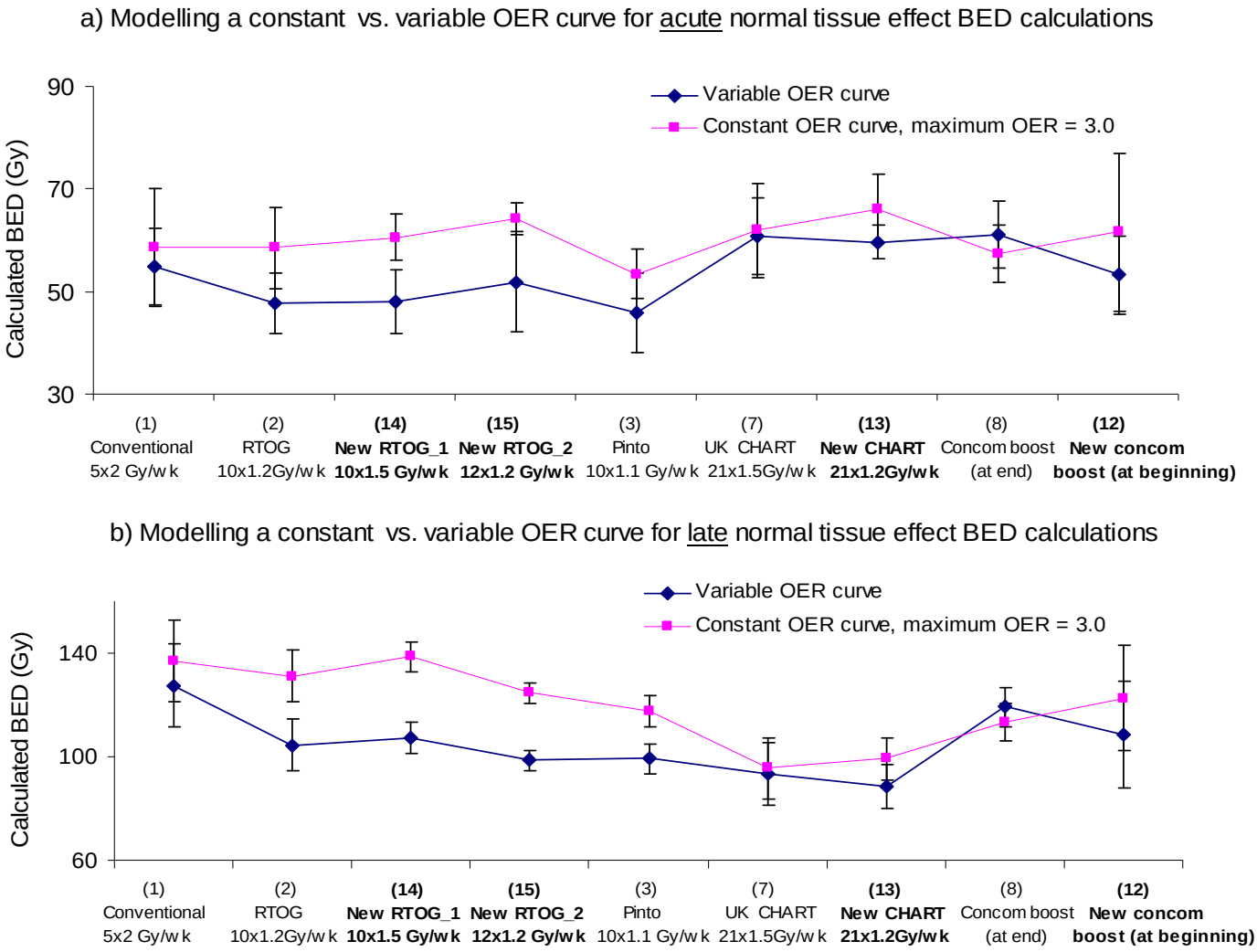

Figure 7.6. BED calculations for predictions of acute and late normal tissue tolerances for the specific case of onset of accelerated repopulation (AR) at 2 weeks and onset of reoxygenation (ROx) at 0 weeks, for hypoxic tumour simulations for four new and five clinically trialled schedules, modelling a fixed vs. variable OER curve (dependent on dose per fraction).

For acute normal tissue effects and the specific case on onset of AR at 0 weeks and ROx at 2 weeks, the Pinto *et al.* schedule remained as having the lowest BED values when a constant OER curve was modelled compared to a variable (dose per fraction dependent) OER curve (Figure 7.6 a). All of the new schedules had significantly increased calculated acute normal tissue BED's using the constant OER curve compared to the variable OER curve, and hence a higher prediction of acute toxicity.

For late normal tissue effect, the two CHART schedule (no. 7 and 13) remained as having the lowest BED's when modelling a constant OER curve (Figure 7.6 b) (95±8 Gy), and

were hence predicted to have the lowest toxicity for late responding normal tissues. The low BED results found here increased the relative benefits of the CHART schedules compared to the Pinto *et al.* schedule (no. 3) found in the previous section.

Overall, for both acute and late normal tissue effects, there were very large differences in calculated BED's, depending on the OER curve used in the model. These were most significant for the hyperfractionated schedules (up to **13 Gy** differences for acute effects and up to **31 Gy** for late effects).

These results highlight the importance of modelling a biologically accurate OER curve that closely resembles the true impact of oxygenation on radiation response. Ideally, the OER curve should be critically assessed and experimentally verified before use, while noting any dose per fraction effects for the fractionation schedule to be used in the simulations.

7.4. Conclusions

After analysing the parameters influencing cell kill in the *HYP-RT* model in chapter 5, and applying clinical trial schedules for model outcomes comparisons and verification in chapter 6, this chapter reported on the first application of the model in exploring new altered fractionation schedules for oxic and hypoxic tumours.

Simulation results from four new altered fractionation schedules have been presented, comparing the total doses required for 100% TCP between the new schedules and the doses prescribed in reported clinical trials (from which the new schedules were derived), as well as a relative toxicity comparison between the clinical trial and new schedules in terms of predicted BED to acute and late responding normal tissues.

Key findings based on total dose and BED results are listed in the dot points below:

- In general, the alteration of the RTOG schedule through both a dose per fraction change (from 1.2 Gy to 1.5 Gy, no. 14) and a fraction per week (from 10 to 12 fractions/week, no.15) change **did not** reduce the total dose required for 100% TCP. The only **small dose reduction** was for observed schedule no. 15 in hypoxic tumours for reducing late normal tissue effects in the specific case of onset of AR at 0 weeks and ROx at 2 weeks (BED reduced by 6±5 Gy).

- The new "less aggressive" CHART schedule (no. 13) with a reduced dose per fraction (from 1.5 down to 1.2 Gy), required the **same total dose** as the UK CHART schedule (no. 7). However, due to the smaller dose per fraction it provided a **therapeutic benefit, having** lower average acute and late normal tissue BED's (by 7 to 10 Gy), making it the schedule with the overall lowest predicted late normal tissue toxicity. For oxic tumour simulations, there were **no significant changes** in the total doses or BED predictions for the new CHART schedule compared to the UK CHART schedule.

- Simulating a boost dose of 1.5 Gy in a 1.8 Gy per fraction in a concomitant schedule, at the beginning *vs.* end of treatment, had a **small benefit** for acute and, to a lesser extent, late normal tissues (BED reduced by 3 to 15 Gy) for hypoxic tumour simulations. However **no predicted benefit** was found for this schedule in oxic tumour simulations. The benefit found for hypoxic tumour simulations was attributed to the boost dose being delivered early in the schedule, at a time when more cells were present in the tumour to receive the extra dose and when the boost would have the most impact on early onset AR.

- Averaging over all combinations of onset times of AR and ROx and all 15 schedules simulated, the **10x1.1 Gy per week schedule** reported by Pinto *et al.* was the schedule predicted to be **most beneficial** by the model (followed by the RTOG and new CHART schedules) because it had lowest BED values for normal tissue effects while achieving 100% TCP using the dose per fraction dependent OER curves.

- The least beneficial schedules based on data this chapter as well as Chapter 6 were the conventional and other 2 Gy per fraction accelerated schedules because of their high late and mid-ranged acute normal tissue BED predictions.

- The shape and maximum value of the **Oxygen Enhancement Ratio curve** used in radiotherapy models, has a significant impact on the rate of cell kill during simulations, affecting the total required dose to achieve 100% TCP and normal tissue BED predictions, especially relevant for hyperfractionated schedules with low doses per fraction. For example, using a constant OER curve, the UK CHART schedule using 1.5 Gy per fraction became relatively more favourable compared against the 1.2 and 1.1 Gy per fraction schedules. In this chapter the choice of OER curve was shown to alter the required total dose by up to **20±10 Gy**. Thus, the OER equation utilised should be critically assessed before being incorporated in radiotherapy models.

Chapter 8

Final Conclusions

Locally advanced hypoxic head and neck carcinomas are often difficult to treat and have poor prognosis after fractionated radiotherapy because of hypoxia related radioresistance and accelerated repopulation. To quantitatively analyse the dynamics of cell propagation, cell death and cellular oxygenation during tumour growth and fractionated radiotherapy, a computer model named *HYP-RT* was developed. The aims of using stochastic methods to model (i) the temporal progression of individual cells during tumour growth and (ii) accelerated repopulation and reoxygenation of hypoxic tumours during radiotherapy have been achieved in this work, while maintaining a high level of computational efficiency.

The model has the flexibility for users to input many different cellular and treatment related parameters within a plausible biological range, and enables tumour hypoxia to be simulated through the use of a single pO_2 histogram corresponding to the pre-treatment oxygenation level of the tumour. The unique and convenient features of the model make it applicable for current radiobiological research investigating the cellular mechanisms influencing radiation induced cell kill during standard and novel radiotherapy fractionation regimens.

8.1. Model Development Summary

The *HYP-RT* model consists of two main algorithms, (i) the tumour growth algorithm, and (ii) the radiation effect algorithm. In the tumour growth algorithm, cells are programmed to divide, starting from one malignant and well oxygenated stem cell. The cell types used to model epithelial cell hierarchy included infinitely proliferating “stem” cells, “transit” cells that could divide up to four times, and non cycling cells including

quiescent stem cells, differentiating/differentiated cells and hypoxia induced quiescent cells. Each living cell was stored in a dynamic and memory efficient vector array containing "object" elements incorporating individual cell data such as cell cycle time, oxygenation and cell type, and their chronological order of division.

Tumour hypoxia was modelled using both log-normal and normal shaped oxygenation probability distributions (pO_2 histogram). As cellular oxygenation has been reported to not only influence cellular radiosensitivity but also cell cycle progression, cells were programmed to both increase their resistance to doses of radiation and have increased cell cycle times with decreasing pO_2. A proportion of cells were assigned to the quiescent phase (G0 phase) if their pO_2 level is $\leq$ 1 mm Hg, which could be later reversed if cellular reoxygenation was simulated.

Random number generation was required in the model to allocate cellular and other parameter values from various mathematical functions, allowing the functions to act as probability distributions. Running the program using different input random seed numbers enabled the associated variation in model output to be statistically analysed and compared against the change in output when purposely altering a parameter value such as symmetrical stem cell division probability (%).

The radiation effect algorithm was developed with the aim of simulating the outcomes of fractionated radiotherapy at the cellular level. Cell kill was modelled to be dependent on the dose per fraction, cellular oxygenation (for which the associated OER curve varied with dose per fraction) and whether or not a cell was cycling or in the G0 quiescent phase.

Modelling the inherent sensitivity of cells for each dose fraction has the potential for incorporating results from genetic assays, which are becoming readily available. The genetic assays may be used to individualise treatment based on genetic profiling, e.g. to examine gene/protein activity and gene mutations that are linked, for example, to either a higher or lower inherent cellular sensitivity to ionising radiation.

Two of the key radiobiological phenomena considered during the development of the radiation effect algorithm were reoxygenation and accelerated repopulation.

Reoxygenation was modelled using small pO_2 increments to the cell population at random, simulating gradual oxygenation increase of the tumour during shrinkage. Reoxygenation related parameter values were based on achieving full oxygenation when all but 10^5 to 10^6 cells remained in the tumour (1 to 2 mm in diameter). Accelerated repopulation was modelled by increasing the stem cell symmetrical division probability (using the *AR boost factor* parameter) from 3% up to 30%, resulting in a reduced rate of cellular differentiation and an increased overall stem cell percentage. A ten fold increase in the *AR boost factor* provided results that correlated closely with clinical data, reporting the extra dose per fraction required to control the accelerated growth (an additional 0.5 to 1.0 Gy per fraction).

The presence and dynamics of tumour hypoxia during radiotherapy were observed in experiments using HNSCC FaDu xenografts in an immuno-deficient mouse model. Immunohistochemical techniques, using the 2-nitromidazole hypoxia marker *Pimonidazole,* and the *in vivo* OxyLab fluorescence probe system (*Oxford Optronix*, Pty. Ltd.) were used to visualise and quantitatively measure hypoxia in the xenografts during an accelerated course of radiotherapy (40 Gy in 2 weeks).

The presence of hypoxia was verified in all of the xenografts, with the spatial distribution of hypoxia observed as chaotic and speckled in appearance, suggesting the dominance of acute hypoxia in the rapidly proliferating tumours and the high probability of hypoxic cells existing in close proximity to endothelial and proliferative cells. Increased cellular oxygenation levels (tumour reoxygenation) were confirmed quantitatively during radiotherapy. However, this result was only significant after the total dose of 40 Gy had been delivered. As such, in the *HYP-RT* model, early as well as late onset reoxygenation was modelled.

The conventional 5x2 Gy per week radiotherapy schedule was simulated with the model, along with nine other clinically trialled HNSCC altered fractionation schedules. Modelling of the schedules allowed for a comparison between model results and clinical trial prescriptions and local control outcomes. Four newly designed altered schedules were also simulated to compare against existing clinical schedules. Model results for the various schedules were compared not only on the basis of the total doses required to achieve tumour control, but also on their relative biological effective doses (BED) to

acute and late responding normal tissues (assuming the normal tissue received 100% of the tumour dose).

8.2. Model Results Summary

The key achievements and outcomes relating to the tumour growth algorithm are listed below:

- The tumour growth algorithm can propagate up to 10^8 cells in approximately 30 minutes on a standard personal computer (2 GB of RAM and a 2 GHz processor). The user can define input values influencing parameters such as the percentage of stem cells, the degree of hypoxia, the rate of natural cell death and cell cycle time.

- Tumour growth rate was found to be most influenced by the stem cell symmetrical division probability (*Spercent*). The default value in the model (3%) generated a tumour that propagated up to 10^8 cells in 2 to 3 years of tumour time and with a final tumour doubling time of 37 to 64 days, depending on the degree of hypoxia.

- Using default parameter values in the model, a tumour consisting of 1% stem cells, 10% transit cells and 89% differentiating/differentiated cells was generated. When hypoxia was simulated, the different cell type percentages were purposely maintained. However, for hypoxic tumours, a percentage of cells (50%) comprised of all cell types were assigned to the quiescent G0 phase if their pO_2 values were $\leq$ 1 mm Hg. Unless reoxygenated, these quiescent cells were eventually eliminated to simulate necrotic cell death, with a default half life of 4 days.

- Tumour hypoxia was defined by the shape of the log-normal or normal pO_2 histogram utilised in the model, with four degrees of tumour oxygenation simulated; oxic, moderately hypoxia, severely hypoxic or extremely hypoxic. Tumour growth rate was significantly decreased by hypoxia because of the associated slowing of the cell cycle and the inducement of necrosis.

- The choice of three digit random seed number, for the model's random number generator algorithm, did not have a significant impact on final tumour doubling times (when approaching 10^8 cells). However, the random seed did impact on the total tumour growth time because of small fluctuations in stem cell percentages that accelerated or decelerated tumour growth rates in the early stages of tumour development.

- Statistical errors caused by the change of random seed, resulted in standard deviations in total dose of approximately 4 to 8 Gy when simulating total cell kill during simulated radiotherapy. This level of statistical error corresponded to tumours grown with three different random seeds in the tumour growth algorithm and treated with a further three random seeds in the radiation effect algorithm.

- In the FaDu xenograft experimental study, the onset of reoxygenation was found to occur relatively late in an accelerated schedule (40 Gy in 2 weeks). This led to the simulation and analysis of a wide range of reoxygenation onset times in the *HYP-RT* model (0 to 3 weeks), among other parameter variables.

- The experimental study led to the development of useful animal handling and restraining techniques, and provided tumour growth rate and radiotherapy tolerance information for the FaDu cell line, for future *in vivo* radiation oncology and medical oncology experiments.

The key outcomes achieved during development and analyses of the radiation effect algorithm are summarised below:

- Using the *HYP-RT* model, fractionated radiotherapy applied to a 10^8 cell virtual tumour was simulated in approximately one minute. The model user is able to input radiobiological parameters such as inherent cellular radiosensitivity (SF_d where d is the dose per fraction), the onset time of accelerated repopulation, the onset time of reoxygenation and the rate of necrotic cell death.

- Simulation results showed that on average the last 3 to 6 dose fractions were responsible for the elimination of the last five tumour cells, while the last 1 to 2 fractions eliminated the very last tumour cell, for the conventional treatment schedule.

- On average, an extra 4 Gy was required in simulations to kill all stem, transit and level 1 differentiating cells (cells normally residing in the basal layer of the epithelium) *vs*. all stem cells alone. This increase in dose was consistently observed, but was within statistical error (4 to 8 Gy).

- Moderately hypoxic tumours required an extra 16±6 Gy to achieve 100% tumour control probability (TCP) compared to well oxygenated tumours, using the conventional treatment schedule.

- Modelling severe and extreme hypoxia by increasing the peak value of the log-normal shaped pO_2 histogram or using a normal function (Figure 5.30) did not have a large impact on model outcomes. This led to the conclusion that the overall shape of the pO_2 histogram is not a critical parameter, however it *was* found that the percentage of cells in the very low pO_2 region of the curve (< 3 mm Hg) is important, primarily due to the associated low OER values (approaching 1.0) and also the relatively slow cell cycle times of the cells.

- Accelerated repopulation increased the total doses required for 100% TCP by approximately 5.0 Gy for every week that the onset of the accelerated growth was brought towards the start of treatment.

- Reoxygenation had a smaller influence on cell death rates during radiotherapy compared to accelerated repopulation using the default model parameters. For example, only an extra 1.0 Gy per week was required for every week that reoxygenation onset was delayed after the start of treatment, to achieve tumour control in the same length schedule.

- When accelerated repopulation and reoxygenation were considered simultaneously in the model, their combined effects were not additive. Consequently, each combination of onset time of accelerated repopulation and reoxygenation must be simulated separately to obtain the correct model prediction.

- Model results have demonstrated the significant variations in total doses that are required to achieve tumour control when accelerated repopulation and reoxygenation are onset at different times throughout treatment (up to 30 Gy). These results provide strong justification for future research to be directed towards the development of predictive assays and quantitative hypoxia imaging assessment on an individual patient basis, to enable a more personalised approach to radiotherapy treatment planning for HNSCC.

- In general, model total delivered doses results agreed well with prescription doses from clinical trials and with the doses predicted with the Linear Quadratic model achieve just under 1.000 cells remaining). However, the linear quadratic model agreement only applied to the simple oxic tumour case.

- When considering specific onset times of accelerated repopulation and reoxygenation, the comparisons between the *HYP-RT* model and clinical trial data were difficult because of the wide heterogeneity of tumour properties in large patient groups. Specific comparisons with the Linear Quadratic model were also difficult because of the level of complication required to model dynamic tumour phenomena in equation based models. These issues make computer model verification challenging, however they highlight that the range of results obtained using different types of models, considering different radiobiological phenomena.

- Modelling the combination of onset of accelerated repopulation at 2 weeks and immediate reoxygenation (0 weeks) provided total delivered dose results (to achieve 100% TCP) that best matched clinical trial prescription doses. Thus, the 2 and 0 week combination for these two phenomena are likely to be the best average patient response. However, for those individuals that deviate from these onset times, the total dose requirements change significantly and should be adapted to suit the specific tumour and patient of consideration to improve the therapeutic ratio.

- Cell survival results from simulations were converted to TCP (Poisson model) for comparisons with clinical trial local control data. This was performed for simulations using threshold total doses equal to the total dose prescriptions from clinical trials. The comparison did not provide clear correlations between model TCP and clinical local control. This was attributed to the sensitivity of the Poisson equation to variations in surviving cell number obtain from the model, which varied with random seed number (over the last 6 fractions), and also due to the large variations in cell kill rates when modelling different onset times of accelerated repopulation and reoxygenation.

- Out of all radiotherapy schedules simulated, the model predicted the Pinto *et al* hyperfractionated 10x1.1 Gy per week schedule to be the most beneficial schedule. This conclusion was based on comparable efficacy (100% TCP) but low toxicity, as reflected in the low calculated BED values for acute and late normal tissue effects.

- The conventional schedule BED results for acute and late normal tissues were mid-ranged to high compared with the altered fractionation schedules simulated, indicating the relatively high toxicity of the conventional schedule (predominately due to late normal tissue toxicity).

- The simulated accelerated schedules, using 2 Gy per fraction, were predicted to have high toxicity (high BED values) for both acute and late normal tissue effects compared to the *b.i.d.* hyperfractionated schedules, in agreement with reported clinical observations.

- The new “less aggressive” CHART schedule (1.2 Gy per fraction) improved upon the UK CHART schedule having slightly reduced BED predictions (by 5 Gy) for acute and late normal tissues, for most combinations of onset times of accelerated repopulation and reoxygenation. Similar small benefits were observed when boosting at the beginning rather than the end of treatment in a concomitant boost schedule.

- Variations made to the 10x1.2 Gy/week RTOG schedule (using 1.5 Gy per fraction or 12 fractions per week) did not have any significant benefits for either acute or normal tissue toxicity.

- The treatment schedules utilising doses per fraction below 1.75 Gy were modelled to have a reduced oxygen effect. This was applied in simulations by flattening the oxygen enhancement ratio (OER) curve and resulting in a more uniform probability of death among cells of different oxygenation. However, when modelling a fixed OER curve for all schedules (with a maximum value of 3.0), there were up to 30 Gy differences in total delivered dose and BED results, compared to modelling a variable OER curve (varying with dose per fraction). This significant dose difference outlines the utility of computer modelling in assessing the quantitative impact of important biological and radiobiological parameters on tumour control, and the need to experimentally validate data before use in models.

8.3. Future Directions

Although further work is needed in terms of clinical verification of model predictions before *HYP-RT* can be used clinically, it is hoped that progress with the model will continue and that within the current decade it will be available as a clinical tool to aid in the process of individualising radiation treatment planning for head and neck squamous cell carcinoma patients.

Future potential extensions to the HYP-RT tumour growth algorithm are listed below:

- addition of spatial parameters to the tumour cell population, to extend model applications to techniques such as IMRT and "dose painting"
- spatial modelling of the tumour vascular system, extra-cellular matrix and the dynamics of cellular migration (microscopic spread)
- modelling of the normal tissue cells surrounding the tumour, to enable more detailed normal tissue toxicity predictions
- modelling alternate disease sites, such as the breast and prostate, by adapting cell type percentages (the cell hierarchy), the degree of hypoxia and cellular differentiation rates during tumour growth and treatment

Future research aims for the radiation effect algorithm include modelling:

- sub-lethal cell damage between radiation treatment fractions
- finite cellular repair times between radiation treatment fractions
- gradual radiation-induced cell death and finite abortive cellular divisions
- tumour reoxygenation in more detail, by extending the model to consider the dependence of the reoxygenation rate on parameters such as the current tumour diameter and/or radiation induced cell death rate
- specific schedules to shed light on the impact of unscheduled treatment breaks during fractionated radiotherapy treatment

To temporally model tumours of a greater size than 10^8 cells will require the use of computers that utilise parallel processing, both to provide convenient tumour growth simulation run times, and well as the use of large amounts of dynamic random access memory during growth and treatment simulations. To model larger tumours in which the

degree of hypoxia extends to the point of large regions of central (or otherwise) tumour necrosis and for the application of IMRT type treatment techniques, spatial coordinates will need to be may for each cell. This will again require an increase in computer requirements. However, with the ever increasing memory capacities and computation speeds of modern computer systems and parallel networks, computational restrictions should not be a major issue in the future.

Other future aims include coding the main algorithms of the *HYP-RT* model into the C++ programming language, to make the code more maintainable, extendable and compatible with up to date programming libraries, and also the modelling of radiation treatment in combination with chemotherapy or cytotoxic drug therapies such as *Tirapazamine*. Problems that may be encountered while fulfilling these aims are likely to include the availability of reliable biological cell data and clinical trial data for model comparison and validation. However, with the increasing quantity, quality and specificity of published data, for example from predicative assays, PET/CT/MRI imaging studies and randomised radiotherapy clinical trials, these issues should not impede future advances and the interest of potential researchers in the field of stochastic tumour modelling.

Appendix A:

HNSCC clinical trials from the 1980's to the present, indicating the conventional and altered fractionation schedules used to treat the disease as the sole modality of treatment. Conventional treatment arms for all studies use 1.8 to 2 Gy per fraction, 1x5 fractions per week, in 7 to 8 weeks (unless otherwise indicated).

Note: Patient number refers to the total patient number in the trial for all trial arms. T_{pot} = tumour potential doubling time, *LC*= local control, *#* = fraction number, *LI* = labelling index, T_{pot} = potential doubling time, *C.T.* = conventional 5x2 Gy per week radiotherapy, *H.T.* = hyperfractionated radiotherapy).

Trial	Fractionation	Total Dose and Dose per Fraction	Patient No.	Local Control	Parameter Stratification	Comments
HYPERFRACTIONATED TREATMENT:						
EORTC Phase III 22791 (Horiot et al 1994)	2 # / day 70 #s 7 weeks	80.5 Gy 1.15 Gy /# 2 #s / day	356	56% LC at 5 years [38% LC in control arm]	T_{pot} less than and more than 4.0 days LC rates reported (65% vs. 62%) [in control arm: T_{pot} less than and more than 4.0 days LC rates reported (28% vs. 60%)]	Improved LC with increase in acute reactions but no increase in late reactions. Ts, Li, Tpot distributions given (11.2+-4.4 hrs, 12.7+-6.0%, 4.7+-3.2 days). Fast growing tumours have much worse LC with C.T. than with A.T. Stage T2 to T3 and N0 to N1 cancers considered in this trial. Benefits only significant for stage T3 tumours.
RTOG Phase III 9003 (Ang et al 1990, Fu et al 2000)	H.T. 2 # / day 68 #s 7 weeks	81.6 Gy 1.2 Gy / #	1073	54% LC at 2 years [46% LC in control arm]		Improved LC with increase in acute reactions but little to no increase in late reactions. Slightly higher grade 3 late effects (13% compared to 6 to 8% for the others regimens)
Brazil Trial Phase III/IV (Pinto et al 1991)	H.T. 2 # / day 6.5 weeks	70.4 Gy 1.1 Gy / # 6.5 weeks	98	62% LC at 2 years [in control arm: 52% LC]		Improved LC with increase in acute reactions but no increase in late reactions. Significant improvement in survival also (not for base of tongue).

Trial Dates	Fractionation Schedule	Dose Regimen (average)	No. Patients	Local Control	Parameter Stratification	Comments
CONTINUOUS ACCELEREATED TREATMENT (CHART and CAIR):						
UK (CHART) (Dische et al 1997)	3 # / day 12 days	54 Gy	918	Same as C.T. LC rate	Poorly differentiated tumour do better with conventional RT i.e. if less differentiated HART is more beneficial.	No significant LC differences but reduced late effects. Fewer side effects specifically in younger patients. Dose reduction cancelled out time reduction effects, to conventional arm
Polish (CAIR) (Skladowski et al 2000)	1 # / day 32 days	64 Gy	279	82% LC at 3 years [35% LC in control arm]		Reduced to 1.8 Gy per day after 12 months sue to high toxicity for early effects
HYPERFRACTIONATED-ACCELERATED FRACTIONATED TREATMENT:						
GORTEC 94-02 Trial (Bourhis et al 2006)	32 # 22 to 23 days 2 # / day	64 Gy 1.8-2.0 Gy / #	268	58% LC at 2 years [34% LC in control arm]		Improved LC with no increase in late effects. Marginal improvement in overall survival. 25% benefit at 2 years 24% benefit at 5 years
Egypt: Influence of cell proliferation (Awwad et al 1992)	30 # 3 # / day 4 hr interval minimum 11 days [C.T.: 6 days / week, 25 #]	42 Gy 1.4 Gy / # [conventional: 50 Gy, 2 Gy / #]	56	46% survival at 3 years (all post-surgery patients)	Improved survival reported compared to control arm for fast growing tumours: LI >10.4% or T_{pot} < 4.5 days. Mean LI=8.1+-5.2% for oral sites.	Similar survival in slow growing tumours and increased/earlier severe acute reactions Late complication rate 20% lower in accelerated arm at 3 years. LI linked to outcome. No change in survival for Tpot > 4.5 days.

Trial Dates	Fractionation Schedule	Dose Regimen	No. Patients	Local Control	Parameter Stratification	Comments
SPLIT-COUSE ACCELERATED FRACTIONATED TREATMENT (SCARF):						
EORTC 22851 Phase I/II (Begg et al 1990)	45 # 5 weeks 3 # / day	72 Gy 1.6 Gy / #	30	56% to 75% LC at 1 year [33% to 73% in control arm]	56% LC for fast tumours with T_{pot}<4.6 days. 75% LC for slow tumours with T_{pot}>4.6 days. [In control arm: 33% LC for fast tumours with T_{pot}<4.6 days and 73% LC for slow tumours with T_{pot}>4.6 days].	47 patients underwent successful cell kinetic investigation. Ts, LI and Tpot distributions: 10.7+-4.7hrs, 11.7+-5.5%, 4.5+-2.5 days. Results from 1999 report of outcomes for most patients receiving conventionally fractionated treatment (476 in total): 35% LC with Tpot not associated with LC, however shorter Ts (synthesis phase) was linked to better survival, and a high LI was linked worse LC.
EORTC phase III 22851 (Horiot et al 1997)	3 # / day with a 2 week break 45 # 5 weeks	72 Gy 1.6 Gy / # 1. up to 28.8 Gy in 18 #s 2. 43.2 Gy with 2 # / day	340	59% LC at 5 years 4 years for high T and N:55% for high T and N: 63% [in control arm: 46% LC at 5 years and for high T and N stage: 37% LC at 4 years for low T and N stage: 58% at 4 years]		Increase LC and increased late effects. Most increase in LC % for patients with the high stage disease. Only T stage and site were significant factors influencing LC. PTV reduced once or twice after 50 Gy.

Trial Dates	Fractionation Schedule	Dose Regimen	No. Patients	Local Control	Parameter Stratification	Comments
ACCELERATED TREATMENT (2 Gy per fraction):						
DAHANCA 7 (Overgaard *et al* 2000)	1 # / day 6 # / week	66-68 Gy 2 Gy / #	1485	76% LC at 5 years [in control arm: 64% LC]	Significant higher incidence of severe mucositis (earlier and longer), but no difference in late effects.	Increased LC and enhanced acute effects, but no increase in late effects. 6 # / week now the standard in Denmark.
Polish Phase III Moderately Accelerated Trial (Hliniak et al 2002)	6 # / 5 days 38 days in total (1 week less than CT)	66 Gy 2 Gy per # 38 days (1 week less than CT)	395	CF and AF showed no difference in terms of loco-regional control (3% to 5% improvement only)		Increased LC and enhanced acute effects, but no increase in late effects. Similar 4 month skin toxicity in both arms.
CAIR (Skladowski *et al* 2000)	1 # / day 7 # / wk	66 to 70 Gy 2 Gy / # (reduced to 1.8 Gy / # after 12 month observations)	100	82% LC at 3 years [in control arm: 37% LC]		Increased severe acute reactions and serious late normal tissue complications (which lead to reduction in dose per fraction)

Trial Dates	Fractionation Schedule	Dose Regimen	No. Patients	Local Control	Parameter Stratification	Comments
CONCOMMITENT BOOST TREATMENT (patient numbers relate to boost arms only):						
RTOG Phase III 9003 (Ang et al 1990, Fu et al 2000)	42 #s (30 fractions and 12 boost fractions) 6 weeks	72 Gy 1.8 Gy / # plus extra 1.5 Gy boost dose for the last 12 #s	24	54.5% LC at 2 years		Increased LC with no increasing in late effects.
MD Anderson, Cancer Centre, (Ang et al 1990)	Boost 1 5 to 6 weeks 1 # / day plus a boost 2 days / week	69 to 72 Gy 1.8 Gy / # for normal # 1.5 Gy / # for boosts	1	Merged LC rates for groups 1 and 2 66% LC at 2 years	Initially 4 hrs between fractions but increased to 6 hrs.	Optimal timing for boost is within the last 2 to 3.5 weeks of the schedule. Boost 3 in this trial has superior LC. LC worse (unexpectedly) if combined with chemotherapy. This effect may have occurred due to earlier induced accelerated repopulation. 79 patients in total.
	Boost 2 5 to 6 weeks 1 # / day plus a boost 5 days / week for first 2.5 weeks	69 to 72 Gy 1.8 Gy / # for normal # 1.5 Gy / # boosts	6			
	Boost 3 1 # / day plus a boost 5 days / week for first 2.5 weeks	69 to 72 Gy 1.8 Gy / # 1.5 Gy / # boosts	10	79% LC at 2 years		
Netherlands (Terhaard et al 2005)	a) 2 # / day and b) 1 # / day then 2 # / day 5 days / wk	a) 70 Gy 2x1.2 Gy / # in wks 1 to 3 2x1.7 Gy / # in weeks 4 to 5 b) 69.5 Gy 2 Gy/# for week 1 and 2 1.8 & 1.5 Gy /# for week 3 and 5	100	a) 59% LC at 3 years b) 78% LC at 3 years	a) Severe/late toxicity = 11 % b) Severe/late toxicity = 16 %	Increased LC in boost arm compared to hyperfractionated accelerated arm, with slight increasing late effects. Accelerated Repopulation onset may be 4 to 6 days earlier in the HART group (at week 2 to 3). Due to Accelerated Repopulation a boost in week 3 is more beneficial than in week 4. Second daily fraction was delivered to a boost volume only.

Appendix B:

i) ***<u>Moderately hypoxic tumour</u> conventional radiotherapy simulation cell kill results, in terms of the number of 2 Gy fractions required to achieve total "basal" (stem, transit and level 1 differentiating cells) and stem cell only elimination, for various reoxygenation (ROx) and accelerated repopulation (AR) onset times.***

Fraction numbers required in the model to achieve tumour control *(averaged over 9 random seed variations)*					
<u>Variations of ROx onset times</u> (weeks: 0 to 3)	**Variations of onset times of AR (weeks: 0 to 3) and the *AR boost factor* *(x3 to x15)***	**#'s to kill all "basal" cells**	**St. Dev. error**	**#'s to kill all stem cells**	**St. Dev. error**
No ROx	0weeks x3	38.2	3.1	35.8	2.7
	0weeks x5	41.3	3.2	38.0	2.9
	0weeks x7	45.4	3.8	42.8	3.9
	0weeks x10	53.8	4.6	51.3	4.3
	0weeks x15	74.1	5.7	71.0	5.0
	1weeks x3	37.4	2.8	35.3	1.9
	1weeks x5	39.9	2.6	37.1	3.2
	1weeks x7	44.9	3.3	43.0	3.3
	1weeks x10	43.4	3.4	41.2	4.2
	1weeks x15	70.6	7.0	69.0	6.4
	2weeks x3	36.9	3.4	34.2	4.2
	2weeks x5	37.6	1.9	34.3	1.9
	2weeks x7	41.7	2.2	38.3	1.8
	2weeks x10	48.8	4.1	46.7	5.0
	2weeks x15	57.3	5.2	54.6	5.4
	3weeks x3	36.2	4.8	34.0	4.6
	3weeks x5	36.6	2.8	33.1	3.1
	3weeks x7	40.1	1.7	37.3	1.8
	3weeks x10	40.7	1.6	38.8	1.5
	3weeks x15	53.8	7.5	50.7	7.9
	No AR	36.2	3.8	30.7	2.3

Appendix B: Table i) Continued:

Variation s of ROx onset times (weeks: 0 to 3)	**Variations of onset times of AR (weeks: 0 to 3) and the *AR boost factor (x3 to x15)***	**#'s to kill all "basal" cells**	**St. Dev. error**	**#'s to kill all stem cells**	**St. Dev. error**
ROx at 0 weeks	0weeks x3	32.2	1.6	29.8	2.3
	0weeks x5	35.6	2.1	33.0	3.2
	0weeks x7	39.8	1.3	37.4	1.0
	0weeks x10	44.7	2.7	42.6	3.4
	0weeks x15	63.9	6.0	62.6	6.3
	1weeks x3	32.0	2.7	30.4	3.1
	1weeks x5	35.2	1.2	32.2	1.4
	1weeks x7	36.8	2.5	34.8	2.4
	1weeks x10	43.9	2.8	42.2	3.7
	1weeks x15	55.7	3.9	54.2	4.0
	2weeks x3	33.1	2.6	31.0	2.4
	2weeks x5	34.9	2.6	32.4	2.8
	2weeks x7	35.8	2.0	33.4	1.9
	2weeks x10	41.1	4.8	39.3	4.9
	2weeks x15	49.7	4.2	47.8	2.9
	3weeks x3	31.9	1.7	29.6	1.2
	3weeks x5	33.7	3.0	30.9	3.9
	3weeks x7	35.2	2.4	33.2	2.4
	3weeks x10	39.1	6.6	36.8	5.4
	3weeks x15	45.4	3.7	43.2	4.4
	No AR	57.1	4.2	55.2	3.7
ROx at 1 weeks	0weeks x10	44.4	1.9	42.7	2.2
	1weeks x10	43.4	3.4	41.2	3.9
	2weeks x10	39.0	2.3	36.7	2.7
	3weeks x10	36.8	2.4	35.0	2.7
	No AR	32.0	2.7	29.2	1.9

Appendix B: Table i) Continued:

Variations of ROx onset times (weeks: 0 to 3)	**Variations of onset times of AR (weeks: 0 to 3) and the *AR boost factor (x3 to x15)***	**#'s to kill all "basal" cells**	**St. Dev. error**	**#'s to kill all stem cells**	**St. Dev. error**
ROx at 2 weeks	0weeks x3	33.0	1.7	30.7	1.8
	0weeks x5	37.9	3.1	36.2	3.1
	0weeks x7	42.0	3.2	40.0	3.5
	0weeks x10	48.9	3.6	45.8	3.5
	0weeks x15	66.0	6.4	65.1	7.0
	1weeks x3	34.7	2.6	31.6	2.5
	1weeks x5	37.1	2.8	34.7	2.7
	1weeks x7	40.8	3.8	38.1	3.0
	1weeks x10	45.9	3.9	44.2	4.0
	1weeks x15	55.7	3.0	53.4	2.6
	2weeks x3	33.1	2.2	30.4	1.9
	2weeks x5	35.4	3.2	33.0	1.9
	2weeks x7	36.4	2.6	34.7	2.3
	2weeks x10	41.1	2.2	39.0	3.4
	2weeks x15	54.7	5.1	54.1	5.2
	3weeks x3	32.7	2.0	30.0	2.6
	3weeks x5	34.2	3.5	33.0	3.9
	3weeks x7	36.1	3.1	33.9	2.6
	3weeks x10	37.3	2.4	36.0	2.9
	3weeks x15	46.9	4.8	45.8	4.7
	No AR	32.2	2.1	30.2	1.2
ROx at 3 weeks	0weeks x10	49.0	4.1	45.8	4.2
	1weeks x10	44.3	2.4	42.1	2.2
	2weeks x10	44.6	4.9	41.9	4.5
	3weeks x10	39.6	3.3	37.3	3.2
	No AR	33.1	2.4	31.6	2.4

Appendix B:

ii) *<u>Oxic tumour</u> Conventional Schedule simulation total cell kill results in terms of the number of 2 Gy fractions required to achieve total "basal" (stem, transit and level 1 differentiating cell) and stem cell only elimination, for accelerated repopulation (AR) onset times, and alpha beta ratios.*

Fraction numbers required in the model to achieve tumour control *(averaged over 9 random seed variations)*				
Variations of onset times of AR (weeks: 0 to 3) and the *AR boost factor* *(x3 to x15)*	**#'s to kill all "basal" cells**	**St. Dev. error**	**#'s to kill all stem cells**	**St. Dev. error**
No AR	30.0	1.2	27.4	1.7
0weeks x3	32.1	2.6	30.0	0.0
0weeks x5	34.8	2.7	33.1	3.0
0weeks x7	36.9	1.6	35.1	0.0
0weeks x10	44.8	4.4	42.7	4.9
0weeks x15	59.0	3.7	57.3	3.3
1weeks x3	33.0	1.4	30.3	0.0
1weeks x5	35.8	2.9	33.4	3.2
1weeks x7	35.8	1.8	33.1	0.0
1weeks x10	41.1	4.2	38.4	4.7
1weeks x15	54.1	6.8	52.8	6.8
2weeks x3	29.9	1.5	27.4	0.0
2weeks x5	33.6	2.5	30.9	2.5
2weeks x7	33.9	2.8	31.8	0.0
2weeks x10	36.9	3.2	35.2	3.4
2weeks x15	50.6	4.6	48.9	5.1
3weeks x3	29.9	1.9	28.0	0.0
3weeks x5	31.7	2.1	29.7	2.3
3weeks x7	33.1	2.4	31.4	0.0
3weeks x10	34.3	2.0	32.6	2.3
3weeks x15	37.2	4.8	35.1	4.5
No AR, alpha/beta = 3.0	23.0	2.1	20.6	1.2
No AR, alpha/beta = 5.0	27.7	1.7	24.7	1.6
No AR, alpha/beta = 10.0 (default)	30.0	1.2	27.4	1.7
No AR, alpha/beta = 20.0	32.0	2.3	29.2	1.8

Appendix C:

i) *Moderately Hypoxic tumour simulation cell kill results for the total elimination of all stem, transit and level 1 differentiating cells, for various onset times of accelerated repopulation (AR) and reoxygenation (ROx). Schedule numbers can be referred to in Tables 6.1 and 7.1 of this report.*

	Onset time variations of AR and ROx	Clinical Trial Schedules 1 to 11:											New Schedules 12 to 15:			
Fraction numbers	**Sch #**	**1**	**2**	**3**	**4**	**5**	**6**	**7**	**8**	**9**	**10**	**11**	**12**	**13**	**14**	**15**
	no AR, no ROx	34.3	58.6	61.7	37.0	34.8	38.8	48.2	40.0	45.2	36.2	55.4	39.8	60.0	49.7	56.0
	AR (0 weeks)	53.8	78.3	86.4	49.7	48.4	45.8	51.2	55.7	53.8	45.0	86.3	56.0	62.3	64.3	74.0
	AR (2 weeks)	48.8	67.3	79.3	45.0	42.9	41.6	48.2	49.4	45.2	41.4	76.3	49.4	54.7	66.0	72.3
	ROx (0 weeks)	30.4	52.7	58.1	31.2	30.9	34.2	41.6	35.7	37.7	30.3	52.3	34.8	52.7	42.3	52.7
	ROx (2 weeks)	32.8	57.2	58.4	34.2	33.2	38.2	47.3	38.3	41.0	33.9	55.6	38.2	56.3	47.7	58.7
	ROx (0 wks)+AR(0 wks)	44.0	68.6	83.9	41.2	42.1	41.9	42.8	48.1	50.1	39.7	85.2	49.4	55.3	58.0	74.0
	ROx (2 wks)+AR(0 wks)	47.1	71.7	81.4	43.0	42.9	45.0	53.2	50.0	50.9	40.8	82.3	52.1	66.0	58.3	69.7
	ROx (0 wks)+AR(2 wks)	38.2	62.1	66.0	37.2	36.8	34.8	41.6	44.4	37.7	35.3	71.1	41.0	52.7	47.7	58.7
	ROx (2 wks)+AR(2 wks)	42.4	61.3	74.8	38.2	38.9	38.9	47.4	45.0	41.0	37.8	74.6	45.4	55.3	55.3	66.7
	(dose per fraction)	**2.0**	**1.2**	**1.1**	**2.0**	**2.0**	**1.8**	**1.5**	**1.8**	**1.6**	**2.0**	**1.2**	**1.8**	**1.2**	**1.5**	**1.2**
	Average	**41.3**	**64.2**	**72.2**	**39.6**	**39.0**	**39.9**	**46.8**	**45.2**	**44.7**	**37.8**	**71.0**	**45.1**	**57.3**	**54.4**	**64.7**
Total Physical Doses (Gy)	**Sch #**	**1**	**2**	**3**	**4**	**5**	**6**	**7**	**8**	**9**	**10**	**11**	**12**	**13**	**14**	**15**
	no AR, no ROx	68.7	70.3	67.8	74.0	69.6	69.8	72.3	68.7	72.4	72.4	66.5	68.6	72.0	74.5	67.2
	AR (0 weeks)	107.6	94.0	95.1	99.3	96.9	82.4	76.8	96.2	86.0	90.0	103.6	97.8	74.8	96.5	88.8
	AR (2 weeks)	97.6	80.8	87.3	90.0	85.8	74.8	72.3	85.9	72.4	82.9	91.6	86.0	65.6	99.0	86.8
	ROx (0 weeks)	60.9	63.2	63.9	62.4	61.8	61.6	62.3	63.2	60.3	60.7	62.8	59.6	63.2	63.5	63.2
	ROx (2 weeks)	65.6	68.7	64.3	68.4	66.4	68.8	71.0	67.6	65.6	67.8	66.7	65.8	67.6	71.5	70.4
	ROx (0 wks)+AR(0 wks)	88.0	82.3	92.3	82.4	84.2	75.4	64.2	83.7	80.2	79.3	102.3	86.0	66.4	87.0	88.8
	ROx (2 wks)+AR(0 wks)	94.2	86.0	89.6	86.0	85.8	81.0	79.8	86.9	81.4	81.6	98.8	90.8	79.2	87.5	83.6
	ROx (0 wks)+AR(2 wks)	76.4	74.5	72.6	74.4	73.6	62.6	62.3	77.7	60.3	70.7	85.3	70.8	63.2	71.5	70.4
	ROx (2 wks)+AR(2 wks)	84.9	73.6	82.3	76.4	77.8	70.0	71.2	78.6	65.6	75.6	89.5	78.8	66.4	83.0	80.0
	Average	**82.6**	**77.0**	**79.5**	**79.3**	**78.0**	**71.8**	**70.3**	**78.7**	**71.6**	**75.7**	**85.2**	**78.2**	**68.7**	**81.6**	**77.7**
	Clinical Trial Dose (Gy)	**70.0**	**81.6**	**70.4**	**66.0**	**66.0**	**63.0**	**54.0**	**72.0**	**72.0**	**64.0**	**81.6**				
Total treatment times (weeks)	**Sch #**	**1**	**2**	**3**	**4**	**5**	**6**	**7**	**8**	**9**	**10**	**11**	**12**	**13**	**14**	**15**
	no AR, no ROx	6.9	5.9	6.2	3.1	5.8	3.9	2.3	5.8	3.0	5.2	7.5	6.0	2.9	5.0	4.7
	AR (0 weeks)	10.8	7.8	8.6	4.1	8.1	4.6	2.4	7.5	3.6	6.4	10.6	9.2	3.0	6.4	6.2
	AR (2 weeks)	9.8	6.7	7.9	3.8	7.1	4.2	2.3	6.8	3.0	5.9	9.6	7.9	2.6	6.6	6.0
	ROx (0 weeks)	6.1	5.3	5.8	2.6	5.1	3.4	2.0	5.5	2.5	4.3	7.2	5.0	2.5	4.2	4.4
	ROx (2 weeks)	6.6	5.7	5.8	2.9	5.5	3.8	2.3	5.7	2.7	4.8	7.6	5.6	2.7	4.8	4.9

Appendix C: Table i) Continued:	ROx (0 wks)+AR(0 wks)	8.8	6.9	8.4	3.4	7.0	4.2	2.0	6.7	3.3	5.7	10.5	7.9	2.6	5.8	6.2
	ROx (2 wks)+AR(0 wks)	9.4	7.2	8.1	3.6	7.1	4.5	2.5	6.9	3.4	5.8	10.2	8.4	3.1	5.8	5.8
	ROx (0 wks)+AR(2 wks)	7.6	6.2	6.6	3.1	6.1	3.5	2.0	6.3	2.5	5.0	9.1	6.2	2.5	4.8	4.9
	ROx (2 wks)+AR(2 wks)	8.5	6.1	7.5	3.2	6.5	3.9	2.3	6.4	2.7	5.4	9.5	7.1	2.6	5.5	5.6
	Average	**8.3**	**6.4**	**7.2**	**3.3**	**6.5**	**4.0**	**2.2**	**6.4**	**3.0**	**5.4**	**9.1**	**7.0**	**2.7**	**5.4**	**5.4**
BED: acute normal tissue effects	**Sch #**	**1**	**2**	**3**	**4**	**5**	**6**	**7**	**8**	**9**	**10**	**11**	**12**	**13**	**14**	**15**
BED equation parameters:	no AR, no ROx	49.9	51.8	46.6	77.2	56.9	66.4	76.0	53.9	72.8	63.8	38.2	53.0	70.3	63.7	54.9
$\alpha/\beta = 10.0$	AR (0 weeks)	75.0	67.4	63.2	101.8	77.0	77.4	80.4	77.0	85.5	77.9	62.6	69.4	72.9	80.8	70.8
	AR (2 weeks)	68.5	58.7	58.4	92.8	68.8	70.8	76.0	68.5	72.8	72.2	54.7	62.8	64.6	82.8	69.3
$T_{pot} = 2.5$	ROx (0 weeks)	44.8	47.1	44.3	66.1	51.1	59.3	66.3	49.6	61.5	54.3	35.8	47.9	62.4	55.1	52.0
	ROx (2 weeks)	47.9	50.7	44.5	71.9	54.6	65.5	74.7	53.3	66.5	60.0	38.3	51.4	66.4	61.3	57.3
$T_k = 7.0$ days	ROx (0 wks)+AR(0 wks)	62.3	59.7	61.5	85.4	67.7	71.3	68.0	66.6	80.0	69.3	61.7	62.8	65.3	73.4	70.8
	ROx (2 wks)+AR(0 wks)	66.4	62.1	59.8	88.9	68.8	76.2	83.3	69.2	81.2	71.1	59.5	65.5	76.8	73.8	67.0
$\alpha = 0.4$ Gy^{-1}	ROx (0 wks)+AR(2 wks)	54.9	54.6	49.5	77.7	59.8	60.1	66.3	61.6	61.5	62.4	50.6	54.2	62.4	61.3	57.3
	ROx (2 wks)+AR(2 wks)	60.3	54.0	55.4	79.6	62.9	66.6	74.9	62.4	66.5	66.3	53.3	58.7	65.3	70.3	64.3
	Average	**58.9**	**56.2**	**53.7**	**82.4**	**63.1**	**68.2**	**74.0**	**62.5**	**72.0**	**66.4**	**50.5**	**58.4**	**67.4**	**69.2**	**62.6**
BED: late normal tissue effects	**Sch #**	**1**	**2**	**3**	**4**	**5**	**6**	**7**	**8**	**9**	**10**	**11**	**12**	**13**	**14**	**15**
BED equation parameters:	no AR, no ROx	114.4	98.4	92.7	123.3	115.9	111.7	108.5	108.0	110.9	120.7	93.1	106.8	100.8	111.8	94.1
$\alpha/\beta = 3.0$	AR (0 weeks)	179.3	131.6	130.0	165.6	161.5	131.8	115.3	151.6	131.9	150.0	145.0	153.5	104.7	144.8	124.3
	AR (2 weeks)	162.6	113.1	119.3	150.0	143.0	119.7	108.5	135.7	110.9	138.1	128.2	134.6	91.8	148.5	121.5
	ROx (0 weeks)	101.5	88.5	87.4	104.1	103.0	98.6	93.5	100.5	92.4	101.1	87.9	92.4	88.5	95.2	88.5
	ROx (2 weeks)	109.3	96.1	87.9	114.1	110.7	110.1	106.5	107.3	100.6	113.0	93.3	102.3	94.6	107.3	98.6
	ROx (0 wks)+AR(0 wks)	146.7	115.2	126.1	137.4	140.4	120.6	96.2	132.3	122.9	132.2	143.2	134.6	93.0	130.5	124.3
	ROx (2 wks)+AR(0 wks)	157.0	120.4	122.4	143.3	143.0	129.6	119.8	137.1	124.8	135.9	138.3	142.3	110.9	131.3	117.0
	ROx (0 wks)+AR(2 wks)	127.4	104.3	99.2	124.1	122.6	100.2	93.5	122.9	92.4	117.8	119.5	110.3	88.5	107.3	98.6
	ROx (2 wks)+AR(2 wks)	141.5	103.0	112.4	127.4	129.6	112.0	106.8	124.4	100.6	125.9	125.3	123.1	93.0	124.5	112.0
	Average	**137.7**	**107.9**	**108.6**	**132.1**	**130.0**	**114.9**	**105.4**	**124.4**	**109.7**	**126.1**	**119.3**	**122.2**	**96.2**	**122.3**	**108.8**

Appendix C:

ii) Oxic tumour simulation cell kill results for the total elimination of all stem, transit and level 1 differentiating cells, for various onset times of accelerated repopulation (AR). Schedule numbers can be referred to in Tables 6.1 and 7.1 of this report.

	Onset time variations of AR	Clinical Trial Schedules 1 to 11:											New Schedules 12 to 15:			
Fraction number	**Sch #**	**1**	**2**	**3**	**4**	**5**	**6**	**7**	**8**	**9**	**10**	**11**	**12**	**13**	**14**	**15**
	no AR, no ROx	30.0	49.3	56.2	30.7	29.7	33.9	40.5	36.1	38.4	32.2	52.2	36.0	48.2	44.9	51.7
	AR (0 weeks)	42.7	69.9	78.9	40.1	41.7	40.1	43.1	47.2	49.6	41.2	81.7	46.6	61.0	55.4	70.0
	AR (2 weeks)	39.6	62.5	66.9	34.3	34.8	34.1	40.5	42.1	38.4	31.6	74.6	42.1	49.7	46.8	59.1
	(dose per fraction)	**2.0**	**1.2**	**1.1**	**2.0**	**2.0**	**1.8**	**1.5**	**1.8**	**1.6**	**2.0**	**1.2**	**1.8**	**1.2**	**1.5**	**1.2**
	Average	**37.4**	**60.6**	**67.3**	**35.0**	**35.4**	**36.0**	**41.4**	**41.8**	**42.1**	**35.0**	**69.5**	**41.6**	**53.0**	**49.0**	**60.3**
Total Physical Dose (Gy)	**Sch #**	**1**	**2**	**3**	**4**	**5**	**6**	**7**	**8**	**9**	**10**	**11**	**12**	**13**	**14**	**15**
	no AR, no ROx	60.0	59.2	56.2	61.4	59.4	61.0	60.8	61.7	61.5	64.4	62.7	61.8	57.8	62.9	62.0
	AR (0 weeks)	85.4	83.9	78.9	80.2	83.4	72.2	64.6	78.3	79.3	82.4	98.0	80.9	73.2	77.6	84.0
	AR (2 weeks)	79.2	75.0	66.9	80.2	69.6	61.4	60.8	70.7	61.5	63.1	89.5	72.8	59.6	65.5	70.9
	Average	**74.9**	**72.7**	**67.3**	**73.9**	**70.8**	**64.9**	**62.1**	**70.2**	**67.4**	**70.0**	**83.4**	**71.8**	**63.6**	**68.6**	**72.3**
	Clinical Trial Dose (Gy)	**70.0**	**81.6**	**70.4**	**66.0**	**66.0**	**63.0**	**54.0**	**72.0**	**72.0**	**64.0**	**81.6**				
Total treatment time (weeks)	**Sch #**	**1**	**2**	**3**	**4**	**5**	**6**	**7**	**8**	**9**	**10**	**11**	**12**	**13**	**14**	**15**
	no AR, no ROx	6.0	4.9	5.6	5.1	5.0	3.4	1.9	6.1	4.4	4.6	7.2	5.2	2.3	4.5	4.3
	AR (0 weeks)	8.5	7.0	7.9	6.7	7.0	4.0	2.1	7.2	5.1	5.9	10.2	7.3	2.9	5.5	5.8
	AR (2 weeks)	7.9	6.3	6.7	5.7	5.8	3.4	1.9	6.7	4.4	4.5	9.5	6.4	2.4	4.7	4.9
	Average	**7.5**	**6.1**	**6.7**	**5.8**	**5.9**	**3.6**	**2.0**	**6.7**	**4.6**	**5.0**	**8.9**	**6.3**	**2.5**	**4.9**	**5.0**
BED: acute normal tissues	**Sch #**	**1**	**2**	**3**	**4**	**5**	**6**	**7**	**8**	**9**	**10**	**11**	**12**	**13**	**14**	**15**
BED equation parameters:	no AR, no ROx	44.3	44.5	36.8	50.9	49.4	58.7	64.7	44.4	52.7	57.4	35.7	48.4	57.6	52.9	51.1
$\alpha/\beta = 10.0$, $\alpha = 0.4$ Gy^{-1}	AR (0 weeks)	60.6	60.8	49.4	64.7	67.1	68.5	68.5	57.9	69.2	71.8	58.9	58.8	71.4	64.0	67.3
$T_{pot} = 2.5$	AR (2 weeks)	56.7	54.9	42.7	70.0	56.9	59.1	64.7	51.7	52.7	56.3	53.3	54.4	59.2	54.9	57.7
$T_k = 7.0$ days	**Average**	**53.9**	**53.4**	**42.9**	**61.9**	**57.8**	**62.1**	**66.0**	**51.4**	**58.2**	**61.8**	**49.3**	**53.9**	**62.7**	**57.3**	**58.7**
BED: late normal tissue s	**Sch #**	**1**	**2**	**3**	**4**	**5**	**6**	**7**	**8**	**9**	**10**	**11**	**12**	**13**	**14**	**15**
BED equation parameters:	no AR, no ROx	100.0	82.9	76.8	102.4	99.1	97.5	91.2	97.0	94.3	107.4	87.7	94.8	81.0	94.3	86.9
$\alpha/\beta = 3.0$	AR (0 weeks)	142.3	117.5	107.8	133.6	139.1	115.6	96.9	122.0	121.6	137.4	137.2	124.0	102.5	116.3	117.6
	AR (2 weeks)	132.0	105.1	91.4	133.6	116.0	98.3	91.2	110.5	94.3	105.2	125.3	111.6	83.5	98.3	99.3
	Average	**124.8**	**101.8**	**92.0**	**123.2**	**118.0**	**103.8**	**93.1**	**109.8**	**103.4**	**116.7**	**116.7**	**110.1**	**89.0**	**103.0**	**101.2**

Reference List

1. Aarnaes E., Clausen O.P., *et al.* (1993), *Heterogeneity in the mouse epidermal cell cycle analysed by computer simulations*. Cell Prolif **26** 205-19.
2. Aarnaes E., Kirkhus B., *et al.* (1990), *Mathematical model analysis of mouse epidermal cell kinetics measured by bivariate DNA/anti-bromodeoxyuridine flow cytometry and continuous [3H]-thymidine labelling*. Cell Tissue Kinet **23** 409-24.
3. Adam M.F., Gabalski E.C., *et al.* (1999), *Tissue oxygen distribution in head and neck cancer patients*. Head Neck **21** 146-53.
4. Alarcon T., Byrne H.M., *et al.* (2004), *A mathematical model of the effects of hypoxia on the cell-cycle of normal and cancer cells*. J Theor Biol **229** 395-411.
5. Alper T. (1979), *Cellular Radiobiology*. (Cambridge: Cambridge University Press).
6. Alper T. and Howard-Flanders P. (1956), *Role of oxygen in modifying the radiosensitivity of E. coli B*. Nature. **178** 978-9.
7. Amellem O. and Pettersen E.O. (1991), *Cell inactivation and cell cycle inhibition as induced by extreme hypoxia: the possible role of cell cycle arrest as a protection against hypoxia-induced lethal damage*. Cell Prolif **24** 127-41.
8. Anderson A.R. and Chaplain M.A. (2000), *A gradient-driven mathematical model of angiogenesis*. Mathematical and Computer Modelling **32** 1142-52.
9. Anderson H.L. (1986), *Metropolis, Monte Carlo and the MANIAC*. Los Alamos Science **14** 98-108.
10. Antipas V.P., Stamatakos G.S., *et al.* (2004), *A spatio-temporal simulation model of the response of solid tumours to radiotherapy in vivo: parametric validation concerning oxygen enhancement ratio and cell cycle duration*. Phys Med Biol **49** 1485-504.
11. Antognoni P., Bignardi M., *et al.* (1996), *Accelerated radiation therapy for locally advanced squamous cell carcinomas of the oral cavity and oropharynx selected according to tumor cell kinetics--a phase II multicenter study*. Int J Radiat Oncol Biol Phys **36** 1137-45.
12. Appleton D.R., Thomson P.J., *et al.* (2002), *Simulation of cell proliferation in mouse oral epithelium, and the action of epidermal growth factor: evidence for a high degree of synchronization of the stem cells*. Cell Prolif **35 Suppl 1** 68-77.
13. Armpilia C.I., Dale R.G., *et al.* (2004), *Determination of the optimum dose per fraction in fractionated radiotherapy when there is delayed onset of tumour repopulation during treatment*. Br J Radiol **77** 765-7.
14. Axelson H., Fredlund E., *et al.* (2005), *Hypoxia-induced dedifferentiation of tumor cells--a mechanism behind heterogeneity and aggressiveness of solid tumors*. Semin Cell Dev Biol. **16** 554-63. Epub 2005 Apr 26.
15. Azuma Y., Chou S., *et al.* (2003), *Hypoxia and differentiation in squamous cell carcinomas of the uterine cervix: pimonidazole and involucrin*. Clin Cancer Res. **9** 4944-52.
16. Barendsen G.W. (1968), *Responses of cultured cells, tumours, and normal tissue to radiations of different linear energy transfer*. Curr Top Radiat Res Q **4** 293-356.
17. Baudelet C., Gallez, B. (2004), *Effect of anesthesia on the signal intensity in tumors using BOLD-MRI: comparison with flow measurements by Laser Doppler flowmetry and oxygen measurements by luminescence-based probes*. Magn Reson Imaging. **22** 905-12.
18. Becker A., Hansgen G., *et al.* (1998), *Oxygenation of squamous cell carcinoma of the head and neck: comparison of primary tumors, neck node metastases, and normal tissue*. Int J Radiat Oncol Biol Phys **42** 35-41.
19. Becker A., P S., *et al.* (2000), *Severe anemia is associated with poor tumor oxygenation in head and neck squamous cell carcinomas*. Int J Radiat Oncol Biol Phys. **46** 459-66.

20. Begg A.C., Haustermans K., *et al.* (1999), *The value of pretreatment cell kinetic parameters as predictors for radiotherapy outcome in head and neck cancer: a multicenter analysis*. Radiother Oncol **50** 13-23.
21. Begg A.C., Hofland I., *et al.* (1991), *Tumour cell repopulation during fractionated radiotherapy: correlation between flow cytometric and radiobiological data in three murine tumours*. Eur J Cancer **27** 537-43.
22. Begg A.C., Hofland I., *et al.* (1990), *The predictive value of cell kinetic measurements in a European trial of accelerated fractionation in advanced head and neck tumors: an interim report*. Int J Radiat Oncol Biol Phys **19** 1449-53.
23. Bentzen S.M. (1993), *Quantitative clinical radiobiology*. Acta Oncol **32** 259-75.
24. Bindra R.S., Schaffer P.J., *et al.* (2004), *Down-regulation of Rad51 and decreased homologous recombination in hypoxic cancer cells*. Mol Cell Biol **24** 8504-18.
25. Bjork-Eriksson T., West C., *et al.* (2000), *Tumor radiosensitivity (SF2) is a prognostic factor for local control in head and neck cancers*. Int J Radiat Oncol Biol Phys **46** 13-9.
26. Borkenstein K., Levegrun S., *et al.* (2004), *Modeling and computer simulations of tumor growth and tumor response to radiotherapy*. Radiat Res **162** 71-83.
27. Bourhis J., Lapeyre M., *et al.* (2006), *Phase III randomized trial of very accelerated radiation therapy compared with conventional radiation therapy in squamous cell head and neck cancer: a GORTEC trial*. J Clin Oncol **24** 2873-8.
28. Brenner D.J. (1993), *Accelerated repopulation during radiotherapy: Quantitative evidence for delayed onset*. Radiation Oncology Investigations **1** 167-72.
29. Brizel D.M., Dodge R.K., *et al.* (1999), *Oxygenation of head and neck cancer: changes during radiotherapy and impact on treatment outcome*. Radiother Oncol **53** 113-7.
30. Brown J.M. (1979), *Evidence for acutely hypoxic cells in mouse tumours, and a possible mechanism of reoxygenation*. Br J Radiol. **52** 650-6.
31. Brown J.M. (1990), *Tumor hypoxia, drug resistance, and metastases*. J Natl Cancer Inst. **82** 338-9.
32. Brown J.M. (1999), *The hypoxic cell: a target for selective cancer therapy--eighteenth Bruce F. Cain Memorial Award lecture*. Cancer Res **59** 5863-70.
33. Brurberg K.G., Skogmo H.K., *et al.* (2005), *Fluctuations in pO2 in poorly and well-oxygenated spontaneous canine tumors before and during fractionated radiation therapy*. Radiother Oncol **77** 220-6. Epub 2005 Oct 27.
34. Chaplain M.A. and Anderson A.R. (1996), *Mathematical modelling, simulation and prediction of tumour-induced angiogenesis*. Invasion Metastasis **16** 222-34.
35. Chin C.W., Foss A.J., *et al.* (2003), *Differences in the vascular patterns of basal and squamous cell skin carcinomas explain their differences in clinical behaviour*. J Pathol **200** 308-13.
36. Chou S.C., Azuma Y., *et al.* (2004), *Evidence that involucrin, a marker for differentiation, is oxygen regulated in human squamous cell carcinomas*. Br J Cancer. **90** 728-35.
37. Clausen O.P., Thorud E., *et al.* (1981), *Evidence of rapid and slow progression of cells through G2 phase in mouse epidermis: a comparison between phase durations measured by different methods*. Cell Tissue Kinet **14** 227-40.
38. Collingridge D.R., Young W.K., *et al.* (1997), *Measurement of tumor oxygenation: a comparison between polarographic needle electrodes and a time-resolved luminescence-based optical sensor*. Radiat Res **147** 329-34.
39. Conti C.J. (2002), *Vascular endothelial growth factor: regulation in the mouse skin carcinogenesis model and use in antiangiogenesis cancer therapy*. Oncologist **7 Suppl 3** 4-11.
40. Corry J. and Rischin D. (2004), *Strategies to overcome accelerated repopulation and hypoxia--what have we learned from clinical trials?* Semin Oncol **31** 802-8.

41. Dale R.G. and Jones B. (2007), *Radiobioloigcal Modelling in Radiation Oncology*. (London, UK: The British Intistitue of Radiology).
42. Dasu A. and Denekamp J. (1998), *New insights into factors influencing the clinically relevant oxygen enhancement ratio*. Radiother Oncol. **46** 269-77.
43. Dasu A. and Denekamp J. (1999), *Superfractionation as a potential hypoxic cell radiosensitizer: prediction of an optimum dose per fraction*. Int J Radiat Oncol Biol Phys **43** 1083-94.
44. Dasu A., Toma-Dasu I., *et al.* (2003), *Theoretical simulation of tumour oxygenation and results from acute and chronic hypoxia*. Phys Med Biol **48** 2829-42.
45. Dasu A., Toma-Dasu I., *et al.* (2005), *The effects of hypoxia on the theoretical modelling of tumour control probability*. Acta Oncol **44** 563-71.
46. Denekamp J. and Dasu A. (1999), *Inducible repair and the two forms of tumour hypoxia--time for a paradigm shift*. Acta Oncol **38** 903-18.
47. Denekamp J., Dasu A., *et al.* (1998), *Hyperfractionation as an effective way of overcoming radioresistance*. Int J Radiat Oncol Biol Phys **42** 705-9.
48. Dinshaw K.A., Agarwal J.P., *et al.* (2006), *Radical radiotherapy in head and neck squamous cell carcinoma: an analysis of prognostic and therapeutic factors*. Clin Oncol (R Coll Radiol) **18** 383-9.
49. Dionysiou D. and Stamatakos G. (2007), *Applying a 4D multiscale in vivo tumor growth model to the exploration of radiotherapy scheduling: The effects of weekend treatment gaps and p53 gene status on the response of fast growing solid tumors*. Cancer Inform. **2** 113-21.
50. Dionysiou D.D., Stamatakos G.S., *et al.* (2008), *Critical parameters determining standard radiotherapy treatment outcome for glioblastoma multiforme: a computer simulation*. Open Biomed Eng J. **2** 43-51.
51. Dionysiou D.D., Stamatakos G.S., *et al.* (2006), *A computer simulation of in vivo tumour growth and response to radiotherapy: new algorithms and parametric results*. Comput Biol Med **36** 448-64.
52. Dionysiou D.D., Stamatakos G.S., *et al.* (2004), *A four-dimensional simulation model of tumour response to radiotherapy in vivo: parametric validation considering radiosensitivity, genetic profile and fractionation*. J Theor Biol **230** 1-20.
53. Dische S., Saunders M., *et al.* (1997), *A randomised multicentre trial of CHART versus conventional radiotherapy in head and neck cancer*. Radiother Oncol **44** 123-36.
54. Dobbs J., Barrett A., *et al.* (1999), *Practical radiotherapy planning*. (London: Arnold ; New York : Oxford University Press).
55. Donaghey C.E. (1980), *CELLSIM: cell cycle simulation made easy*. Int Rev Cytol **66** 171-210.
56. Donaghey C.E. (1983), *CELLSIM and CELLGROW: tools for cell kinetic modeling*. ISA Trans **22** 21-4.
57. Dorr W. (1997), *Three A's of repopulation during fractionated irradiation of squamous epithelia: Asymmetry loss, Acceleration of stem-cell divisions and Abortive divisions*. Int J Radiat Biol **72** 635-43.
58. Douglas R.M., Farahani R., *et al.* (2005), *Hypoxia induces major effects on cell cycle kinetics and protein expression in Drosophila melanogaster embryos*. Am J Physiol Regul Integr Comp Physiol **288** R511-21. Epub 2004 Oct 21.
59. Duchting W., Ginsberg T., *et al.* (1995), *Modeling of radiogenic responses induced by fractionated irradiation in malignant and normal tissue*. Stem Cells **13** 301-6.
60. Duchting W., Ulmer W., *et al.* (1992), *Computer simulation and modelling of tumor spheroid growth and their relevance for optimization of fractionated radiotherapy*. Strahlenther Onkol **168** 354-60.

61. Duchting W. and Vogelsaenger T. (1981), *Three-dimensional pattern generation applied to spheroidal tumor growth in a nutrient medium*. Int J Biomed Comput **12** 377-92.
62. Duchting W. and Vogelsaenger T. (1985), *Recent progress in modelling and simulation of three-dimensional tumor growth and treatment*. Biosystems **18** 79-91.
63. Dunst J., Stadler P., *et al.* (2003), *Tumor volume and tumor hypoxia in head and neck cancers. The amount of the hypoxic volume is important*. Strahlenther Onkol **179** 521-6.
64. Durand R.E. and Sham E. (1998), *The lifetime of hypoxic human tumor cells*. Int J Radiat Oncol Biol Phys **42** 711-5.
65. Elkind M.M., Swain R.W., *et al.* (1965), *Oxygen, nitrogen,recovery and radiation therapy* In: University of Texas, M.D. Anderson Hospital and Tumor Institute of Cellular Radiation Biology: A symposium considering radiation effects in the cell and possible implications for cancer therapy, a collection of papers 442– 61.
66. Eschwege F., Bourhis J., *et al.* (1997), *Predictive assays of radiation response in patients with head and neck squamous cell carcinoma: a review of the Institute Gustave Roussy experience*. Int J Radiat Oncol Biol Phys **39** 849-53.
67. Forsythe J.A., Jiang B.H., *et al.* (1996), *Activation of vascular endothelial growth factor gene transcription by hypoxia-inducible factor 1*. Mol Cell Biol. **16** 4604-13.
68. Fowler J. (2010), *21 years of biologically effective dose*. Br J Radiol. **83** 554-68.
69. Fowler J.F. (1989), *The linear-quadratic formula and progress in fractionated radiotherapy*. Br J Radiol **62** 679-94.
70. Fowler J.F. (1991), *Rapid repopulation in radiotherapy: a debate on mechanism. The phantom of tumor treatment--continually rapid proliferation unmasked*. Radiother Oncol **22** 156-8.
71. Fowler J.F. (2007), *Is there an optimum overall time for head and neck radiotherapy? A review, with new modelling*. Clin Oncol (R Coll Radiol) **19** 8-22.
72. Fowler J.F. and Harari P.M. (2000), *Confirmation of improved local-regional control with altered fractionation in head and neck cancer*. Int J Radiat Oncol Biol Phys. **48** 3-6.
73. Fowler J.F., Harari P.M., *et al.* (2003), *Acute radiation reactions in oral and pharyngeal mucosa: tolerable levels in altered fractionation schedules*. Radiother Oncol **69** 161-8.
74. Fowler J.F., Welsh J.S., *et al.* (2004), *Loss of biological effect in prolonged fraction delivery*. Int J Radiat Oncol Biol Phys **59** 242-9.
75. Fu K.K., Pajak T.F., *et al.* (2000), *A Radiation Therapy Oncology Group (RTOG) phase III randomized study to compare hyperfractionation and two variants of accelerated fractionation to standard fractionation radiotherapy for head and neck squamous cell carcinomas: first report of RTOG 9003*. Int J Radiat Oncol Biol Phys **48** 7-16.
76. Gardner L.B., Li Q., *et al.* (2001), *Hypoxia inhibits G1/S transition through regulation of p27 expression*. J Biol Chem **276** 7919-26. Epub 2000 Dec 8.
77. Gatenby R.A., Kessler H.B., *et al.* (1988), *Oxygen distribution in squamous cell carcinoma metastases and its relationship to outcome of radiation therapy*. Int J Radiat Oncol Biol Phys **14** 831-8.
78. Gray L.H., Conger A.D., *et al.* (1953), *The concentration of oxygen dissolved in tissues at the time of irradiation as a factor in radiotherapy*. Br J Radiol **26** 638-48.
79. Hall E.J. and Garcia A.G. (2006), *Radiobiology for the Radiologist.* Lippincott Williams and Wilkins, PA, USA).
80. Harriss W., Bezak E., *et al.* (2010), *Measurement of reoxygenation during fractionated radiotherapy in head and neck squamous cell carcinoma xenografts*. Australas Phys Eng Sci Med. **33** 251-63. Epub 2010 Sep 28.

81. Harting C., Peschke P., *et al.* (2007), *Single-cell-based computer simulation of the oxygen-dependent tumour response to irradiation*. Phys Med Biol **52** 4775-89. Epub 2007 Jul 24.
82. Henrikson (1997), *NMS Histology*. (USA
83. Hill R.P. (1990), *Tumor progression: potential role of unstable genomic changes*. Cancer Metastasis Rev. **9** 137-47.
84. Hill R.P., Bush R.S., *et al.* (1971), *The effect of anaemia on the fraction of hypoxic cells in an experimental tumour*. Br J Radiol **44** 299-304.
85. Hill S.E. (1928), *A Simple Visual Method for Demonstrating the Diffusion of Oxygen through Rubber and Various Other Substances*. Science. **67** 374-6.
86. Hirst D.G. and Denekamp J. (1979), *Tumour cell proliferation in relation to the vasculature*. Cell Tissue Kinet **12** 31-42.
87. Hliniak A., Gwiazdowska. B, *et al.* (2002), *A multicentre randomized/controlled trial of a conventional versus modestly accelerated radiotherapy in the laryngeal cancer: influence of a 1 week shortening overall time*. Radiother Oncol. **62** 1-10.
88. Horiot J., Begg A., *et al.* (1994), *Present status of EORTC trials of hyperfractionated and accelerated radiotherapy on head and neck carcinoma: Recent Results Cancer Res*. **134** 111-9.
89. Horiot J.C., Bontemps P., *et al.* (1997), *Accelerated fractionation (AF) compared to conventional fractionation (CF) improves loco-regional control in the radiotherapy of advanced head and neck cancers: results of the EORTC 22851 randomized trial*. Radiother Oncol **44** 111-21.
90. Hume W.J. and Thompson J. (1990), *Double labelling of cells with tritiated thymidine and bromodeoxyuridine reveals a circadian rhythm-dependent variation in duration of DNA synthesis and S phase flux rates in rodent oral epithelium*. Cell Tissue Kinet **23** 313-23.
91. ICRP (2007), The 2007 Recommendations of the International Commission on Radiological Protection. ICRP Publication 103. Ann. ICRP 37 (2-4). ed J. Valentin
92. Izquierdo J.N. and Gibbs S.J. (1972), *Circadian rhythms of DNA synthesis and mitotic activity in hamster cheek pouch epithelium*. Exp Cell Res **71** 402-8.
93. Joiner M. and van der Kogel A. (2009), *Basic Clinical Radiobiology* (London, UK: Edward Arnold).
94. Joiner M.C. and Johns H. (1988), *Renal damage in the mouse: the response to very small doses per fraction*. Radiat Res. **114** 385-98.
95. Kaanders J.H., Bussink J., *et al.* (2004), *Clinical studies of hypoxia modification in radiotherapy*. Semin Radiat Oncol **14** 233-40.
96. Kansal A.R., Torquato S., *et al.* (2000a), *Emergence of a subpopulation in a computational model of tumor growth*. J Theor Biol **207** 431-41.
97. Kansal A.R., Torquato S., *et al.* (2000b), *Simulated brain tumor growth dynamics using a three-dimensional cellular automaton*. J Theor Biol **203** 367-82.
98. Kelvin L. (1901), *Nineteenth century clouds over the dynamical theory of heat and light*. Philosophical magazine **6**
99. Kirkpatrick J.P., Cardenas-Navia L.I., *et al.* (2004), *Predicting the effect of temporal variations in PO2 on tumor radiosensitivity*. Int J Radiat Oncol Biol Phys **59** 822-33.
100. Kitakabu Y., Shibamoto Y., *et al.* (1991), *Variations of the hypoxic fraction in the SCC VII tumors after single dose and during fractionated radiation therapy: assessment without anesthesia or physical restraint of mice*. Int J Radiat Oncol Biol Phys **20** 709-14.
101. Kocher M., Treuer H., *et al.* (1997), *Quantification of tumor reoxygenation during accelerated radiation therapy*. Radiology **205** 263-8.

102. Kocher M., Treuer H., *et al.* (2000), *Computer simulation of cytotoxic and vascular effects of radiosurgery in solid and necrotic brain metastases*. Radiother Oncol **54** 149-56.
103. Koh W.J., Bergman KS, *et al.* (1995), *Evaluation of oxygenation status during fractionated radiotherapy in human nonsmall cell lung cancers using [F-18]fluoromisonidazole positron emission tomography*. Int J Radiat Oncol Biol Phys. **33** 391-8.
104. Koritzinsky M., Wouters B.G., *et al.* (2001), *Cell cycle progression and radiation survival following prolonged hypoxia and re-oxygenation*. Int J Radiat Biol **77** 319-28.
105. Koukourakis M.I., Bentzen S.M., *et al.* (2006), *Endogenous markers of two separate hypoxia response pathways (hypoxia inducible factor 2 alpha and carbonic anhydrase 9) are associated with radiotherapy failure in head and neck cancer patients recruited in the CHART randomized trial*. J Clin Oncol **24** 727-35. Epub 2006 Jan 17.
106. Kummermehr J., Dorr W., *et al.* (1992), *Kinetics of accelerated repopulation in normal and malignant squamous epithelia during fractionated radiotherapy*. BJR Suppl **24** 193-9.
107. Lallemant B., Evrard A, *et al.* (2010), *Gene expression profiling in head and neck squamous cell carcinoma: Clinical perspectives*.
108. Lartigau E., Lusinchi A., *et al.* (1998), *Variations in tumour oxygen tension (pO2) during accelerated radiotherapy of head and neck carcinoma*. Eur J Cancer **34** 856-61.
109. Le Q. (2004), *Hypoxic gene expression and metastasis*. Cancer Metastasis Rev. **23** 293-310.
110. Lee D.J., Moini M., *et al.* (1996), *Hypoxic sensitizer and cytotoxin for head and neck cancer*. Ann Acad Med Singapore **25** 397-404.
111. Lehtio K., Eskola O., *et al.* (2004), *Imaging perfusion and hypoxia with PET to predict radiotherapy response in head-and-neck cancer*. Int J Radiat Oncol Biol Phys **59** 971-82.
112. Ljungkvist A.S., Bussink J., *et al.* (2005), *Hypoxic cell turnover in different solid tumor lines*. Int J Radiat Oncol Biol Phys **62** 1157-68.
113. Ljungkvist A.S., Bussink J., *et al.* (2006), *Dynamics of hypoxia, proliferation and apoptosis after irradiation in a murine tumor model*. Radiat Res **165** 326-36.
114. Ljungkvist A.S., Bussink J., *et al.* (2002), *Vascular architecture, hypoxia, and proliferation in first-generation xenografts of human head-and-neck squamous cell carcinomas*. Int J Radiat Oncol Biol Phys **54** 215-28.
115. Maciejewski B., Withers H.R., *et al.* (1989), *Dose fractionation and regeneration in radiotherapy for cancer of the oral cavity and oropharynx: tumor dose-response and repopulation*. Int J Radiat Oncol Biol Phys **16** 831-43.
116. Mantel C., Hendrie P., *et al.* (2001), *Steel factor regulates cell cycle asymmetry*. Stem Cells **19** 483-91.
117. Marcu L., Bezak E., *et al.* (2006a), *Scheduling cisplatin and radiotherapy in the treatment of squamous cell carcinomas of the head and neck: a modelling approach*. Phys Med Biol. **51** 3625-37. Epub 2006 Jul 12.
118. Marcu L., Bezak E., *et al.* (2005), *Tumour resistance to cisplatin: a modelling approach*. Phys Med Biol. **50** 93-102.
119. Marcu L. and Olver I. (2006b), *Tirapazamine: from bench to clinical trials*. Curr Clin Pharmacol. **1** 71-9.
120. Marcu L., van Doorn T., *et al.* (2003), *Cisplatin and radiotherapy in the treatment of locally advanced head and neck cancer--a review of their cooperation*. Acta Oncol **42** 315-25.

121. Marcu L., van Doorn T., *et al.* (2004), *Modelling of post-irradiation accelerated repopulation in squamous cell carcinomas*. Phys Med Biol **49** 3767-79.
122. Marcu L., van Doorn T., *et al.* (2002), *Growth of a virtual tumour using probabilistic methods of cell generation*. Australas Phys Eng Sci Med **25** 155-61.
123. Marsaglia G. and Tsang W.W. (2000), *The Ziggurat method for generating random variables*. Journal of Statistical Software **5** 1 - 7.
124. Maseide K. and Rofstad E.K. (2000), *Mathematical modeling of chronical hypoxia in tumors considering potential doubling time and hypoxic cell lifetime*. Radiother Oncol **54** 171-7.
125. McElwain D.L., Callcott R., *et al.* (1979), *A model of vascular compression in solid tumours*. J Theor Biol **78** 405-15.
126. McElwain D.L. and Pettet G.J. (1993), *Cell migration in multicell spheroids: swimming against the tide*. Bull Math Biol **55** 655-74.
127. Mehanna H., Paleri V., *et al.* (2010), *Head and neck cancer--Part 1: Epidemiology, presentation, and prevention*. BMJ **341** 4684.
128. Nilsson J., Lind B.K., *et al.* (2002), *Radiation response of hypoxic and generally heterogeneous tissues*. Int J Radiat Biol **78** 389-405.
129. Nordsmark M., Bentzen S.M., *et al.* (2005), *Prognostic value of tumor oxygenation in 397 head and neck tumors after primary radiation therapy. An international multi-center study*. Radiother Oncol **77** 18-24.
130. Nordsmark M. and Overgaard J. (2004), *Tumor hypoxia is independent of hemoglobin and prognostic for loco-regional tumor control after primary radiotherapy in advanced head and neck cancer*. Acta Oncol **43** 396-403.
131. Nordsmark M., Overgaard M., *et al.* (1996), *Pretreatment oxygenation predicts radiation response in advanced squamous cell carcinoma of the head and neck*. Radiother Oncol **41** 31-9.
132. Núñez M., Villalobos M., *et al.* (1995), *Radiation-induced DNA double-strand break rejoining in human tumour cells*. Br J Cancer. **71** 311-6.
133. Overgaard J., Alsner J., *et al.* (2000), *Importance of overall treatment time for the response to radiotherapy in patients with squamous cell carcinoma of the head and neck*. Rays. **25** 313-9.
134. Patel A.A., Gawlinski E.T., *et al.* (2001), *A cellular automaton model of early tumor growth and invasion*. J Theor Biol **213** 315-31.
135. Pescarmona G.P., Scalerandi M., *et al.* (1999), *Non-linear model of cancer growth and metastasis: a limiting nutrient as a major determinant of tumor shape and diffusion*. Med Hypotheses **53** 497-503.
136. Peters L.J. and Withers H.R. (1997), *Applying radiobiological principles to combined modality treatment of head and neck cancer--the time factor*. Int J Radiat Oncol Biol Phys **39** 831-6.
137. Petersen C. and Eicheler W., et al (2003), *Proliferation and micromilieu during fractionated irradiation of human FaDu squamous cell carcinoma in nude mice*. Int J Radiat Biol. **79** 469-77.
138. Pinto L.H., Canary P.C., *et al.* (1991), *Prospective randomized trial comparing hyperfractionated versus conventional radiotherapy in stages III and IV oropharyngeal carcinoma*. Int J Radiat Oncol Biol Phys **21** 557-62.
139. Popple R.A., Ove R., *et al.* (2002), *Tumor control probability for selective boosting of hypoxic subvolumes, including the effect of reoxygenation*. Int J Radiat Oncol Biol Phys **54** 921-7.
140. Potten C.S. (1981), *The cell kinetic mechanism for radiation-induced cellular depletion of epithelial tissue based on hierarchical differences in radiosensitivity*. Int J Radiat Biol Relat Stud Phys Chem Med **40** 217-25.

141. Potten C.S. (1986), *Cell cycles in cell hierarchies*. Int J Radiat Biol Relat Stud Phys Chem Med **49** 257-78.
142. Qi A.S., Zheng X., *et al.* (1993), *A cellular automaton model of cancerous growth*. J Theor Biol **161** 1-12.
143. Ramaley J.F. (1969), *Buffon's Noodle Problem*. The American Mathematical Monthly (Mathematical Association of America) **76** 916–8.
144. Reid B., Winn D., *et al.* (2000), *Head and neck in situ carcinoma: incidence, trends, and survival*. Oral Oncol. **36** 414-20.
145. Rijken P.F.J.W., Bernsen H.J.J.A., *et al.* (2000), *Spatial relationship between hypoxia and the (perfused) vascular network in a human glioma xenograft: a quantitative multi-parameter analysis*. Int J Radiat Oncol Biol Phys. **48** 571-82.
146. Rijken P.F.J.W., Peters J.P.W., *et al.* (2002), *Quantitative analysis of varying profiles of hypoxia in relation to functional vessels in different human glioma xenograft lines*. Radiat Res. **157** 626-32.
147. Rischin D., Hicks R.J., *et al.* (2006), *Prognostic significance of [18F]-misonidazole positron emission tomography-detected tumor hypoxia in patients with advanced head and neck cancer randomly assigned to chemoradiation with or without tirapazamine: a substudy of Trans-Tasman Radiation Oncology Group Study 98.02*. J Clin Oncol **24** 2098-104.
148. Rosenthal D.I. and Ang K.K. (2004), *Altered radiation therapy fractionation, chemoradiation, and patient selection for the treatment of head and neck squamous carcinoma*. Semin Radiat Oncol **14** 153-66.
149. Royds J.A., Dower S.K., *et al.* (1998), *Response of tumour cells to hypoxia: role of p53 and NFkB*. Mol Pathol. **51** 55-61.
150. Scott O.C. (1990), *Mathematical models of repopulation and reoxygenation in radiotherapy*. Br J Radiol **63** 821-3.
151. Selek U., Garden A.S., *et al.* (2004), *Radiation therapy for early-stage carcinoma of the oropharynx*. Int J Radiat Oncol Biol Phys **59** 743-51.
152. Skladowski K., Maciejewski B., *et al.* (2000), *Randomized clinical trial on 7-day-continuous accelerated irradiation (CAIR) of head and neck cancer - report on 3-year tumour control and normal tissue toxicity*. Radiother Oncol. **55** 101-10.
153. Smolle J. and Stettner H. (1993), *Computer simulation of tumour cell invasion by a stochastic growth model*. J Theor Biol **160** 63-72.
154. Sovik A., Malinen E., *et al.* (2007), *Optimization of tumour control probability in hypoxic tumours by radiation dose redistribution: a modelling study*. Phys Med Biol **52** 499-513. Epub 2006 Dec 29.
155. Spiro I.J., Rice G.C., *et al.* (1984), *Cell killing, radiosensitization and cell cycle redistribution induced by chronic hypoxia*. Int J Radiat Oncol Biol Phys **10** 1275-80.
156. Stadler P., Becker A., *et al.* (1999), *Influence of the hypoxic subvolume on the survival of patients with head and neck cancer*. Int J Radiat Oncol Biol Phys **44** 749-54.
157. Stadler P., Feldmann H.J., *et al.* (1998), *Changes in tumor oxygenation during combined treatment with split-course radiotherapy and chemotherapy in patients with head and neck cancer*. Radiother Oncol **48** 157-64.
158. Stamatakos G.S., Antipas V.P., *et al.* (2006), *A four-dimensional computer simulation model of the in vivo response to radiotherapy of glioblastoma multiforme: studies on the effect of clonogenic cell density*. Br J Radiol. **79** 389-400.
159. Stamatakos G.S., Zacharaki E.I., *et al.* (2001), *Modeling tumor growth and irradiation response in vitro--a combination of high-performance computing and web-based technologies including VRML visualization*. IEEE Trans Inf Technol Biomed **5** 279-89.
160. Stanley J.A., Shipley W.U., *et al.* (1977), *Influence of tumour size on hypoxic fraction and therapeutic sensitivity of Lewis lung tumour*. Br J Cancer **36** 105-13.

161. Steel G.G. (2002), *Basic Clinical Radiobiology*. Hodder Arnold, London, UK).
162. Stuschke M. and Thames H.D. (1997), *Hyperfractionated radiotherapy of human tumors: overview of the randomized clinical trials*. Int J Radiat Oncol Biol Phys **37** 259-67.
163. Tannock I.F. (1968), *The relation between cell proliferation and the vascular system in a transplanted mouse mammary tumour*. Br J Cancer **22** 258-73.
164. Tannock I.F. (1972), *Oxygen diffusion and the distribution of cellular radiosensitivity in tumours*. Br J Radiol **45** 515-24.
165. Tannock I.F. and Hill R.P. (1998), *The basic science of oncology*. (N Y: McGraw-Hill Professional).
166. Tannock I.F. and Steel G.G. (1970), *Tumor growth and cell kinetics in chronically hypoxic animals*. J Natl Cancer Inst **45** 123-33.
167. Terhaard C.H., Kal H.B., *et al.* (2005), *Why to start the concomitant boost in accelerated radiotherapy for advanced laryngeal cancer in week 3*. Int J Radiat Oncol Biol Phys **62** 62-9.
168. Thomlinson R.H. and Gray L.H. (1955), *The histological structure of some human lung cancers and the possible implications for radiotherapy*. Br J Cancer **9** 539-49.
169. Titz B. and Jeraj R. (2008), *An imaging-based tumour growth and treatment response model: investigating the effect of tumour oxygenation on radiation therapy response*. Phys Med Biol. **53** 4471-88. Epub 2008 Aug 1.
170. Trott K.R. (1999), *The mechanisms of acceleration of repopulation in squamous epithelia during daily irradiation*. Acta Oncol **38** 153-7.
171. Trott K.R. and Kummermehr J. (1991), *Rapid repopulation in radiotherapy: a debate on mechanism. Accelerated repopulation in tumours and normal tissues*. Radiother Oncol **22** 159-60.
172. Tucker S.L. (1999), *Pitfalls in estimating the influence of overall treatment time on local tumor control*. Acta Oncol **38** 171-8.
173. Tucker S.L. and Chan K.S. (1990), *The selection of patients for accelerated radiotherapy on the basis of tumor growth kinetics and intrinsic radiosensitivity*. Radiother Oncol. **18** 197-211.
174. Tuckwell W., Bezak E., *et al.* (2008), *Efficient Monte Carlo modelling of individual tumour cell propagation for hypoxic head and neck cancer*. Phys Med Biol **53** 4489-507. Epub 2008 Aug 1.
175. Urano M., Chen Y., *et al.* (2002), *Measurements of tumor tissue oxygen tension using a time-resolved luminescence-based optical oxylite probe: comparison with a paired survival assay*. Radiat Res **158** 167-73.
176. Vaupel P. (2004), *Tumor microenvironmental physiology and its implications for radiation oncology*. Semin Radiat Oncol. **14** 198-206.
177. Villaret D.B., Wang T., *et al.* (2000), *Identification of genes overexpressed in head and neck squamous cell carcinoma using a combination of complementary DNA subtraction and microarray analysis*. Laryngoscope. **110** 374-81.
178. Vokes E.E., Weichselbaum R.R., *et al.* (1993), *Head and neck cancer*. N Engl J Med. **328** 184-94.
179. Wang T., Hopkins D., *et al.* (2000), *Identification of genes differentially over-expressed in lung squamous cell carcinoma using combination of cDNA subtraction and microarray analysis*. Oncogene. **19** 1519-28.
180. Ward J.F. (1994), *DNA damage as the cause of ionizing radiation-induced gene activation*. Radiat Res. **138** S85-8.
181. Webster L., Hodgkiss R.J., *et al.* (1998), *Cell cycle distribution of hypoxia and progression of hypoxic tumour cells in vivo*. Br J Cancer **77** 227-34.

182. Wijffels K.I., Marres H.A., *et al.* (2008), *Tumour cell proliferation under hypoxic conditions in human head and neck squamous cell carcinomas*. Oral Oncol **44** 335-44. Epub 2007 Aug 6.
183. Wilson G.D. (2007), *Cell kinetics*. Clin Oncol (R Coll Radiol) **19** 370-84. Epub 2007 Mar 30.
184. Wilson G.D., Dische S., *et al.* (1995), *Studies with bromodeoxyuridine in head and neck cancer and accelerated radiotherapy*. Radiother Oncol **36** 189-97.
185. Wilson G.D., McNally N.J., *et al.* (1988), *Measurement of cell kinetics in human tumours in vivo using bromodeoxyuridine incorporation and flow cytometry*. Br J Cancer **58** 423-31.
186. Withers H.R., Peters L.J., *et al.* (1995), *Local control of carcinoma of the tonsil by radiation therapy: an analysis of patterns of fractionation in nine institutions*. Int J Radiat Oncol Biol Phys **33** 549-62.
187. Withers H.R., Taylor J.M., *et al.* (1988), *The hazard of accelerated tumor clonogen repopulation during radiotherapy*. Acta Oncol **27** 131-46.
188. Wong D., Todd R., *et al.* (1996), *Molecular biology of human oral cancer*. Crit Rev Oral Biol Med **7** 319-28.
189. Wouters B.G. and Brown J.M. (1997), *Cells at intermediate oxygen levels can be more important than the "hypoxic fraction" in determining tumor response to fractionated radiotherapy*. Radiat Res **147** 541-50.
190. Wright E.A. and Howard-Flanders P. (1957), *The influence of oxygen on the radiosensitivity of mammalian tissues*. Acta radiol **48** 26-32.
191. Wright N., and Alison, M. (1984), *The biology of epithelial cell populations.* vol **2** (Oxford and NY: Oxford Univerisy Press and Clarendon Press).
192. Young M.R. (2006), *Protective mechanisms of head and neck squamous cell carcinomas from immune assault*. Head Neck **28** 462-70.